



ANDRÉA ARRUDA MARTINS SHIMOJO

**PLASMA RICO EM PLAQUETAS ASSOCIADO A ÁCIDO HIALURÔNICO  
E/ OU QUITOSANA PARA APLICAÇÕES EM MEDICINA  
REGENERATIVA**

***PLATELET-RICH PLASMA ASSOCIATED TO HYALURONIC ACID AND/  
OR CHITOSAN FOR APPLICATIONS IN REGENERATIVE MEDICINE***

Campinas, 2015





**UNIVERSIDADE ESTADUAL DE CAMPINAS**  
**Faculdade De Engenharia Química**

**ANDRÉA ARRUDA MARTINS SHIMOJO**

**PLASMA RICO EM PLAQUETAS ASSOCIADO A ÁCIDO HIALURÔNICO  
E/OU QUITOSANA PARA APLICAÇÕES EM MEDICINA  
REGENERATIVA**

***PLATELET-RICH PLASMA ASSOCIATED TO HYALURONIC ACID AND/  
OR CHITOSAN FOR APPLICATIONS IN REGENERATIVE MEDICINE***

Tese apresentada à Faculdade de Engenharia Química da Universidade Estadual de Campinas como parte dos requisitos exigidos para obtenção do título de Doutora em Engenharia Química.

*Thesis presented to the School of Chemical Engineering of the University of Campinas in partial fulfillment of the requirements for the degree of Doctor in Chemical Engineering*

**Orientadora: Professora Doutora Maria Helena Andrade Santana**

Este exemplar corresponde à versão final da tese defendida pela aluna Andréa Arruda Martins Shimojo, e orientada pela profa. Dra. Maria Helena Andrade Santana.

  
Assinatura do orientador

Campinas, 2015

Ficha catalográfica  
Universidade Estadual de Campinas  
Biblioteca da Área de Engenharia e Arquitetura  
Rose Meire da Silva - CRB 8/5974

Sh62p Shimojo, Andréa Arruda Martins, 1971-  
Plasma rico em plaquetas associado a ácido hialurônico e/ ou quitosana para aplicações em medicina regenerativa / Andréa Arruda Martins Shimojo. – Campinas, SP : [s.n.], 2015.

Orientador: Maria Helena Andrade Santana.  
Tese (doutorado) – Universidade Estadual de Campinas, Faculdade de Engenharia Química.

1. Plasma rico em plaquetas. 2. Ácido hialurônico. 3. Quitosana. 4. Biomateriais. 5. Medicina regenerativa. 6. Micropartículas. I. Santana, Maria Helena Andrade, 1951-. II. Universidade Estadual de Campinas. Faculdade de Engenharia Química. III. Título.

Informações para Biblioteca Digital

**Título em outro idioma:** Platelet-rich plasma associated to hyaluronic acid and/ or chitosan for applications in regenerative medicine

**Palavras-chave em inglês:**

Platelet-rich plasma

Hyaluronic acid

Chitosan

Biomaterials

Regenerative medicine

Microparticles

**Área de concentração:** Engenharia Química

**Titulação:** Doutora em Engenharia Química

**Banca examinadora:**

Maria Helena Andrade Santana [Orientador]

Aline Mara Barbosa Pires

Giuliana Piovesan Alves

Marco Vinícius Chaud

Mariana Altenhofen da Silva

**Data de defesa:** 27-03-2015

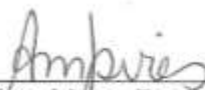
**Programa de Pós-Graduação:** Engenharia Química

Tese de Doutorado defendida por Andréa Arruda Martins Shimojo e aprovada em  
27 de março de 2015 pela banca examinadora constituída pelos doutores:



---

Profa. Dra. Maria Helena Andrade Santana



---

Profa. Dra. Aline Mara Barbosa Pires



---

Profa. Dra. Giuliana Piovesan Alves



---

Prof. Dr. Marco Vinicius Chaud



---

Profa. Dra. Mariana Altenhofen da Silva



# RESUMO

---

Este trabalho teve como objetivo estudar o desempenho *in vitro* do plasma rico em plaquetas (PRP) com *scaffolds* de ácido hialurônico (AH) ou quitosana (CHT) como um *scaffold* compósito para a proliferação e diferenciação osteogênica de células tronco mesenquimais derivadas de tecido adiposo humano (h-AdMSCs). O PRP é um produto autólogo obtido do sangue total (WB). O ácido hialurônico é um glicosaminoglicano e principal componente do fluido sinovial. A quitosana é um polissacarídeo natural encontrado principalmente na carapaça de crustáceos. O PRP puro (P-PRP, rico em plaquetas e pobre em leucócitos) foi obtido a partir da centrifugação controlada do WB, e ativado com os agonistas soro autólogo e cálcio. Os *scaffolds* foram estruturados em micropartículas ou esponjas, para atender os requisitos de formulações injetáveis ou sólidas, respectivamente. Nesse contexto, os seguintes *scaffolds* foram preparados e caracterizados: sólidos porosos (esponjas) de quitosana não estabilizados (PCHTs) e estabilizados (SPCHTs); micropartículas de quitosana-tripolifosfato de sódio (iCHT-TPPs); micropartículas e esponjas de ácido hialurônico autorreticulado (ACPs) e de ácido hialurônico reticulado com 1,4-butanodiol diglicidil éter (HA-BDDE); e esponjas e micropartículas de ACP e CHT (PECs). PCHTs foram preparados por congelamento e liofilização de soluções de CHT, variando a concentração e as condições de congelamento. As estabilizações foram realizadas pelo tratamento dos PCHTs com hidróxido de sódio, série de etanol ou reticulação com tripolifosfato. Os iCHT-TPPs foram preparados por reticulação iônica de quitosana com TPP em diferentes razões mássicas. ACPs foram obtidos por autoesterificação organocatalisada. HA-BDDE foi preparado por eterificação dos grupos hidroxílicos do HA com o epóxido BDDE. PECs foram preparados por reticulação iônica do ACP com a CHT. Para a preparação de *scaffolds* compósitos, P-PRP ativado contendo h-AdMSCs foi imediatamente pipetado sobre a superfície dos *scaffolds*. Os resultados mostraram que os *scaffolds* não apresentam citotoxicidade. Micrografias obtidas por microscopia eletrônica de varredura mostraram compatibilidade estrutural com as redes de fibrina formadas no interior dos poros ou na superfície de *scaffolds* compósitos. Os *scaffolds* compósitos estimularam o crescimento de h-AdMSCs e a diferenciação osteogênica. Os *scaffolds* compósitos também promoveram liberação gradual dos fatores de crescimento PDGF-AB e TGF- $\beta$ 1. Assim, concluímos que os *scaffolds* compósitos estudados neste trabalho são promissores para engenharia de tecidos, particularmente para a cicatrização e regeneração óssea, no âmbito da medicina regenerativa.

*Palavras-chave: Plasma rico em Plaquetas, Scaffolds, Ácido hialurônico, Quitosana, Medicina regenerativa.*





# ABSTRACT

---

This work aimed to study the *in vitro* performance of platelet-rich plasma (PRP) with scaffolds of hyaluronic acid (HA) and/ or chitosan (CHT) as a composite scaffold for proliferation and osteogenic differentiation of human adipose-derived mesenchymal stem cells (h-AdMSCs). The PRP is an autologous product obtained from whole blood (WB). Hyaluronic acid is a glycosaminoglycan and the main component of the synovial fluid. Chitosan is a natural polysaccharide found mainly in the carapace of crustaceans. The pure PRP (P-PRP, rich in platelet and poor in leukocytes) was obtained from controlled centrifugation of WB, and activated with the agonists autologous serum and calcium. The scaffolds were structured in microparticles or sponges, to comply the requirements of injectable or solid formulations, respectively. In this context, the following scaffolds were prepared and characterized: chitosan porous solid (sponge) unstabilized (PCHTs) and stabilized (SPCHTs); chitosan-sodium tripolyphosphate microparticles (iCHT-TPPs); microparticles and sponges of auto-crosslinked hyaluronic acid (ACPs) and of hyaluronic acid crosslinked with 1,4-butanediol diglycidyl ether (HA-BDDE); and microparticles and sponges of ACP and CHT (PECs). PCHTs were prepared by freezing and lyophilization of CHT solutions, varying the concentration and freezing conditions. Stabilization was performed by treating the PCHTs with sodium hydroxide, an ethanol series or by crosslinking with tripolyphosphate. The iCHT-TPPs were prepared by ionic crosslinking of chitosan with TPP at different mass ratios. ACPs was prepared by organocatalyzed auto-esterification. HA-BDDE was prepared by etherification of the hydroxyl groups of HA with the epoxide BDDE. PECs were prepared by ionic crosslinking of ACP with CHT. For the preparation of composite scaffolds, activated P-PRP containing h-AdMSCs was immediately pipetted onto the surface of the scaffolds. The results showed that the scaffolds do not exhibit cytotoxicity. Micrographs obtained by scanning electron microscopy (SEM) showed structural compatibility with fibrin networks formed inside the pores or on the surface of scaffolds. The composite scaffolds stimulated the growth of h-AdMSCs and osteogenic differentiation. Composite scaffolds also promoted gradual release of growth factors PDGF-AB and TGF- $\beta$ 1 and osteogenic differentiation. Thus, we conclude that the composite scaffolds studied in this work are promising for tissue engineering, particularly for healing and bone regeneration in regenerative medicine.

*Keywords: Platelet-rich plasma, hyaluronic acid, chitosan, scaffolds, regenerative medicine.*



# SUMÁRIO

---

RESUMO.....	vii
ABSTRACT .....	ix
AGRADECIMENTOS .....	xxi
LISTA DE FIGURAS .....	xxiii
LISTA DE TABELAS .....	xxix
CAPÍTULO 1 – INTRODUÇÃO .....	1
1.1. Apresentação .....	1
1.2. Relevância do Trabalho .....	2
1.3. Objetivo .....	5
CAPÍTULO 2 – REVISÃO BIBLIOGRÁFICA .....	7
2.1. Engenharia de Tecidos e Medicina Regenerativa .....	7
2.2. Plasma Rico em Plaquetas .....	8
2.2.1. Definições .....	8
2.2.2. PRP na regeneração de tecidos .....	10
2.3. <i>Scaffolds</i> .....	12
2.3.1. Definições .....	12
2.3.2. <i>Scaffolds</i> na regeneração de tecidos .....	13
2.3.3. Propriedades requeridas dos <i>scaffolds</i> .....	14
2.3.4. Materiais utilizados na fabricação de <i>scaffolds</i> .....	15
2.3.4.1. Ácido hialurônico (AH) .....	16
2.3.4.2. Quitosana .....	20
2.3.4.3. Complexos Polieletrólitos de Ácido Hialurônico e Quitosana .....	22
2.4. Células Tronco Mesenquimais .....	23
2.5. <i>Scaffolds</i> Compósitos .....	25
2.6. Referências .....	27

CAPÍTULO 3 – PERFORMANCE OF PRP ASSOCIATED WITH POROUS CHITOSAN AS A COMPOSITE SCAFFOLD FOR REGENERATIVE MEDICINE.....	41
3.1. Introduction .....	42
3.2. Experimental .....	45
3.2.1. Materials .....	45
3.2.2. Methods.....	45
3.2.2.1. Preparation of Porous Chitosan Scaffolds (PCHTs).....	45
3.2.2.2. Characterization of Porous Chitosan Scaffolds (PCHTs) .....	46
3.2.2.3. PRP Preparations.....	47
3.2.2.4. The Composite Scaffolds ( $\alpha$ P-PRP/PCHTs).....	48
3.2.2.5. Images of the h-AdMSCs-Seeded Composite Scaffolds .....	50
3.2.2.6. Induction of Osteogenic Differentiation.....	50
3.2.2.7. Statistical Analysis.....	50
3.3. Results and Discussion .....	51
3.3.1. Experimental Design.....	51
3.3.2. Effects of Freezing Conditions and Chitosan Concentration on PCHTs ....	51
3.3.2.1. Images of Porous Structure.....	51
3.3.2.2. Characterization of PCHTs.....	53
3.3.2.3. Cell Compatibility.....	56
3.3.3. Characterization of the Composite Scaffolds .....	57
3.3.3.1. Images of the Cell-Seeded $\alpha$ P-PRP/PCHTs.....	57
3.3.3.2. Growth Factor Release .....	58
3.3.3.3. h-AdMSCs-Seeded Proliferation .....	60
3.3.3.4. Induction of Osteogenic Differentiation.....	61
3.4. Conclusions.....	61
3.5. References.....	62
CAPÍTULO 4 – STABILIZATION OF POROUS CHITOSAN IMPROVES THE PERFORMANCE OF ITS ASSOCIATION WITH PLATELET-RICH PLASMA AS A COMPOSITE SCAFFOLD.....	69
4.1. Introduction .....	70

4.2. Materials and Methods .....	72
4.2.1. Materials .....	73
4.2.2. Methods .....	73
4.2.2.1. Preparation of porous chitosan (PCHT).....	73
4.2.2.2. Stabilization of PCHT .....	73
4.2.3. Characterization of SPCHTs.....	74
4.2.3.1. Chemical modification .....	74
4.2.3.2. Morphology and pore size .....	74
4.2.3.3. Swelling profile .....	74
4.2.3.4. Porosity .....	75
4.2.3.5. Mechanical resistance.....	75
4.2.3.6. Degradation in phosphate buffered saline .....	75
4.2.3.7. Cell compatibility .....	76
4.2.4. Preparation of pure platelet-rich plasma (P-PRP).....	76
4.2.5. Preparation of activated P-PRP (aP-PRP).....	76
4.2.6. Preparation of composite scaffold (aP-PRP/SPCHTs) .....	76
4.2.7. h-AdMSCs isolation and pre-cultivation .....	77
4.2.8. h-AdMSCs-seeding in the composite scaffolds.....	77
4.2.9. Characterization of the composite scaffold .....	77
4.2.9.1. Release of GFs .....	77
4.2.9.2. Images of the cell-seeded composite scaffolds.....	78
4.2.9.3. h-AdMSCs proliferation .....	78
4.2.9.4. Induction of osteogenic differentiation .....	79
4.2.9.5. Alkaline phosphatase activity (ALP) .....	79
4.2.10. Statistical analysis .....	79
4.3. Results and discussion.....	79
4.3.1. Modifications and surface chemistry.....	79
4.3.2. Physicochemical and mechanical properties of SPCHTs .....	80
4.3.3. Biological properties of SPCHTs.....	85
4.4. Conclusions.....	88

4.5. References .....	89
CAPÍTULO 5 – IN VITRO BIOLOGICAL PERFORMANCE OF INJECTABLE CHITOSAN-TRIPOLYPHOSPHATE SCAFFOLDS COMBINED WITH PLATELET-RICH PLASMA.....	95
5.1. Introduction .....	96
5.2. Materials and Methods .....	97
5.2.1. Materials .....	97
5.2.2. Preparation of injectable scaffolds of chitosan-sodium tripolyphosphate (iCHT-TPPs) .....	98
5.2.3. Physicochemical Characterization .....	98
5.2.3.1. Chemical modification. ....	98
5.2.3.2. Crosslink density Flory-Rehner calculations.....	98
5.2.3.3. Particle diameter measurements.....	99
5.2.3.4. Rheology measurements.....	99
5.2.3.5. Extrusion force. ....	99
5.2.3.6. Swelling ratio (SR).....	99
5.2.3.7. Degradation in phosphate buffered saline.....	100
5.2.4. Biological characterization .....	100
5.2.4.1. Cell compatibility. ....	100
5.2.5. Preparation of pure platelet-rich plasma (P-PRP).....	100
5.2.5.1. Activation of P-PRP (aP-PRP).....	101
5.2.6. Preparation of composite scaffold (aP-PRP/iCHT-TPPs) .....	101
5.2.7. Characterization of aP-PRP/iCHT-TPPs.....	101
5.2.7.1. Release of GFs .....	101
5.2.8. h-AdMSCs isolation and pre-cultivation .....	102
5.2.9. Culture of h-AdMSCs-seeding in the composite scaffolds .....	102
5.2.9.1. h-AdMSCs proliferation .....	102
5.2.9.2. Images of the cell-seeded composite scaffolds.....	103
5.2.9.3. Induction of osteogenic differentiation .....	103
5.2.9.4. Alkaline phosphatase activity (ALP) .....	103

5.2.10. Statistical analysis .....	104
5.3. Results and discussion.....	104
5.3.1. Crosslinking in the injectable scaffolds of chitosan-sodium tripolyphosphate (iCHT-TPPs).....	104
5.3.2. Physicochemical and mechanical properties of iCHT-TPPs.....	105
5.3.3. Biological characterization .....	108
5.4. Conclusions.....	112
5.5. References.....	113
<b>CAPÍTULO 6 – IMPROVEMENTS IN PLATELET-RICH PLASMA PERFORMANCE BY ASSOCIATION WITH MICROPARTICLES OR SPONGES OF AUTO-CROSSLINKED HYALURONIC ACID .....</b>	<b>117</b>
6.1. Introduction .....	118
6.2. Experimental .....	120
6.2.1. Materials .....	121
6.2.2. Methods.....	121
6.2.2.1. Preparation of HA-TBA.....	121
6.2.2.2. Preparation of ACP .....	121
6.2.2.3. Characterization of ACP .....	122
6.2.2.4. Preparation of structured ACP.....	122
6.2.2.5 Characterization of structured ACP .....	122
6.2.2.6. Preparation of PRP .....	125
6.2.2.7. Preparation of activated P-PRP (aP-PRP) .....	125
6.2.2.8 Preparation of composite scaffolds .....	125
6.2.2.9. Characterization of composite scaffolds .....	126
6.2.2.10. Statistical analysis .....	128
6.3. Results .....	128
6.3.1. Characterization of ACP .....	128
6.3.2. Characterization of ACPs structured scaffolds.....	129
6.3.3. Characterization of the composite scaffolds .....	132
6.4. Discussion.....	136

6.5. Conclusions.....	140
6.6. References.....	141
CAPÍTULO 7 – STRUCTURATION OF HIGH MOLECULAR WEIGHT HYALURONIC ACID IN MICROPARTICLES OR SPONGES IMPROVES ITS PERFORMANCE WHEN ASSOCIATED TO PLATELET-RICH PLASMA .....	
	147
7.1. Introduction .....	148
7.2. Experimental Section .....	150
7.2.1. Materials .....	150
7.2.2. Methods.....	151
7.2.2.1. Preparation and characterization of HA crosslinked with BDDE.....	151
7.2.2.2. Preparation of structured HA-BDDE .....	151
7.2.3. Characterization of the structures .....	151
7.2.3.1. mHA-BDDE .....	152
7.2.3.2. sHA-BDDE .....	153
7.2.4. PRP preparation and activation .....	154
7.2.5. Release of growth factors .....	154
7.2.6. Association of mHA-BDDE or sHA-BDDE with P-PRP and h-AdMSCs-seeding .....	155
7.2.7. h-AdMSCs cultivation .....	155
7.2.8. Images of the cell-seeded composite scaffolds .....	156
7.2.9. Induction of osteogenic differentiation .....	156
7.2.10. Alkaline phosphatase activity (ALP).....	156
7.2.11. Statistical analysis .....	157
7.3. Results and Discussion .....	157
7.3.1. Experimental design .....	157
7.3.2. Chemical modifications.....	157
7.3.3. Physicochemical and mechanical properties of HA forms .....	158
7.3.3.1. mHA-BDDE .....	159
7.3.3.2. sHA-BDDE .....	161



7.3.4. Effects of the association with P-PRP .....	162
7.3.4.1. SEM images .....	162
7.3.4.2. Release of growth factors .....	163
7.3.4.3. Proliferation of h-AdMSCs and ALP activity .....	164
7.4. Conclusions .....	165
7.5. References .....	166
<b>CAPÍTULO 8 – STERILIZATION OF AUTO-CROSSLINKED HYALURONIC ACID STRUCTURED IN MICROPARTICLES OR SPONGES .....</b>	<b>171</b>
8.1. Introduction .....	172
8.2. Materials and Methods .....	173
8.2.1. Materials .....	173
8.2.2. Methods .....	173
8.2.2.1. Preparation of the HA-ACP scaffolds .....	173
8.2.2.2. Sterilization Treatments .....	174
8.2.2.3. HA-ACP sponges characterization .....	175
8.2.2.4. HA-ACP microparticles characterization .....	175
8.2.2.5. Sterility Tests .....	175
8.3. Results and Discussion .....	176
8.3.1. Effects of the treatments on physicochemical properties of the HA-ACP sponges .....	176
8.3.2. Effects of the treatments on physicochemical properties of HA-ACP microparticles .....	178
8.3.3. Sterility evaluation .....	179
8.4. Conclusion .....	181
8.5. References .....	181
<b>CAPÍTULO 9 – CONCLUSÕES .....</b>	<b>183</b>
9.1. Conclusões .....	183
9.2. Trabalhos Futuros .....	184
<b>ANEXO 1 .....</b>	<b>187</b>



*Ao meu marido Luther, que me apoiou em todos os momentos e às minhas filhas, Laura e Júlia, que de uma forma especial e carinhosa me deram força e coragem para concluir esta jornada.*



# AGRADECIMENTOS

---

À Professora Dra. Maria Helena Andrade Santana pela oportunidade, orientação, carinho e confiança durante a execução deste trabalho.

Ao amigo Gilson Barbosa Maia Jr., técnico do Laboratório de Desenvolvimento de Processos Biotecnológicos (LDPB), pela paciência, dedicação e amizade em todos os momentos.

Ao Professor Dr. Edvaldo Sabadini do Departamento de Físico-Química do Instituto de Química da Unicamp pela utilização do reômetro e ao seu aluno de doutorado Thiago Heiji Ito pela colaboração e disponibilidade.

Ao Professor Dr. William Dias Belangero e à sua aluna Ana Amélia Rodrigues do Laboratório de Biomateriais em Ortopedia da Faculdade de Ciências Médicas da Unicamp pela disponibilização de seu laboratório e pelas análises de citotoxicidade.

À Dra. Ângela Cristina Malheiros Luzo e à funcionária Adriana da Silva Santos Duarte do Centro de Hematologia e Hemoterapia do Banco de Sangue de Cordão Umbilical e Placentário da Unicamp pela disponibilização de seu laboratório e isolamento e caracterização das células mesenquimais.

Ao Dr. José Fábio Lana (Instituto de Osso e Cartilagem - IOC) por nos instigar a estudar esse assunto.

À Profa. Dra. Mariana Altenhofen da Silva, do Centro de Ciências Agrárias (CCA) da UFSCAR, pelo carinho em participar de todas as minhas bancas de qualificação e defesa do mestrado e doutorado.

Aos meus colegas do LDPB Amanda, Bruna, Fernanda, Yara, Patrícia, Rafaela, Rhelvis. Em especial à minha querida amiga Sofia Elisa Moraga Galdames que me apoiou em todos os momentos bons e ruins deste trabalho. Obrigada amiga, você tornou isso bem mais leve e engraçado.

Às minhas amigas do Laboratório de Nano & Biotecnologia para Desenvolvimentos Avançados (LaNBda), Caroline, Micaela, Aline e Lucimara.

Aos meus alunos de Iniciação Científica, Rafael Lichy, Isabela Cambraia de Souza Brissac e Lucas Martins Pina pela ajuda e principalmente para imensa paciência.

Ao meu marido Luther, pelo amor, incentivo, dedicação, paciência, apoio e compreensão em todos os momentos. Sem você nada disso teria se realizado.

As minhas filhas Laura e Júlia, pelas férias perdidas, pelas incontáveis horas no laboratório, pela compreensão, amor e paciência.

Em especial à minha querida amiga Aline Mara Barbosa Pires, aluna de pós-doutorado da Universidade Federal do Rio de Janeiro (UFRJ) que mesmo de muito longe, me apoiou e incentivou em todos os momentos. Obrigada sempre.

A toda minha família, pelo apoio e incentivo. Em especial, quero agradecer minha tia Therezinha Zani pelo amor, apoio e pela torcida em todos os momentos mais importantes da minha vida.

Ao Conselho Nacional de Desenvolvimento Científico e Tecnológico (CNPq) pelo financiamento.

# LISTA DE FIGURAS

---

<b>Figura 1.</b> Disciplinas que contribuem atualmente na medicina regenerativa (Daar & Greenwood, 2007).....	7
<b>Figura 2.</b> Triângulo da proliferação celular (Adaptado de Barnett & Pomeroy, 2007; Crane & Everts, 2008).....	8
<b>Figura 3.</b> Ilustração esquemática da arquitetura da matriz e das células das quatro categorias de concentrados de plaquetas classificados segundo Ehrenfest <i>et al.</i> (2009). P-PRP=plasma rico em plaquetas puro; L-PRP=plasma rico em plaquetas e leucócitos; P-PRF=fibrina rica em plaquetas pura e L-PRF=fibrina rica em plaquetas e leucócitos. ....	10
<b>Figura 4.</b> Mecanismo de ação do PRP (Mishra <i>et al.</i> , 2012). ....	11
<b>Figura 5.</b> Estrutura molecular do ácido hialurônico.....	16
<b>Figura 6.</b> Grupos de modificação química da molécula de AH: (1) carboxílico, (2) hidroxílico, (3) acetamida, (4) Terminal Reduzido do Polímero (Adaptado de Garg & Hales, 2004).....	17
<b>Figura 7.</b> Preparação de ACP por autoesterificação organocatalisada usando o intermediário ativado AH-CPMI (Schanté <i>et al.</i> , 2011).....	19
<b>Figura 8.</b> Ácido hialurônico reticulado com BDDE em meio alcalino (Malson & Lindqvist, 1986).....	20
<b>Figura 9.</b> Estrutura molecular da quitosana.....	21
<b>Figure 10.</b> SEM micrographs of PCHTs. Cross-sectional morphologies of (a) PCHTs 1% (-20°C); (b) PCHTs 2% (-20°C); (c) PCHTs 3% (-20°C); (d) PCHTs 3% (-80°C); and (e) PCHTs 3% (-196°C). Original magnification is ×100 and the scale bar represents 200 µm. ....	52
<b>Figure 11.</b> The weight loss of scaffolds with time in PBS at 37°C as a percentage of the original weight of the scaffold ( $n = 3$ ). The data are plotted with the mean $\pm$ standard	

error. (■) PCHTs 1% (-20°C); (●) PCHTs 2% (-20°C); (▲) PCHTs 3% (-20°C); (□) PCHTs 3% (-80°C); and (O) PCHTs 3% (-196°C). .....56

**Figure 12.** Proliferation of h-AdMSCs exposed to the PCHTs scaffolds after 24 hours of cultivation. Negative control (NTC) = DMEM with 10%FBS; positive control (PTC) =DMEM with phenol 0.5%. Mean ± standard deviation  $n = 3$ . The population means are significantly different from positive control at  $*P < 0.05$ . .....57

**Figure 13.** Scanning electron microscopic images of  $\alpha$ P-PRP/PCHTs after 5 days of cultivation of h-AdMSCs. (a)  $\alpha$ -PRP; (b)  $\alpha$ P-PRP/PCHTs 1% (-20°C); (c)  $\alpha$ P-PRP/PCHTs 2% (-20°C); (d)  $\alpha$ P-PRP/PCHTs 3% (-20°C); (e)  $\alpha$ P-PRP/PCHTs 3% (-80°C); and (f)  $\alpha$ P-PRP/PCHTs 3% (-196°C). Original magnification is  $\times 5,000$  and the scale bar represents 3  $\mu\text{m}$ . .....58

**Figure 14.** Release profiles of growth factors from  $\alpha$ P-PRP in porous chitosan scaffolds as a function of [(a), (b)] chitosan concentrations and [(c), (d)] freezing conditions. (■) PCHTs 1% (-20°C); (●) PCHTs 2% (-20°C); (▲) PCHTs 3% (-20°C); (□) PCHTs 3% (-80°C), (O) PCHTs 3% (-196°C), and ( $\Delta$ ) P-PRP activated with  $\text{Ca}^{+2}$ /thrombin (used as control); TGF- $\beta$ 1 [(a), (c)]; and PDGF-AB [(b), (d)]. The concentration of platelets in P-PRP was 472,250  $\text{pq}/\text{mm}^3$ . Activated P-PRP alone was used as control. ....59

**Figure 15.** Proliferation kinetic profiles of h-AdMSCs seeded in  $\alpha$ P-PRP/PCHTs. (a) CHT concentration and (b) freezing conditions. (■) PCHTs 1% (-20°C); (●) PCHTs 2% (-20°C); (▲) PCHTs 3% (-20°C); (□) PCHTs 3% (-80°C), (O) PCHTs 3% (-196°C), and ( $\Delta$ ) P-PRP activated with  $\text{Ca}^{+2}$ /thrombin (control). The concentration of platelets in P-PRP was 374,000  $\text{pq}/\text{mm}^3$ . Activated P-PRP alone was used as control. ....60

**Figure 16.** ALP activities of cells cultured on  $\alpha$ P-PRP/PCHTs scaffolds prepared with different CHT concentrations and freezing conditions (statistically significant differences from blank,  $n = 3$ ,  $*P < 0.05$ ). Blank = the reagents used in the assay only. The concentration of platelets in whole blood donors (average of 2 donors) was 163,500  $\text{pq}/\text{mm}^3$ . After preparation of the PRP, the platelets were concentrated approximately 1.74 times, with an average final concentration of 303,000  $\text{pq}/\text{mm}^3$ . .....61

**Figure 17.** ATR-FTIR spectra of SPCHTs/TNaOH, SPCHTs/TEtOH, SPCHTs/CTPP and NTPCHTs. ....80

**Figure 18.** Physicochemical and mechanical properties of the PCHTs. (a) Photographs



and SEM micrographs of the cross-section of the scaffolds. Original magnification is  $\times 100$  and the scale bar represents 200  $\mu\text{m}$ . (b) Young's moduli and pore size; (c) Porosity (\*The means difference are significant at level at  $p < 0.05$ ); (d) Swelling profile in PBS pH 7.4 at 37°C; (e) Degradation profile in PBS pH 7.4 at 37°C expressed as weight loss. Values are the mean  $\pm$  standard deviation. (■) SPCHTs/TNaOH; (●) SPCHTs/TEtOH; (▲) SPCHTs/CTPP and (□) NTPCHTs. ....84

**Figure 19.** (a) SEM images of cells on aP-PRP/SPCHTs after 5 days of culture. Scale bars indicate 3  $\mu\text{m}$  (magnification = 5,000x). (b) The compatibility of h-AdMSCs that were exposed to SPCHTs. Negative control (NTC) = DMEM with 10% FBS; positive control (PTC) = DMEM with phenol 0.5%. Mean  $\pm$  standard deviation  $n = 3$ . The population means are significantly different from the positive control at  $*p < 0.05$ . (c) Proliferation profile of h-AdMSCs cultured in aP-PRP/SPCHTs as a function of time. aP-PRP and NTPCHTs were used as controls. Platelets were concentrated in aP-PRP at approximately 1.84 times the basal value. The average concentration was 393,000  $\text{pq}/\text{mm}^3$ . (d) PDGF-AB release profile from aP-PRP/SPCHTs. Platelets were concentrated in aP-PRP at approximately 2.09 times the basal value. The average concentration was 472,250  $\text{pq}/\text{mm}^3$ . (e) TGF- $\beta 1$  release profile from aP-PRP/PCHTs. Platelets were concentrated in aP-PRP at approximately 2.09 times the basal value. The average concentration was 472,250  $\text{pq}/\text{mm}^3$ . (f) ALP activity of cells cultured on SPCHTs (statistically significant differences from blank,  $n=3$ ,  $*p < 0.05$ ). NTPCHTs is the control group, blank = the reagents used in the assay only. Platelets were concentrated in aP-PRP at approximately 1.79 times the basal value. The average concentration was 280,500  $\text{pq}/\text{mm}^3$ . ( $\Delta$ ) aP-PRP and (□) NTPCHT were both used as controls; (●) SPCHTs/TEtOH; (■) SPCHTs/TNaOH, and (▲) SPCHTs/CTPP.....87

**Figure 20.** Interaction of chitosan with TPP by (a) ionic crosslinking or (b) deprotonation. ....104

**Figure 21.** FTIR spectrum of pure chitosan and iCHT-TPPs 2:1. ....105

**Figure 22.** Degradation profile of iCHT-TPPs in PBS pH 7.4 at 37°C. (■) iCHT-TPPs 2:1; (●) iCHT-TPPs 5:1 and (▲) iCHT-TPPs 10:1.....107

**Figure 23.** Growth factor release profiles from aP-PRP combined with CHT-TPP scaffolds. (a) PDGF-AB and (b) TGF- $\beta 1$ . ( $\Delta$ ) PRP activated with  $\text{Ca}^{+2}$ /serum used as control; (■) aP-PRP/iCHT-TPPs 2:1; (●) aP-PRP/iCHT-TPPs 5:1 and (▲) aP-PRP-iCHT-

TPPs 10:1. The concentration of platelets in whole blood donors (average of 2 donors) was 234,250  $\text{pq}/\text{mm}^3$ . After preparation of the P-PRP, the platelets were concentrated approximately 2.09 times, with an average final concentration of 472,250  $\text{pq}/\text{mm}^3$ . .... 109

**Figure 24.** Scanning electron microscopic images of aP-PRP and aP-PRP/iCHT-TPPs after 5 days of cultivation of h-AdMSCs..... 110

**Figure 25.** (a) % of NTC as a measurement of the compatibility of h-AdMSCs that were exposed to the iCHT-TPPs. Negative control (NTC) = DMEM with 10% FBS; positive control (PTC) = DMEM with phenol 0.5%. The population means are significantly different from positive control at  $*p < 0.05$ . (b) Proliferation profile of h-AdMSCs cultured in aP-PRP/iCHT-TPPs scaffolds as a function of time. Activated PRP was used as control. ( $\Delta$ ) aP-PRP; ( $\blacksquare$ ) aP-PRP/iCHT-TPPs 2:1; ( $\bullet$ ) aP-PRP/iCHT-TPPs 5:1 and ( $\blacktriangle$ ) aP-PRP/iCHT-TPPs 10:1. The concentration of platelets in whole blood donors (average of 2 donors) was 215,375  $\text{pq}/\text{mm}^3$ . After preparation of the P-PRP, the platelets were concentrated approximately 1.79 times, with an average final concentration of 383,500  $\text{pq}/\text{mm}^3$ . Mean  $\pm$  standard deviation  $n = 3$ . .... 111

**Figure 26.** ALP activities of h-AdMSCs cultured on composite scaffolds (\*statistically significant differences from blank,  $n=3$ ,  $p < 0.05$ ). Blank = the reagents used in the assay only). The concentration of platelets in whole blood donors (average of 2 donors) was 214,000  $\text{pq}/\text{mm}^3$ . After preparation of the P-PRP, the platelets were concentrated approximately 2.31 times, with an average final concentration of 473,500  $\text{pq}/\text{mm}^3$ . .... 112

**Figure 27.** Auto-crosslinking reaction using CMPI-activated HA intermediate (Schanté *et al.*, 2011). .... 122

**Figure 28.** ATR-FTIR spectra of ACP with 5% of carboxylic groups esterified. .... 128

**Figure 29.** (a) Oscillation spectrum and (b) flow curve of ( $\blacksquare$ ) ACP Microparticles and ( $\blacktriangle$ ) fluid HA (1% wt.).  $G'$  (closed symbol) and  $G''$  (open symbol)..... 129

**Figure 30.** Figure 4. SEM micrographs of cross-sectional of (a) ACP sponges and (b) HA sponge..... 131

**Figure 31.** (a) Viability of h-AdMSCs exposed to the structured ACP or HA (fluid and sponge). Negative control (NTC) = DMEM with 10% FBS; positive control (PTC) = DMEM with phenol 0.5%. Mean  $\pm$  standard deviation  $n = 3$ . The population means are

significantly different from the positive control at  $*p < 0.05$ . (b) The weight remaining of the structured ACP under the time course of degradation (at 37°C, in PBS). (■) ACP microparticles and (▲) ACP sponges.....132

**Figure 32.** Growth factor release profiles from P-PRP combined with HA and ACP structured scaffolds. (a) PDGF-AB and (b) TGF-β1. (●) ACP microparticles; (▲) fHA; (■) P-PRP alone; (O) ACP sponges and (Δ) sHA. The concentration of platelets in P-PRP was 407,000 pq/mm<sup>3</sup>.....133

**Figure 33.** The proliferation profiles of h-AdMSCs cultured in structured HA and ACP composite scaffolds as a function of time. (a) Microparticles (concentration of platelets in P-PRP = 393,000 pq/mm<sup>3</sup>) and (b) sponges (concentration of platelets in P-PRP = 472,250 pq/mm<sup>3</sup>). Activated P-PRP alone was used as control. ....134

**Figure 34.** Scanning electron microscopy images of HA and ACP composite scaffolds after 5 days of cultivation of h-AdMSCs. (a) ACP microparticles; (b) fluid HA; (c) ACP sponges and (d) HA sponge. Original magnification is ×5,000 and the scale bar represents 3 μm. ....135

**Figure 35.** Alkaline phosphatase (ALP) activity of h-AdMSCs-seeded cultured in the HA and ACP composite scaffolds on day 14. Blank = the reagents used in the assay only. Statistically significant differences from blank, n=3,  $*p < 0.05$ . The concentration of platelets in P-PRP was 473,500 pq/mm<sup>3</sup>.....135

**Figure 36.** (a) The weight remaining of the HA-BDDE structures under the time course of degradation (At 37°C, in PBS). (■) sHA-BDDE and (□) mHA-BDDE. (b) Viability of h-AdMSC exposed to the HA-BDDE structures, sHA and fHA for 24 hours. Negative control (NTC) = DMEM with 10% FBS; positive control (PTC) = DMEM with phenol 0.5%. Mean ± standard deviation n = 3. The population means are significantly different from positive control at  $p < 0.05$ . ....159

**Figure 37.** (a) Oscillation spectrum of mHA-BDDE and mHA-BDDE/aP-PRP. (■) aP-PRP; (▲) mHA-BDDE; (●) mHA-BDDE/aP-PRP 2:1; (●) mHA-BDDE/aP-PRP 1:1; (◆) mHA-BDDE/aP-PRP 1:2. G' (closed symbol) and G'' (open symbol). (b) Shear viscosity spectra of (▲) fluid HA (1% wt.) and (■) mHA-BDDE.....160

**Figure 38.** Scanning electron micrographs. Cross-section morphologies of (a) HA-BDDE scaffold and (b) sHA.....162

<b>Figure 39.</b> Scanning electron microscopic images of aP-PRP/HA-BDDE scaffolds after 5 days of cultivation of h-AdMSCs. Microparticles: (a) magnification of 2,500X and (b) magnification of 10,000X. Sponges: (c) magnification of 1,000X and (d) magnification of 10,000X.....	163
<b>Figure 40.</b> Growth factor release profile from PRP combined with HA-BDDE scaffolds. PDGF-AB (a) and TGF- $\beta$ 1 (b). (■) PRP activated with serum/ $\text{Ca}^{+2}$ was used as control; (●) sHA-BDDE; (▲) mHA-BDDE. The GFs were measurements from activated P-PRP containing average platelet concentration 495,000 pq/mm <sup>3</sup> .....	164
<b>Figure 41.</b> (a) Kinetic proliferation profiles of h-AdMSCs seeded in aP-PRP/HA-BDDE scaffolds structured in sponges and microparticles. aP-PRP was used as control. The concentration of platelets in P-PRP was 273,000 pq/mm <sup>3</sup> . (b) ALP activities of cells cultured on aP-PRP/HA-BDDE scaffolds structured in sponges and microparticles (statistically significant differences from blank, n=3, *p<0.05). Blank = the colorimetric reagent used in the assay only. The concentration of platelets in whole blood donors (average of 2 donors) was 468,500 pq/mm <sup>3</sup> .....	165
<b>Figure 42.</b> SEM cross-section images of HA-ACP sponges. (a) Unsterile; (b) UV (5 cm); (c) UV (60 cm); (d) Plasma and (e) Ethanol disinfection. Bar = 100 $\mu\text{m}$ .....	176
<b>Figure 43.</b> (a) FT-IR spectra and (b) DSC of HA-ACP sponges after the different treatments. (1) Unsterile; (2) UV irradiation (5 cm); (3) UV irradiation (60 cm); (4) plasma radiation and (5) ethanol disinfection.....	177
<b>Figure 44.</b> Rheological characterization of HA-ACP microparticles after treatment in autoclave at 126°C, under a vapor pressure of 1.5 kgf/cm <sup>2</sup> for: (■) 0 minute; (●) 1 minute; (▲) 2.5 minutes; (◆) 5 minutes; (◆) 10 minutes and (★) 15 minutes. (a) Oscillation spectrum and (b) flow curves. G' (closed symbol) and G'' (open symbol) moduli.....	178
<b>Figure 45.</b> Rheological characterization of HA-ACP microparticles after the treatments: (■) untreated; (●) UV1; (▲) UV2; (◆) plasma and (◆) ethanol disinfection. (a) Oscillation spectrum and (b) flow curves. G' (closed symbol) and G'' (open symbol) moduli.....	179

# LISTA DE TABELAS

---

<b>Table 1.</b> Physicochemical characterization of PCHTs.....	54
<b>Table 2.</b> Physicochemical and mechanical properties of iCHT-TPPs. ....	106
<b>Table 3.</b> Properties of fHA, sHA, and structured ACP (microparticles and sponges). ..	130
<b>Table 4.</b> Physicochemical and mechanical properties of HA in the forms: free (fHA), structured in sponge (sHA), crosslinked with BDDE and structured in sponges (sHA-BDDE) or microparticles (mHA-BDDE).....	158
<b>Table 5.</b> Results of heterotrophic plate count (bacteria) and fungal count (molds and yeasts) obtained after treatment of HA-ACP sponges.....	180
<b>Table 6.</b> Results of heterotrophic plate count (bacteria) and fungal count (molds and yeasts) obtained after sterilization of HA-ACP microparticles.....	180



# LISTA DE ABREVIações DA REVISÃO BIBLIOGRÁFICA

---

ACP.....	Auto-crosslinked polymer
ACPs.....	Scaffolds de ácido hialurônico autorreticulado
aP-PRP.....	Plasma rico em plaquetas ativado
BDDE.....	1,4-butanodiol diglicidil éter
bFGF.....	Fator de crescimento de fibroblastos básico
BMP-2.....	Proteína morfogênica óssea
CHT.....	Quitossana
CMPI.....	Iodeto de 2-cloro-1-metilpiridínio
DMF.....	Dimetilformamida
DMSO.....	Dimetilsulfóxido
EGF.....	Fator de crescimento epitelial
FCs.....	Fatores de crescimento
FTC.....	Fosfato tricálcico
GD.....	Grau de desacetilação
GlcNAc.....	N-acetilglucosamina
GlcUA.....	Ácido D-glucurônico
HA-BDDE.....	Scaffolds de ácido hialurônico reticulado com 1,4-butanodiol diglicidil éter
h-AdMSCs.....	Células tronco mesenquimais derivadas de tecido adiposo humano
iCHT-TPPs.....	Scaffolds injetáveis de quitossana-tripolifosfato de sódio
IGF.....	Fator de crescimento semelhante à insulina
L-PRF.....	Fibrina rica em plaquetas e leucócitos
L-PRP.....	Plasma rico em plaquetas e em leucócitos
$\overline{MM}$ .....	Massa molar média

MSCs.....	Células tronco mesenquimais
PCHTs.....	Scaffolds porosos de quitosana
PDGF-AB.....	fator de crescimento derivado de plaquetas
PECs.....	Complexos polieletrólíticos
PPP.....	Plasma pobre em plaquetas
P-PRF.....	Fibrina rica em plaquetas pura
P-PRP.....	Plasma rico em plaquetas puro
PRP.....	Plasma rico em plaquetas
Ser.....	Soro autólogo
SPCHTs.....	Scaffolds porosos de quitosana estabilizados
TBA.....	Tetrabutylamônio
TGF- $\beta$ 1.....	fator de crescimento transformador beta 1
TPP.....	Tripolifosfato de sódio
VEGF.....	Fator de crescimento endotelial vascular



# CAPÍTULO 1 — INTRODUÇÃO

---

## 1.1. Apresentação

O presente trabalho foi redigido na forma de capítulos, contendo uma introdução geral (Capítulo 1), o objetivo e uma revisão bibliográfica (Capítulo 2) direcionada para os principais fundamentos considerados no desenvolvimento do trabalho.

O desempenho individual dos scaffolds estudados, assim como as metodologias, os resultados e as conclusões específicas estão apresentados na forma de artigos científicos submetidos a periódicos internacionais e na forma de uma patente cujo *abstract* também é apresentado em anexo neste trabalho.

**CAPÍTULO 3 – PERFORMANCE OF PRP ASSOCIATED WITH POROUS CHITOSAN AS A COMPOSITE SCAFFOLD FOR REGENERATIVE MEDICINE** (artigo publicado em fevereiro de 2015 no periódico *The Scientific World Journal*).

**CAPÍTULO 4 – STABILIZATION OF POROUS CHITOSAN IMPROVES THE PERFORMANCE OF ITS ASSOCIATION WITH PLATELET-RICH PLASMA AS A COMPOSITE SCAFFOLD** (artigo submetido ao periódico *Materials Science and Engineering C: Materials for Biological Applications*).

**CAPÍTULO 5 – IN VITRO BIOLOGICAL PERFORMANCE OF INJECTABLE CHITOSAN-TRIPOLYPHOSPHATE SCAFFOLDS COMBINED WITH PLATELET-RICH PLASMA** (artigo submetido ao periódico *Tissue Engineering and Regenerative Medicine*).

**CAPÍTULO 6 – IMPROVEMENTS IN PLATELET-RICH PLASMA PERFORMANCE BY ASSOCIATION WITH MICROPARTICLES OR SPONGES OF AUTO-CROSSLINKED HYALURONIC ACID** (artigo submetido ao periódico *Journal of Applied Polymer Science*).

**CAPÍTULO 7 – THE STRUCTURATION OF HIGH MOLECULAR WEIGHT HYALURONIC ACID IN MICROPARTICLES OR SPONGES IMPROVES ITS**

**PERFORMANCE WHEN ASSOCIATED TO PLATELET-RICH PLASMA** (artigo submetido ao periódico *Trends in Biomaterials & Artificial Organs*).

**CAPÍTULO 8 – STERILIZATION OF AUTO-CROSSLINKED HYALURONIC ACID STRUCTURED IN MICROPARTICLES OR SPONGES** (artigo submetido ao periódico *Biotechnology Letters*).

**ANEXO 1 – COMPOSIÇÃO E FORMULAÇÃO DE SCAFFOLDS DE ÁCIDO HIALURÔNICO E QUITOSANA PARA ASSOCIAÇÃO COM PLASMA RICO EM PLAQUETAS E SEUS USOS EM TERAPIA REGENERATIVA** somente *abstract*).

O último capítulo (Capítulo 9) apresenta as conclusões gerais comparativas entre os desempenhos dos *scaffolds* e as sugestões para trabalhos futuros.

## **1.2. Relevância do Trabalho**

O aumento da expectativa de vida, o mau funcionamento e/ ou a perda de tecidos causados por lesões ou por doenças, têm levado à redução da qualidade de vida de muitos pacientes e a um aumento do custo socioeconômico. Mesmo com o progresso da engenharia de tecidos e da medicina regenerativa, as terapias atuais ainda apresentam inúmeras limitações.

Assim, o desenvolvimento de matrizes tridimensionais (*scaffolds*) combinadas com diferentes tipos de células e moléculas bioativas com atividades específicas tem se tornado uma alternativa atrativa aos tratamentos atuais.

A obtenção de *scaffolds* biodegradáveis onde células específicas possam crescer e se multiplicar em uma estrutura similar aos tecidos é a base da engenharia de tecidos, que constitui um ramo da medicina regenerativa.

O principal objetivo de um *scaffold* é mimetizar a matriz extracelular nativa do tecido desejado, permitindo adesão, migração, proliferação, diferenciação e manutenção do fenótipo celular. Além disso, um *scaffold* deve ainda promover a vascularização e a migração de nutrientes, e possuir taxa de degradação e propriedades mecânicas adequadas para suportar a formação do novo tecido (Langer & Vacanti, 1993; Hutmacher, 2000; Lin *et al.*, 2009).

Várias matrizes têm sido empregadas para a proliferação e multiplicação de diferentes células progenitoras, incluindo as células-tronco mesenquimais. Entretanto, a

maioria destas matrizes não fornece o ambiente biológico adequado para que as células possam proliferar e se multiplicar de forma semelhante aos sistemas *in vivo*. O desenvolvimento de um *scaffold* para cultivo celular que seja mecanicamente estável, biocompatível e biodegradável e que possa atender a especificidade das células que compõem os diferentes tecidos representa ainda um grande desafio para a engenharia de tecidos (George *et al.*, 2008).

Os polímeros naturais são os materiais mais atraentes para a preparação de *scaffolds*, principalmente devido às suas semelhanças com a matriz extracelular, versatilidade química, bom desempenho biológico, e interações celulares específicas (Costa-Pinto *et al.*, 2011).

O plasma rico em plaquetas (PRP) é um concentrado de plaquetas autólogas e de outros componentes do plasma capaz de liberar fatores de crescimento (FCs) e citocinas utilizadas na regeneração de tecidos (Anitua *et al.*, 2012; Foster *et al.*, 2009). O PRP tem sido amplamente utilizado com sucesso na prática clínica da medicina regenerativa (Crane & Everts, 2008; Cole *et al.*, 2010).

Quando ativado com soro autólogo (ser) e CaCl<sub>2</sub>, o PRP produz a rede de fibrina com estrutura semelhante a um *gel* que suporta a proliferação e diferenciação celular, sendo assim um *scaffold* natural (Marx, 2004).

O PRP pode ser aplicado em feridas, na forma sólida ou injetável, ou pode ser utilizado como um suplemento em cirurgias, para promover hemostasia e acelerar a cicatrização através da liberação dos FCs e citocinas (Singh *et al.*, 2014).

Embora o PRP seja um *scaffold* natural eficaz, a liberação da maior parte dos FCs ocorre dentro da primeira hora após a ativação plaquetária. Além disso, a rede de fibrina não apresenta estabilidade mecânica adequada para suportar a formação do novo tecido (McCarrel & Fortier, 2009).

Assim, nossa hipótese é que a associação de PRP com ácido hialurônico (AH) e/ou quitosana (CHT), produza *scaffolds* compósitos com melhores propriedades físico-químicas, mecânicas e biológicas, que possam promover a liberação gradual dos FCs e estimular a proliferação e a diferenciação celular.

O AH é um polissacarídeo natural linear composto de repetidas unidades dissacarídicas de ácido D-glicurônico (GlcUA) e N-acetilglicosamina (GlcNAc) unidas alternadamente por ligações glicosídicas  $\beta$ -1,3 e  $\beta$ -1,4 (Ruhela *et al.*, 2006, Meyer & Palmer, 1934).

As funções e aplicações do AH na engenharia de tecidos e medicina regenerativa estão associadas basicamente às suas propriedades biológicas

favoráveis, características estruturais, e às possíveis modificações químicas do polímero, as quais determinam suas propriedades reológicas, de solubilidade, de hidratação e de reconhecimento celular específico.

Entretanto, a rápida degradação *in vivo* e as propriedades mecânicas inadequadas do AH exigem sua modificação e/ ou estabilização para aplicações na medicina em especial na medicina regenerativa.

Assim, para a preparação de um *scaffold* compósito de AH com prolongado tempo de residência *in vivo* e melhores propriedades mecânicas em relação ao AH nativo, foram utilizados o derivado autorreticulado ACP (*auto-crosslinked polymers*) completamente biocompatível e o derivado reticulado com 1,4-butanodiol diglicidil éter (HA-BDDE) que apresenta baixa citotoxicidade em relação a outros agentes reticulante disponíveis no mercado. O ACP foi preparado através de reação de autoesterificação organocatalisada na qual é formada uma ligação covalente entre os grupos hidroxílicos e carboxílicos de uma mesma cadeia e/ ou de cadeias diferentes de AH sem a adição de agentes reticulantes tóxicos (Bellini *et al.*, 2001). O HA-BDDE foi preparado por reação de eterificação dos grupos hidroxílicos do AH com o epóxido BDDE em meio alcalino (Malson & Lindqvist, 1986).

A quitosana é um polissacarídeo derivado da quitina (copolímeros  $\beta$ -(1 $\rightarrow$ 4)-2-amino 2-desoxi-D-glicose e  $\beta$ -(1 $\rightarrow$ 4)-2-acetamida 2-desoxi-D-glicose) encontrada nas carapaças de crustáceos marinhos e paredes celulares de alguns fungos (Muzzarelli, 1973; Berger *et al.*, 2004).

Propriedades como biodegradabilidade, biocompatibilidade, adesividade, capacidade de moldagem em diferentes formas e versatilidade de modificação química fazem com que a quitosana seja um biomaterial promissor para diversas aplicações na engenharia de tecidos e medicina regenerativa (Adekogbe & Ghanem, 2005; Agnihotri *et al.*, 2004).

A liofilização é a técnica mais empregada para a preparação de *scaffolds* de quitosana. Neste processo, as condições de congelamento induzem a separação de fase entre o sal de acetato de quitosana e a fase de cristal de gelo. A remoção de gelo por sublimação gera um material poroso, cujo tamanho e orientação dos poros podem ser controlados pela variação da temperatura e da taxa de congelamento. Na maioria dos casos, estes *scaffolds* podem conter acetato de quitosana que pode levar ao intumescimento e dissolução do *scaffold* em meio aquoso neutro. Neste caso também é necessária modificação ou estabilização, realizadas normalmente por reidratação ou reticulação (Shen *et al.*, 2000) com hidróxido de sódio (Madihally & Matthew, 1999;

Manjubala *et al.*, 2006), tripolifosfato de sódio (TPP) (Seol *et al.*, 2004; Lee *et al.*, 2000) e/ou série de etanol (Nwe *et al.*, 2009, Reis *et al.*, 2008).

Embora existam inúmeros trabalhos na literatura utilizando *scaffolds* de AH e CHT, combinados ou não, para a regeneração de diferentes tecidos, estudos avaliando a performance *in vitro* destes *scaffolds* combinados ao PRP ainda são escassos.

Além disso, os poucos trabalhos existentes na literatura enfatizam as aplicações *in vitro* ou *in vivo* desses *scaffolds*, ou simplesmente apresentam as suas aplicações clínicas ou a cinética de liberação dos FCs do PRP, sem no entanto, estudar a relação estrutura – função ou a combinação dos vértices do triângulo de proliferação celular: *scaffolds*, células e moléculas bioativas (Crane & Everts, 2008).

Sendo assim, este trabalho se diferencia dos demais da literatura, pois além da extensa caracterização físico-química e mecânica dos *scaffolds*, ele correlaciona essas propriedades com as capacidades: condutiva dos *scaffolds*, indutiva do PRP e gênica das células tronco mesenquimais derivadas de tecido adiposo humano (h-AdMSCs) baseado no triângulo de proliferação celular.

Dessa forma, neste trabalho foram preparados e caracterizados *scaffolds* de AH e/ou CHT estruturados em micropartículas ou esponjas, para atender os requisitos de formulações injetáveis ou sólidas, respectivamente. Estes *scaffolds* foram combinados com PRP ativado na forma de *scaffolds* compósitos e avaliados *in vitro* quanto a cinética de liberação de fatores de crescimento (fator de crescimento derivado de plaquetas (PDGF-AB) e fator de crescimento transformador  $\beta$ 1 (TGF- $\beta$ 1)), proliferação de h-AdMSCs e diferenciação osteogênica através do marcador fosfatase alcalina (ALP).

### 1.3. Objetivo

O presente trabalho teve por objetivo estudar o desempenho *in vitro* do plasma rico em plaquetas ativado (aP-PRP) associado ao ácido hialurônico e/ou quitosana como um *scaffold* compósito para a proliferação e diferenciação osteogênica de células tronco mesenquimais derivadas de tecido adiposo humano (h-AdMSCs).

Para atingir o objetivo mencionado, foram realizadas as seguintes etapas:

- Preparação e caracterização do PRP;
- Preparação e caracterização de *scaffolds* porosos sólidos (esponjas) de quitosana não estabilizados (PCHTs), variando a concentração de CHT e as condições de congelamento;

- Preparação e caracterização de *scaffolds* porosos sólidos (esponjas) de quitosana estabilizados (SPCHTs);
- Preparação e caracterização de *scaffolds* injetáveis compostos de micropartículas de quitosana reticulada com tripolifosfato de sódio (iCHT-TPPs) em diferentes razões mássicas;
- Preparação e caracterização de *scaffolds* de ácido hialurônico autorreticulado (ACPs) estruturados em micropartículas ou em esponjas.
- Preparação e caracterização de *scaffolds* de ácido hialurônico reticulado com 1,4-butanodiol diglicidil éter (HA-BDDE) estruturados em micropartículas ou em esponjas.
- Preparação e caracterização de *scaffolds* de ACP e CHT (PECs) em diferentes razões mássicas, e estruturados em micropartículas ou em esponjas.
- Avaliação de diferentes processos de esterilização na estabilidade de *scaffolds* de ácido hialurônico autorreticulado (ACPs) estruturados em micropartículas e em esponjas.
- Avaliação da citotoxicidade dos *scaffolds*;
- Preparação de *scaffolds* compósitos de aP-PRP e *scaffolds* de ácido hialurônico e/ou quitosana;
- Avaliação da cinética de liberação de fatores de crescimento nos *scaffolds* compósitos;
- Avaliação *in vitro* da performance biológica dos *scaffolds* compósitos quanto a proliferação e diferenciação osteogênica de h-AdMSCs.

# CAPÍTULO 2 – REVISÃO BIBLIOGRÁFICA

---

## 2.1. Engenharia de Tecidos e Medicina Regenerativa

O termo medicina regenerativa vem sendo utilizado muitas vezes como sinônimo de engenharia de tecidos, embora a medicina regenerativa frequentemente implique na utilização de células tronco como fonte de células (Berthiaume *et al.*, 2011).

Segundo Greenwood *et al.* (2006), “medicina regenerativa é um campo interdisciplinar (Figura 1) de pesquisa e aplicações clínicas, focado no reparo, substituição ou regeneração de células, tecidos ou órgãos visando restaurar funções prejudicadas por defeitos congênitos, doenças, traumas e envelhecimento e que utiliza a combinação de várias abordagens tecnológicas que incluem a utilização de moléculas solúveis, terapia gênica, terapia com células-tronco e progenitoras, engenharia de tecidos e reprogramação de células e de tecidos”.

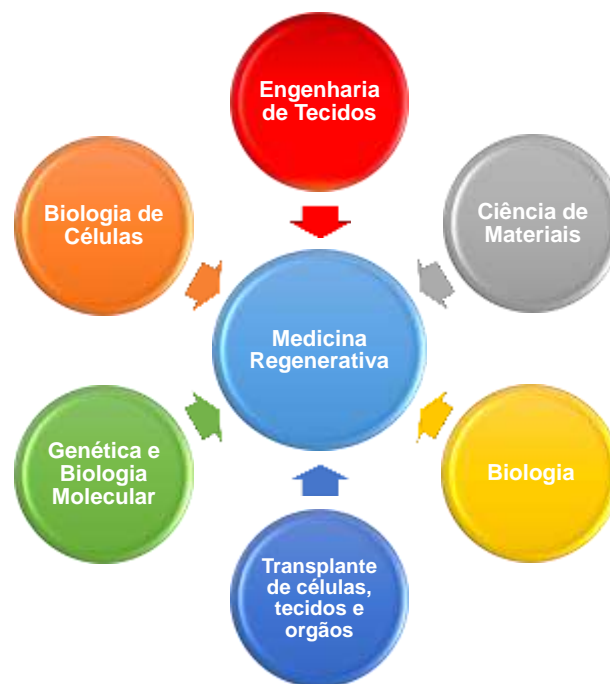


**Figura 1.** Disciplinas que contribuem atualmente na medicina regenerativa (Daar & Greenwood, 2007).

Por outro lado, “engenharia de tecidos é definida como um campo interdisciplinar

que aplica os princípios da engenharia e de ciências da vida para o desenvolvimento de substitutos biológicos que restauram, mantêm ou melhoram a função do tecido ou de um conjunto de órgãos” (Langer & Vacanti, 1993). Seu objetivo é superar as limitações dos tratamentos convencionais com base em transplantes de órgãos.

A medicina regenerativa e a engenharia de tecidos têm se tornado campos de pesquisa promissores e importantes, uma vez que podem oferecer alternativas viáveis e menos invasivas para o reparo e regeneração de órgãos e tecidos (Vindigni *et al.*, 2009).

A engenharia de tecidos é um campo relativamente novo dentro da medicina regenerativa, que utiliza como base o triângulo de proliferação celular proposto por Crane & Everts (2008) (Figura 2), o qual é composto pelas capacidades indutiva dos fatores de crescimento, condutiva dos *scaffolds* e gênica das células tronco ou progenitoras.

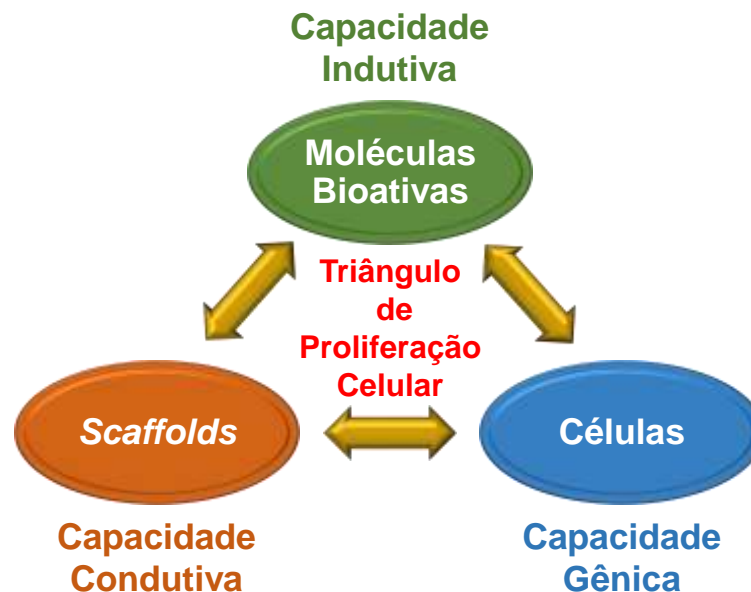


**Figura 2.** Triângulo da proliferação celular (Adaptado de Barnett & Pomeroy, 2007; Crane & Everts, 2008).

## 2.2. Plasma Rico em Plaquetas

### 2.2.1. Definições

Plasma rico em plaquetas (PRP) é um produto autólogo, preparado a partir do



sangue total, composto por um concentrado de plaquetas, leucócitos e proteínas, disperso em uma pequena fração de plasma (Marx *et al.*, 1998; Marx, 2004).

Plaquetas são fragmentos citoplasmáticos anucleados presentes no sangue e produzidos na medula óssea a partir dos megacariócitos. São os menores componentes do sangue, e apresentam formato irregular e diâmetro de 2-3  $\mu\text{m}$ . As plaquetas contêm um grande número de proteínas, citocinas e outros fatores bioativos, tais como fatores de crescimento, que iniciam e regulam aspectos básicos da cicatrização de tecidos.

Leucócitos são as células brancas do sangue, compostos de linfócitos, granulócitos e agranulócitos.

Plasma é a porção fluida do sangue que contém fatores de coagulação e outras proteínas e íons.

A contagem normal de plaquetas no sangue é de 150.000 a 400.000 plaquetas/ $\mu\text{L}$  (Foster *et al.*, 2009, Engebretsen *et al.*, 2010).

O plasma rico em plaquetas (PRP) contém uma concentração de plaquetas de pelo menos 1.000.000 plaquetas/ $\mu\text{L}$  em 5 mL de plasma e está associado com a cicatrização. O PRP contém de 1,5 a 7 vezes a concentração de FCs do sangue total e é normalmente obtido por centrifugação diferencial (Foster *et al.*, 2009).

A liberação de fatores de crescimento ocorre após o processo de degranulação das plaquetas. As plaquetas são o primeiro tipo celular recrutado para o local da lesão e são responsáveis pela ativação da resposta inflamatória inicial do processo de cicatrização (Cole *et al.*, 2010).

Fatores de crescimento (FCs) são mediadores biológicos naturais que exercem vários efeitos sobre os processos de reparo e de regeneração. São polipeptídios capazes de regular diversos eventos celulares que incluem síntese de DNA, quimiotaxia, diferenciação e síntese de matriz extracelular.

No PRP estes fatores de crescimento incluem 3 isômeros do fator de crescimento derivado de plaquetas (PDGF- $\alpha\alpha$ , PDGF- $\beta\beta$  e PDGF- $\alpha\beta$ ), 2 isômeros do fator de crescimento transformador  $\beta$  (TGF- $\beta$ 1 e TGF- $\beta$ 2), o fator de crescimento endotelial vascular (VEGF), o fator de crescimento semelhante à insulina (IGF), o fator de crescimento de fibroblastos básico (bFGF) e o fator de crescimento epitelial (EGF) (Cole *et al.*, 2010; Engebretsen *et al.*, 2010).

Várias técnicas para a preparação do PRP têm sido utilizadas gerando diferentes produtos com diferentes propriedades biológicas e aplicações.

A classificação mais atual (Figura 3) é a estabelecida por Ehrenfest *et al.* (2009)

de acordo com o conteúdo de leucócitos e de fibrina: plasma rico em plaquetas puro (P-PRP): plasma rico em plaquetas e leucócitos (L-PRP), fibrina rica em plaquetas pura (P-PRF) e fibrina rica em plaquetas e leucócitos (L-PRF).

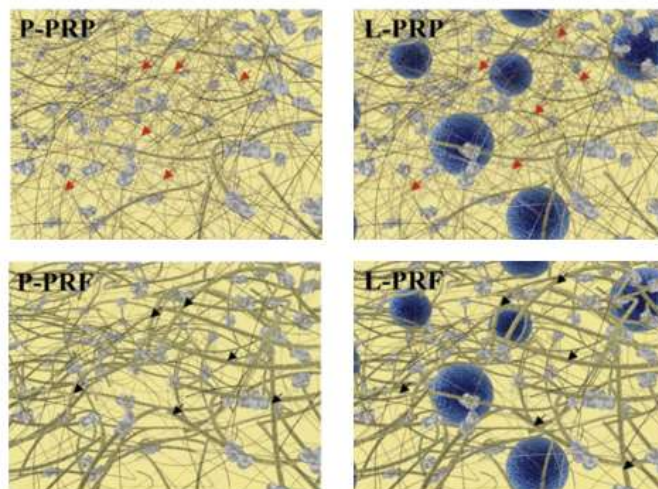


**Figura 3.** Ilustração esquemática da arquitetura da matriz e das células das quatro categorias de concentrados de plaquetas classificados segundo Ehrenfest *et al.* (2009). P-PRP=plasma rico em plaquetas puro; L-PRP=plasma rico em plaquetas e leucócitos; P-PRF=fibrina rica em plaquetas pura e L-PRF=fibrina rica em plaquetas e leucócitos.

### 2.2.2. PRP na regeneração de tecidos

O plasma rico em plaquetas é uma terapia simples, eficiente e minimamente invasiva para a obtenção de FCs autólogos. Sendo uma preparação autóloga, o PRP tem a vantagem de evitar a transmissão de doenças e o aparecimento de reações imunogênicas.

Mariani *et al.* (2014) demonstraram que o PRP pode ser utilizado na inibição do crescimento bacteriano contra diferentes patógenos, fornecendo proteção adicional contra possíveis contaminações bacterianas durante intervenções cirúrgicas.

Na regeneração de tecidos, o PRP atua como um selante do tecido e como um carreador de fatores de crescimento, onde as plaquetas iniciam a regeneração do tecido através da liberação local dos FCs via degranulação de seus  $\alpha$ -grânulos.

As plaquetas no PRP são transportadas através de um coágulo, que contém moléculas de adesão celular incluindo fibronectina, fibrina e vitronectina. Na cicatrização de feridas, este coágulo age como uma matriz condutora ou *scaffold* natural sobre o qual as células aderem e iniciam o processo de cicatrização.

As plaquetas atuam no processo de hemostasia, cicatrização de feridas e re-epitelização. Elas liberam diversos FCs que estimulam a angiogênese, promovendo crescimento vascular e proliferação de fibroblastos, que por sua vez proporcionam um aumento na síntese de colágeno (Marx, 2004). Além disso, os FCs promovem a proliferação celular e influenciam a diferenciação atuando diretamente na reparação e regeneração de tecidos (Nguyen *et al.*, 2011)

Nos estágios iniciais do processo de cicatrização (Figura 4), as plaquetas são ativadas na cascata de coagulação via colágeno endógeno, e os fatores de crescimento e as citocinas são liberados por estas plaquetas ativadas para auxiliar na cicatrização. A sequência de eventos que conduz à formação do novo tecido (quimiotaxia, migração, proliferação e diferenciação celular) é regulada pelos fatores de crescimento, muitos dos quais estão presentes no PRP (Tsay *et al.*, 2005).

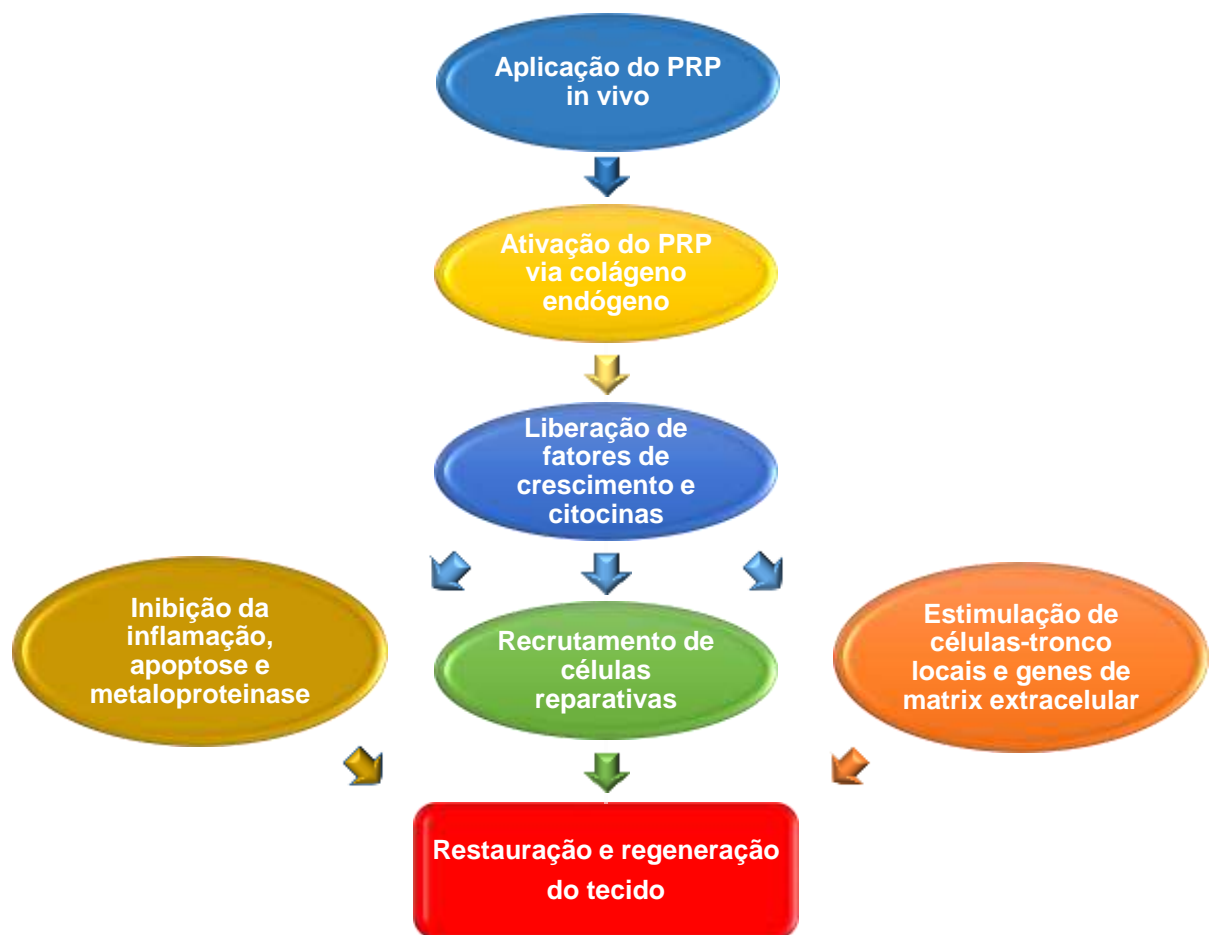


**Figura 4.** Mecanismo de ação do PRP (Mishra *et al.*, 2012).

O processo de cicatrização, na qual os fatores de crescimento participam,

envolve três fases interpostas: (1) a fase inflamatória, (2) a fase de proliferação e (3) a fase de maturação e/ ou de remodelação.

A fase inicial ocorre imediatamente após a lesão e envolve hemostasia e recrutamento de mediadores inflamatórios com duração de aproximadamente 1 semana. A lesão tecidual ativa a ciclooxigenase-2 e leva à vasodilatação. Os FCs atraem os macrófagos e fibroblastos. A fase de proliferação permanece durante as 2 semanas seguintes com formação de matriz extracelular, granulação, contração e reepitelização. A fase de remodelagem continua até que a produção de colágeno e do tecido de cicatrização seja finalizada. Esta fase pode durar até 1 ano e nela o colágeno tipo I substitui os proteoglicanos e a fibronectina para formar uma matriz mais forte com maior resistência à tração (Nguyen *et al.*, 2011).

Embora os mecanismos envolvidos na utilização do PRP ainda não estejam completamente elucidados, sua fácil aplicação na prática clínica e seu possível resultado benéfico tornam o PRP uma promissora ferramenta para a área médica (Alsousou *et al.*, 2009).

O plasma rico em plaquetas foi utilizado pela primeira vez por Ferrari *et al.* (1987) em cirurgia cardíaca com coração aberto como um componente de transfusão autólogo. Inicialmente, o PRP foi utilizado principalmente em cirurgias orais para promover a cicatrização do tecido e integração do implante, e controlar hemorragias (Anitua, 1999; Marx *et al.*, 1998). Subsequentemente, também foi empregado em outras cirurgias incluindo cirurgias nos ombros (Everts *et al.*, 2008), quadris (Everts *et al.*, 2007), procedimentos nas articulações dos joelhos (Sánchez *et al.*, 2008; Ishida *et al.*, 2007), reconstrução de ligamentos (Radice *et al.*, 2010) e cicatrização óssea (Kawasumi *et al.*, 2008).

Mais recentemente, o PRP com suas variantes tem sido empregado na forma injetável visando a cicatrização de diversos tecidos incluindo pele (Judith *et al.*, 2010; Judith *et al.*, 2012), músculos (van Ark *et al.*, 2013), tendões (de Vos *et al.*, 2010; Kaux & Crielaard, 2013), cartilagem (Kon *et al.*, 2010; Kon *et al.*, 2011) e osso (Jia *et al.*, 2011; Jiang *et al.*, 2012).

## **2.3. Scaffolds**

### **2.3.1. Definições**

*Scaffolds* são matrizes tridimensionais temporárias que funcionam como a matriz extracelular, organizando as células tridimensionalmente e estimulando o crescimento e

a formação do tecido desejado (Hutmacher, 2000).

Os *scaffolds* são divididos em fluídos (injetáveis) e sólidos (convencionais), e podem ser fabricados em diversos formatos, os quais dependem da aplicação desejada e do processo de fabricação utilizado: esponjas (Amaral *et al.*, 2006; Manferdini *et al.*, 2010), hidrogéis (Bhattacharyya *et al.*, 2008, Kim *et al.*, 2010), fibras (Yamane *et al.*, 2005, Iwasaki *et al.*, 2011), membranas (Mathews *et al.*, 2011; Mucha *et al.*, 2012) micro e nano partículas (Cruz *et al.*, 2008; Custódio *et al.*, 2014), tubos (Venkatesan *et al.*, 2012) e esferas (Shu & Zhu, 2002).

Vários processos têm sido desenvolvidos para fabricar diferentes tipos de *scaffolds* entre eles destacam-se: evaporação de solvente/ lixiviação de partículas (*solvent casting/ particulate leaching*) (Mikos *et al.*, 1994); espuma de gás (*gas foaming*) (Nam *et al.*, 2000), liofilização (*freeze-drying*) (Madihally and Mathew, 1999); eletrofiação (*electrospinning*) (Huang *et al.*, 2003), prototipagem rápida (*rapid prototyping*) (Peltola *et al.*, 2008) e separação de fases termicamente induzida (*thermally induced phase separation*) (Pavia *et al.*, 2008).

A técnica de processamento escolhida deve obedecer, em termos gerais, aos seguintes critérios (Boccaccini *et al.*, 2002):

- O processo ou produção não deve afetar as propriedades dos materiais, isto é, a sua biocompatibilidade ou propriedades físico-químicas;
- A técnica deve permitir um controle da porosidade, tamanho de poros, sua distribuição e interconectividade;
- Grupos diferentes de matrizes devem exibir variações mínimas nas suas propriedades, quando processadas nas mesmas condições.

As principais características que diferenciam as várias técnicas são a aplicação desejada e/ ou o uso de solventes; calor ou pressão; ou a utilização de aditivos responsáveis pela geração dos poros (Agrawal & Ray, 2001).

### 2.3.2. *Scaffolds* na regeneração de tecidos

Na engenharia de tecidos e medicina regenerativa, os *scaffolds* representam a capacidade condutiva e podem ser utilizados para transportar as células antes da sua implantação *in vivo*, ou servirem apenas como um material bioativo atraindo as células do tecido onde é implantado.

Além de permitir a adesão e a migração celular dentro do suporte e promover a proliferação e a diferenciação celular, o *scaffold* deve fornecer um ambiente no qual as células possam manter seu fenótipo e sintetizar as proteínas e/ou outras moléculas

necessárias (Monteiro, 2008).

### 2.3.3. Propriedades requeridas dos *scaffolds*

*Scaffolds* utilizados em engenharia de tecidos e medicina regenerativa devem apresentar propriedades biológicas e físicas compatíveis com as condições fisiológicas *in vitro* e *in vivo*. Como mencionado anteriormente, a principal função dos *scaffolds* é proporcionar um suporte temporário adequado que permita os processos celulares necessários para a regeneração do tecido. Para isso, vários requisitos, dependentes do tipo de célula utilizada e do tecido a ser regenerado, devem ser considerados no desenvolvimento de *scaffolds* (Sachlos & Czernuszka, 2003). Os *scaffolds* devem:

- Possuir estrutura tridimensional;
- Possuir poros interconectados e de tamanho apropriado para favorecer a integridade e a vascularização do tecido;
- Possuir porosidade que proporcione elevada área superficial para interação célula-*scaffold*;
- Ser biodegradável e biocompatível;
- Não apresentar nenhum componente ou subproduto de sua degradação que provoque reações inflamatórias ou tóxicas;
- Apresentar superfície química que favoreça a adesão, proliferação e diferenciação das células;
- Apresentar propriedades mecânicas adequadas para implantação e manipulação;
- Ter bioatividade satisfatória para explorar o processo de reparação natural do tecido;
- Ser facilmente fabricado em uma variedade de formas e tamanhos.

Além dos requisitos necessários para a preparação dos *scaffolds* sólidos, os *scaffolds* fluidos devem apresentar as seguintes propriedades (Hou *et al.*, 2004):

- Injetabilidade;
- Solidificação sob condições brandas;
- Coesividade;
- Força mecânica e resistência a forças *in situ*;
- Possibilidade de incorporação de moléculas bioativas.

Do ponto de vista clínico, a utilização de *scaffolds* fluidos é muito interessante, pois minimiza o desconforto do paciente, o risco de infecção, a formação de cicatrizes e o custo do tratamento já que não requer intervenção cirúrgica para sua implantação

(Hou *et al.*, 2004).

O material fluido pode preencher de forma homogênea o defeito ou ponto de reparo, pode incorporar vários agentes terapêuticos, e, finalmente, não exige procedimento cirúrgico invasivo para sua implantação (Gutowska *et al.*, 2001).

Além disso, a alta hidratação destes materiais mimetiza a matriz extracelular sendo, portanto, ideais para a proliferação e diferenciação celular.

#### 2.3.4. Materiais utilizados na fabricação de *scaffolds*

A seleção dos materiais para a produção dos *scaffolds* é uma das etapas mais importantes e vários materiais têm sido propostos para sua fabricação, entre eles estão os metais, os polímeros de origem natural ou de origem sintética, os materiais cerâmicos e os compósitos.

Embora os materiais metálicos e cerâmicos tenham contribuído para muitos avanços na área médica, principalmente na substituição de tecidos ortopédicos, eles apresentam duas importantes desvantagens para a aplicação em engenharia de tecidos: não são biodegradáveis e a processabilidade destes materiais é bastante limitada (Liu & Ma, 2004).

Os polímeros biodegradáveis são considerados os materiais ideais para a produção destas matrizes e podem ser divididos em naturais e sintéticos.

Os polímeros biodegradáveis naturais podem ser obtidos de fontes animais ou vegetais. São idênticos ou semelhantes às substâncias já encontradas no corpo e, portanto, a probabilidade de toxicidade ou de estimular uma reação inflamatória crônica é reduzida. Estes materiais também têm, geralmente, atividade biológica inerente, proporcionando assim sinalização para células sem a necessidade de adição de fatores exógenos. Eles também são susceptíveis a enzimas presentes no organismo e, portanto, são inerentemente biodegradáveis, sendo possível controlar suas taxas de degradação através de modificações químicas.

No entanto, são frequentemente imunogênicos e sua manipulação e/ ou processamento são muito mais difíceis que a de polímeros sintéticos devido a sua complexidade.

Além disso, o processo de extração desses materiais a partir de um tecido muitas vezes altera sua estrutura natural. Outra desvantagem é a variabilidade natural dos materiais derivados de fontes animais (Mann, 2003).

Assim, a escolha do material para a produção dos *scaffolds* deve levar em consideração as vantagens e desvantagens desses materiais bem como a aplicação

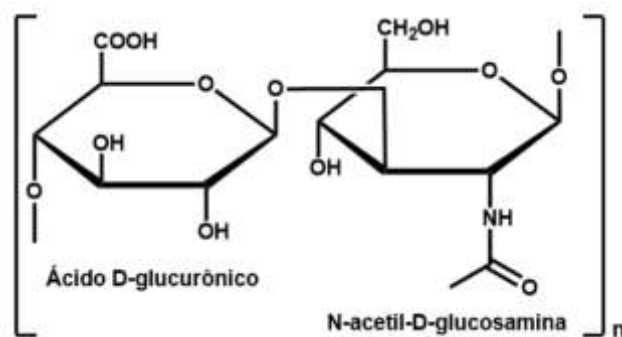
pretendida.

A seguir são apresentadas as principais características dos biomateriais, ácido hialurônico e quitosana, utilizados neste trabalho para preparar os *scaffolds* compósitos estudados.

#### 2.3.4.1. Ácido hialurônico (AH)

O AH é um biopolímero viscoelástico linear, composto de repetidas unidades dissacarídicas de ácido D-glicurônico (GlcUA) e N-acetilglicosamina (GlcNAc) unidas alternadamente por ligações glicosídicas  $\beta$ -1,3 e  $\beta$ -1,4 (Figura 5), encontrado naturalmente nos tecidos conjuntivos de mamíferos (Kuo *et al.*, 2000) e produzido por bactérias do gênero *Streptococcus* (Pires *et al.*, 2010).

Devido a suas propriedades físicas, o AH tem funções no preenchimento de espaços, na lubrificação, na absorção de choque e na exclusão de proteínas. Além disso, suas propriedades bioquímicas incluem a modulação da resposta inflamatória das células, a interação com os proteoglicanos da matriz extracelular e a captura de radicais livres (Monheit & Coleman, 2006). Estudos também mostraram que o AH ligado a proteínas e a receptores específicos desempenha importante papel na embriogênese, na transdução de sinais, na motilidade celular e está ainda associado ao câncer e a metástase (Kogan *et al.*, 2007).



n = número de repetições de unidades dissacarídicas

**Figura 5.** Estrutura molecular do ácido hialurônico.

Sendo assim, o ácido hialurônico tem sido amplamente aplicado nas áreas médicas e cosméticas, principalmente em cirurgias oftálmicas (Balazs, 1983); em terapias para o controle da artrite (Balazs & Denlinger, 1993), implante de próteses; cicatrização de feridas; prevenção de adesão de tecidos (Garg & Hales, 2004) e preenchimento dérmico (Holmström & Ricici, 1967). Além disso, devido a suas



propriedades físico-químicas e funções biológicas, o ácido hialurônico e seus derivados modificados também têm sido amplamente utilizados na administração de fármacos (Kim *et al.*, 2005; Hahn *et al.*, 2006) e na engenharia de tecidos (Ohri *et al.*, 2004; West *et al.*, 1985).

As funções e aplicações do ácido hialurônico (AH) estão associadas basicamente às suas características estruturais e às possíveis modificações químicas do polímero, as quais determinam suas propriedades reológicas, de solubilidade, de hidratação e de reconhecimento celular específico.

O AH é não-imunogênico, biocompatível e biodegradável, e por isso, possui diversas aplicações como biomateriais. Entretanto, sua aplicação na preparação de *scaffolds* requer prévia modificação do polímero visando melhorar suas propriedades mecânicas e químicas, e principalmente aumentar seu tempo de residência nos tecidos (biodisponibilidade). Como o AH natural apresenta um tempo de residência de 1 a 2 dias e a maioria das aplicações médicas desse biopolímero requer um tempo de residência maior, modificações químicas do AH tem se tornado essenciais na preparação de produtos para aplicações médicas e cosméticas (Romagnoli & Belmontesi, 2008, Monheit & Coleman, 2006).

A molécula de AH apresenta quatro grupos funcionais que podem ser modificados quimicamente: carboxílico, hidroxílico, acetamida e o terminal reduzido do polímero (Figura 6). Além disso, as ligações glicosídicas também podem ser hidrolisadas para formar cadeias menores ou oligossacarídeos.

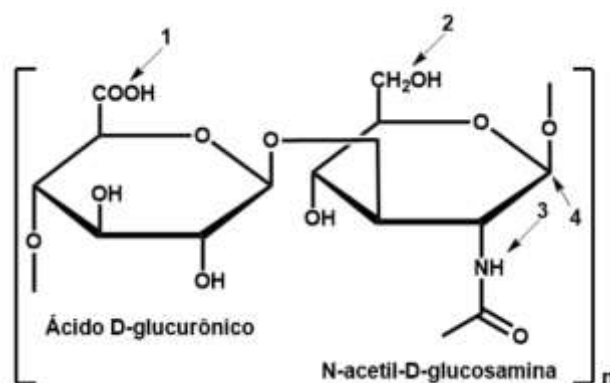


**Figura 6.** Grupos de modificação química da molécula de AH: (1) carboxílico, (2) hidroxílico, (3) acetamida, (4) Terminal Reduzido do Polímero (Adaptado de Garg & Hales, 2004).

Além das modificações do AH através da adição de moléculas em sua cadeia (conjugação), o AH pode também ser modificado através de reticulação.

A reticulação do AH fornece moléculas maiores e mais estáveis, com biocompatibilidade similar à do AH não modificado. O polímero pode ser reticulado através de ligações covalentes irreversíveis (reticulação química), ou através da formação de várias ligações iônicas reversíveis (reticulação física).

A reticulação pode ser realizada através da exposição direta do AH ao agente reticulante, ou através da reação de um derivado de AH altamente reativo primariamente sintetizado com o agente reticulante em uma reação secundária.

A maioria dos métodos reportados na literatura para reticular o AH emprega reagentes polifuncionais tais como bis-epóxidos, carbodiimidas, dihidrazidas e divinil sulfona (Band, 1998). Entretanto, os agentes reticulantes mais comuns normalmente apresentam elevada citotoxicidade, a qual limita sua aplicação nas áreas médica e cosmética.

A seguir serão discutidas brevemente as reações de modificações químicas do AH utilizadas neste trabalho.

- *Modificação do grupo carboxílico por amidação com iodeto de 2-cloro-1-metilpiridínio (CMPI).* Magnani *et al.* (2000) descreveram a reação de amidação usando CMPI como o agente de ativação dos grupos carboxílicos do AH. Esta reação é normalmente realizada em dimetilformamida (DMF) ou dimetilsulfóxido (DMSO), um solvente orgânico anidro, para minimizar a hidrólise do CMPI. Inicialmente, o hialuronato de sódio é convertido no sal de tetrabutylamônio (TBA) para permitir a sua solubilização no solvente orgânico. Para formar as ligações cruzadas entre as cadeias de AH, CMPI reage com o grupo carboxílico do HA, forma um intermediário piridíneo e libera o íon cloreto, o qual é neutralizado pelo tetrabutylamônio. Trietilamina neutraliza o íon iodeto liberado (Figura 7). Quando nenhuma amina é adicionada ao meio reacional, a esterificação ocorre entre o intermediário AH-CMPI ativado e os grupos hidroxílicos de uma mesma cadeia ou de cadeias diferentes de AH, formando uma ligação éster entre as cadeias de AH. Neste caso, temos uma reação de autoesterificação na qual é formado o derivado autorreticulado de ácido hialurônico (ACP = *auto-crosslinked polymers*) (Della Valle, 1994; Della Valle & Romeo, 1989). Os grupos carboxílicos do AH ativados por CMPI também podem reagir com um grupo carboxílico não ativado, porém o anidrido resultante é instável e subsequentemente reage com um grupo hidroxílico formando a mesma ligação éster. A desvantagem desse método é a necessidade de uma etapa adicional para a preparação do TBA-AH e de ter que ser realizado em um solvente orgânico que requer um processo de purificação longo.

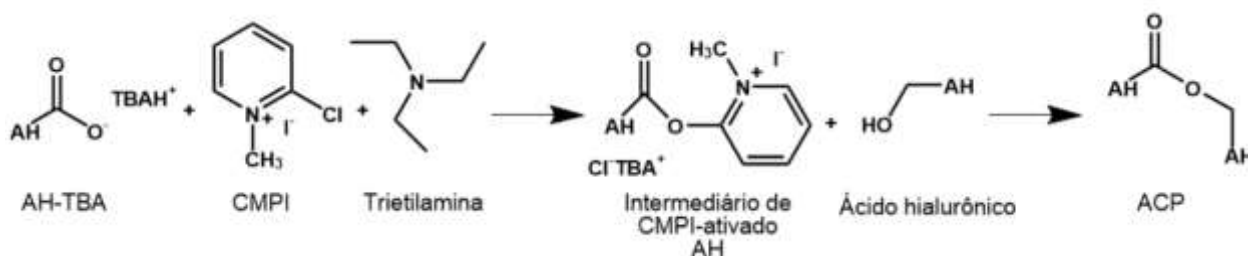


**Figura 7.** Preparação de ACP por autoesterificação organocatalisada usando o intermediário ativado AH-CMPI (Schanté *et al.*, 2011).

Na reação de autoesterificação organocatalisada é formada uma ligação covalente entre os grupos hidroxílicos e carboxílicos de uma mesma cadeia e/ ou de cadeias diferentes de AH, formando assim lactonas ou ligações ésteres intermoleculares. Nos derivados ACP, os grupos carboxílicos do AH estão completamente ou parcialmente esterificados. No caso de ésteres parcialmente esterificados, os grupos carboxílicos remanescentes podem ainda ser totalmente ou parcialmente esterificados com álcoois mono- ou polivalentes, formando assim grupos ésteres externos; podem permanecer livres e/ou serem salinizados com bases metálicas ou orgânicas (Bellini *et al.*, 2001).

A reticulação por autoesterificação da molécula de AH é uma excelente alternativa para preparação de derivados reticulados completamente biocompatíveis e que apresentam prolongado tempo de residência *in vivo* e/ ou melhores propriedades mecânicas em relação ao AH nativo.

Embora sejam utilizados compostos orgânicos como os solventes e os catalisadores da reação, as etapas de lavagem do produto final mantêm sua biocompatibilidade (Bellini *et al.*, 2001, Collins & Birkinshaw, 2007).

A principal vantagem da formação das ligações ésteres sem a adição de agentes reticulantes tóxicos em relação a outros métodos de reticulação é ausência de moléculas estranhas inseridas nas cadeias de AH. Sendo assim, durante o processo de degradação do ACP *in vivo*, somente AH nativo é gerado.

Além disso, o ACP pode ser preparado com vários graus de reticulação, os quais permitem adequar suas propriedades para inúmeras aplicações.

- *Modificação do grupo hidroxílico por formação de ligações éter utilizando epóxidos.* Malson & Lindqvist (1986) patentearam a reticulação de AH utilizando 1,4-butanodiol-diglicidil éter (BDDE) em uma solução 0.25 M NaOH. A reação consiste da abertura do anel epóxido para formar ligações éter com os grupos hidroxílicos do AH

(Figura 8). Quando AH é submetido a valores de pH ( $\text{pH} > 13$ ) acima do  $\text{pK}_a$  dos grupos hidroxílicos do AH ( $\text{pK}_a \sim 10$ ), estes são desprotonados e se tornam mais nucleofílicos que os grupos carboxílicos desprotonados. Os epóxidos, portanto, reagem preferencialmente com os grupos hidroxílicos para formar ligações éter.

No entanto, quando o pH é menor do que o valor de  $\text{pK}_a$  do grupo hidroxílico, uma quantidade menor de grupos hidroxílicos é desprotonada e os grupos carboxílicos aniônicos tornam-se predominantes, promovendo assim a formação da ligação éster. Isto tem sido demonstrado por De Belder & Malson (1986), que realizaram a reticulação de AH com BDDE em condições ácidas ( $\text{pH} 2-4,5$ ).

Atualmente, BDDE é usado na preparação da maioria dos hidrogéis de AH reticulados disponíveis no mercado. Além da síntese fácil, a degradação dos produtos de AH-BDDE não demonstram citotoxicidade e os compostos epóxidos são hidrolisados em dióis simples (Nishi *et al.*, 1995).

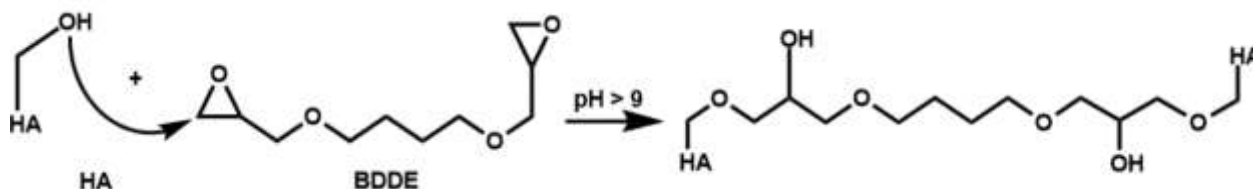


**Figura 8.** Ácido hialurônico reticulado com BDDE em meio alcalino (Malson & Lindqvist, 1986).

#### 2.3.4.2. Quitosana

Quitosana (CHT) é um polissacarídeo derivado da quitina (copolímeros  $\beta$ -(1 $\rightarrow$ 4)-2-amino 2-desoxi-D-glicose e  $\beta$ -(1 $\rightarrow$ 4)-2-acetamida 2-desoxi-D-glicose), encontrada em abundância na natureza, principalmente na carapaça de crustáceos. A quitosana pode ser obtida a partir da quitina por meio de desacetilação alcalina, podendo também estar naturalmente presente em alguns fungos pertencentes aos gêneros *Mucor* e *Zygomycetes* (Silva *et al.*, 2006).

A Figura 9 representa a estrutura química parcial da quitosana.

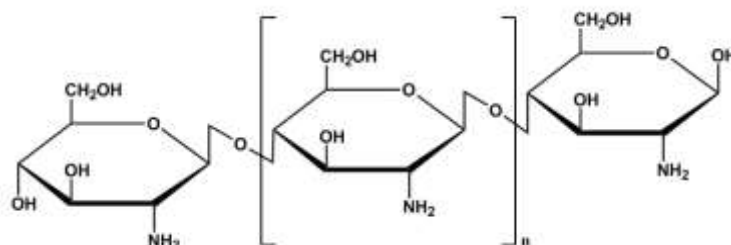


**Figura 9.** Estrutura molecular da quitosana.

Os principais parâmetros que influenciam as características da quitosana são a sua massa molar (MM) e seu grau de desacetilação (GD), o qual representa o conteúdo de unidades desacetiladas. Em geral, o produto N-desacetilado da quitina só passa a ser considerado quitosana quando o GD se torna igual ou superior a 60%, percentagem a partir da qual o biopolímero se torna solúvel em soluções ácidas diluídas. O grau de desacetilação é um parâmetro muito importante, pois é capaz de influenciar as características químicas, físicas e biológicas do biopolímero.

Do ponto de vista químico, o GD da quitosana exerce influência sobre algumas de suas propriedades, tais como hidrofiliabilidade, capacidade de reticulação na presença de determinados agentes reticulantes, solubilidade e viscosidade (Gonsalves *et al.*, 2011).

Na sua forma cristalina, a quitosana é normalmente insolúvel em solução aquosa acima de pH 7, no entanto, em ácidos diluídos (pH < 6.0), os grupos amino livres protonados da glicosamina facilitam a solubilidade da molécula (Madhally & Matthew, 1999).

Nos últimos anos, pesquisadores das áreas médica e farmacêutica têm demonstrado grande interesse na utilização de quitosana devido principalmente a suas propriedades intrínsecas. A quitosana é um polímero biocompatível, devido à sua metabolização por certas enzimas humanas como a lisozima, sendo considerado, portanto, biodegradável (Nordtveit *et al.*, 1996; Muzzarelli, 1997). Além disso, devido à sua carga positiva em pH fisiológico, a quitosana é também bioadesiva (He *et al.*, 1998; Calvo *et al.*, 1997; Bertram & Bodmeier, 2006), o que aumenta sua retenção no local da aplicação. A quitosana também promove a cicatrização de feridas (Antonov *et al.*, 2008; Dai *et al.*, 2011) e tem efeito antimicrobiano (Muzzarelli *et al.*, 1990; Liu *et al.*, 2001; Li *et al.*, 2013). Finalmente, a quitina é muito abundante, e a produção da quitosana é de baixo custo e ecologicamente interessante (Berger *et al.*, 2004).

Além destas propriedades, estudos recentes mostraram que a quitosana e seus derivados são candidatos promissores a *scaffolds* principalmente devido à facilidade de

modificação química, possibilidade de ser moldada em várias formas (membranas, géis, esferas, esponjas, micro- e nanopartículas) e à sua elevada afinidade às macromoléculas *in vivo*.

A versatilidade química da quitosana resulta principalmente da presença dos grupos amino em sua estrutura. Apesar da maioria das modificações químicas da quitosana ocorrer em seus grupos amino C-2, as hidroxilas em C-3 e C-6 das unidades estruturais do biopolímero também são susceptíveis a reações.

A natureza química da quitosana fornece possibilidades para as modificações covalentes e iônicas, as quais também permitem a modulação das propriedades mecânicas e biológicas dos biomateriais produzidos, ampliando seu espectro de aplicação na engenharia de tecidos e medicina regenerativa. (Gonsalves *et al.*, 2011).

#### 2.3.4.3. Complexos Polieletrólíticos de Ácido Hialurônico e Quitosana

Complexos polieletrólíticos (PECs) são complexos poliméricos formados pela reação entre polímeros de cargas opostas. A formação e as propriedades dos PECs dependem da razão das cargas aniônicas e catiônicas dos polímeros, do grau de neutralização, da força iônica e da valência dos íons na solução eletrolítica. Os PECs preparados a partir polímeros naturais, tais como ácido hialurônico e quitosana, têm a vantagem de serem não tóxicos e bioabsorvíveis (Kim *et al.*, 2004a; Kim *et al.*, 2004b).

Como dito anteriormente, o ácido hialurônico tem sido amplamente utilizado como *scaffolds* na cicatrização de feridas e na regeneração de tecidos, entretanto, a elevada densidade de cargas negativas do AH pode reduzir a adesão celular e interferir nos processos biológicos envolvidos na regeneração tecidual limitando sua aplicação (Ren *et al.*, 2005; Correia *et al.*, 2011). Uma boa alternativa para contornar esta limitação é combinar o AH com policátions tais como a quitosana.

Testes *in vitro* mostraram que os PECs formados de CHT e AH podem ser utilizados como um material de suporte para o transplante de condrócitos autólogos e/ou como *scaffolds* para a engenharia de tecidos, principalmente de tecidos da cartilagem (Sechriest *et al.*, 1999).

Correia *et al.* (2011) prepararam *scaffolds* de CHT com diferentes concentrações de AH (1, 5, 10%) por liofilização. Os *scaffolds* de CHT-AH não apresentaram citotoxicidade e promoveram adesão celular. Além disso, a incorporação de AH até uma

concentração de 5% melhorou as propriedades físico-químicas e biológicas dos *scaffolds* de CHT, favorecendo a adesão de condrócitos, proliferação celular e a produção de cartilagem, quando comparados aos *scaffolds* de CHT e a outras razões CHT-AH.

*Scaffolds* porosos de AH e CHT foram preparados por Coimbra *et al.* (2011) visando regeneração de polpa dentária. Estudos *in vitro* mostraram que as células tronco mesenquimais (MSCs) aderiram e proliferaram sobre a superfície do *scaffold*, o que demonstrou a biocompatibilidade e não citotoxicidade do biomaterial.

Majima *et al.* (2007) prepararam fibras de CHT com 0,1 % de ácido hialurônico que foram utilizadas como *scaffolds* para a engenharia de tecidos de ligamentos e tendões. Ensaio *in vivo* mostraram baixa toxicidade e baixa indução da inflamação. Além disso, ensaios *in vivo* mostraram que as propriedades mecânicas do ligamento ou do tendão engenheirado podem conferir maior estabilização das articulações.

Lee *et al.* (2003) prepararam esponjas de AH-CHT em vários pHs por liofilização e avaliaram seu efeito de cicatrização de feridas na pele de ratos Wistar com ou sem o agente antimicrobiano sulfadiazina de prata. Os resultados mostraram a proliferação de fibroblastos na ferida e uma redução significativa de agentes infecciosos.

## 2.4. Células Tronco Mesenquimais

Células tronco mesenquimais são células indiferenciadas tradicionalmente encontradas na medula óssea. No entanto, as MSCs podem também ser isoladas a partir de outros tecidos, incluindo o tecido adiposo (h-AdMSCs).

Atualmente, as h-AdMSCs são as células mais utilizadas na medicina regenerativa devido principalmente à facilidade de obtenção de grandes quantidades de células.

As h-AdMSCs podem ser facilmente obtidas através de lipoaspiração, que é um método mais barato e menos invasivo que o procedimento de punção realizado para a obtenção das MSCs derivadas da medula óssea.

Além disso, a frequência de h-AdMSCs no tecido adiposo (5000 células/g de gordura) é muito maior em relação às MSCs da medula óssea (100-1000 células/g) (Chavez-Munoz *et al.*, 2013; Lin *et al.*, 2008).

Morfologicamente, as h-AdMSCs são fibroblastoides, com formato fusiforme.

Quando submetidas a diferentes estímulos, as h-AdMSCs apresentam potencial para se diferenciarem, *in vitro* ou *in vivo*, em células de tecidos mesodérmicos, como os adipócitos, as cartilagens, os ossos e o músculo esquelético; e não mesodérmicos, como os hepatócitos, as células pancreáticas endócrinas, os neurônios, os hepatócitos e as células endoteliais vasculares, possibilitando assim um vasto campo de aplicações na medicina regenerativa (Yarak & Okamoto, 2010)

As h-AdMSCs também compartilham algumas características importantes das MSCs adultas, incluindo plasticidade, alto potencial proliferativo, capacidade de secretar moléculas protetoras bioativas e capacidade para modular a resposta imune (Bailey *et al.*, 2010).

Apesar das h-AdMSCs e PRP apresentarem propriedades benéficas para os processos celulares utilizados na regeneração de tecidos, estudos utilizando a combinação de h-AdMSCs e PRP ainda são escassos.

A seguir são citados os principais trabalhos da literatura utilizando a combinação de PRP e h-AdMSCs, sem a presença de scaffolds.

Baseados na avaliação clínica por ultrassonografia, Guercio *et al.* (2014) verificaram que a combinação de PRP e AdMSCs é uma terapia promissora para o tratamento de lesões em tendões de cavalos de competição.

Pak *et al.* (2013) mostraram que terapias com h-AdMSCs/ PRP podem ser consideradas seguras quando utilizadas na forma de injeções percutâneas locais para o tratamento de diferentes condições ortopédicas.

Em estudos realizados por van Pham *et al.* (2013), PRP promoveu a proliferação de h-AdMSCs e a diferenciação condrogênica. Além disso, estes autores observaram que PRP combinado com h-AdMSCs melhorou a cicatrização da cartilagem das articulações em modelos murinos quando comparados com PRP sem a presença de células.

O efeito da liberação de FC do PRP e de BMP-2 (proteína morfogênica óssea) encapsulada em microesferas na proliferação e diferenciação osteogênica de h-AdMSCs foi verificado por Chen *et al.* (2012). Para isso, estes autores prepararam 5 compósitos: h-AdMSCs/ plasma pobre em plaquetas (PPP); h-AdMSCs/ PRP; BMP-2/ PPP; h-AdMSCs/BMP/PRP e h-AdMSCs/ BMP-2/ PPP. Os resultados mostraram que a liberação controlada de BMP-2 em combinação com o PRP é melhor do que uma única administração de PRP ou de BMP-2 na diferenciação osteogênica de h-AdMSCs.

Kakudo *et al.* (2008) verificaram que concentrações menores que 20% de PRP ativado promovem significativamente a proliferação de h-AdMSCs.



## 2.5. *Scaffolds* Compósitos

Embora o PRP seja uma fonte de FCs plaquetários, a liberação da maior parte desses fatores de crescimento ocorre dentro da primeira hora após a ativação plaquetária, apesar da liberação continuar durante todo o período de viabilidade das plaquetas (7 dias) (McCarrel & Fortier, 2009)

Hokugo *et al.* (2005) mostraram que nenhuma regeneração óssea foi observada com o tratamento usando PRP livre, devido a sua rápida excreção do sítio de aplicação.

Além disso, segundo Rossi *et al.* (2013), a eficácia dos FCs no processo de regeneração depende também da forma como esses FCs são disponibilizados no tecido lesionado.

Assim, a liberação gradual dos FCs tem sido considerada benéfica nas terapias utilizando PRP.

Em adição, na preparação do PRP, ocorre a formação de uma rede de fibrina, *scaffold* natural, decorrente da ativação das plaquetas e decomposição do fibrinogênio. No entanto, a rede de fibrina formada é frágil e possui viscoelasticidade e viscosidade limitadas pelo endurecimento das fibras sob altos níveis de cisalhamento, além de sofrer degradação rápida no meio biológico.

Para proteger os FCs contra proteólise, prolongando assim sua atividade *in vivo* e melhorar a estabilidade da rede de fibrina do PRP, Tabata (2003) sugeriu combinar as funções dos *scaffolds* com a tecnologia de liberação controlada.

Entretanto, trabalhos utilizando PRP associado a *scaffolds* visando potencializar a utilização dos FCs do PRP ainda são escassos.

O desenvolvimento de *scaffolds* adequados para a utilização eficaz do PRP é ainda um grande desafio para a engenharia de tecidos.

Embora vários trabalhos tenham descrito as propriedades físico-químicas, mecânicas e biológicas, e/ou as aplicações clínicas de diferentes *scaffolds* de quitosana e ácido hialurônico, ainda existem poucos trabalhos usando a combinação desses *scaffolds* com PRP, ou seja, utilizando *scaffolds* compósitos.

Além disso, somente o trabalho descrito por Rossi *et al.* (2013) utilizou os três vértices da proliferação celular, usando *scaffolds* de quitosana, PRP e fibroblastos como fonte de células.

Os principais trabalhos da literatura que descrevem a utilização de *scaffolds* compósitos de AH e CHT, que foram utilizados como base para este trabalho são descritos a seguir.

Ouyang *et al.* (2013) patentearam diferentes *scaffolds* compósitos de quitosana solúvel combinada com PRP para a reparação de tecidos, usando trombina e/ ou CaCl<sub>2</sub> como agonistas.

Esponjas de glutamato de quitosana e de hialuronato de sódio combinadas com lisado de plaquetas e preparadas por liofilização utilizando glicina como crioprotetor, foram usadas por Rossi *et al.* (2013) como matrizes para a incorporação de FCs derivados do PRP. Os resultados de crescimento celular para fibroblastos obtidos para as esponjas de CHT e de AH foram similares aos valores encontrados para o lisado de plaquetas fresco.

Kutlu *et al.* (2012) prepararam compósitos de quitosana/ PRP por 2 métodos diferentes: PRP foi adicionado ao gel de quitosana antes da liofilização e PRP foi embebido no *scaffold* liofilizado. Estes autores demonstraram que *scaffolds* de quitosana, especialmente na forma de géis, podem ser apropriados carreadores para o PRP fornecendo liberação controlada dos fatores de crescimento.

Uma terapia de etapa única para o tratamento de defeitos osteocondrais de coelhos utilizando fragmentos autólogos de cartilagem e *scaffolds* compostos de ácido hialurônico (AH), cola de fibrina humana e PRP foi proposta por Marmotti *et al.* (2012). Esses autores observaram que os fragmentos de cartilagem autólogos em AH/ cola de fibrina/ PRP fornecem uma fonte eficiente de células e permitem uma melhor reparação do defeito. A cola de fibrina, no entanto, dificultou o processo de cicatrização nos coelhos.

Fathi (2012) demonstrou que a utilização de PRP sozinho ou em combinação com AH acelerou a cicatrização de feridas em coelhos adultos comparado ao AH livre usado como controle.

A eficácia do uso de PRP e da viscosuplementação com injeções intra-articulares de AH para o tratamento de lesões degenerativas da cartilagem do joelho e osteoartrite foram comparadas por Kon *et al.* (2011). Injeções autólogas de PRP mostraram maior eficácia e maior duração que as injeções de AH na redução da dor e dos sintomas; e recuperação da função articular. Melhores resultados foram conseguidos em pacientes mais jovens e em degenerações da cartilagem menos intensas, enquanto que um pior resultado foi obtido em articulações mais degeneradas e em pacientes mais idosos, em quem os resultados foram semelhantes aos da viscosuplementação.

He *et al.* (2010) estudaram a ativação e a adesão plaquetária em *scaffolds* de quitosana e quitosana-heparina combinados com PRP. Eles observaram, *in vitro*, que

os *scaffolds* de quitosana-heparina quando combinados com PRP apresentam supressão da adesão e ativação das plaquetas em relação com os *scaffolds* de quitosana/PRP.

O efeito de PRP, de esponjas de quitosana e da combinação deles, na regeneração óssea de defeitos cranianos de coelhos foi investigado por Oktay *et al.* (2010). Para isso, eles criaram e enxertaram 4 defeitos cranianos, com um diâmetro de 4,5 mm com os 3 grupos. Os coelhos foram mortos entre a quarta e oitava semana, e os defeitos foram analisados histologicamente. Maior formação óssea foi observada no grupo contendo PRP com preenchimento completo do defeito com osso trabecular. Os defeitos que foram preenchidos somente com esponjas de quitosana mostraram uma quantidade limitada de osso, e a presença de tecido fibroso.

Uma nova abordagem terapêutica para estimular a regeneração de feridas complexas em membros inferiores, com base em um tratamento composto de PRP e curativo de AH foi avaliada por Cervelli *et al.* (2011). Após um único tratamento, os autores observaram que o tempo médio de re-epitelização foi de 8,1 semanas em 73,3% dos pacientes tratados com o PRP-AH versus 30% dos pacientes tratados apenas com AH.

Um compósito injetável de fosfato tricálcico/ quitosana (FTC/CHT) e PRP para a reconstrução de defeitos de tíbias de cabras foi preparado por Bi *et al.* (2010). Esses autores mostraram que a adição de PRP aumentou a biocompatibilidade e a osteocondutividade do FTC/CHT sem comprometer sua força mecânica e injetabilidade.

Chang *et al.* (2009) mostraram que compósitos preparados pela associação de PRP ativado e microesferas de CaSO<sub>4</sub>/ quitosana, preparadas utilizando campo eletrostático de alta tensão, melhoraram a regeneração óssea em torno dos alvéolos orais de porcos.

A possibilidade de utilizar quitosana como substituto da trombina durante a preparação PRP foi avaliada por Shen *et al.* (2006). Os resultados obtidos por estes autores mostraram aumento na adesão e da agregação de plaquetas, além de maiores concentrações de fatores de crescimento do PRP após utilização da quitosana, sugerindo que quitosana e/ ou seus derivados podem substituir a trombina em preparações do PRP.

## 2.6. Referências

ADEKOGBE, I.; GHANEM, A. Fabrication and characterization of DTBP-crosslinked

chitosan scaffolds for skin tissue engineering. **Biomaterials**, vol.26, p.7241–7250, 2005.

AGNIHOTRI, S.A.; MALLIKARJUNA, N.N.; AMINABHAVI, T.M. Recent advances on chitosan-based micro- and nanoparticles in drug delivery. **Journal Controlled Release**, vol.100, n.1, p.5-28, 2004.

AGRAWAL, C.M.; RAY, R.B. Biodegradable polymeric scaffolds for musculoskeletal tissue engineering. **Journal of Biomedical Materials Research – Part A**, vol.55, p.141–150, 2001.

ALSOUSOU, J.; THOMPSON, M.; HULLEY, P.; NOBLE, A.; WILLETT, K. The biology of platelet-rich plasma and its application in trauma and orthopaedic surgery. **Journal of Bone and Joint Surgery – Part B**, vol.91, p.987-96, 2009.

AMARAL, I.F.; SAMPAIO, P.; BARBOSA, M.A. Three-dimensional culture of human osteoblastic cells in chitosan sponges: The effect of the degree of acetylation. **Journal of Biomedical Materials Research – Part A**, vol.76, p.335–346, 2006.

ANITUA, E. Plasma rich in growth factors: preliminary results of use in the preparation of future sites for implants. **International Journal of Oral & Maxillofacial Implants**, vol.4, p.529-535, 1999.

ANITUA, E.; ALKHRAISAT, M.H.; ORIVE, G. Perspectives and challenges in regenerative medicine using plasma rich in growth factors. **Journal of Controlled Release**, vol.157, p.29-38, 2012.

ANTONOV, S.F.; KRYZHANOVSKAYA, E.V.; FILIPPOV, Y.I.; SHINKAREV, S.M.; FROLOVA, M.A. Study of Wound-Healing Properties of Chitosan. **Russian Agricultural Sciences**, vol.34, n.6, p.426–427, 2008.

BAILEY, A.; KAPUR, S.; KATZ, A.J. Characterization of adipose-derived stem cells: an update. **Current Stem Cell Research & Therapy**, vol.5, p.95–102, 2010.

BALAZS, E.A. Sodium hyaluronate and viscosurgery. In: MILLER, D.; STEGMANN, R. (Ed.). **Healon (sodium hyaluronate). A guide to its use in Ophthalmic Surgery**. New York: Wiley, 1983, p. 5-28.

BALAZS, E.A.; DENLINGER, J.L. Viscosupplementation: a new concept in the treatment of osteoarthritis. **Journal of Rheumatology**, vol.39, p.3-9, 1993.

BAND, P.A. **Hyaluronan derivatives: chemistry and clinical applications**. In: LAURENT T.C. (Eds.). **The chemistry biology and medical applications of hyaluronan and its derivatives**. London: Portland Press, p. 33-42, 1998.

BARNETT, M.D.; POMEROY, G.C. Use of Platelet-Rich Plasma and Bone Marrow Y Derived Mesenchymal Stem Cells. **Techniques in Foot and Ankle Surgery**, vol.6, n.2, p.89–94, 2007.

BELLINI, D.; PAPARELLA, A.; O'REGAN, M.; CALLEGARO, L. Autocross-linked hyaluronic acid and related pharmaceutical compositions for the treatment of arthropathies. **United States Patent: U.S. 6,251,876 B1**, 2001.

BERGER, J.; REIST, M.; MAYER, J.; FELT, O.; PEPPAS, N.; GURNY, R. Structure and interactions in covalently and ionically crosslinked chitosan hydrogels for biomedical applications. **European Journal of Pharmaceutics and Biopharmaceutics**, vol.57, p.19–34, 2004.

BERTHIAUME, F.; MAGUIRE, T.J.; YARMUSH, M.L. Tissue Engineering and Regenerative Medicine: History, Progress, and Challenges. **Annual Review of Chemical and Biomolecular Engineering**, vol.2, p.403–30, 2011.

BERTRAM, U.; BODMEIER, R. In situ gelling, bioadhesive nasal inserts for extended drug delivery: In vitro characterization of a new nasal dosage form. **European Journal of Pharmaceutical Sciences**, vol.27, n.1, p.62-71, 2006.

BHATTACHARYYA, S.; GUILLOT, S.; DABBOUE, H.; TRANCHANT, J.F.; SALVETAT, J.P. Carbon nanotubes as structural nanofibers for hyaluronic acid hydrogel scaffolds. **Biomacromolecules**, vol.9, n.2, p.505-509, 2008.

BI, L.; CHENG, W.; FAN, H.; PEI, G. Reconstruction of goat tibial defects using an injectable tricalcium phosphate/chitosan in combination with autologous platelet-rich plasma. **Biomaterials**, vol.31, p.3201–3211, 2010.

BOCCACCINI, AR.; ROETHER, J.A.; HENCH, L.L.; MAQUET, V.; JEROME, R. Composites approach to tissue engineering. **Ceramic Engineering and Science**, vol.23, n.4, p.805-816, 2002.

CALVO, P.; VILA-JATO, J.L.; ALONSO, M.J. Evaluation of cationic polymer-coated nanocapsules as ocular drug carriers. **International Journal of Pharmaceutics**, vol.153, p.41–50, 1997.

CERVELLI, V.; LUCARINI, L.; SPALLONE, D.; PALLA, L.; COLICCHIA, G.M.; GENTILE, P.; ANGELIS, B. Use of Platelet-Rich Plasma and Hyaluronic Acid in the Loss of Substance with Bone Exposure. **Advances in Skin & Wound Care**, vol.24, n.4, p.176-181, 2011.

CHANG, S.J.; KUO, S.M.; LAN, C-W.; MANOUSAKAS, I.; TSAI, P.H. Evaluation of chitosan/CaSO<sub>4</sub>/ platelet-rich plasma microsphere composites as alveolus osteogenesis material. **Biomedical Engineering: Applications, Basis and Communications**, vol.21, n.2, p.115–122, 2009.

CHAVEZ-MUNOZ, C.; NGUYEN, K.T.; XU, W.; HONG, S.J.; MUSTOE, T.A.; GALIANO, R.D. Transdifferentiation of adipose-derived stem cells into keratinocyte-like cells: engineering a stratified epidermis. **PLOS One**, vol.8, n.12, p.1-13, 2013.

CHEN, L.; LU, X.; LI, S.; SUN, Q.; LI, W.; SONG, D. Sustained Delivery of BMP-2 and

Platelet rich Plasma-released Growth Factors Contributes to Osteogenesis of Human Adipose-derived Stem Cells. **Orthopedics**, vol.35, n.9, p.e1402–e1409, 2012.

COIMBRA, P.; ALVES, P.; VALENTE, T.A.M.; SANTOS, R.; CORREIA, I.J.; FERREIRA, P. Sodium hyaluronate/chitosan polyelectrolyte complex scaffolds for dental pulp regeneration: Synthesis and characterization. **International Journal of Biological Macromolecules**, vol.49, p.573– 579, 2011.

COLE, B.J.; SEROYER, S.T.; FILARDO, G.; BAJAJ, S.; FORTIER, L.A. Platelet-Rich Plasma: Where Are We Now and Where Are We Going? **Sports Health**, vol.2, n.3, p.203-210, 2010.

COLLINS, M.N.; BIRKINSHAW, C. Investigation of the Swelling Behavior of Crosslinked Hyaluronic Acid Films and Hydrogels Produced Using Homogeneous Reactions. **Journal of Applied Polymer Science**, vol.109, p.923-931, 2008.

CORREIA, C.R.; TEIXEIRA, L.S.M.; MORONI, L.; REIS, R.L.; VAN BLITTERSWIJK, C.A.; KARPERIEN, M.; MANO, J.F. Chitosan Scaffolds Containing Hyaluronic Acid for Cartilage Tissue Engineering. **Tissue Engineering – Part C**, vol.17, n.7, p. 717-730, 2011.

COSTA-PINTO, A.R.; REIS, R.L.; NEVES, N.M. Scaffolds Based Bone Tissue Engineering: The Role of Chitosan. **Tissue Engineering – Part B**, vol.17, p.331–347, 2011.

CRANE, D.; EVERTS, P.A.M. Platelet Rich Plasma (PRP) Matrix Grafts, **PPM Communications**, vol.8, p.1-10, 2008.

CRUZ, D.M.G.; IVIRICO, J.L.E.; GOMES, M.M.; RIBELLES, J.L.G.; SÁNCHEZ, M.S.; Reis, R.L.; MANO, J.F. Chitosan microparticles as injectable scaffolds for tissue engineering. **Journal of Tissue Engineering and Regenerative Medicine**, vol.2, p.378–380, 2008.

CUSTÓDIO, C.A.; SANTO, V.R.; OLIVEIRA, M.B.; GOMES, M.E.; REIS, R.L.; MANO, J.F. Functionalized Microparticles Producing Scaffolds in Combination with Cells. **Advanced Functional Materials**, vol.24, p.1391–1400, 2014.

DAAR, A.S.; GREENWOOD, H.L. A proposed definition of regenerative medicine. **Journal of Tissue Engineering and Regenerative Medicine**, vol.1, p.179–184, 2007.

DAI, T.; TANAKA, M.; HUANG, Y.Y.; HAMBLIN, M.R. Chitosan preparations for wounds and burns: antimicrobial and wound-healing effects. **Expert Review of Anti-infective Therapy**, vol.9, p.857–879, 2011.

DE BELDER, A.; MALSON, T. Gel for preventing adhesion between body tissues and process for its production. **Patent: WO 1986/000/912 A1**, 1986.

DE VOS, R.J.; WEIR, A.; VAN SCHIE, H.T.M.; BIERMA-ZEINSTRA, S.M.A.; VERHAAR,

J.A.N.; WEINANS, H.; TOL, J.L. Platelet-Rich Plasma Injection for Chronic Achilles Tendinopathy. **Journal of the American Medical Association**, vol.303, n.2, p.144-149, 2010.

DELLA VALLE, F. Crosslinked carboxy polysaccharides. **Patent: EP 341,745**, 1994

DELLA VALLE, F.; ROMEO, A. Cross-linked carboxy polysaccharides. **Patent: WO/1989/10941**, 1989.

EHRENFEST, D.M.D.; RASMUSSEN, L.; ALBREKTSSON, T. Classification of platelet concentrates: from pure platelet-rich plasma (P-PRP) to leucocyte- and platelet-rich fibrin (L-PRF). **Trends Biotechnology**, vol.27, p.158-167, 2009.

ENGBRETSSEN, L.; STEFFEN, K.; ALSOUSOU, J.; ANITUA, E.; BACHL, N.; DEVILEE, R.; EVERTS, P.; HAMILTON, B.; HUARD, J.; JENOURE, P.; KELBERINE, F.; KON, E.; MAFFULLI, N.; MATHESON, G.; MEI-DAN, O.; MENETREY, J.; PHILIPPON, M.; RANDELLI, P.; SCHAMASCH, P.; SCHWELLNUS, M.; VERNEC, A.; GEOFFREY, V. IOC consensus paper on the use of platelet-rich plasma in sports medicine. **British Journal of Sports Medicine**, vol.44, p.1072–1081, 2010.

EVERTS P.A.; JAKIMOWICZ, J.J.; VAN BEEK, M.; SCHÖNBERGER, J.P.A.M.; DEVILEE, R.J.J.; OVERDEVEST E.P.; KNAPE, J.T.A.; VAN ZUNDERT, A. Reviewing the Structural Features of Autologous Platelet-Leukocyte Gel and Suggestions for Use in Surgery. **European Surgical Research**, vol.39, p.199–207, 2007.

EVERTS, P.A.; DEVILEE, R.J.J.; MAHONEY, C.B.; VAN, E.R.P.A.; OOSTERBOS, C.J.M.; STELLENBOOM, M.; KNAPE, J.T.A.; VAN ZUNDERT, A. Exogenous application of platelet-leukocyte gel during open subacromial decompression contributes to improved patient outcome. **European Surgical Research**, vol.40, p.203-210, 2008.

FATHI, W.K. The Effect of Hyaluronic Acid and Platelet - Rich Plasma on Soft Tissue Wound Healing: An Experimental Study on Rabbits. **Al-Rafidain Dental Journal**, vol.12, n.1, p.115-125, 2012.

FERRARI, M.; ZIA, S.; VALBONESI, M.; HENRIQUET, F.; VENERE, G.; SPAGNOLO, S.; GRASSO, M.A.; PANZANI, I. A new technique for hemodilution, preparation of autologous platelet-rich plasma and intraoperative blood salvage in cardiac surgery. **International journal of artificial organs**, vol.10, n.1, p.47-50, 1987.

FOSTER, T.E.; PUSKAS, B.L.; MANDELBAUM, B.R.; GERHARDT, M.B.; RODEO, S.A. Platelet-Rich Plasma From Basic Science to Clinical Applications. **American Journal of Sports Medicine**, vol.37, n.11, p.2258-2272, 2009.

GARG, H.G.; HALES, C.A. Chemistry and Biology of Hyaluronan, Boston, USA, Elsevier, 2004.

GEORGE, J.; ONODERA, J.; MIYATA, T. Biodegradable honeycomb collagen scaffold for dermal tissue engineering. **Journal of Biomedical Materials Research – Part A**,

vol.87, p.1103-1111, 2008.

GONSALVES, A.A.; ARAÚJO, C.R.M.; SOARES, N.A.; GOULART, M.O.F.; DE ABREU, F.C. Diferentes estratégias para a reticulação de quitosana. **Química Nova**, vol.XY, n.00, p.1-9, 2011.

GREENWOOD, H.L.; SINGER, P.A.; DOWNEY, G.P.; MARTIN, D.K.; THORSTEINSDÓTTIR, H.; DAAR, A.S. Regenerative Medicine and the Developing World. **PLoS Medicine**, vol.3, n.9, p.1496-1500, 2006.

GUERCIO, A.; DI MARCO, P.; CASELLA, S.; RUSSOTTO, L.; PUGLISI, F.; MAJOLINO, C.; GIUDICE, E.; DI BELLA, S.; PURPARI, G.; CANNELLA, V.; PICCIONE, G.; Mesenchymal stem cells derived from subcutaneous fat and platelet-rich plasma used in athletic horses with lameness of the superficial digital flexor tendon. **Journal of Equine Veterinary Science**, vol.35, n.1, p. 19-26, 2014.

GUTOWSKA, A.; JEONG, B.; JASIONOWSKI, M. Injectable Gels for Tissue Engineering. **Anatomical Record**, vol.263, p.342-349, 2001.

HAHN, S.K.; OH, E.J.; MIYAMOTO, H.; SHIMOBOUJI, T. Sustained release formulation of erythropoietin using hyaluronic acid hydrogels crosslinked by Michael addition. **International Journal of Pharmaceutics**, vol.322, p.44-51, 2006.

HE, P.; DAVIS, S.S.; ILLUM, L. In vitro evaluation of the mucoadhesive properties of chitosan microspheres. **International Journal of Pharmaceutics**, vol.166, p.75–88, 1998.

HOKUGO, F.; OZEKI, M.; KAWAKAMI, O.; SUGIMOTO, K.; MUSHIMOTO, K.; MORITA, S.; TABATA, Y. Augmented Bone Regeneration Activity of Platelet-Rich Plasma by Biodegradable Gelatin Hydrogel. **Tissue Engineering**, vol.11, n.7/8, p.1224–1233, 2005.

HOLMSTRÖM, B.; RICICI, J. Production of Hyaluronic Acid by a Streptococcal Strain in Batch Culture. **Journal of Applied Microbiology**, vol.15, p.1409-1413, 1967.

HOU, Q.; DE BANK, P.A.; SHAKESHEFF, K.M. Injectable scaffolds for tissue regeneration. **Journal of Materials Chemistry**, vol.14, p.1915-1923, 2004.

HUANG, Z-M.; ZHANG, Y-Z.; KOTAKI, M.; RAMAKRISHN, S. A review on polymer nanofibers by electrospinning and their applications in nanocomposites. **Composites Science and Technology**, vol.63, n.15, p.2223–2253, 2003.

HUTMACHER, D.W. Scaffolds in tissue engineering bone and cartilage. **Biomaterials**, vol.21, p.2529-2543, 2000.

ISHIDA, K.; KURODA, R.; MIWA, M.; TABATA, Y.; HOKUGO, A.; KAWAMOTO, T.; SASAKI, K.; DOITA, M.; KUROSAKA, M. The Regenerative Effects of Platelet-Rich Plasma on Meniscal Cells In Vitro and Its In Vivo Application with Biodegradable Gelatin



Hydrogel. **Tissue Engineering**, vol.13, n.5, p.1103-1115, 2007.

IWASAKI, N.; KASAHARA, Y.; YAMANE, S.; IGARASHI, T.; MINAMI, A.; NISIMURA, S.-I. Chitosan-Based Hyaluronic Acid Hybrid Polymer Fibers as a Scaffold Biomaterial for Cartilage Tissue Engineering. **Polymers**, vol.3, p.100-113, 2011.

JIA, X.; PETERS, P.G.; SCHON, L. The use of platelet-rich plasma in the management of foot and ankle conditions. **Operative Techniques in Sports Medicine**, vol.19, p.177-184, 2011.

JIANG, Z-Q.; LIU, H-Y.; ZHANG, L-P.; WU, Z-Q.; SHANG, D-Z. Repair of calvarial defects in rabbits with platelet-rich plasma as the scaffold for carrying bone marrow stromal cells. **Oral Surgery, Oral Medicine, Oral Pathology, Oral Radiology, and Endodontology**, vol.113, p.327-333, 2012.

JUDITH, R.; NITHYA, M.; ROSE, C.; MANDAL, A.B. Biopolymer gel matrix as acellular scaffold for enhanced dermal tissue regeneration. **Biologicals**, vol.40, p.231-239, 2012.

JUDITH, R.; NITHYA, M.; ROSE, C.; MANDAL, AB. Application of a PDGF-containing novel gel for cutaneous wound healing. **Life Sciences**, vol.87, p.1–8, 2010.

KAKUDO, N.; MINAKATA, T.; MITSUI, T.; KUSHIDA, S.; NOTODIHARDJO, F.Z.; KUSUMOTO, K. Proliferation-promoting effect of platelet-rich plasma on human adipose-derived stem cells and human dermal fibroblasts. **Plastic and Reconstructive Surgery**, vol.122, p.1352–1360, 2008.

KAUX, J-F.; CRIELAARD, J-M. Platelet-rich plasma application in the management of chronic tendinopathies. **Acta Orthopaedica Belgica**, vol.79, p.10-15, 2013.

KAWASUMI, M.; KITO, H.; SIWICKA, K.A.; ISHIGURO, N. The effect of the platelet concentration in platelet-rich plasma gel on the regeneration of bone. **Journal of bone and joint surgery**, vol.90B, p.966-972, 2008.

KIM, J.; KIM, I.S.; CHO, T.H.; KIM, H.C.; YOON, S.J.; CHOI, J.; PARK, Y.; SUN, K.; HWANG, S.J.; In vivo evaluation of MMP sensitive high-molecular weight HA-based hydrogels for bone tissue engineering. **Journal of Biomedical Materials Research – Part A**, vol.95, p.673–681, 2010.

KIM, S.J.; HAHN, S.K.; KIM, M.J.; KIM, D.H.; LEE, Y.P. Development of a novel sustained release formulation of recombinant human growth hormone using sodium hyaluronate microparticles. **Journal of Controlled Release**, vol.104, p.323–335, 2005.

KIM, S.J.; LEE, K.J.; KIM, S.I. Swelling Behavior of Polyelectrolyte Complex Hydrogels Composed of Chitosan and Hyaluronic Acid. **Journal of Applied Polymer Science**, vol.93, p.1097-1101, 2004a.

KIM, S.J.; SHIN, S.R.; LEE, K.B.; PARK, Y.D.; KIM, S.I. Synthesis and Characteristics of Polyelectrolyte Complexes Composed of Chitosan and Hyaluronic Acid. **Journal of**

**Applied Polymer Science**, vol.91, p.2908-2913, 2004b.

KOGAN, G.; ŠOLTÉS, L.; STERN, R. Hyaluronic Acid: a natural biopolymer with a broad range of biomedical and industrial applications. **Biotechnology Letters**, vol.29, p.17-25, 2007.

KON, E.; BUDA, R.; FILARDO, G.; DI MARTINO, A.; TIMONCINI, A.; CENACCHI, A.; FORNASARI, PA.; GIANNINI, S.; MARCACCI, M. Platelet-rich plasma: intra-articular knee injections produced favorable results on degenerative cartilage lesions. **Knee Surgery, Sports Traumatology, Arthroscopy**, vol.18, p.472–479, 2010.

KON, E.; MANDELBAUM, B.; BUDA, R.; FILARDO, G.; DELCOGLIANO, M.; TIMONCINI, A.; FORNASARI, P.M.; GIANNINI, S.; MARCACCI, M. Platelet-Rich Plasma Intra-Articular Injection Versus Hyaluronic Acid Viscosupplementation as Treatments for Cartilage Pathology: From Early Degeneration to Osteoarthritis. **Arthroscopy: The Journal of Arthroscopic and Related Surgery**, vol.27, n.11, p.1490-1501, 2011.

KUO, J.W.; SWANN, D.A.; PRESTWICH, G.D. Water-insoluble derivatives of hyaluronic acid and their methods of preparation and use. **United States Patent: U.S. 6,013,679**, 2000.

KUTLU, B.; AYDIN, R.S.T.; AKMAN, A.C.; GÜMÜŞDERELIOĞLU, M.; NOHUTCU, R.M. Platelet-rich plasma-loaded chitosan scaffolds: Preparation and growth factor release kinetics. **Journal of Biomedical Materials Research – Part B**, vol.101, p.28–35, 2012.

LANGER, P.; VACANTI, J.P. Tissue Engineering. **Science**, vol.260, n.5110, p.920-926, 1993.

LEE, S.B.; LEE, Y.M.; SONG, K.W.; PARK, M.H. Preparation and Properties of Polyelectrolyte Complex Sponges Composed of Hyaluronic Acid and Chitosan and Their Biological Behaviors. **Journal of Applied Polymer Science**, vol.90, p.925–932, 2003.

LEE, Y.M.; PARK, Y.J.; LEE, S.J.; KU, Y.; HAN, S.B.; CHOI, S.M.; KLOKKEVOLD, P.R.; CHUNG, C.P. Tissue engineered bone formation using chitosan/tricalcium phosphate sponges. **Journal of Periodontology**, vol.71, p.410-417, 2000.

LI, X.; MIN, M.; DU, N.; GU, Y.; HODE, T.; NAYLOR, M.; CHEN, D.; NORDQUIST, R.E.; CHEN, W.R. Chitin, chitosan, and glycated chitosan regulate immune responses: the novel adjuvants for cancer vaccine. **Clinical and Developmental Immunology**, vol.387023, p.1-8, 2013.

LIN, G.; GARCIA, M.; NING, H.; BANIE, L.; GUO, Y-L.; LUE, T.F.; LIN, C-S. Defining Stem and Progenitor Cells within Adipose Tissue. **Stem cells and development**, vol.17, p.1053–1064, 2008.

LIN, Y-C.; TAN, F-J.; MARRA, K.G.; JAN, S-S.; LIU, D-C. Synthesis and characterization of collagen/ hyaluronan/ chitosan composite sponges for potential

biomedical applications. **Acta Biomaterialia**, vol.5, p.2591-2600, 2009.

LIU, X.; MA, P.X. Polymeric Scaffolds for Bone Tissue Engineering. **Annals of Biomedical Engineering**, vol.32, n.3, p.477–486, 2004.

LIU, X.F.; GUAN, Y.L.; YANG, D.Z.; LI, Z.; YAO, K.D. Antibacterial action of chitosan and carboxymethylated chitosan. **Journal of Applied Polymer Science**, vol.79, p.1324–1335, 2001.

MADHALLY, S.V.; MATTHEW, H.W.T. Porous chitosan scaffolds for tissue engineering. **Biomaterials**, vol.20, p.1133–1142, 1999.

MAGNANI, A.; RAPPUOLI, R.; LAMPONI, S.; BARBUCCI, R. Novel Polysaccharide Hydrogels: Characterization and Properties. **Polymers for Advanced Technologies**, vol.11, p.488-495, 2000.

MAJIMA, T.; IRIE, T.; SAWAGUCHI, N.; FUNAKOSHI, T.; IWASAKI, N.; HARADA, K.; MINAMI, A.; NISHIMURA, S.-I. Chitosan-based hyaluronan hybrid polymer fiber scaffold for ligament and tendon tissue engineering. **Proceedings of the Institution of Mechanical Engineers – Part H: J. Engineering in Medicine**, vol. 221, p.537-546, 2007.

MALSON, T.; LINDQVIST, B. Gels of crosslinked hyaluronic acid for use as a vitreous humor substitute. **Patent WO 1986/000/079**, 1986.

MANFREDINI, C.; GUARINO, V.; ZINI, N.; RAUCCI, M.G.; FERRARI, A.; GRASSI, F.; GABUSI, E.; SQUARZONI, S.; FACCHINI, A.; AMBROSIO, L.; LISIGNOLI, G. Mineralization behavior with mesenchymal stromal cells in a biomimetic hyaluronic acid-based scaffold. **Biomaterials**, vol.31, p.3986–3996, 2010.

MANJUBALA, I.; SCHELER, S.; BÖSSERT, J.; JANDT, K.D. Mineralisation of chitosan scaffolds with nano-apatite formation by double diffusion technique. **Acta Biomaterialia**, vol.2, p.75-84, 2006.

MANN, B.K. Biologic gels in tissue engineering. **Clinics in Plastic Surgery**, vol.30, p.601– 609, 2003.

MARIANI, E.; FILARDO, G.; CANELLA, V.; BERLINGERI, A.; BIELLI, A.; CATTINI, L.; LANDINI, M.P.; KON, E.; MARCACCI, M.; FACCHINI, A. Platelet-rich plasma affects bacterial growth in vitro. **Cytotherapy**, vol.16, p.1294-1304, 2014.

MARMOTTI, A.; BRUZZONE, M.; BONASIA, D.E.; CASTOLDI, F.; ROSSI, R.; PIRAS, L.; MAIELLO, A.; REALMUTO, C.; PERETI, G.M. One-step osteochondral repair with cartilage fragments in a composite scaffold. **Knee Surgery, Sports Traumatology, Arthroscopy**, vol.20, n.12, p.2590-2601, 2012.

MARX, R.E. Platelet-rich plasma: Evidence to support its use. **Journal of Oral and Maxillofacial Surgery**, vol.62, p.489–496, 2004.

MARX, R.E.; CARLSON, E.R.; EICHSTAEDT, R.M.; SCHIMMELE, S.R.; STRAUSS, J.E.; GEORGEFF, K.R. Platelet-rich plasma Growth factor enhancement for bone grafts. **Oral Surgery, Oral Medicine, Oral Pathology, Oral Radiology**, vol.85, p.638-646, 1998.

MATHEWS, S.; BHONDE, R.; GUPTA, P.K.; TOTEY, S. A novel tripolymer coating demonstrating the synergistic effect of chitosan, collagen type 1 and hyaluronic acid on osteogenic differentiation of human bone marrow derived mesenchymal stem cells. **Biochemical and Biophysical Research Communications**, vol.414, p.270–276, 2011.

MCCARREL, T.; FORTIER, L. Temporal Growth Factor Release from Platelet-Rich Plasma, Trehalose Lyophilized Platelets, and Bone Marrow Aspirate and Their Effect on Tendon and Ligament Gene Expression. **Journal of Orthopaedic Research**, vol.27, p.1033–1042, 2009.

MEYER, K.; PALMER, J. The polysaccharide of vitreous humor. **Journal of Biological Chemistry**, vol.107, p.629-634, 1934.

MIKOS, A.G.; THORSEN, A.J.; CZERWONKA, L.A.; BAO, Y.; LANGER, R.; WINSLOW, D.N.; VACANTI, J.P. Preparation and characterization of (L-Lactic Acid) foams. **Polymer**, vol.35, p.1068-1077, 1994.

MISHRA, A.; HARMON, K.; WOODALL, J.; VIEIRA, A. Sports Medicine Applications of Platelet Rich Plasma. **Current Pharmaceutical Biotechnology**, vol.13, p.1185-1195, 2012.

MONHEIT, G.D.; COLEMAN, K.M. Hyaluronic Acid Fillers. **Dermatology and Therapy**, vol.19, p.141-150, 2006.

MONTEIRO, N.S. **Caracterização de matrizes de Quitosana para a regeneração de tecidos produzidas pela técnica de TIPS**. Dissertação de Mestrado em Engenharia Biomédica, Faculdade de Ciências e Tecnologia da Universidade Nova de Lisboa, 2008.

MUCHA, M.; MICHALAK, I.; BALCERZAK, J.; TYLMAN, M. Chitosan scaffolds, films and microgranules for medical application - preparation and drug release studies, **Polimery**, vol.57, n.10, p.714-721, 2012.

MUZZARELLI, R. Chitosan in: MUZZARELLI R. (Ed.). **Natural Chelating Polymers**. Oxford: Pergamon Press, 1973, p.144–176.

MUZZARELLI, R.; TARSI, R.; FILIPPINI, O.; GIOVANETTI, E.; BIAGINI, G.; VARALDO, P.E. Antimicrobial properties of N-carboxybutyl chitosan. **Antimicrobial Agents and Chemotherapy**, vol.34, p.2019-2023, 1990.

MUZZARELLI, R.A.A. Human enzymatic activities related to the therapeutic administration of chitin derivatives. **Cellular and Molecular Life Sciences**, vol.53, p.131–140, 1997.

NAM, Y.S.; YOON, J.J.; PARK, T.G. A novel fabrication method for macroporous scaffolds using gas foaming salt as porogen additive. **Journal of Biomedical Materials Research – Part B**, vol.53, p.1–7, 2000.

NGUYEN, R.T.; BORG-STEIN, J.; MCINNIS, K. Applications of Platelet-Rich Plasma in Musculoskeletal and Sports Medicine: An Evidence-Based Approach. **American Journal of Physical Medicine & Rehabilitation**, vol.3, p.226-250, 2011.

NISHI, C.; NAKAJIMA, N.; IKADA, Y. In vitro evaluation of cytotoxicity of diepoxy compounds used for biomaterial modification. **Journal of Biomedical Materials Research**, vol.29, n.7, p.829–834, 1995.

NORDTVEIT, R.J.; VÂRUM, K.M.; SMIDSRD, O. Degradation of partially N-acetylated chitosans with hen egg white and human lysozyme. **Carbohydrate Polymers**, vol.29, p.163-167, 1996.

NWE, N.; FURUIKE, T.; TAMURA, H. The Mechanical and Biological Properties of Chitosan Scaffolds for Tissue Regeneration Templates Are Significantly Enhanced by Chitosan from *Gongronella butleri*. **Materials**, vol.2, p.374-398, 2009.

OHRI, R.; HAHN, S.K.; STAYTON, P.S.; HOFFMAN, A.S.; GIACHELLI, M. Hyaluronic acid grafting mitigates calcification of glutaraldehyde-fixed bovine pericardium. **Journal of Biomedical Materials Research – Part A**, vol.70, p.159–165, 2004.

OKTAY, E.O.; DEMIRALP, B.; DEMIRALP, B.; SENEL, S.; AKMAN, A.; ERATALAY, K.; AKINCIBAY, H. Effects of platelet-rich plasma and chitosan combination on bone regeneration in experimental rabbit cranial defects. **Journal of Oral Implantology**, vol.36, p.175–184, 2010.

OUYANG, W.; BUSCHMANN, M.; CHEVRIER, A. Soluble physiological chitosan formulations combined with platelet-rich plasma (PRP) for tissue repair. **United States Patent Application Publication: U.S. 0,004,474 A1**, 2013.

PAK, J.; CHANG, J-J.; LEE, J.H.; LEE, S.H. Safety reporting implantation of autologous adipose tissue-derived stem cells with platelet-rich plasma into human articular joints. **BMC Musculoskeletal Disorders**, vol.14, n.337, p.1-8, 2013.

PAVIA, F.C.; CARRUBBA, V.L.; PICCAROLO, S.; BRUCATO, V. Characterization of Chitosan Based Hybrid Nanofiber Scaffolds for Tissue Engineering. **Journal of Biomedical Materials Research – Part A**, vol.86, n.2, p.459–466, 2008.

PELTOLA, S.M.; MELCHELS, F.P.; GRIJPMMA, D.W.; KELLOMÄKI, M. A review of rapid prototyping techniques for tissue engineering purposes. **Annals of Medicine**, vol.40, n.4, p.268-280, 2008.

PIRES, A.M.B.; MACEDO, A.C.; EGUCHI, S.Y.; SANTANA, M.H.A. Microbial production of hyaluronic acid from agricultural resource derivatives. **Bioresource Technology**, vol.101, p.6506-6509, 2010.

RADICE, F.; YÁNEZ, R.; GUTIÉRREZ, V.; ROSALES, J.; PINEDO, M.; CODA, S. Comparison of Magnetic Resonance Imaging Findings in Anterior Cruciate Ligament Grafts With and Without Autologous Platelet-Derived Growth Factors. **Arthroscopy: The Journal of Arthroscopic and Related Surgery**, vol.26, n.1, p.50-57, 2010.

REIS, R.L.; NEVES, N.M.; MANO, J.F.; GOMES, M.E.; MARQUES, A.P.; AZEVEDO H.S. (Eds.). **Natural-based polymers for biomedical applications**. Cambridge: Woodhead Publishing, 2008.

REN, D.; YI, H.; WANG, W.; MA, X. The enzymatic degradation and swelling properties of chitosan matrices with different degrees of N-acetylation. **Carbohydrate Research**, vol.340, p.2403-2410, 2005.

ROMAGNOLI, M.; BELMONTESI, M. Hyaluronic acid-based fillers: theory and practice. **Clinics in Dermatology**, vol.26, p.123-159, 2008.

ROSSI, S.; FACCENDINI, A.; BONFERONI, M.C.; FERRARI, F.; SANDRI, G.; DEL FANTE, C.; PEROTTI, C.; CAMELLA, C.M.; Sponge-like dressings based on biopolymers for the delivery of platelet lysate to skin chronic wounds. **International Journal of Pharmaceutics**, vol.440, p.207-215, 2013.

RUHELA, D.; RIVIERE, K.; SZOKA JR, F.C. Efficient synthesis of an aldehyde functionalized hyaluronic acid and its application in the preparation of hyaluronan-lipid conjugates. **Bioconjugate Chemistry**, p.17, p.1360-1363, 2006.

SACHLOS, E.; CZERNUSZKA, J.T. Making tissue engineering scaffolds work. Review on the application of solid freeform fabrication technology to the production of tissue engineering scaffolds. **European Cells & Materials**, vol.5, p.29-40, 2003.

SÁNCHEZ, M.; ANITUA, E.; AZOFRA, J.; AGUIRRE, J.J.; ANDIA, I. Intra-articular injection of an autologous preparation rich in growth factors for the treatment of knee OA: a retrospective cohort study. **Clinical and experimental rheumatology**, vol.26, p.910-913, 2008.

SCHANTÉ, C.E.; ZUBER, G.; HERLIN, C.; VANDAMME, T.F. Chemical modifications of hyaluronic acid for the synthesis of derivatives for a broad range of biomedical applications. **Carbohydrate Polymers**, vol.85, p.469–489, 2011.

SECHRIEST, V.F.; MIAO, Y.J.; NIYIBIZI, C.; WESTERHAUSEN-LARSON, A.; MATTHEW, H.W.; EVANS, C.H.; FU, F.H.; SUH, J.K. GAG-augmented polysaccharide hydrogel: A novel biocompatible and biodegradable material to support chondrogenesis. **Journal of Biomedical Materials Research – Part A**, vol.49, p.534–541, 1999.

SEOL, Y.J.; LEE, J.Y.; PARK, Y.J.; LEE, Y.M.; YOUNG, K.; RHYU, I.C.; LEE, S.J.; HAN, S.B.; CHUNG, C.P.; Chitosan sponges as tissue engineering scaffolds for bone formation. **Biotechnology Letters**, vol.26, p.1037-1041, 2004.

SHEN, E.C.; CHOU, T.C.; GAU, C.H.; TU, H.P.; CHEN, Y.T.; FU, E. Releasing growth

factors from activated human platelets after chitosan stimulation: a possible bio-material for platelet-rich plasma preparation. **Clinical Oral Implants Research**, vol.17, p.572–578, 2006.

SHEN, F.; CUI, Y.L.; YANG, L.F.; YAO, K.D.; DONG, X.H.; JIA, W.Y.; SHI, H.D. A study on the fabrication of porous chitosan/gelatin network scaffold for tissue engineering. **Polymer International**, vol.49, p.1596-1599, 2000.

SHU, X.Z.; ZHU, K.J. Controlled drug release properties of ionically cross-linked chitosan beads: the influence of anion structure. **International Journal of Pharmaceutics**, vol.233, p.217–225, 2002.

SILVA, H.S.R.C.; DOS SANTOS, K.S.C.R.; FERREIRA, E.I. Quitosana: derivados hidrossolúveis, aplicações farmacêuticas e avanços. **Química Nova**, vol.29, n.4, p.776-785, 2006.

SINGH, A.; ALI, S.; MAHDI, A.A.; SRIVASTAVA, R.N. Role of Platelets Rich Plasma in Management of Osteoporotic Fractures. **Annual Research & Review in Biology**, vol.4, n.8, p.1187-1210, 2014.

TABATA, Y. Tissue regeneration based on growth factor release. **Tissue engineering**, vol.9, n.1, p.S5-15, 2003.

TSAY, R.C.; VO, J.; BURKE, A.; EISIG, S.B.; LU, H.H.; LANDESBURG, R. Differential Growth Factor Retention by Platelet-Rich Plasma Composites. **Journal of Oral and Maxillofacial Surgery**, vol.63, p.521-528, 2005.

VAN ARK, M.; VAN DEN AKKER-SCHEEK, I.; MEIJER, L.T.B; ZWERVER, J. An exercise-based physical therapy program for patients with patellar tendinopathy after platelet-rich plasma injection. **Physical Therapy in Sport**, vol.14, p.124-130, 2013.

VAN PHAM, P.; BUI, K.H.; NGO, D.Q.; VU, N.B.; TRUONG, N.H.; PHAN, N.L-C.; LE, D.M.; DUONG, T.D.; NGUYEN, T.D.; LE, V.T.; PHAN, N.K. Activated platelet-rich plasma improves adipose-derived stem cell transplantation efficiency in injured articular cartilage. **Stem Cell Research & Therapy**, vol.4, n.4, p.91-102, 2013.

VENKATESAN, J.; RYUA, B.; SUDHAC, P.N.; KIMA, S-K. Preparation and characterization of chitosan–carbon nanotube scaffolds for bone tissue engineering. **International Journal of Biological Macromolecules**, vol.50, p.393– 402, 2012.

VINDIGNI, V.; CORTIVO, R.; IACOBELLIS, L.; ABATANGELO, G.; ZAVAN, B.; Hyaluronan Benzyl Ester as a Scaffold for Tissue Engineering. **International Journal of Molecular Sciences**, vol.10, p.2972-2985, 2009.

WEST, D.C.; HAMPSON, IN.; ARNOLD, F.; KUMAR, S. Angiogenesis induced by degradation products of hyaluronic acid. **Science**, vol.228, p.1324–1326, 1985.

YAMANE, S.; IWASAKI, N.; MAJIMA, T.; FUNAKOSHI, T.; MASUKO, T.; HARADA, K.;

MINAMI, A.; MONDE, K.; NISHIMURA, S-I. Feasibility of chitosan-based hyaluronic acid hybrid biomaterial for a novel scaffold in cartilage tissue engineering. **Biomaterials**, vol.26, p.611–619, 2005.

YARAK, S.; OKAMOTO, O.K. Células-tronco derivadas de tecido adiposo humano: desafios atuais e perspectivas clínicas. **Anais Brasileiros De Dermatologia**, vol.85, n. 5, p.647-56, 2010.



# CAPÍTULO 3 – PERFORMANCE OF PRP ASSOCIATED WITH POROUS CHITOSAN AS A COMPOSITE SCAFFOLD FOR REGENERATIVE MEDICINE

---

Artigo publicado em fevereiro de 2015 no periódico *The Scientific World Journal*.

Andréa Arruda Martins Shimojo, Amanda Gomes Marcelino Perez, Sofia Elisa Moraga Galdames, Isabela Cambraia de Souza Brissac and Maria Helena Andrade Santana\*

Department of Engineering of Materials and of Bioprocesses, School of Chemical Engineering, UNICAMP, P.O. Box 6066, 13083-970 Campinas, SP, Brazil

\*Correspondence should be addressed to Maria Helena Andrade Santana; [mariahelena.santana@gmail.com](mailto:mariahelena.santana@gmail.com)

**Abstract.** This study aimed to evaluate the *in vitro* performance of activated platelet-rich plasma associated with porous sponges of chitosan as a composite scaffold for proliferation and osteogenic differentiation of human adipose tissue-derived mesenchymal stem cells. The sponges were prepared by controlled freezing ( $-20$ ,  $-80$ , or  $-196^{\circ}\text{C}$ ) and lyophilization of chitosan solutions (1, 2, or 3% w/v). The platelet-rich plasma was obtained from controlled centrifugation of whole blood and activated with calcium and autologous serum. The composite scaffolds were prepared by embedding the sponges with the activated platelet-rich plasma. The results showed the performance of the scaffolds was superior to that of activated platelet-rich plasma alone, in terms of delaying the release of growth factors and increased proliferation of the stem cells. The best preparation conditions of chitosan composite scaffolds that coordinated the physicochemical and mechanical properties and cell proliferation were 3% (w/v) chitosan and a  $-20^{\circ}\text{C}$  freezing temperature, while  $-196^{\circ}\text{C}$  favored osteogenic

differentiation. Although the composite scaffolds are promising for regenerative medicine, the structures require stabilization to prevent the collapse observed after five days.

### **3.1. Introduction**

In tissue engineering, a scaffold is a three-dimensional matrix for the stimulation of cell proliferation and the formation of new tissue. To achieve this goal, scaffolds must meet some specific requirements such as mimicking the native extracellular matrix (ECM) of the target tissue; allowing cell attachment, migration, proliferation, and differentiation and maintenance of the target phenotype; promoting vascularization and nutrient delivery; and having a biodegradation rate and mechanical properties that are adequate to support the formation of the new tissue (Langer & Vacanti, 1993).

According to Crane & Everts (2008), tissue regeneration is based on a proliferation triangle composed of the three fundamental elements: cells, growth factors (GFs) and scaffolds, which are in a close relationship through their capabilities. Thus, scaffolds provide the conductive matrix for supporting the genic capability of progenitor cells mediated by the inductive capability of GFs (Chen *et al.*, 2002). Optimal conditions for tissue regeneration must come from the interaction of the properties of those elements.

The cell responses to the surface chemistry of scaffolds depend on their hydrophobicity, protein adsorption, surface charge, and roughness, softness, and stiffness. Additionally, the porous architecture characterized by the pore size, porosity, connectivity, and tortuosity plays important roles, as described and discussed by Chang & Wang (2011). Therefore, bringing together all these properties in solid scaffolds is an enormous technological challenge.

The fibrin matrix is the natural scaffold formed from the coagulation cascade in the healing process. Under injury, thrombin cleaves the soluble plasma protein fibrinogen into peptide fragments, yielding insoluble fibrin peptides that aggregate and form fibrils. A fibrin network is then formed, which entraps platelets and other blood components (Bensaïd *et al.*, 2003; Weisel & Nagaswami, 1992). Calcium acts as a

cofactor of thrombin, modulates the elongation of fibers during polymerization by promoting lateral branching, and functions in clot stability (Falvo *et al.*, 2010; Ryan *et al.*, 1999). Calcium and thrombin also activate platelets, allowing the release of GFs and cytokines. Therefore, the fibrin matrix provides an optimized medium for cell proliferation and healing.

Based on these features, platelet-rich plasma (PRP) has been widely used in regenerative medicine. PRP is an autologous product prepared from whole blood by separating the red blood cells and concentrating the platelets and other components of plasma. However, although viscoelastic, the fibrin matrix alone lacks stability to be efficient when regenerative medicine is the goal.

To mimic the natural healing process and improve the stability of the fibrin matrix, we propose in this work the use of the fibrin network from activated PRP with porous chitosan as a composite scaffold for tissue regeneration.

Our hypothesis is that the chemical nature of the chitosan surface supports the fibrin network by electrostatic attachment, thus prolonging its stability, without changing the paracrine affinity of mesenchymal cells to fibrin fibers. As a consequence, the composite scaffold must improve cell proliferation and tissue differentiation compared to PRP alone.

Related works showed the effects of chitosan on blood coagulation through the strong adhesion of platelets to the surface of chitosan particles, as well as chitosan (0.1–1mg/mL) incorporated with PRP to enhance the release of PDGF-AB and TGF- $\beta$ 1 from platelets (Kojima *et al.*, 2004; Okamoto *et al.*, 2003). Shen *et al.* (2006) demonstrated that chitosan could be an appropriate substitute for thrombin, as an agonist in PRP preparation. Chang *et al.* (2009) showed that growth factors could sustain release until 12 h at approximately 1 ng/mL from chitosan/CaSO<sub>4</sub>/PRP microspheres after activation with thrombin. Kutlu *et al.* (2012) showed that scaffolds prepared by the freeze-drying of PRP added to chitosan gel (2% w/v) were more effective than chitosan sponges soaked with PRP on controlled GF release. Oktay *et al.* (2010) applied PRP-embedded chitosan sponges to defects and showed a histological tendency toward increased bone formation. Mathews *et al.* (2011) demonstrated that chitosan enhanced mineralization by upregulating the genes associated with

mineralization and calcium-binding proteins.

Chitosan is a polysaccharide derived from chitin (copolymers  $\beta$ -(1 $\rightarrow$ 4)-2-amino-2-deoxy-D-glucose and  $\beta$ -(1 $\rightarrow$ 4)-2-acetamido 2-deoxy-D-glucose) found in the shells of marine crustaceans and insects and the cell walls of some fungi (Muzzarelli, 1973; Berger *et al.*, 2004).

In the last ten years, considerable attention has been given to chitosan-based materials in the field of tissue engineering (Nwe *et al.*, 2009; Martins *et al.*, 2014). The beneficial properties of chitosan have been proven, such as biodegradability (Nordtveit *et al.*, 1996; Koga, 1998), biocompatibility (Molinaro *et al.*, 2002; R cker *et al.*, 2006), antibacterial activity (Muzzarelli *et al.*, 1990; Li *et al.*, 2013), cell adhesion (He *et al.*, 1998; Bertram & Bodmeier, 2006), and wound healing properties (Antonov *et al.*, 2008; Dai *et al.*, 2011). Moreover, the chemical nature of chitosan gives many possibilities for ionic and covalent modifications that allow for the modulation of the mechanical and biological properties of biomaterials (Agnihotri *et al.*, 2004; Adekogbe & Ghanem, 2005).

Regarding the technological aspects, chitosan can be easily processed in diverse forms in the absence of toxic solvents, such as films (Mucha *et al.*, 2012), sponges (Madihally & Matthew, 1999; Amaral *et al.*, 2006), fibers (Majima *et al.*, 2007), beads (Shu & Zhu, 2002), hydrogels (Tan *et al.*, 2009), and microparticles/nanoparticles (Lavertu *et al.*, 2006). Furthermore, chitosan supports sterilization (Rao & Sharma, 1995), is abundant in nature, and requires only low-cost processing in nonaggressive ecological conditions before being used as a raw material (Berger *et al.*, 2004).

Freeze-drying is the most common and simplest method to produce porous chitosan scaffolds. The freezing process provides the nucleation of ice crystals from solution and further growth along the lines of thermal gradients. Exclusion of the chitosan acetate salt from the ice crystal phase and subsequent ice removal by lyophilization generate a porous material (Cardea *et al.*, 2010; Costa-Pinto *et al.*, 2011).

Madihally & Matthew (1999) reported that the pore size of chitosan scaffolds produced by lyophilization can be controlled within the range of 1–250  $\mu\text{m}$ . A more uniform and interconnected pore structure can be obtained when lower freezing temperatures are used. Furthermore, the pore orientation is related to the geometry of the moldings used and can also be controlled by changing thermal gradients during

freezing (Shen *et al.*, 2000).

The microstructure, crystallinity, and mechanical strength of the porous chitosan matrix also can be controlled by the chitosan concentration, molecular weight, and deacetylation degree (Madhally & Matthew, 1999; Nettles *et al.*, 2002).

In this work, the effects of PRP association were studied regarding to the porous structure of solid sponges, which were produced by varying chitosan concentration and freezing conditions. The biological performance of association was evaluated in terms of growth factor release kinetics, proliferation, and osteogenic differentiation of seeded human adipose tissue-derived mesenchymal stem cells (h-AdMSCs).

## **3.2. Experimental**

### **3.2.1. Materials**

Chitosan (average molecular weight [Mw] =  $4 \times 10^5$  Da, degree of deacetylation =  $83 \pm 4\%$ ) was purchased from Polymar (Fortaleza, CE, Brazil) and purified according to the protocol described by Nasti *et al.* (2009). Other chemicals were of reagent grade and were used without any further purification. All biological experiments were performed with human adipose tissue-derived stem mesenchymal cells (h-AdMSCs) and approved by the Ethics Committee of the Medical Sciences School of the University of Campinas (UNICAMP; CAAE: 0972.0.146.000-11). The donors were healthy individuals aged between 30 and 40 years old who were previously assessed through clinical examinations.

### **3.2.2. Methods**

#### **3.2.2.1. Preparation of Porous Chitosan Scaffolds (PCHTs)**

PCHTs were prepared by freezing at a controlled temperature of a chitosan solution previously poured in 24-well culture plates (TPP, polystyrene, diameter = 15.4 mm) to give them a cylindrical shape, followed by lyophilizing in lyophilizer L101 (Liobras, São Carlos, SP, Brazil) at a temperature of approximately  $-30^\circ\text{C}$  for 48 hours.

*Effects of Chitosan Concentration.* Chitosan solutions with concentrations of 1, 2, or 3% (w/v) were prepared by dissolution in 0.2 mol.L<sup>-1</sup> acetic acid for 24 hours at room temperature. The solutions were frozen at -20°C for 24 hours and lyophilized.

*Effects of Freezing Conditions.* Chitosan solution (3% w/v) was prepared as previously described. The solution was frozen at -20°C in a freezer for 24 hours; -80°C in an ultrafreezer for 24 hours; or -196°C by immersion in liquid N<sub>2</sub>; and lyophilized.

#### 3.2.2.2. Characterization of Porous Chitosan Scaffolds (PCHTs)

*Morphology and Pore Size.* The morphology of PCHTs was evaluated by scanning electron microscopy (SEM) using an LEO 440i Electron Microscopy/Oxford (Cambridge, England) operated at 5 kV accelerating voltage. The scaffolds were gold-coated using a sputter coater POLARON SC7620, VG Microtech (Uckfield, England) for 180 s at a current of 3 mA. Pore size ( $n = 20$ ) was measured using software Image J 1.47t.

*Mechanical Properties.* Mechanical compression tests of PCHTs ( $n = 3$ ) were performed using a Universal Testing Machine, MTS model 810-Flex Test 40 (MTS Systems Corporation, Eden Prairie, MN, USA) up to 60% strain, according to Correia *et al.* (2011). The testing machine was equipped with a 1.5 kN load cell, and the loading rate was 5 mm/min. Young's modulus was calculated in the initial linear section of the stress-strain curve, when the strain was lower than 10%.

*Degradation in PBS.* The degradation profile of the PCHTs in PBS at 37°C was performed by the gravimetric method described by Tang & Spector (2007) through measurements of loss weight.

*Water Sorption.* The water sorption was determined by swelling of PCHTs (previously weighted) in PBS (LB Laborclin, Pinhais, PR, Brazil) at pH 7.4 for 24 hours at 37°C. The swollen PCHTs were weighed after the removal of excess water by keeping the surfaces on a filter paper. The swelling ratio (SR) was also calculated using

Equation (1):

$$SR = \frac{ws}{wd} \quad \text{Equation (1)}$$

where  $ws$  and  $wd$  are the weights of the scaffolds in the swelled state and the dry state, respectively.

*Porosity.* The porosity ( $\varepsilon$ ) of the PCHTs was determined according to the protocol used by Wang *et al.* (2003) and calculated by Equation (2):

$$\varepsilon (\%) = \frac{Vm - \left(\frac{wm}{\rho}\right)}{Vm} \times 100 \quad \text{Equation (2)}$$

where  $Vm$  is the total volume of PCHTs ( $\text{cm}^3$ ),  $\rho$  is the density of nonporous CHT ( $1.342 \text{ g/cm}^3$ ), and  $wm$  is the weight of sponge (g). Values are expressed as the mean  $\pm$  standard deviation ( $n = 3$ ).

*Cell Compatibility.* The compatibility was carried out by exposing PCHTs to h-AdMSCs followed by cultivation at  $37^\circ\text{C}$  for 24 hours and evaluation by MTT assay (3-[4,5-dimethyl-thiazol-2-yl]-2,5-diphenyltetrazolium bromide) (MTT, Molecular Probes) according to a modified Mosmann method (1983). The MTT assay is a colorimetric test based on the reduction of yellow tetrazolium salt into a purple formazan product in presence of cells (Gümüdereliolu & Aday, 2011).

### 3.2.2.3. PRP Preparations

*PRP Concentration.* P-PRP (plasma rich in platelets and poor in leukocytes) was prepared according to Perez *et al.* (2013). Briefly, whole blood (WB) was collected into 3.5 mL vacuum tubes (Vacuette, Campinas, SP, Brazil) containing sodium citrate 3.2% (w/v) as an anticoagulant. WB was initially centrifuged in a Rotina 380R centrifuge (Hettich Zentrifugen, Tuttlingen, Germany) at  $100 \times g$  for 10 minutes at  $25^\circ\text{C}$ . After the formation of three layers (a bottom layer composed mainly of red blood cells (RBCs); an upper layer composed of plasma, platelets, and some WB cells; and an intermediate

layer, or buffy coat, composed mostly of WB cells), only the upper layer was collected to obtain PPRP. The concentration of platelets, WB cells, and RBCs in WB and P-PRP were determined using the ABX Micros ES 60 hematology analyzer (HORIBA ABX Diagnostics, Montpellier, France).

*P-PRP Activation.* Activated P-PRP (*aP-PRP*) was obtained by adding autologous serum (Ser) and 10% (w/v) CaCl<sub>2</sub> solution as agonists using the following proportions: agonist/P-PRP = 20% (v/v), Ser/CaCl<sub>2</sub> volumetric ratio = 9. Autologous serum was prepared by collecting 5 mL of WB in tubes without anticoagulant. After 30 minutes to form clots, WB was centrifuged at 2000 ×g for 10 minutes (Perez *et al.*, 2014).

#### 3.2.2.4. The Composite Scaffolds (*aP-PRP/PCHTs*)

*Preparation.* *aP-PRP/PCHTs* was prepared for embedding by dripping *aP-PRP*, immediately after activation, into PCHTs. The preparation was carried out in 48-well microplates using a ratio of 200 µL of *aP-PRP* to 10–20 mg of PCHTs.

*Release of GFs.* The release of platelet-derived growth factor AB (PDGF-AB) and transforming growth factor β1 (TGF-β1) was performed after 1 hour of gelation of *aP-PRP* associated with PCHTs in the presence of the culture medium (Dulbecco's Modified Eagle's Medium (DMEM-LG) (Gibco, Grand Island, NY, USA) with low glucose concentration). The culture medium (1.5 mL) was added to *aP-PRP/PCHTs* in 48-well microplates, which were maintained in an incubator with 5% CO<sub>2</sub> throughout the assays. The total volume of culture medium was withdrawn at 3, 6, 12, 24, and 72 hours, and the same volume of fresh medium was replaced without removing the hydrogels from the wells. The samples were stored at -80°C for further characterization. The concentrations of the released GFs PDGF-AB and TGF-β1 were measured using enzyme-linked immunosorbent assay (ELISA) kits (R&D Systems, Minneapolis, MN, USA) according to the manufacturer's instructions and specifications.

*h-AdMSCs Proliferation.* The cultivation of h-AdMSCs was carried out in 24-well



tissue culture plates by adding 1 mL DMEM to the seeded composite scaffolds ( $n = 4$ ). The composite scaffolds seeded were maintained at 37°C for 10 days. Cell proliferation was quantified using the thiazolyl blue tetrazolium bromide (MTT) assay. At 3, 5, 7, and 10 cultivation days, the composite scaffolds were removed and transferred to 24-well plates. MTT (1 mL of 1 mg/mL) was then added, and the cultivation proceeded at 37°C for 4 hours. The MTT solution was then discarded, and 1 mL of DMSO was added to dissolve the purple formazan crystals. The samples were shaken at 120 rpm for 30 min to ensure homogeneous dissolution of the formazan dye, and then 200  $\mu$ L of each sample was transferred to a 96-well plate. Optical density was measured at 595 nm using a microplate reader (Filter Max F5, Molecular Devices). The isolation and pre-cultivation of h-AdMSCs as well as the cell seeding were performed as described below.

*h-AdMSCs Isolation and Pre-cultivation.* Human subcutaneous adipose tissue that was initially acquired from liposuction surgery was washed with sterile PBS, separated into fractions of 10 g, digested with 20 mg of collagenase type 1A and maintained in 20 mL of DMEM-LG containing 10% BSA (bovine serum albumin) and 10  $\mu$ L of gentamicin for 30 min in a 37°C bath. After complete digestion, the reaction was quenched with 10 mL fetal bovine serum (FBS) and immediately centrifuged for 15 min at 1500 rpm. The supernatant was discarded, and the pellet was suspended in 10 mL DMEM-LG with 10% FBS. After pre-cultivation for 24 h, the culture medium was changed every 3 days; after the fourth passage, the cells were characterized by immunophenotyping (data not shown) using flow cytometry and according to their adipogenic, osteogenic, and chondrogenic differentiation and then used in the subsequent experiments.

*h-AdMSCs-Seeding.* The pre-cultured h-AdMSCs were trypsinized and resuspended in P-PRP to a final cell concentration of  $1 \times 10^4$  cells/mL. P-PRP containing h-AdMSCs was activated and immediately embedded to the PCHTs in a 24-well tissue culture plate, using 200  $\mu$ L of h-AdMSCs +  $\alpha$ P-PRP per 10–20 mg of PCHTs. The composite scaffolds with h-AdMSCs were kept at room temperature for 45 minutes for consolidation of the fibrin network. Pure PRP was used as control.

### 3.2.2.5. Images of the h-AdMSCs-Seeded Composite Scaffolds

The images of the cell-seeded composite scaffolds were obtained by scanning electron microscopy after 5 days of h-AdMSCs proliferation. The cell-seeded composite scaffolds were fixed in a solution of 4% paraformaldehyde and 2.5% glutaraldehyde in phosphate buffer, pH 7.4, for 2 hours. The samples were then dehydrated in ethanol for 15 min intervals in aqueous 50%, 70%, 95%, and 100% ethanol solutions (2x) and dried at the critical point dryer BAL-TEC CPD 030 (Schalksmühle, Germany). After gold coating (Sputter Coater POLARON, SC7620, VG Microtech), the cell-seeded composite scaffolds were visualized with a SEM (Leo440i, LEO) with an accelerating voltage of 20 kV.

### 3.2.2.6. Induction of Osteogenic Differentiation

h-AdMSCs seeded in the composite scaffolds were induced to differentiate into the osteogenic lineage by providing the osteogenic medium containing DMEM-LG supplemented with 10% FBS, 1%  $\beta$ -glycerol-phosphate (Sigma-Aldrich, St. Louis, MO, USA), 1% L-ascorbic acid (Sigma-Aldrich, St. Louis, MO, USA), 1% dexamethasone (Sigma-Aldrich, St. Louis, MO, USA), and 1% penicillin/streptomycin solution (Gibco, Grand Island, NY, USA). The medium was changed every 7 days.

*Evaluation of Differentiation.* Differentiation was evaluated by measuring the alkaline phosphatase activity (ALP) on day 14. The supernatant (200  $\mu$ L) was collected and mixed with the same volume of p-nitrophenyl phosphate (SIGMAFAST p-nitrophenyl phosphate tablets, Sigma, Saint Louis, MO, USA) as substrate and incubated at room temperature for 30 minutes. Absorbance was read immediately at 405 nm.

### 3.2.2.7. Statistical Analysis

Each experiment was carried out in triplicate unless otherwise specified. All results are presented as the mean  $\pm$  standard deviation (SD). The experimental data from all the studies were analyzed using Analysis of Variance (ANOVA). Statistical significance was set to  $P$  value  $\leq 0.05$ .

## 3.3. Results and Discussion

### 3.3.1. Experimental Design

In this study, we prepared novel composite scaffolds by association of PRP with the 3D-porous structure of chitosan. First, different 3D-porous structures of chitosan (PCHTs) were prepared by freeze-drying by varying the CHT concentration and freezing conditions (temperature and freezing rate). Second, the microstructure and mechanical properties of the PCHTs were characterized and evaluated for cell compatibility. The surface chemistry, hydrophilicity, and positive charge of  $-NH_2$  groups in acidic medium were maintained unaltered.

The composite scaffolds (*a*P-PRP/PCHTs) were obtained by embedding the PCHTs with immediately activated P-PRP in a 24-well microplate. The release of the GFs (PDGF-AB and TGF- $\beta$ 1) from the composite scaffolds was evaluated in DMEM culture medium. Afterwards, pre-cultured h-AdMSCs were added to PRP before activation in order to obtain cell-seeded composite scaffolds. In vitro examination of h-AdMSCs proliferation kinetics was performed over 10 days by using the cell-seeded composite scaffolds in DMEM. Additionally, osteogenic differentiation was evaluated by ALP activity measurements after 14 days. Thus, we verified the correlation between the structure and function of PCHTs by controlling the concentration and freezing conditions of chitosan solution.

### 3.3.2. Effects of Freezing Conditions and Chitosan Concentration on PCHTs

#### 3.3.2.1. Images of Porous Structure

Figures 10(a) – 10(c) show images of the porous structure from controlled freezing at  $-20^\circ\text{C}$  by varying the concentration of the chitosan solution (1, 2, or 3%) and subsequent lyophilization. The images show highly porous structures with rounded pores that interconnected, regardless of CHT concentration. Differences in chitosan molecular weight, deacetylation degree, and purity make difficult comparisons even for

similar treatment. Madihally & Matthew (1999) showed a higher pore interconnectivity degree and more open pores for 1% (w/w) chitosan concentration for a similar deacetylation degree, but other properties were not characterized.

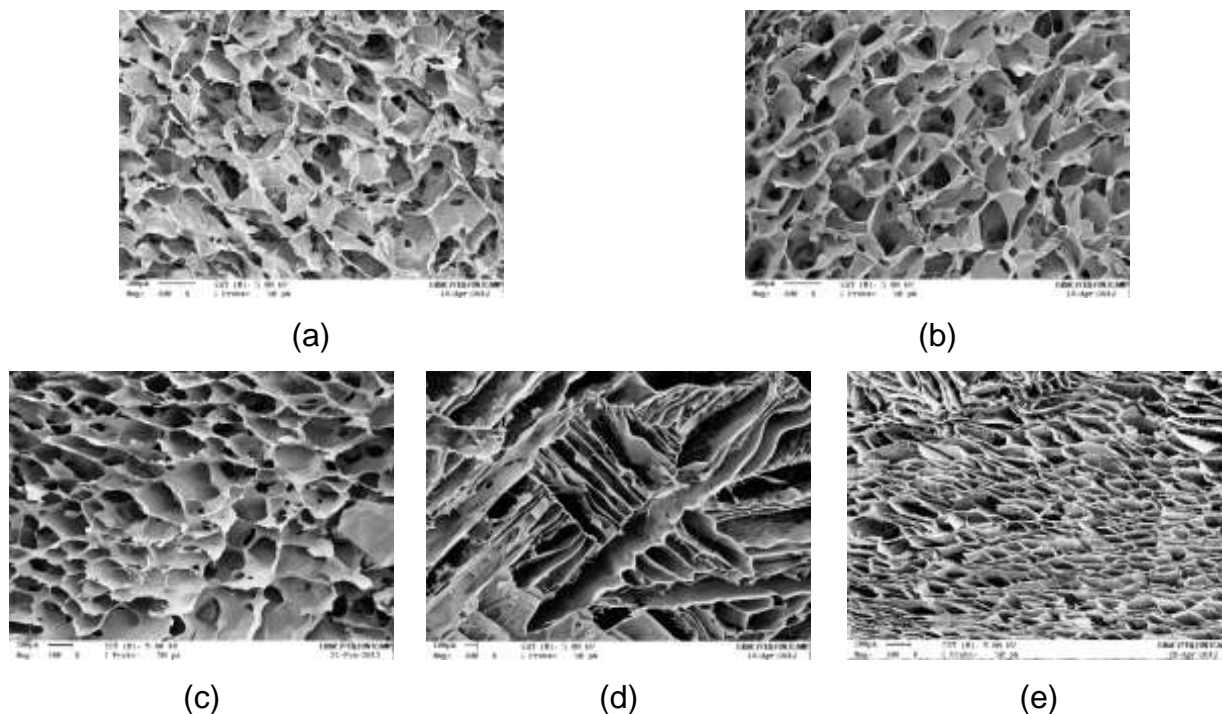


**Figure 10.** SEM micrographs of PCHTs. Cross-sectional morphologies of (a) PCHTs 1% ( $-20^{\circ}\text{C}$ ); (b) PCHTs 2% ( $-20^{\circ}\text{C}$ ); (c) PCHTs 3% ( $-20^{\circ}\text{C}$ ); (d) PCHTs 3% ( $-80^{\circ}\text{C}$ ); and (e) PCHTs 3% ( $-196^{\circ}\text{C}$ ). Original magnification is  $\times 100$  and the scale bar represents  $200\ \mu\text{m}$ .

Freezing conditions produced a more prominent effect on the morphology of the pores [Figures 10(d) – 10(e)] attributed the variations in the freezing rate used to achieve the temperatures evaluated. In contrast with rounded pores at  $-20^{\circ}\text{C}$  (3% CHT) [Figure 10(c)], we observed pores with leaf structure at  $-80^{\circ}\text{C}$  [Figure 10(d)], while smaller and elongated open pores were produced at  $-196^{\circ}\text{C}$  [Figure 10(e)]. In all cases, the pores were uniformly distributed and radially oriented and had a high degree of interconnectivity.

The pore structures allow uniform cell spatial distribution throughout the scaffold, facilitating homogeneous tissue formation. Moreover, the differences in pore morphologies obtained are suitable to several cell lineage and type of tissue to be

regenerated.

### 3.3.2.2. Characterization of PCHTs

*Physicochemical and Mechanical Properties.* Table 1 shows physicochemical characterization of the PCHTs. At  $-20^{\circ}\text{C}$ , the mean diameter of rounded pores could be controlled around the 300–400  $\mu\text{m}$ , regardless of the CHT concentration, although there is a large distribution.

However, the elongated pores from Figures 10(d) – 10(e) were markedly decreased with freezing conditions from 2615  $\mu\text{m}$  ( $-80^{\circ}\text{C}$ ) to 280  $\mu\text{m}$  ( $-196^{\circ}\text{C}$ ) because crystal growth and hence pore size are functions of both heat and mass transfer rates, determined by the temperature and freezing rate. At  $-80^{\circ}\text{C}$ , the observed differences in pore shape and size suggest parallel ice crystal growth, which in turn was caused by the strongly one-dimensional nature of the thermal gradients established during freezing, as discussed by Madihally & Matthew (1999).

The diverse nature of tissue architectures requires scaffolds with optimal pore sizes, such as 5  $\mu\text{m}$  for neovascularization (Brauker *et al.*, 1995), 5–15  $\mu\text{m}$  for fibroblast ingrowth (Klawitter & Hulbert, 1971), 20  $\mu\text{m}$  for the ingrowth of hepatocytes (Yang *et al.*, 2001), 200–900  $\mu\text{m}$  for osteoconduction (Salgado *et al.*, 2004), and 20–125  $\mu\text{m}$  for regeneration of adult mammalian skin (Yannas *et al.*, 1989).

According to these data, the rounded pores obtained at  $-20^{\circ}\text{C}$  or elongated at  $-196^{\circ}\text{C}$  are adequate for bone tissue, although other properties could also influence the choice. Moreover, because human adipose tissue-derived mesenchymal stem cells (h-AdMSCs) exhibit a spindle-like shape and are 80–100  $\mu\text{m}$  in diameter and  $\sim 200$   $\mu\text{m}$  in length (Chavez-Munoz *et al.*, 2013), the range of pore sizes in our PCHTs allows cells to migrate freely into the scaffolds, favoring the formation of a new tissue.

**Table 1.** Physicochemical characterization of PCHTs.

CHT concentration (%)	Freezing temperature (°C)	Swelling ratio (n=3)	Pore size (µm) (n=20)	Porosity (%) (n=3)	Young's Moduli (MPa) (n=3)
1	-20	6.5 ± 0.4	425 ± 102	97.1 ± 0.3	0.037 ± 0.002
2	-20	5.5 ± 0.9	418 ± 113	94.7 ± 0.8	0.5 ± 0.1
3	-20	4.7 ± 0.9	336 ± 138	93.1 ± 0.5	1.1 ± 0.1
3	-80	5.1 ± 0.9	2615 ± 600*	91.7 ± 0.3	0.28 ± 0.01
3	-196	6.4 ± 0.6	280 ± 62*	92.5 ± 0.1	1.01 ± 0.05

\*mean longitudinal size.

The porosity is also an important aspect of cell migration and proliferation, guiding and promoting the formation of new tissue. Porosity is defined as the percentage of void space in a solid and is a morphological property independent of material (Léon y Léon, 1998). A porosity higher than 90% and pore interconnectivity are basic requirements for scaffolds in tissue engineering because they affect the diffusion of physiological nutrients and gases to and the removal of metabolic waste and byproducts from cells that have penetrated the scaffold (Leong *et al.*, 2003; Liu & Ma, 2004). Moreover, the porosity often compromises the mechanical and structural stability of the scaffolds and must be evaluated in accordance with the application and degradation rate of materials utilized (Loh & Choong, 2013).

The porosity values of PCHTs scaffolds ranged from 91.0 to 97.0% (Table 1), which are adequate for TE, independent of CHT concentration or freezing conditions. However, the porosity decreased with increasing chitosan concentration. The highest porosity was provided from 1% chitosan solution, but there was not a direct relationship with freezing conditions. The PCHTs prepared at -80°C showed a significantly lower porosity even with higher pore size, probably due to their leaf structure.

To guide tissue regeneration, scaffolds should also have sufficient mechanical strength during in vitro culturing to maintain the spaces required for cell in-growth and matrix elaboration (Leong *et al.*, 2003). Moreover, their mechanical properties should be similar to the properties of tissues generated to provide an adequate structural support in the stage of healing (Cheung *et al.*, 2007).

Scaffolds for the regeneration of hard tissue must exhibit a mechanical modulus in the range of 10–1,500 MPa, while scaffolds for soft tissues must exhibit a mechanical modulus in the range of 0.4–350 MPa (Hollister, 2005).

In this work, we observed a drastic decrease in Young's modulus (Table 1) with a decrease in CHT concentration. Better mechanical properties were found for a CHT concentration of 3%.

The PCHTs 3% (w/v) prepared at  $-80^{\circ}\text{C}$  showed lower mechanical strength than those prepared at  $-20^{\circ}\text{C}$  and  $-196^{\circ}\text{C}$  with the same CHT concentration, which could be attributed to its leaf structure and pore size. There was no significant difference ( $P < 0.05$ ) in mechanical properties for PCHTs 3% (w/v) frozen at  $-20^{\circ}\text{C}$  or  $-196^{\circ}\text{C}$ . Thus, the range of Young's moduli found for PCHTs suggests their application for soft tissue engineering. For hard tissues, these scaffolds must be crosslinked and/or reinforced by the addition of fillers.

The water absorption capacity (swelling ratio) of the scaffolds affects cell growth indirectly (Enrione *et al.*, 2010). The hydration of the scaffolds is a necessary step for cell incorporation and proliferation.

PCHTs scaffolds showed a high swelling capacity in PBS (pH 7.4) regardless of chitosan concentration and freezing conditions, allowing for rapid hydration when culture medium was added.

*Degradation in PBS.* Scaffold degradation is also an important parameter for the formation of new tissue. The scaffold degradation rate must be tuned appropriately with the growth rate of the new tissue in such a way that by the time the injury site is completely regenerated, the scaffold is completely degraded (Salgado *et al.*, 2004). Degradation can occur through mechanisms that involve physical or chemical processes and/or biological processes that are mediated by biological agents, such as enzymes (Langer & Vacanti, 1993).

Here, we evaluated in vitro the profile degradation of PCHTs in PBS (pH 7.4) at  $37^{\circ}\text{C}$ ; we supposed that degradation occurred by solubilization due to the presence of residual acetate molecules.

Figure 11 shows the degradation profile of PCHTs.

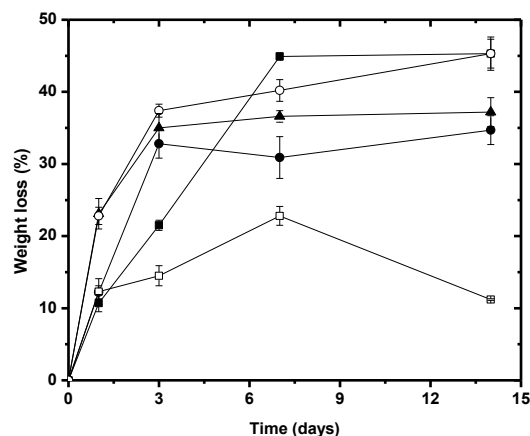


**Figure 11.** The weight loss of scaffolds with time in PBS at 37°C as a percentage of the original weight of the scaffold ( $n = 3$ ). The data are plotted with the mean  $\pm$  standard error. (■) PCHTs 1% (-20°C); (●) PCHTs 2% (-20°C); (▲) PCHTs 3% (-20°C); (□) PCHTs 3% (-80°C); and (○) PCHTs 3% (-196°C).

We observed the highest weight loss, approximately 45%, for PCHT 1% (-20°C) after 7 days, while for PCHTs 2% (-20°C), 3% (-20°C), and 3% (-196°C) weight loss was approximately 35% after 3 days. The PCHTs 3% (-80°C) showed the lowest weight loss (~20%), probably due to their leaf structure retaining lower concentration of acetate molecules.

Our results suggest that the PCHTs need further stabilization, to ensure the balance between tissue regeneration and degradation rate of the scaffold.

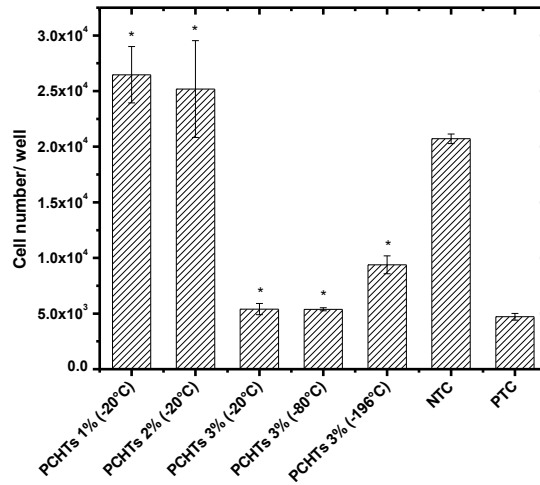
### 3.3.2.3. Cell Compatibility

Figure 12 shows the cell compatibility of h-AdMSCs cultured in the presence of PCHTs, as assayed by MTT. The results revealed no potential cytotoxicity in 24 hours for the scaffolds according to the standard values (PTC).

However, we observed lower proliferation of h-AdMSCs on PCHTs prepared with chitosan concentration of 3% (w/v) compared to the negative control.

Nevertheless, the PCHTs are potentially useful for in vivo applications regardless of CHT concentration and freezing conditions.



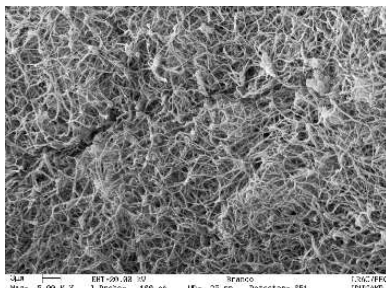


**Figure 12.** Proliferation of h-AdMSCs exposed to the PCHTs scaffolds after 24 hours of cultivation. Negative control (NTC) = DMEM with 10%FBS; positive control (PTC) =DMEM with phenol 0.5%. Mean  $\pm$  standard deviation  $n = 3$ . The population means are significantly different from positive control at  $*P < 0.05$ .

### 3.3.3. Characterization of the Composite Scaffolds

#### 3.3.3.1. Images of the Cell-Seeded $\alpha$ P-PRP/PCHTs

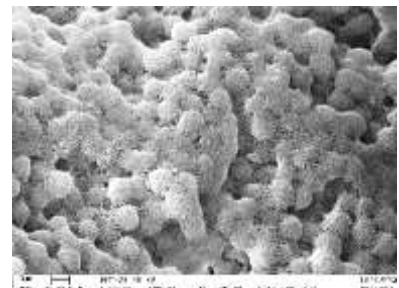
SEM characterization (Figure 13) of the  $\alpha$ P-PRP/PCHTs on the 5<sup>th</sup> day of culture showed fibrin networks covering the pores and surface of PCHTs, as a consequence of the interaction of fibrin fibers and CHT. This interaction supported cell proliferation by improving the mechanical strength of the fibrin network, in addition to providing additional surface area to cell adhesion, proliferation and differentiation.



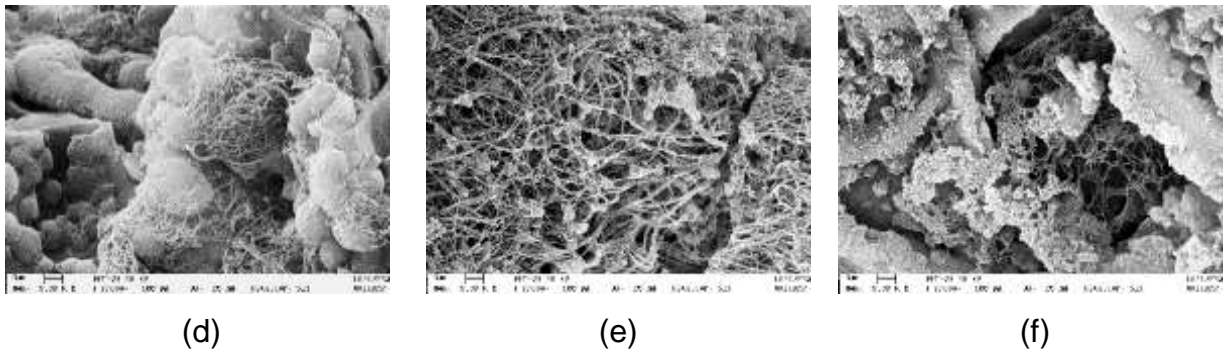
(a)



(b)



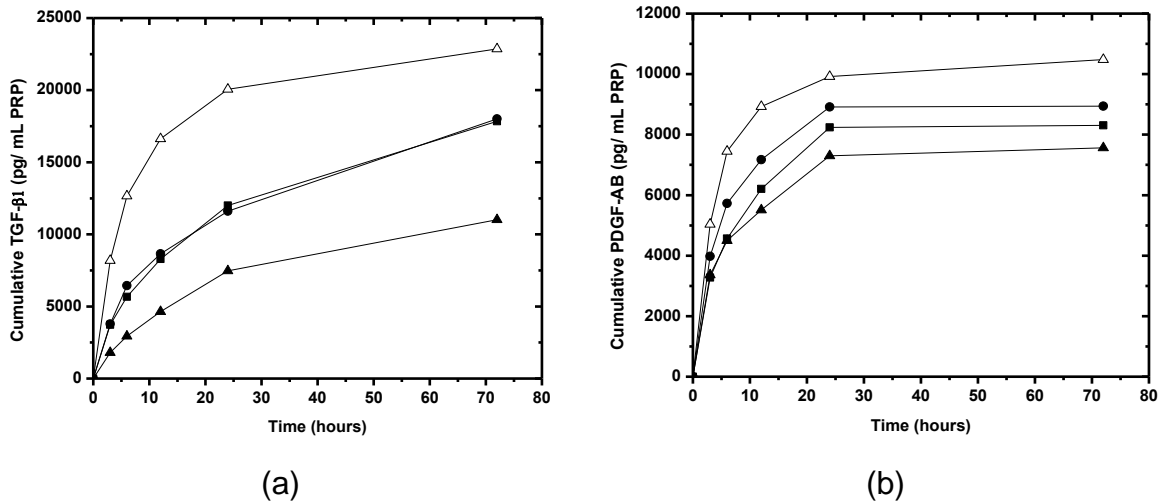
(c)

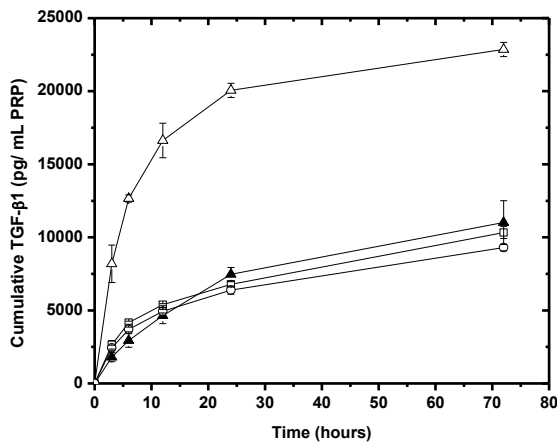


**Figure 13.** Scanning electron microscopic images of *aP-PRP/PCHTs* after 5 days of cultivation of h-AdMSCs. (a) *a-PRP*; (b) *aP-PRP/PCHTs* 1% (-20°C); (c) *aP-PRP/PCHTs* 2% (-20°C); (d) *aP-PRP/PCHTs* 3% (-20°C); (e) *aP-PRP/PCHTs* 3% (-80°C); and (f) *aP-PRP/PCHTs* 3% (-196°C). Original magnification is  $\times 5,000$  and the scale bar represents 3  $\mu\text{m}$ .

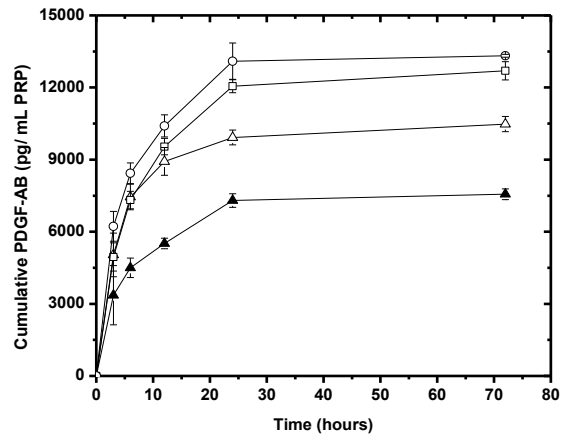
### 3.3.3.2. Growth Factor Release

Figure 14 shows PDGF-AB and TGF- $\beta 1$  release kinetics from *aP-PCHTs* determined by ELISA.





(c)



(d)

**Figure 14.** Release profiles of growth factors from  $\alpha$ P-PRP in porous chitosan scaffolds as a function of [(a), (b)] chitosan concentrations and [(c), (d)] freezing conditions. (■) PCHTs 1% ( $-20^{\circ}\text{C}$ ); (●) PCHTs 2% ( $-20^{\circ}\text{C}$ ); (▲) PCHTs 3% ( $-20^{\circ}\text{C}$ ); (□) PCHTs 3% ( $-80^{\circ}\text{C}$ ), (O) PCHTs 3% ( $-196^{\circ}\text{C}$ ), and ( $\Delta$ ) P-PRP activated with  $\text{Ca}^{+2}$ /thrombin (used as control); TGF- $\beta$ 1 [(a), (c)]; and PDGF-AB [(b), (d)]. The concentration of platelets in P-PRP was  $472,250 \text{ pg}/\text{mm}^3$ . Activated P-PRP alone was used as control.

The curves show diffusion profiles, indicating no collapse of the porous structure of chitosan scaffolds during the course of the assays, regardless of the CHT concentration and freezing conditions.

PDGF-AB released from PCHTs ended within 24 hours of incubation, whereas TGF- $\beta$ 1 tended to continue after 72 hours.

A controlled release of TGF- $\beta$ 1 and PDGF-AB was achieved for all CHT concentrations, related to the scaffolds of activated P-PRP only. The slowest release was observed for a chitosan concentration of 3%.

In contrast, for the PCHTs 3% freezing at  $-80^{\circ}\text{C}$  and  $-196^{\circ}\text{C}$ , we observed a controlled release of TGF- $\beta$ 1, but a strong burst release of PDGF-AB.

Thus, PCHTs prepared with 3% CHT at  $-20^{\circ}\text{C}$  provided a controlled release of PDGF-AB and TGF- $\beta$ 1 and can be an efficient vehicle for release of GFs from PRP.

### 3.3.3.3. h-AdMSCs-Seeded Proliferation

Figure 15 shows the proliferation profile of h-AdMSCs cultured in  $\alpha$ P-PRP/PCHTs.

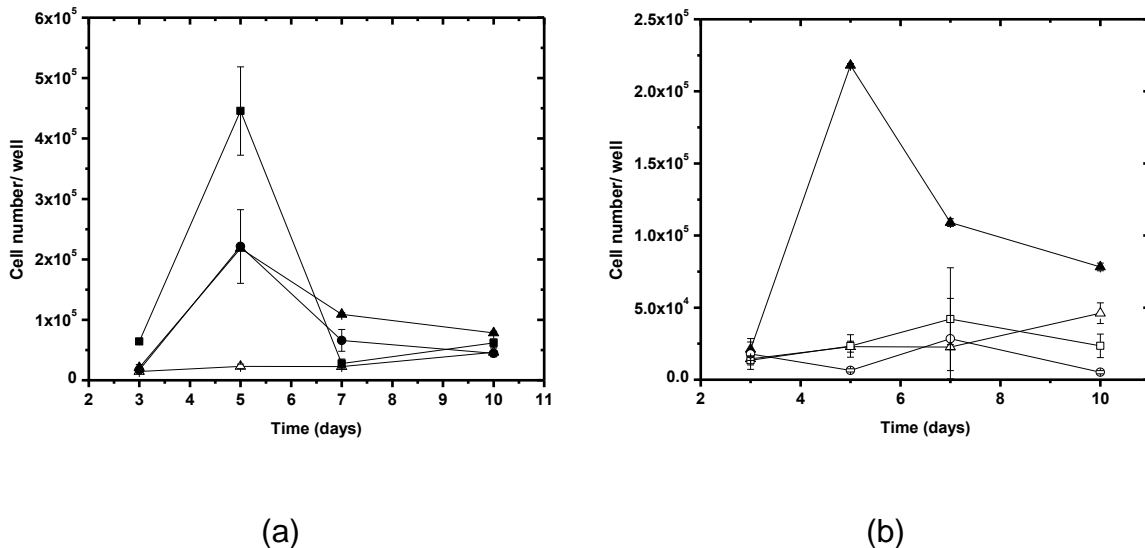


**Figure 15.** Proliferation kinetic profiles of h-AdMSCs seeded in  $\alpha$ P-PRP/PCHTs. (a) CHT concentration and (b) freezing conditions. (■) PCHTs 1% ( $-20^\circ\text{C}$ ); (●) PCHTs 2% ( $-20^\circ\text{C}$ ); (▲) PCHTs 3% ( $-20^\circ\text{C}$ ); (□) PCHTs 3% ( $-80^\circ\text{C}$ ), (○) PCHTs 3% ( $-196^\circ\text{C}$ ), and (Δ) P-PRP activated with  $\text{Ca}^{+2}$ /thrombin (control). The concentration of platelets in P-PRP was  $374,000 \text{ pq}/\text{mm}^3$ . Activated P-PRP alone was used as control.

The cell number per well determined after 3 days exceeded the number of seeded cells ( $1.4 \times 10^4$  cells/well) in all the  $\alpha$ P-PRP/PCHTs, meaning that the cells kept in the matrices retained their viability, regardless of the CHT concentration and freezing conditions.

The cell number per well of  $\alpha$ P-PRP/PCHTs prepared with 1, 2, and 3% (w/v) of chitosan [Figure 15(a)] showed significant differences ( $P < 0.05$ ) compared to control ( $\alpha$ P-PRP). Therefore, PCHTs must have stabilized fibrin networks as we initially hypothesized.

However, regarding freezing condition, no significant variations for  $\alpha$ P-PRP/PCHTs prepared at  $-80^\circ\text{C}$  or  $-196^\circ\text{C}$  and  $\alpha$ P-PRP were observed [Figure 15(b)]. In all cases, cell viability decreased after 7 days, probably due to collapse of the structure.

We also observed that the exponential phase of the cultures [Figure 15(a)]

started after the maximum release of GFs (Figure 14), and the decline phase matched the largest weight loss of the PCHTs (Figure 11).

#### 3.3.3.4. Induction of Osteogenic Differentiation

Osteogenic differentiation of h-AdMSCs was investigated 14 days after cell seeding. ALP, an early marker of osteogenic differentiation, was determined, and the results are shown in Figure 16. The expression of ALP activity showed no significant difference ( $P < 0.05$ ) with CHT concentration. However, higher osteogenic differentiation was obtained with  $\alpha$ P-PRP/PCHTs 3% ( $-196^{\circ}\text{C}$ ).

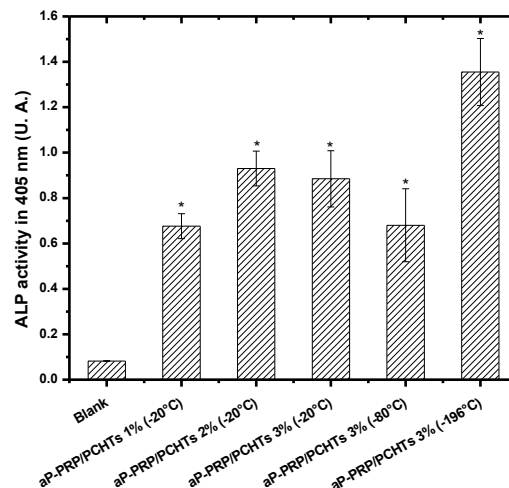


**Figure 16.** ALP activities of cells cultured on  $\alpha$ P-PRP/PCHTs scaffolds prepared with different CHT concentrations and freezing conditions (statistically significant differences from blank,  $n = 3$ ,  $*P < 0.05$ ). Blank = the reagents used in the assay only. The concentration of platelets in whole blood donors (average of 2 donors) was  $163,500 \text{ pq/mm}^3$ . After preparation of the PRP, the platelets were concentrated approximately 1.74 times, with an average final concentration of  $303,000 \text{ pq/mm}^3$ .

## 3.4. Conclusions

Composite scaffolds were prepared with porous chitosan and  $\alpha$ -PRP. The performance of the composite scaffolds was superior to  $\alpha$ P-PRP alone, indicating that the porous chitosan stabilized the fibrin network, supporting our initial hypothesis.

Chitosan concentration and freezing conditions influenced the physicochemical and biological properties of the scaffolds. On the average, physicochemical, mechanical, and h-AdMSCs proliferation improved by the use of 3% (w/v) chitosan and  $-20^{\circ}\text{C}$  freezing temperature, while  $-196^{\circ}\text{C}$  favored osteogenic differentiation. Additional stabilization of the porous structure is needed for applications in regenerative medicine.

**Conflict of Interests.** The authors declare that there is no conflict of interests regarding the publication of this paper.

**Acknowledgments.** The authors acknowledge the financial support from the National Council of Technological and Scientific Development (CNPq, Brazil). They also thank Dr. William Dias Belangero and Dr. Ana Amélia Rodrigues of the Faculty of Medical Sciences (University of Campinas) for assistance and Dr. Ângela Cristina Malheiros Luzo of the Haematology and Hemotherapy Center (University of Campinas) for the donation of h-AdMSCs.

### 3.5. References

ADEKOGBE, I.; GHANEM, A. Fabrication and characterization of DTBP-crosslinked chitosan scaffolds for skin tissue engineering. **Biomaterials**, vol.26, p.7241–7250, 2005.

AGNIHOTRI, S.A.; MALLIKARJUNA, N.N.; AMINABHAVI, T.M. Recent advances on chitosan-based micro- and nanoparticles in drug delivery. **Journal of Controlled Release**, vol.100, n.1, p.5-28, 2004.

AMARAL, F.; SAMPAIO, P.; BARBOSA, M.A. Three-dimensional culture of human osteoblastic cells in chitosan sponges: The effect of the degree of acetylation. **Journal of Biomedical Materials Research**, vol.76A, p.335–346, 2006.

ANTONOV, S.F.; KRYZHANOVSKAYA, E.V.; FILIPPOV, Y.I.; SHINKAREV, S.M.; FROLOVA, M.A. Study of Wound-Healing Properties of Chitosan. **Russian Agricultural Sciences**, vol.34, n.6, p.426-427, 2008.

BENSAÏD, W.; TRIFFITT, J.T.; BLANCHAT, C.; OUDINA, K.; SEDEL, L.; PETITE, H.A. biodegradable fibrin scaffold for mesenchymal stem cell transplantation. **Biomaterials**, vol.24, n.14, p.2497–502, 2003.

BERGER, J.; REIST, M.; MAYER, J.; FELT, O.; PEPPAS, N.; GURNY, R. Structure and interactions in covalently and ionically crosslinked chitosan hydrogels for biomedical applications. **European journal of pharmaceutics and biopharmaceutics**, vol.57, p.19–34, 2004.

BERTRAM, U.; BODMEIER, R. In situ gelling, bioadhesive nasal inserts for extended drug delivery: In vitro characterization of a new nasal dosage form. **European Journal of Pharmaceutical Sciences**, vol.27, n.1, p.62-71, 2006.

BRAUKER, H.; CARR-BRENDEL, V.E.; MARTINSON, L.A.; CRUDELE, J.; JOHNSTON, W.D.; JOHNSON, R.C. Neovascularization of synthetic membranes directed by membrane micro architecture. **Journal of Biomedical Materials Research**, vol.29, p.1517–1524, 1995.

CARDEA, S.; PISANTI, P.; REVERCHON, E. Generation of chitosan nanoporous structures for tissue engineering applications using a supercritical fluid assisted process. **Journal of Supercritical Fluids**, vol.54, p.290–295, 2010.

CHANG, H-I.; WANG, Y. Cell Responses to Surface and Architecture of Tissue Engineering Scaffolds. In: EBERLI D., (Ed.). **Regenerative Medicine and Tissue Engineering – Cells and Biomaterials**, Croatia: InTech, chapter 27, p. 569-588, 2011.

CHANG, S.J.; KUO, S.M.; LAN, C-W.; MANOUSAKAS, I.; TSAI, P.H. Evaluation of chitosan/CaSO<sub>4</sub>/ platelet-rich plasma microsphere composites as alveolus osteogenesis material. **Biomedical Engineering: Applications, Basis and Communications**, vol.21, n.2, p.115–122, 2009.

CHAVEZ-MUNOZ, C; NGUYEN, K.T.; XU, W.; HONG, S.J.; MUSTOE, T.A.; GALIANO, R.D. Transdifferentiation of adipose-derived stem cells into keratinocyte-like cells: engineering a stratified epidermis. **Public Library of Science One**, vol.8, n.12, p.1-13, 2013.

CHEN, G.; USHIDA, T.; TATEISHI, T. Scaffold Design for Tissue Engineering. **Macromolecular Bioscience**, vol.2, pp.67-77, 2002.

CHEUNG, H-Y.; LAU, Q-T.; LU, T-P.; HUI, D. A critical review on polymer-based bio-engineered materials for scaffold development. **Composites: Part B**, vol.38, p.291-300, 2007.

CORREIA, C.R.; TEIXEIRA, L.S.M.; MORONI, L.; REIS, R.L.; VAN BLITTERSWIJK, C.A.; KARPERIEN, M.; MANO, J.F. Chitosan Scaffolds Containing Hyaluronic Acid for Cartilage Tissue Engineering, **Tissue Engineering: Part C**, vol.17(7), p.717-730, 2011.

COSTA-PINTO, R.; REIS, R.L.; NEVES, N.M. Scaffolds Based Bone Tissue Engineering: The Role of Chitosan. **Tissue Eng. Part B**, vol.17, p.331–347, 2011.

CRANE, D.; EVERTS, P.A.M. Platelet Rich Plasma (PRP) Matrix Grafts, **PPM**

**Communications**, vol.8, p.1-10, 2008.

DAI, T.; TANAKA, M.; HUANG, Y.Y.; HAMBLIN, M.R. Chitosan preparations for wounds and burns: antimicrobial and wound-healing effects. **Expert Review of Anti-infective Therapy**, vol.9, p.857–879, 2011.

ENRIONE, J.; OSORIO, F.; LOPEZ, P.; WEINSTEIN-OPPENHEIMER, C.; FUENTES, M.A.; CERIANI, R.; BROWN, D.I.; ALBORNOZ, F.; SÁNCHEZ, E.; VILLALOBOS, P.; SOMOZA, R.A.; YOUNG, M.E.; ACEVEDO, C.A. Characterization of a gelatin/chitosan/hyaluronan scaffold-polymer. **Electronic Journal of Biotechnology**, vol.13, n.5, p.1-11, 2010.

FALVO, M.R.; GORKUN, O.V.; LORD, S.T. The molecular origins of the mechanical properties of fibrin. **Biophysical Chemistry**, vol.152, p.15–20, 2010.

GÜMÜŞDERELIOĞLU, M.; ADAY, S. Heparin-functionalized chitosan scaffolds for bone tissue engineering. **Carbohydrate Research**, vol.346, p.606–613, 2011.

HE, P.; DAVIS, S.S.; ILLUM, L. In vitro evaluation of the mucoadhesive properties of chitosan microspheres. **International Journal of Pharmaceutics**, vol.166, p.75–88, 1998.

HOLLISTER, S. J. Porous scaffold design for tissue engineering. **Nature Materials**, vol.4, p.518-590, 2005.

KLAWITTER, J.; HULBERT, S.F. Application of porous ceramics for the attachment of load-bearing internal orthopedic applications. **Journal of Biomedical Materials Research A Symposium**, vol.2, p.161–168, 1971.

KOGA, D. Chitin enzymology—chitinase, In: Chen, R.; Chen, H.C. (Eds.). **Advances in Chitin Science**, vol.3, p.16–23, 1998.

KOJIMA, K.; OKAMOTO, Y.; MIYATAKE, K.; FUJISE, H.; SHIGEMASA, Y.; MINAMI, S. Effects of chitin and chitosan on collagen synthesis in wound Healing. **Journal of Veterinary Medical Science**, vol.66, p.1595–1598, 2004.

KUTLU, B.; AYDIN, R.S.T.; AKMAN, A.C.; GÜMÜŞDERELIOĞLU, M.; NOHUTCU, R.M. Platelet-rich plasma-loaded chitosan scaffolds: Preparation and growth factor release kinetics. **Journal of Biomedical Materials Research**, vol.101B, p.28–35, 2012.

LANGER, R.; VACANTI, J.P. Tissue engineering. **Science**, vol.260, n.5110, pp. 920–926, 1993.

LAVERTU, M.; METHOT, S.; TRAN-KHANH, N.; BUSCHMANN, M.D. High efficiency gene transfer using chitosan/DNA nanoparticles with specific combinations of molecular weight and degree of deacetylation. **Biomaterials**, vol.27, p.4815-4824, 2006.



LEÓN Y LEÓN, C.A. New perspectives in mercury porosimetry. **Advances in Colloid and Interface Science**, vol.76-77, p.341-372, 1998.

LEONG, F.; CHEAH, C.M.; CHUA, C.K. Solid freeform fabrication of three-dimensional scaffolds for engineering replacement tissues and organs. **Biomaterials**, vol.24, p.2363–2378, 2003.

LI, X.; MIN, M.; DU, N.; GU, Y.; HODE, T.; NAYLOR, M.; CHEN, D.; NORDQUIST, R.E.; CHEN, W.R. Chitin, Chitosan, and Glycated Chitosan Regulate Immune Responses: The Novel Adjuvants for Cancer Vaccine, **Hindawi Publishing Corporation Clinical and Developmental Immunology**, p.1-8, 2013.

LIU, X.; MA, P.X. Polymeric Scaffolds for Bone Tissue Engineering. **Annals of Biomedical Engineering**, vol.32, n.3, p.477–486, 2004.

LOH, Q.L.; CHOONG, C.; Three-Dimensional Scaffolds for Tissue Engineering Applications: Role of Porosity and Pore Size. **Tissue Engineering: Part B**, vol.19, n.6, p.485-503, 2013.

MADIHALLY, S.V.; MATTHEW, H.W.T. Porous chitosan scaffolds for tissue engineering. **Biomaterials**, vol.20, p.1133-1142, 1999.

MAJIMA, T.; IRIE, T.; SAWAGUCHI, N.; FUNAKOSHI, T.; IWASAKI, N.; HARADA, K.; MINAMI, A.; NISHIMURA, S.-I. Chitosan-based hyaluronan hybrid polymer fiber scaffold for ligament and tendon tissue engineering. **Proceedings of the Institution of Mechanical Engineers – Part H: J. Engineering in Medicine**, vol. 221, p.537-546, 2007.

MARTINS, M.; ENG, G.; CARIDADE, S.G.; MANO, J.F.; REIS, R.L.; VUNJAK-NOVAKOVIC, G. Electrically Conductive Chitosan/Carbon Scaffolds for Cardiac Tissue Engineering. **Biomacromolecules**, vol.15, p.635–643, 2014.

MATHEWS, S.; BHONDE, R.; GUPTA, P.K.; TOTEY, S. A novel tripolymer coating demonstrating the synergistic effect of chitosan, collagen type 1 and hyaluronic acid on osteogenic differentiation of human bone marrow derived mesenchymal stem cells. **Biochemical and Biophysical Research Communications**, vol.414, p.270–276, 2011.

MOLINARO, G.; LEROUX, J.C.; DAMAS, J.; ADAM, A. Biocompatibility of thermosensitive chitosan-based hydrogels: an in vivo experimental approach to injectable biomaterials. **Biomaterials**, vol.23, p.2717-2722, 2002.

MOSSMAM, T.J. A rapid colorimetric assay of cellular growth and survival: application to proliferation and cytotoxicity assays. **Journal of Immunological Methods**, vol.65, p.55-63, 1983.

MUCHA, M.; MICHALAK, I.; BALCERZAK, J.; TYLMAN, M. Chitosan scaffolds, films and microgranules for medical application — preparation and drug release studies.

**Polimery**, vol.57, n.10, p.714-721, 2012.

MUZZARELLI, R. Chitosan. In: MUZZARELLI R. (Eds.). **Natural Chelating Polymers**. Oxford: Pergamon Press, 1973, p. 144–176.

MUZZARELLI, R.; TARSI, R.; FILIPPINI, O.; GIOVANETTI, E.; BIAGINI, G.; VARALDO, P.E. Antimicrobial Properties of N-Carboxybutyl Chitosan. **Antimicrobial agents and chemotherapy**, vol.34, n.10, p.2019-2023, 1990.

NASTI, A.; ZAKI, M.N.; DE LEONARDIS, P.; UNGPHAIBOON, S.; SANSONGSAK, P.; RIMOLI, M.G.; TIRELLI, N. Chitosan/TPP and Chitosan/TPP-hyaluronic Acid Nanoparticles: Systematic Optimisation of the Preparative Process and Preliminary Biological Evaluation. **Pharmaceutical Research**, vol.26, n.8, p.1918-1930, 2009.

NETTLES, D.L.; ELDER, S.H.; GILBERT, J.A. Potential Use of Chitosan as a Cell Scaffold Material for Cartilage Tissue Engineering. **Tissue Engineering**, vol.8, n.6, p.1009-1016, 2002.

NORDTVEIT, R.J.; VÂRUM, K.M.; SMIDSRD, O. Degradation of partially N-acetylated chitosans with hen egg white and human lysozyme. **Carbohydrate Polymers**, vol.29, p.163-167, 1996.

NWE, N.; FURUIKE, T.; TAMURA, H. The Mechanical and Biological Properties of Chitosan Scaffolds for Tissue Regeneration Templates Are Significantly Enhanced by Chitosan from *Gongronella butleri*. **Materials**, vol.2, p.374-398, 2009.

OKAMOTO, Y.; YANO, R.; MIYATAKE, K.; TOMOHIRO, I.; SHIGEMASA, Y.; MINAMI, S. Effects of chitin and chitosan on blood coagulation. **Carbohydrate Polymers**, vol.53, p.337–342, 2003.

OKTAY, E.O.; DEMIRALP, B.; DEMIRALP, B.; SENEL, S.; CEVDET A.; ERATALAY, K.; AKINCIBAY, H. Effects of platelet-rich plasma and chitosan combination on bone regeneration in experimental rabbit cranial defects. **Journal of Oral Implantology**, vol.36, p.175–184, 2010.

PEREZ, A.G.M.; LICHY, R.; LANA, J.F.S.D.; RODRIGUES, A.A.; LUZO, A.C.M.; BELANGERO, W.D.; SANTANA, M.H.A. Prediction and Modulation of Platelet Recovery by Discontinuous Centrifugation of Whole Blood for the Preparation of Pure Platelet-Rich Plasma. **BioResearch Open Access**, vol.2, p. 307-314, 2013.

PEREZ, A.G.M.; RODRIGUES, A.A.; LUZO, A.C.M.; LANA, J.F.S.D.; BELANGERO, W.D.; SANTANA M. H. A. Fibrin network architectures in pure platelet-rich plasma as characterized by fiber radius and correlated with clotting time. **Journal of Materials Science: Materials in Medicine**, vol.25(8), p.1967-1977, 2014.

RAO, S.B.; SHARMA, C.P. Sterilization of chitosan: implications. **Journal of Biomaterials Applications**, vol.10, n.2, p.136-43, 1995.

RUCKER, M.; LASCHKE, M. W.; JUNKER, D.; CARVALHO, C.; SCHRAMM, A.; MULHAUPT, R.; GELLRICH, N.C; MENGER, M.D. Angiogenic and inflammatory response to biodegradable scaffolds in dorsal skinfold chambers of mice. **Biomaterials**, vol.27, p.5027-5038, 2006.

RYAN, E.; MOCKROS, L.F.; WEISEL, J.W.; LORAND, L. Scientific Commons: Structural origins of fibrin clot rheology. **Biophysical Journal**, vol.77, p.2813-2826, 1999.

SALGADO, J.; COUTINHO, O.P.; REIS, R.L. Bone Tissue Engineering: State of the Art and Future Trends. **Macromolecular Bioscience**, vol.4, p.743-765, (2004).

SHEN, E.C.; CHOU, T.C.; GAU, C.H.; TU, H.P.; CHEN, Y.T.; FU, E. Releasing growth factors from activated human platelets after chitosan stimulation: a possible bio-material for platelet-rich plasma preparation. **Clinical Oral Implants Research**, vol.17, p.572–578, 2006.

SHEN, F.; CUI, Y.L.; YANG, L.F.; YAO, K.D.; DONG, X.H.; JIA, W.Y.; SHI, H.D. A study on the fabrication of porous chitosan/gelatin network scaffold for tissue engineering. **Polymer International**, vol.49, p.1596-1599, 2000.

SHU, X.Z.; ZHU, K.J. Controlled drug release properties of ionically cross-linked chitosan beads: the influence of anion structure. **International Journal of Pharmaceutics**, vol.233, p.217–25, 2002.

TAN, H.P.; CHU, C.R.; PAYNE, K.A.; MARRA, K.G. Injectable in situ forming biodegradable chitosan-hyaluronic acid based hydrogels for cartilage tissue engineering. **Biomaterials**, vol.30, p.2499–2506, 2009.

TANG, S.; SPECTOR, M. Incorporation of hyaluronic acid into collagen scaffolds for the control of chondrocyte-mediated contraction and chondrogenesis. **Biomedical Materials**, vol.2, p.S135–S141, 2007.

WANG, Y.; LIN, M.; WANG, D.; HSIEH, H. Fabrication of a novel porous PGA–chitosan hybrid matrix for tissue engineering. **Biomaterials**, vol.24, p.1047–57, 2003.

WEISEL, J.W.; NAGASWAMI, C. Computer modeling of fibrin polymerization kinetics correlated with electron microscope and turbidity observations: clot structure and assembly are kinetically controlled. **Biophysical Journal**, vol.63, n.1, p.111–128, 1992.

YANG, S.; LEONG, K.F.; DU, Z.; CHUA, C.K. The design of scaffolds for use in tissue engineering—part I: traditional factors. **Tissue Engineering**, vol.7, n.6, p.679–689, 2001.

YANNAS, V.; LEE, E.; ORGILL, D.P.; SKRABUT, E.M.; MURPHY, G.F. Synthesis and characterization of a model extracellular matrix that induces partial regeneration of adult mammalian skin. **Proceedings of the National Academy of Sciences of the**

**United States of America**, vol.86, p.933-937, 1989.

# CAPÍTULO 4 – STABILIZATION OF POROUS CHITOSAN IMPROVES THE PERFORMANCE OF ITS ASSOCIATION WITH PLATELET-RICH PLASMA AS A COMPOSITE SCAFFOLD

---

Artigo submetido ao periódico *Materials Science and Engineering C: Materials for Biological Applications*.

A. A. M. Shimojo<sup>1</sup>, A. G. M. Perez<sup>1</sup>, S. E. M. Galdames<sup>1</sup>, I. C. S. Brissac<sup>1</sup>, M. H. A. Santana<sup>1</sup>

<sup>1</sup>Department of Engineering of Materials and of Bioprocesses, School of Chemical Engineering, UNICAMP, P.O. Box 6066, 13083-970 Campinas, SP, Brazil.

\*Correspondence to: Andréa Arruda Martins Shimojo, phone: +55-19-35213969, FAX: +55-19-35213890, e-mail: [lshimojo51@gmail.com](mailto:lshimojo51@gmail.com)

**Abstract.** This study offers innovative perspectives for optimizing of scaffolds based on correlation structure-function aimed the regenerative medicine. Thus, we evaluated *in vitro* the performance of stabilized porous chitosan (SPCHTs) associated with activated platelet-rich plasma (aP-PRP) as a composite scaffold for the proliferation and osteogenic differentiation of human adipose-derived mesenchymal stem cells (h-AdMSCs). The porous structure of chitosan (PCHT) was prepared similarly to solid sponges by controlled freezing (-20°C) and lyophilization of a 3% (w/v) chitosan solution. Stabilization was performed by treating the PCHT with sodium hydroxide (TNaOH), an ethanol series (TEtOH) or by crosslinking with tripolyphosphate (CTPP). The aP-PRP was obtained from the controlled centrifugation of whole blood and activated with autologous serum and calcium. Imaging of the structures showed fibrin networks inside and on the surface of SPCHTs as a consequence of electrostatic interactions. SPCHTs were non-cytotoxic, and the porosity, pore size and Young's modulus were

approximately 96%, 145  $\mu\text{m}$  and 1.5 MPa for TNaOH and TEtOH and 94%, 110  $\mu\text{m}$  and 1.8 MPa for CTPP, respectively. Stabilization maintained the integrity of the SPCHTs for at least 10 days of cultivation. SPCHTs showed controlled release of the growth factors TGF- $\beta$ 1 and PDGF-AB. Although generating different patterns, all of the stabilization treatments improved the proliferation of seeded h-AdMSCs on the composite scaffold compared to aP-PRP alone, and differentiation of the composite scaffold treated with TEtOH was significantly higher than for non-stabilized PCHT. We conclude that the stabilized porous chitosan scaffolds improved the *in vitro* performance of PRP and have potential in regenerative medicine.

**Keywords:** Regenerative medicine; scaffolds; chitosan; platelet-rich plasma; growth factors.

## 4.1. Introduction

Platelet-rich plasma (PRP) is an autologous product from whole blood (WB) comprised primarily of a high concentration of platelets dispersed in plasma (P-PRP) but that can also include concentrated leukocytes (L-PRP) (Ehrenfest *et al.*, 2009). Currently, PRP therapy has been used in various medical specialties and has been responsible for several successful outcomes. Various clinical uses including sports medicine, orthopedics and the recovery of musculoskeletal injuries have been reported recently (Lana *et al.*, 2014).

Activated PRP (aPRP) releases growth factors (GFs) and various cytokines from platelets and leukocytes as well as stimulating the decomposition of fibrinogen in fibrin fibers, which arrange themselves in a network structure that supports cell proliferation and differentiation (Marx, 2004). Therefore, tissue repair occurs from a cascade of multiple reactions mediated by GFs (Jacobson *et al.*, 2008), in which cytokines play an important role (Kanaji *et al.*, 2011).

Preparation of PRP first involves the separation of red blood cells and the concentration of platelets and other components of WB. Usually, separation is performed by centrifugation, and activation is promoted by thrombin and calcium.

Adequate centrifugation conditions and multiple spins must be used to obtain a high yield of platelets and preserve integrity (Perez *et al.*, 2013). The architecture of the fibrin network is determined by the activation conditions (Perez *et al.*, 2014) and plays an important role in GF release and cell proliferation.

Crane & Everts (2008) described tissue regeneration based on the triangle of proliferation, which represents cooperation between genic, conductive and inductive capabilities, using the cells, scaffold and GFs as basic elements. PRP is beneficial to tissue regeneration because it acts as an inducer and conductive matrix (scaffold) for cell proliferation. Furthermore, aPRP influences the paracrine activity of mesenchymal cells (MSCs), which is an important mechanism determining their efficacy in regenerative therapies (Liu *et al.*, 2002; Hom *et al.*, 2007).

In regenerative PRP therapies, we would consider first generation therapies to be PRP alone, followed by the second generation of PRP associated with bone marrow cells, and finally a third generation using PRP and h-AdMSCs. However, the performance of the fibrin network as a scaffold in regeneration requires further attention. Structural stability is an important issue because MSCs needs the maintenance of a 3-dimensional fibrin architecture for proliferation, migration and differentiation.

Some of the available literature suggests that the association of PRP with chitosan is beneficial to osteogenic regeneration (Ouyang *et al.*, 2013; Rossi *et al.*, 2013; Kutlu *et al.*, 2013; Bi *et al.*, 2010; Oktay *et al.*, 2010; Chang *et al.*, 2009; Shen *et al.*, 2006; Kojima *et al.*, 2004; Okamoto *et al.*, 2003).

In our previous studies, we observed the association of aP-PRP with PCHTs controlled the release of GFs and also improved the *in vitro* proliferation and differentiation of h-AdMSCs compared to aP-PRP only. However, the PCHTs collapsed after five days of cell cultivation and required stabilization.

Porous chitosan scaffolds are produced primarily by a freezing process, which provides the nucleation of ice crystals from solution and further growth along the lines of thermal gradients. Exclusion of the chitosan acetate salt from the ice crystal phase and subsequent ice removal by lyophilization generates a porous material. After freeze-drying, the acetate molecules are in solid form in the scaffold cavities as ions bound to the cationic amine groups in the chitosan. When the acetate is not removed or

neutralized, the scaffold will swell rapidly and ultimately dissolve upon rehydration in a neutral aqueous medium, requiring stabilization of the scaffold.

Stabilization using multiple methods has been studied, including rehydration and/or crosslinking (Shen *et al.*, 2000), immersion in sodium hydroxide (Madhally & Mathew, 1999; Manjubala *et al.*, 2006), tripolyphosphate (Seol *et al.*, 2004; Lee *et al.*, 2000) and/or an ethanol series (Nwe *et al.*, 2009; Reis *et al.*, 2008). Neutralization with NaOH removes acid remnants and regenerates the NH<sub>2</sub> groups on the chitosan, yielding a hydrophilic surface. The stabilization occurs by inhibition of the repulsion between chitosan chains and the formation of hydrogen bonds, hydrophobic interactions and chitosan crystallites (Noriega & Subramanian, 2011). An adequate NaOH concentration must be applied to maintain the shape and volume of the chitosan scaffold during the cell culture period (Nwe *et al.*, 2009).

Stabilization with an ethanol series occurs because CHT decreases in solubility as the polarity of mixed solvents decreases, and affects not only the solubility of CHT but also the elasticity of the hydrogel (Sano *et al.*, 1999).

Cationic chitosan can be crosslinked by multivalent counterions such as tripolyphosphate to form an intermolecular and/or intramolecular network structure. The reaction occurs through the ionic interaction between the NH<sub>3</sub><sup>+</sup> protonated groups of chitosan and the negatively charged counterions of TPP, including the OH<sup>-</sup> and P<sub>3</sub>O<sub>10</sub><sup>5-</sup> ions coexisting in the TPP solution (Bhumkar & Pokharkar, 2006).

In this work, we extended previous findings by studying the effects of PCHT stabilization on the performance of the composite scaffold aP-PRP/SPCHT. Stabilization was performed by treating PCHT with sodium hydroxide (TNaOH), an ethanol series (TEtOH) or by crosslinking with tripolyphosphate (CTPP). The *in vitro* performance of the composite scaffolds was evaluated based on physicochemical and biological properties, and these results are important to optimize composite scaffolds for use in implants or for wound healing.

## 4.2. Materials and Methods



### 4.2.1. Materials

Chitosan (average molecular weight [Mw] =  $4 \times 10^5$  Da, degree of deacetylation =  $83 \pm 4\%$ ) was purchased from Polymar® (Fortaleza, CE, Brazil) and purified according to a protocol described by Nasti *et al.* (2009). Other chemicals were reagent grade and were used without any further purification. PRP was prepared from whole blood (WB) of donors, who were healthy individuals aged between 30 and 40 years old and previously assessed through their clinical examinations. The human adipose tissue-derived mesenchymal stem cells, h-AdMSCs, were provided by Umbilical Cord Blood Bank of Haematology and Hemotherapy Center of University of Campinas. All biological experiments were approved by the Ethics Committee of the Medical Sciences School of the University of Campinas (UNICAMP; CAAE: 0972.0.146.000-11).

### 4.2.2. Methods

#### 4.2.2.1. Preparation of porous chitosan (PCHT)

PCHT was prepared from a chitosan solution 3% (w/v) prepared by dissolving chitosan in  $0.2 \text{ mol.L}^{-1}$  acetic acid. To obtain a cylindrical shape, the solution was added to the wells of a 24 well culture plate (TPP®, polystyrene, diameter=15.4 mm). The sponge-like porous structure was generated by freezing at  $-20^\circ\text{C}$  for 24 hours and lyophilizing in a lyophilizer Liobras L101 (Liobras, São Carlos, SP, Brazil) at a temperature of approximately  $-30^\circ\text{C}$  for 48 hours.

#### 4.2.2.2. Stabilization of PCHT

PCHT was stabilized by treatment with dilute NaOH (TNaOH), an ethanol series (TEtOH) or by crosslinking with tripolyphosphate (CTPP) (Madhally & Matthew, 1999). All of these treatments began with the slow immersion of PCTS in specific aqueous solutions, some of which were followed by washing. For TNaOH,  $0.05 \text{ mol.L}^{-1}$  NaOH solution was used, and the PCHT was equilibrated for  $\sim 10$  min and then washed twice with water and twice with phosphate buffered saline (pH 7.4). TEtOH treatment was performed by immersing the PCHT in absolute ethanol for  $\sim 1$  h, then immersing sequentially in 70% and 50% (v/v) ethanol for  $\sim 30$  min each. For CTPP treatment, the

PCHT was immersed in 5% (w/v) TPP solution, equilibrated for ~2 h and then washed twice with water and twice with phosphate buffered saline (pH 7.4). The final mass ratio in the stabilized scaffold of CHT/TPP was 2:1. The stabilized PCHT (SPCHTs) were frozen at -20°C and lyophilized at a temperature of approximately -30°C for 48 hours again.

### 4.2.3. Characterization of SPCHTs

#### 4.2.3.1. Chemical modification

Infrared spectrometry (FT-IR) was used to identify the chemical modifications in the SPCHT scaffolds. Infrared spectra of PCHTs were obtained using an Infrared Spectrometer Fourier Transform (FT-IR) Thermo Scientific Nicolet Model 6700 (Thermo Fisher Scientific, Waltham, MA, USA) in the spectral range of 4000–675  $\text{cm}^{-1}$ . Measurements were made in ATR mode with the SMART OMNI-SAMPLER accessory in the spectral range between 4000-675  $\text{cm}^{-1}$  at a resolution of 4  $\text{cm}^{-1}$  and 64 scans. ATR-IR<sub>(chitosan)</sub>: 3500–3000 ( $\nu$  OH and  $\text{NH}_2$ ), 2875 ( $\nu$ CH), 1645 (amide I), 1550 (amide II) 1380, 1067, 1020  $\text{cm}^{-1}$  (Nasti *et al.*, 2009).

#### 4.2.3.2. Morphology and pore size

The morphology of the SPCHTs was evaluated by scanning electron microscopy (SEM) using a LEO 440i Electron Microscopy/Oxford (Cambridge, England) operated at 5 kV accelerating voltage. The scaffolds were gold-coated using a sputter coater POLARON SC7620, VG Microtech (Uckfield, England) for 180 s at a current of 3 mA. Pore size ( $n=20$ ) was measured using an Image J 1.47t.

#### 4.2.3.3. Swelling profile

The swelling profile in function of time of the SPCHTs was determined by swelling freeze-dried scaffolds of known weight in phosphate buffered saline (PBS) (LB Laborclin, Pinhais, PR, Brazil) at pH 7.4 and 37°C. The swelling ratio (SR) was calculated using Equation (1):

$$SR = \frac{w_s}{w_d} \quad \text{Equation (1)}$$

in which  $w_s$  and  $w_d$  are the weights of the scaffolds at the swelling state and the dry state, respectively.

#### 4.2.3.4. Porosity

Porosity ( $\varepsilon$ ) of the SPCHTs was measured according to the protocol used by Wang *et al.* (2003), and calculated using Equation (2):

$$\varepsilon (\%) = \frac{V_m - \left(\frac{w_m}{\rho}\right)}{V_m} \times 100 \quad \text{Equation (2)}$$

in which  $V_m$  is the total volume of CHT scaffolds ( $\text{cm}^3$ ),  $\rho$  is the density of the non-porous chitosan scaffold ( $1.342 \text{ g/cm}^3$ ) and  $w_m$  is the weight of scaffold (g). Values are expressed as the mean  $\pm$  standard deviation ( $n=3$ ).

#### 4.2.3.5. Mechanical resistance

Mechanical compression tests of the SPCHTs ( $n=3$ ) were performed using a Universal Testing Machine, MTS model 810-Flex Test 40 (MTS Systems Corporation, Eden Prairie, MN, USA) at up to 60% of strain, according to Correia *et al.* (2011). The testing machine was equipped with a 1.5 kN load cell, and the loading rate was 5 mm/min. The Young's modulus was calculated in the initial linear section of the stress-strain curve, when the strain was lower than 10%.

#### 4.2.3.6. Degradation in phosphate buffered saline

Degradation of SPCHTs was examined by the weight loss of previously weighed SPCHTs ( $w_0$ ), which was monitored as a function of incubation time in PBS at  $37^\circ\text{C}$ . At specified time intervals, PCHTs were removed from the PBS and weighed ( $w_t$ ). The weight loss ratio is defined in Equation (3) (Tan *et al.*, 2009).

$$\text{weight loss } (\%) = \frac{(w_0 - w_t)}{w_0} \times 100 \quad \text{Equation (3)}$$

#### 4.2.3.7. Cell compatibility

The compatibility of the SPCHTs was performed by exposing h-AdMSCs to SPCHTs followed by cultivation at 37°C for 24 hours and evaluation by MTT (3-[4,5-dimethyl-thiazol-2-yl]-2,5-diphenyltetrazolium bromide) assay (MTT, Molecular Probes), according to a modified Mosmann method (1983). The MTT assay is a colorimetric test based on the reduction of yellow tetrazolium salt into a purple formazan product in the presence of cells (Gümüşderelioğlu & Aday, 2011).

#### 4.2.4. Preparation of pure platelet-rich plasma (P-PRP)

P-PRP, which is rich in platelets and poor in leukocytes, was prepared according to Perez *et al.* 2013. Briefly, whole blood (WB) was collected in 3.5 mL vacuum tubes (Vacurette®, Campinas, SP, Brazil) containing sodium citrate 3.2% (w/v) as an anticoagulant. WB was initially centrifuged in a Rotina 380R centrifuge (Hettich® Zentrifugen, Tuttlingen, Germany) at 100xg for 10 minutes at 25°C. After the formation of three layers: a bottom layer of red blood cells (RBCs); an upper layer of plasma, platelets and some WBCs; and an intermediate layer, or buffy coat, composed mostly of WBCs; only the upper layer was collected as P-PRP. The concentration of platelets, WBCs and RBCs in WB and P-PRP was determined using the ABX Micros ES 60 hematology analyzer (HORIBA ABX Diagnostics, Montpellier, France).

#### 4.2.5. Preparation of activated P-PRP (aP-PRP)

aP-PRP was prepared by activation of P-PRP using autologous serum (Ser) and 10% (w/v) CaCl<sub>2</sub> solution as agonists in the following proportions: agonist/P-PRP=20% (v/v); Ser/CaCl<sub>2</sub> volumetric ratio=9. Autologous serum was prepared by collecting 5 mL of WB in tubes without anticoagulant. After 30 minutes of clot formation, WB was centrifuged at 2000xg for 10 minutes (Perez *et al.*, 2014).

#### 4.2.6. Preparation of composite scaffold (aP-PRP/SPCHTs)

aP-PRP/SPCHTs were prepared by dripping aP-PRP, immediately after activation, onto SPCHTs. The preparation was carried out in 48-well microplates using

200  $\mu$ L of aP-PRP/10-20 mg of PCHTs.

#### 4.2.7. h-AdMSCs isolation and pre-cultivation

Human subcutaneous adipose tissue initially acquired from liposuction surgery was washed with sterile PBS, separated into 10 g samples, digested with 20 mg of collagenase type 1A and maintained in 20 mL of DMEM-LG containing 10% bovine serum albumin (BSA) and 10  $\mu$ L of gentamicin for 30 min in a 37°C bath. After complete digestion, the reaction was quenched with 10 mL fetal bovine serum (FBS) and immediately centrifuged for 15 min at 1500 rpm. The supernatant was discarded, and the pellet was suspended in 10 mL DMEM-LG with 10% FBS. After pre-cultivation for 24 h, the culture medium was changed every 3 days and after the fourth passage, the cells were characterized by immunophenotyping using flow cytometry and adipogenic, osteogenic and chondrogenic differentiation (data not shown), then were used in the subsequent experiments.

#### 4.2.8. h-AdMSCs-seeding in the composite scaffolds

The pre-cultured h-AdMSCs were trypsinized and re-suspended in P-PRP to a final cell concentration of  $1 \times 10^4$  cells/ mL. P-PRP containing h-AdMSCs was activated and immediately embedded in the SPCHTs in a 24-well tissue culture plate using 200  $\mu$ L of h-AdMSCs+aP-PRP/10-20 mg of SPCHTs. The composite scaffolds seeded were with h-AdMSCs and incubated at room temperature for 45 minutes for the consolidation of the fibrin network. aP-PRP was used as the control.

#### 4.2.9. Characterization of the composite scaffold

##### 4.2.9.1. Release of GFs

The release of platelet-derived growth factor AB (PDGF-AB) and transforming growth factor  $\beta$ 1 (TGF- $\beta$ 1) was assessed after 1 hour gelation of aP-PRP associated to SPCHTs in the presence of the culture medium (Dulbecco's Modified Eagle's Medium (DMEM-LG) (Gibco, Grand Island, NY, USA) with low glucose concentration). The culture medium (1.5 mL) was added to aP-PRP/SPCHTs in 48 well microplates, which

were maintained in an incubator with 5% CO<sub>2</sub> for the duration of the assays. The total volume of culture medium was removed at 3, 6, 12, 24 and 72 hours, and the same volume of fresh medium was replaced without removing the hydrogels from the wells. The samples were stored at -80°C for further characterization. The concentration of the released GFs PDGF-AB and TGF-β1 were measured using enzyme-linked immunosorbent assay (ELISA) kits (R&D Systems, Minneapolis, MN, USA) according to the manufacturer's instructions and specifications.

#### 4.2.9.2. Images of the cell-seeded composite scaffolds

The images of cell-seeded composite scaffolds were obtained by scanning electron microscopy after 5 days of h-AdMSCs proliferation. The cell-seeded composite scaffolds were fixed in a solution of 4% paraformaldehyde and 2.5% glutaraldehyde in phosphate buffer, pH 7.4, for 2 hours. The samples were then dehydrated in ethanol for 15 min intervals in aqueous 50%, 70%, 95% and 100% ethanol solutions (2x) and dried at the critical point dryer BAL-TEC CPD 030 (Schalksmühle, Germany). After gold coating (Sputter Coater POLARON, SC7620, VG Microtech), the cell-seeded composite scaffolds were visualized with a scanning electron microscope (Leo 440i LEO) with an accelerating voltage of 20 kV.

#### 4.2.9.3. h-AdMSCs proliferation

The cultivation of h-AdMSCs was performed in 24-well tissue culture plates by adding 1 mL of the DMEM culture medium to the seeded composite scaffolds (n=4) and controlling the temperature at 37°C for 10 days. Cell proliferation was quantified by MTT assay. After 3, 5, 7 and 10 days of cultivation, the composite scaffolds were removed and transferred to 24-well plates. Then, MTT (1 mL of 1 mg/mL) was added, and the cultivation proceeded at 37°C for 4 hours. The MTT solution was discarded, and 1 mL of DMSO was added to dissolve the purple formazan crystals. The samples were shaken at 120 rpm for 30 min to ensure homogeneous dissolution of the formazan dye, and then 200 µL of each sample was transferred to a 96-well plate. The optical density was measured at 595 nm using a microplate reader (FilterMax F5 Molecular Devices).

#### 4.2.9.4. Induction of osteogenic differentiation

h-AdMSCs-seeded in the composite scaffolds were induced to differentiate into the osteogenic lineage by providing osteogenic medium containing DMEM-LG supplemented with 10% FBS, 1%  $\beta$ -glycerol-phosphate (Sigma-Aldrich, St. Louis, MO, USA), 1% L-ascorbic acid (Sigma-Aldrich, St. Louis, MO, USA), 1% dexamethasone (Sigma-Aldrich, St. Louis, MO, USA) and 1% Penicillin/Streptomycin solution (Gibco, Grand Island, NY, USA). The medium was changed every 7 days.

#### 4.2.9.5. Alkaline phosphatase activity (ALP)

The level of alkaline phosphatase (ALP) activity in h-AdMSCs was determined on day 14. The supernatant (200  $\mu$ L) was collected and mixed with 200  $\mu$ L of the substrate p-nitrophenyl phosphate (SIGMAFAST™ p-nitrophenyl phosphate tablets, Sigma, Saint Louis, MI, USA) and incubated at room temperature for 30 minutes. Absorbance was read immediately on a spectrophotometer at 405 nm.

#### 4.2.10. Statistical analysis

Each experiment was performed in triplicate unless otherwise specified. All of the results are presented as the mean  $\pm$  standard deviation (SD). The experimental data from all of the studies were analyzed using Analysis of Variance (ANOVA). Statistical significance was set to p-value  $\leq$  0.05.

### 4.3. Results and discussion

#### 4.3.1. Modifications and surface chemistry

The FTIR spectra of the SPCHTs from the various treatments is shown in Figure 17. The FTIR spectra of non-treated scaffolds (NTPCHTs) were included as controls.

FTIR spectra of SPCHTs/TNaOH and SPCHTs/TEtOH showed no significant modification of the chemical structure of chitosan compared to the NTPCHTs, which showed peaks at 1550  $\text{cm}^{-1}$  and 1400  $\text{cm}^{-1}$  corresponding to asymmetric and symmetric carboxylate ion stretching, characteristic of the presence of acetate ions in the chitosan

acetate salt and suggesting incomplete deacetylation of chitosan (Noriega & Subramanian, 2011; Demarger-Andre & Domard, 1994). Therefore, the chemical groups of SPCHTs/TNaOH and SPCHTs/TEtOH exposed to PRP and h-AdMSCs during *in vitro* assays are  $-\text{NH}_3^+$  and  $-\text{OH}$  from the chitosan chain, which favor osteoblast differentiation (Chang & Wang, 2011).

The formation of an intermolecular complex between the  $-\text{NH}_3^+$  group of chitosan and the  $\text{P}_3\text{O}_{10}^{5-}$  of TPP in the SPCHTs/CTPP was characterized by the presence of the P=O and P-O groups at the frequencies of  $1100\text{ cm}^{-1}$  and  $1232\text{ cm}^{-1}$ , respectively (Mi *et al.*, 1999). In this case, the crosslinking decreased the positive charge on the chitosan exposed to PRP and h-AdMSCs during the *in vitro* assays. However, there is increased scaffold hydrophilicity due to the presence of  $-\text{OH}$  and P=O groups from TPP that favor cell spreading, proliferation and differentiation (Chang & Wang, 2011).

Thus, the stabilized scaffolds prepared in this work show chemical surfaces favorable for cell processes required for tissue regeneration as well as being suitable for the adhesion and support of the fibrin network from PRP, which has a negative charge.

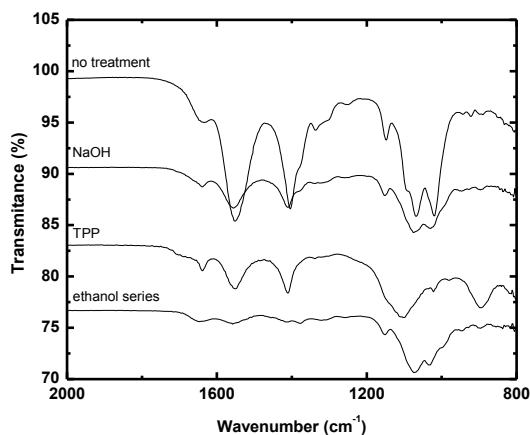


**Figure 17.** ATR-FTIR spectra of SPCHTs/TNaOH, SPCHTs/TEtOH, SPCHTs/CTPP and NTPCHTs.

#### 4.3.2. Physicochemical and mechanical properties of SPCHTs

In addition to surface chemistry, physicochemical and mechanical properties such as porous structure, Young's modulus, swelling and degradation over time play important roles in the performance of scaffolds. It is known that the microstructural



characteristics such as pore size and distribution, porosity and pore shape have prominent influences on cell intrusion, proliferation and function in tissue engineering (Ma *et al.*, 2003). When PRP is associated, the microstructure might also induce activation as well as support the fibrin network on the internal and external surfaces. These properties in conjunction are shown in Figure 18, for an easier comparison of the SPCHTs.

The micrographs obtained by SEM [Figure 18(a)] showed three-dimensional structures with visually interconnected pores in all cases. Scaffolds with open and interconnected pores are essential for cell nutrition, proliferation and migration promoting the vascularization and formation of new tissues (Loh & Choong, 2013). However, the surface chemistry provided by the treatments produced significant differences in the scaffolds.

The Young's modulus values [Figure 18(b)] were similar for SPCHT/TNaOH and SPCHT/TEtOH, approximately 1.4 MPa, but significantly larger than NTPCHTs (1.1 MPa). SPCHT/CTPP exhibited the highest mechanical resistance (1.8 MPa) due to the physical crosslinking, as expected.

Regardless of the type of treatment, the mean pore diameter [Figure 18(b)] could be controlled around 100-200  $\mu\text{m}$ . Tiğli *et al.* (2007) also obtained a pore size in the range of 100  $\mu\text{m}$ . Although controversial, several researchers have suggested optimal pore structures for the regeneration of specific tissues. Pore sizes of 100–400  $\mu\text{m}$  and 200–350  $\mu\text{m}$  have been suggested for bone tissue regeneration and osteoconduction, respectively (Oh *et al.*, 2007).

The smallest pores from TPP treatment are from crosslinking and entanglement of the chains of chitosan.

According to Ma *et al.* (2003), an additional freeze-drying can induce the fusion of some smaller pores to generate larger ones, or the slight collapse of the scaffold of the structure might reduce pore size. Therefore, in our scaffolds, the collapse effect was more prominent than fusion because the pores were smaller for all treatments. In addition, this effect seemed to be homogeneous in the structures.

According to Liu & Ma (2004), high porosity of scaffolds (such as  $\geq 90\%$ ) is important for any tissue engineering applications, including bone.

Porosity was similar for SPCHT/TNaOH and NTPCHT. A significant reduction in porosity and pore size was observed after rehydration and new lyophilization for SPCHT/CTPP. Final porosities were in the range of 93-97% [Figure 18(c)]. These values agree with those reported by Amaral *et al.* (2006) for similar scaffolds.

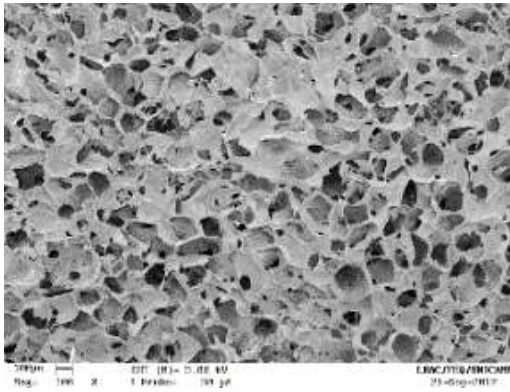
The water uptake property of the raw materials primarily influences the maintenance of the chitosan scaffolds' shape. Deformations in the structure affect cell proliferation and migration. The SPCHTs/TNaOH and SPCHTs/TEtOH [Figure 18(d)] exhibited rapid swelling in PBS pH 7.4 within 5 minutes. After 24 h their SR values were  $11 \pm 1$  and  $14 \pm 3$ , respectively, indicating extremely hydrophilic structures with the capacity to accommodate in their 3D structure large amounts of saline solution. SPCHTs/CTPP showed smaller SR in 24 hours ( $5.9 \pm 0.4$ ) because the crosslinking that reduces the functional groups that hydrogen bond with water and decreased the pore size and porosity. NTPCHT rehydrated in a neutral aqueous medium after 24 hours of rapid swelling and ultimately dissolved, indicating that the lyophilized structure was composed of soluble chitosan acetate.

The swelling was stabilized after 7.5 hours and increased in the following order: SPCHTs/TEtOH > SPCHTs/TNaOH > SPCHTs/CTPP. It was not possible to measure the swelling of NTPCHTs after 7 days due to the fragility of its structure.

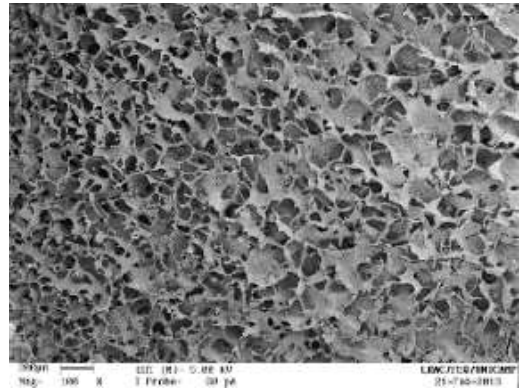
Degradation profiles were similar over 30 days. These results indicated that the treatments reduced the solubility of chitosan, providing stability to the scaffolds compared to NTPCHTs. The high weight loss (approximately 40%) of SPCHTs/TNaOH and SPCHTs/TEtOH likely occurs due to the presence of residual chitosan acetate that can cause rapid swelling and subsequently dissolution in a neutral aqueous medium.

Both processes, degradation and swelling, occur simultaneously and compete with other.

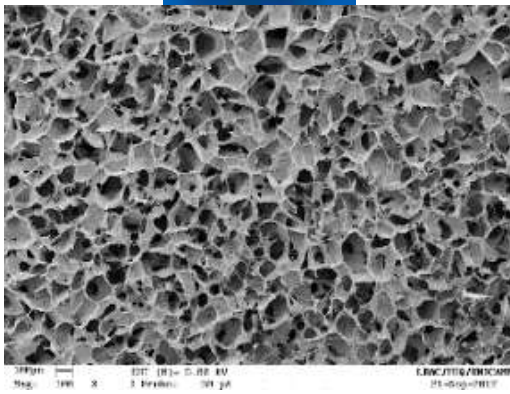




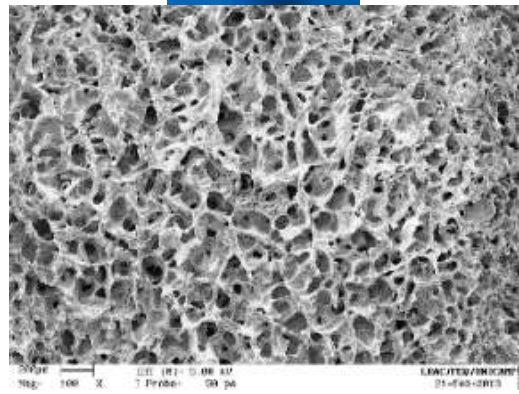
No treatment



Ethanol series



NaOH



TPP

(a)

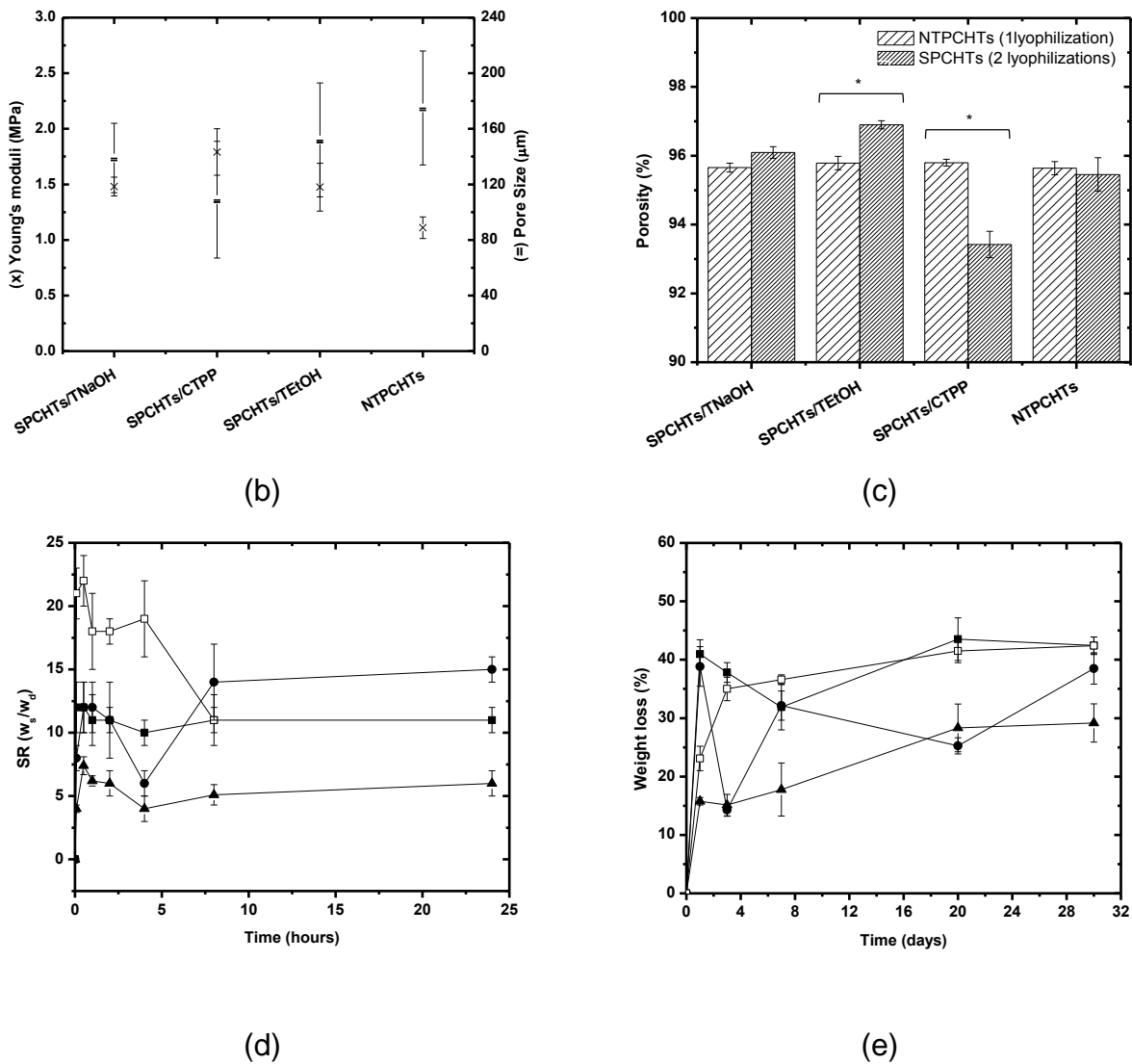


**Figure 18.** Physicochemical and mechanical properties of the PCHTs. (a) Photographs and SEM micrographs of the cross-section of the scaffolds. Original magnification is  $\times 100$  and the scale bar represents  $200 \mu\text{m}$ . (b) Young's moduli and pore size; (c) Porosity (\*The means difference are significant at level at  $p < 0.05$ ); (d) Swelling profile in PBS pH 7.4 at  $37^\circ\text{C}$ ; (e) Degradation profile in PBS pH 7.4 at  $37^\circ\text{C}$  expressed as weight loss. Values are the mean  $\pm$  standard deviation. (■) SPCHTs/TNaOH; (●) SPCHTs/TEtOH; (▲) SPCHTs/CTPP and (□) NTPCHTs.

The freeze-drying technique limits the pores to medium sizes and the mechanical properties of the porous structures even after cross-linking (Costa-Pinto *et al.*, 2011).

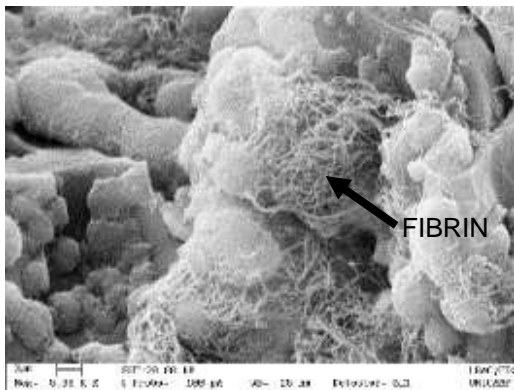
Therefore, the physicochemical characterization suggests that the SPCHTs might

be useful for bone regeneration. Stabilization provided pore sizes in the range of 100-150  $\mu\text{m}$  and porosities higher than 90%. In addition, they prevented the collapse of the structures after at least 10 days in PBS at pH 7.4 with swelling capacity. However, mechanical resistance was low, requiring further treatments for application in regions exposed to high shear.

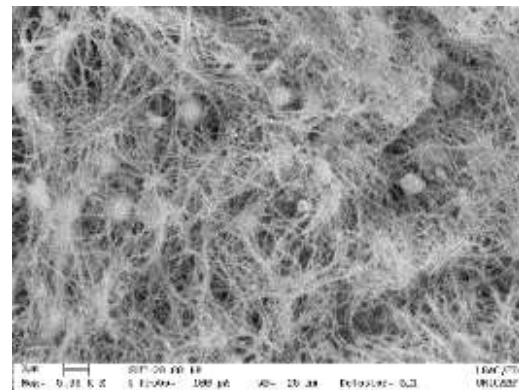
#### 4.3.3. Biological properties of SPCHTs

SEM characterization [Figure 19(a)] of the *aP*-PRP/PCHTs composite scaffolds after 5<sup>th</sup> days of culture indicated cell attachment and a fibrin network inside the pores and on the surface of SPCHTs. *aP*-PRP was used as control.

The cell compatibility, as assayed by MTT, of h-AdMSCs cultured in the presence of SPCHTs is shown in [Figure 19(b)]. This assay is widely used to determine cellular toxicity, viability and proliferation (Gümüřdereliolu & Aday, 2011). The results revealed no potential cytotoxicity over 24 hours for the SPCHTs according to the standard values (PCT). However, we observe reduced viability compared to the negative control toxicity (NCT) for SPCHTs/TNaOH and SPCHTs/CTPP.

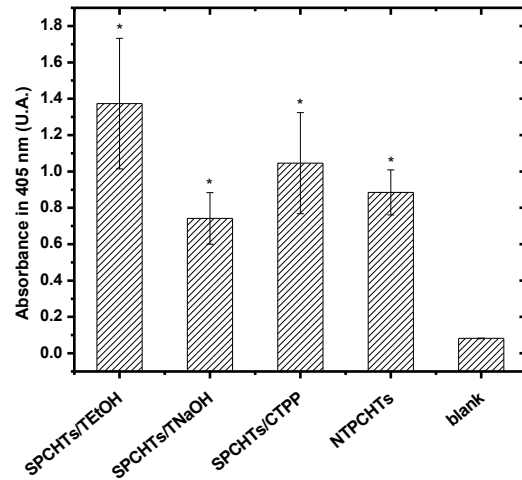


NTPCHTs



SPCHTs/TEtOH





(f)

**Figure 19.** (a) SEM images of cells on aP-PRP/SPCHTs after 5 days of culture. Scale bars indicate 3  $\mu\text{m}$  (magnification = 5,000x). (b) The compatibility of h-AdMSCs that were exposed to SPCHTs. Negative control (NTC) = DMEM with 10% FBS; positive control (PTC) = DMEM with phenol 0.5%. Mean  $\pm$  standard deviation  $n = 3$ . The population means are significantly different from the positive control at  $*p < 0.05$ . (c) Proliferation profile of h-AdMSCs cultured in aP-PRP/SPCHTs as a function of time. aP-PRP and NTPCHTs were used as controls. Platelets were concentrated in aP-PRP at approximately 1.84 times the basal value. The average concentration was 393,000  $\text{pq}/\text{mm}^3$ . (d) PDGF-AB release profile from aP-PRP/SPCHTs. Platelets were concentrated in aP-PRP at approximately 2.09 times the basal value. The average concentration was 472,250  $\text{pq}/\text{mm}^3$ . (e) TGF- $\beta$ 1 release profile from aP-PRP/SPCHTs. Platelets were concentrated in aP-PRP at approximately 2.09 times the basal value. The average concentration was 472,250  $\text{pq}/\text{mm}^3$ . (f) ALP activity of cells cultured on SPCHTs (statistically significant differences from blank,  $n=3$ ,  $*p < 0.05$ ). NTPCHTs is the control group, blank = the reagents used in the assay only. Platelets were concentrated in aP-PRP at approximately 1.79 times the basal value. The average concentration was 280,500  $\text{pq}/\text{mm}^3$ . ( $\Delta$ ) aP-PRP and ( $\square$ ) NTPCHT were both used as controls; ( $\bullet$ ) SPCHTs/TEtOH; ( $\blacksquare$ ) SPCHTs/TNaOH, and ( $\blacktriangle$ ) SPCHTs/CTPP.

The cell number per well as a function time for aP-PRP/ SPCHTs [Figure 19(c)]

showed that the number of viable cells determined after 3 days exceeded the number of seeded cells ( $1.4 \times 10^4$  cells/well) in all of the composite scaffolds, indicating that the cells grown in the matrices retained their viability, regardless of the treatment. The results also indicated cell proliferation was significantly higher ( $p < 0.05$ ) for the aP-PRP/SPCHTs compared to the control aP-PRP. Cultivation in aP-PRP/SPCHTs/TNaOH showed faster cell proliferation, and the stationary phase was reached in 5<sup>th</sup> days, whereas for aP-PRP/SPCHTs/CTPP the proliferation shows a nearly linear increasing profile. In aP-PRP/SPCHTs/TEtOH, the cells had a longer lag phase (5 days) followed by an exponential phase in the subsequent period.

TEtOH has the added advantage of allowing direct sterilization of samples in 70% ethanol; however, after treatment, the scaffolds should be equilibrated with culture medium or PBS for several hours prior to any cell seeding or *in vivo* implantation activity (Oh *et al.*, 2007).

Cultivation in aP-PRP/NTPCHT reached the exponential phase in 5<sup>th</sup> days and decreased sharply afterward due to the collapse of the non-stabilized structure.

The curves of Figure 19(d) and 19(e) show PDGF-AB and TGF- $\beta$ 1 release kinetics from aP-PRP/SPCHTs with aP-PRP and aP-PRP/NTPCHTs used as controls. The curves show diffusive controlled profiles, indicating no collapse of the porous structure of chitosan scaffolds over the duration of the assays. The differences in the profiles are due to interactions of the GFs with the surface groups generated by the various stabilizing treatments.

The ALP activity of h-AdMSCs assayed after 14 days of cultivation is shown in Figure 19(f). The ALP activity of the cells cultured on aP-PRP/SPCHTs and aP-PRP/NTPCHTs scaffolds showed significant differences from the control ( $p < 0.05$ ), suggesting that the composite scaffolds favored osteogenic differentiation. Moreover, the differentiation of the composite scaffold treated with TEtOH was significantly higher than for non-stabilized PCHT.

#### **4.4. Conclusions**

Composite scaffolds of stabilized porous chitosan and activated P-PRP were



prepared and characterized. The stabilization of the porous chitosan was accomplished by using various treatments. In general, the composite scaffolds controlled the release of growth factors and improved proliferation of h-AdMSCs that were seeded compared to activated P-PRP. Osteogenic differentiation evaluated by ALP marker was favored by the stabilization provided mainly by the ethanol series treatment. These findings are important for optimizing composite scaffolds for applications in regenerative medicine.

**Acknowledgements.** The authors acknowledge the financial support from the National Council of Technological and Scientific Development (CNPq, Brazil). They also thank Prof. Dr. William Dias Belangero and Dr. Ana Amélia Rodrigues of the Faculty of Medical Sciences (University of Campinas) for assistance and Dr. Ângela Cristina Malheiros Luzo of the Haematology and Hemotherapy Center (University of Campinas) for the donation of h-AdMSCs.

## 4.5. References

AMARAL, I.F., SAMPAIO, P., BARBOSA, M.A. Three-dimensional culture of human osteoblastic cells in chitosan sponges: The effect of the degree of acetylation. **Journal of Biomedical Materials Research**, vol.76A p.335-346, 2006.

BHUMKAR, D.R.; POKHARKAR, V.B. Studies on Effect of pH on Cross-linking of Chitosan with Sodium Tripolyphosphate: A Technical Note. **AAPS Pharm Sci Tech**, vol.7, n.2, p.E1-E6, 2006.

BI, L.; CHENG, W.; FAN, H.; PEI, G. Reconstruction of goat tibial defects using an injectable tricalcium phosphate/chitosan in combination with autologous platelet-rich plasma. **Biomaterials**, vol.31, p.3201–3211, 2010.

CHANG, H-I.; WANG, Y. Cell Responses to Surface and Architecture of Tissue Engineering Scaffolds. In: Eberli, D. (Eds.). **Regenerative Medicine and Tissue Engineering - Cells and Biomaterials**, Croatia: InTech, chapter 27, p. 569-588, 2011.

CHANG, S.J.; KUO, S.M.; LAN, C-W.; MANOUSAKAS, I.; TSAI P.H. Evaluation of chitosan/CaSO<sub>4</sub>/ platelet-rich plasma microsphere composites as alveolus osteogenesis material. **Biomedical Engineering: Applications, Basis and Communications**, vol.21, n.2, p.115–122, 2009.

CORREIA, C.R.; TEIXEIRA, L.S.M.; MORONI, L.; REIS, R.L.; VAN BLITTERSWIJK, C.A.; KAPERIEN, M.; MANO J.F. Chitosan Scaffolds Containing Hyaluronic Acid for Cartilage Tissue Engineering. **Tissue Engineering Part C**, vol.17, n.7, p.717-730, 2011.

COSTA-PINTO, A.R.; REIS, R.L.; NEVES, N.M. Scaffolds Based Bone Tissue Engineering: The Role of Chitosan. **Tissue Engineering Part B**, vol.17, p.331-347, 2011.

CRANE, D.; EVERTS, P.A.M. Platelet Rich Plasma (PRP) Matrix Grafts, **PPM Communications**, vol.8, p.1-10, 2008.

DEMARGER-ANDRE, S.; DOMARD, A. Chitosan carboxylic acid salts in solution and in the solid state. **Carbohydrate Polymers**, vol.23, n.3, p.211-219, 1994.

EHRENFEST, D.M.D.; RASMUSSEN, L.; ALBREKTSSON, T. Classification of platelet concentrates: from pure platelet-rich plasma (P-PRP) to leucocyte- and platelet-rich fibrin (L-PRF). **Trends in Biotechnology**, vol.27, p.158-167, 2009.

GÜMÜŞDERELIOĞLU, M.; ADAY, S. Heparin-functionalized chitosan scaffolds for bone tissue engineering. **Carbohydrate Research**, vol.346, p.606-613, 2011.

HOM, D.B.; LINZIE, B.M.; TREVOR, C.; HUANG, T.C. The Healing Effects of Autologous Platelet Gel on Acute Human Skin Wounds. **Archives of Facial Plastic Surgery**, vol.9, n.3, p.174-183, 2007.

JACOBSON, M.; FUFA, D.; ABREU, E.L.; KEVY, S.; MURRAY, M.M. Platelets, but not erythrocytes, significantly affect cytokine release and scaffold contraction in a provisional scaffold model. **Wound Repair Regeneration**, vol.16, n.3, p.370-378, 2008.

KANAJI, N.; SATO, T.; NELSON, A.; WANG, X.; LI, Y.; KIM, M.; NAKANISHI, M.; BASMA, H.; MICHALSKI, J.; FARID, M.; CHANDLER, M.; PEASE, W.; PATIL, A.; RENNARD, S.I.; LIU, X. Inflammatory cytokines regulate endothelial cell survival and tissue repair functions via NF- $\kappa$ B signaling. **Journal of Inflammation Research**, vol.4 p.127–138, 2011.

KOJIMA, K.; OKAMOTO, Y.; MIYATAKE, K.; FUJISE, H.; SHIGEMASA, Y.; MINAMI, S. Effects of chitin and chitosan on collagen synthesis in wound Healing. **Journal of Veterinary Medical Science**, vol.66, p.1595-1598, 2004.

KUTLU, B.; AYDIN, R.S.T.; AKMAN, A.C.; GÜMÜŞDERELIOĞLU, M.; NOHUTCU, R.M. Platelet-rich plasma-loaded chitosan scaffolds: Preparation and growth factor release kinetics. **Journal of Biomedical Materials Research**, vol.101B, p.28-35, 2012.

LANA, J.F.S.D.; SANTANA, M.H.A.; BELANGERO, W.D.; LUZO, A.C.M. **Platelet-Rich Plasma: Regenerative Medicine: Sports Medicine, Orthopedic, and Recovery of Musculoskeletal Injuries** (Lecture Notes in Bioengineering), 1st ed., Springer, 2014.

LEE, Y.M.; PARK, Y.J.; LEE, S.J.; KU, Y.; HAN, S.B.; CHOI, S.M.; KLOKKEVOLD, P.R.; CHUNG, C.P. Tissue engineered bone formation using chitosan/tricalcium phosphate sponges. **Journal of Periodontology**, vol.71, p.410-417, 2000.

LIU, X.; MA, P.X. Polymeric Scaffolds for Bone Tissue Engineering. **Annals of Biomedical Engineering**, vol.32, n.3, p.477-486, 2004.

LIU, Y.B.A.; KALÉN, A.; RISTO, O.; WAHLSTRÖM, O. Fibroblast Proliferation due to Exposure to a Platelet Concentrate in Vitro is pH Dependent. *Wound Regeneration*, vol.10 p.336-340, 2002.

LOH, Q.L.; CHOONG, C. Three-Dimensional Scaffolds for Tissue Engineering Applications: Role of Porosity and Pore Size. **Tissue Engineering - Part B**, vol.19, n.6, p.485-503, 2013.

MA, L.; GAO, C.; MAO, Z.; ZHOU, J.; SHEN, J.; HU, X.; HAN, C. Collagen/chitosan porous scaffolds with improved biostability for skin tissue engineering. **Biomaterials**, vol.242, p.4833-4841, 2003.

MADIHALLY, S.V.; MATTHEW, H.W.T. Porous chitosan scaffolds for tissue engineering. **Biomaterials**, vol.20, p.1133-1142, 1999.

MANJUBALA, I.; SCHELER, S.; BÖSSERT, J.; JANDT, K.D. Mineralisation of chitosan scaffolds with nano-apatite formation by double diffusion technique. **Acta Biomaterialia**, vol.2, p.75-84, 2006.

MARX, R.E. Platelet-rich plasma: Evidence to support its use. **Journal of Oral and Maxillofacial Surgery**, vol.62, p. 489–496, 2004.

MI, F-L.; SHYU, S-S.; LEE, S-T.; WONG, T-B. Kinetic Study of Chitosan-Tripolyphosphate Complex Reaction and Acid-Resistive Properties of the Chitosan-Tripolyphosphate Gel Beads Prepared by in-Liquid Curing Method. **Journal of Polymer Science Part B: Polymer Physics**, vol.37 p.1551-1564, 1999.

MOSSMAM, T.J. A rapid colorimetric assay of cellular growth and survival: application to proliferation and cytotoxicity assays. **Journal of Immunological Methods**, vol.65, p.55-63, 1983.

NASTI, A.; ZAKI, M.N.; DE LEONARDIS, P.; UNGPHAIBOON, S.; SANSONGSAK, P.; RIMOLI, M.G.; TIRELLI, N. Chitosan/TPP and Chitosan/TPP-hyaluronic Acid Nanoparticles: Systematic Optimisation of the Preparative Process and Preliminary Biological Evaluation. **Pharmaceutical Research**. vol.26, n.8, p.1918-1930, 2009.

NORIEGA, S.E.; SUBRAMANIAN, A. Consequences of Neutralization on the Proliferation and Cytoskeletal Organization of Chondrocytes on Chitosan-Based Matrices. **International Journal of Carbohydrate Chemistry**, p.1-13, 2011.

NWE, N.; FURUIKE, T.; TAMURA, H. The Mechanical and Biological Properties of Chitosan Scaffolds for Tissue Regeneration Templates Are Significantly Enhanced by Chitosan from *Gongronella butleri*. **Materials**, vol.2, p.374-398, 2009.

OH, S.H.; PARK, I.K.; KIM, J.M.; LEE, J.H. In vitro and in vivo characteristics of PCL scaffolds with pore size gradient fabricated by a centrifugation method. **Biomaterials**, vol.28, p.1664-1671, 2007.

OKAMOTO, Y.; YANO, R.; MIYATAKE, K.; TOMOHIRO, I.; SHIGEMASA, Y.; MINAMI, S. Effects of chitin and chitosan on blood coagulation. **Carbohydrate Polymers**, vol.53, p.337-342, 2003.

OKTAY, E.O.; DEMIRALP, B.; DEMIRALP, B.; SENEL, S.; AKMAN, A.; ERATALAY, K.; AKINCIBAY, H. Effects of platelet-rich plasma and chitosan combination on bone regeneration in experimental rabbit cranial defects. **Journal of Oral Implantology**, vol.36, p.175–184, 2010.

OUYANG, W.; BUSCHMANN, M.; CHEVRIER, A. Soluble physiological chitosan formulations combined with platelet-rich plasma (PRP) for tissue repair. **United States Patent: U.S. 0,004,474 A1**, 2013.

PEREZ, A.G.M.; LANA, J.F.S.D.; RODRIGUES, A.A.; LUZO, A.C.M.; BELANGERO, W.D.; SANTANA, M.H.A. Relevant Aspects of Centrifugation Step in the Preparation of Platelet-Rich Plasma. **ISRN Hematology**, vol.2014, p.1-8, 2014.

PEREZ, A.G.M.; LICHY, R.; LANA, J.F.S.D.; RODRIGUES, A.A.; LUZO, A.C.M.; BELANGERO, W.D.; SANTANA, M.H.A. Prediction and Modulation of Platelet Recovery by Discontinuous Centrifugation of Whole Blood for the Preparation of Pure Platelet-Rich Plasma. **BioResearch Open Access**, vol.2, p.307-314, 2013.

REIS, R.L.; NEVES, N.M.; MANO, J.F.; GOMES, M.E.; MARQUES, A.P.; AZEVEDO, H.S. **Natural-based polymers for biomedical applications**. Cambridge: Woodhead Publishing, 2008.

ROSSI, S.; FACCENDINI, A.; BONFERONI, M.C.; FERRARI, F.; SANDRI, G.; DEL FANTE, C.; PEROTTI, C.; CAMELLA, C.M. Sponge-like dressings based on biopolymers for the delivery of platelet lysate to skin chronic wounds. **International Journal of Pharmaceutics**, vol.440, p.207-215, 2013.

SANO, M.; HOSOYA, O.; TAOKA, S.; SEKI, T.; KAWAGUCHI, T.; SUGIBAYASHI, K.; JUNI, K.; MORIMOTO, Y. Relationship between Solubility of Chitosan in Alcoholic Solution and Its Gelation. **Chemical and pharmaceutical bulletin**, vol.47, n.7, p.1044-1046, 1999.

SEOL, Y.J.; LEE, J.Y.; PARK, Y.J.; LEE, Y.M.; YOUNG, K.; RHYU, I.C.; LEE, S.J.; HAN, S.B.; CHUNG, C.P. Chitosan sponges as tissue engineering scaffolds for bone formation. **Biotechnology Letter**, vol.26; p.1037-1041, 2004.

SHEN, E.C.; CHOU, T.C.; GAU, C.H.; TU, H.P.; CHEN, Y.T.; FU, E. Releasing growth factors from activated human platelets after chitosan stimulation: a possible bio-material for platelet-rich plasma preparation. **Clinical Oral Implants Research**, vol.17, p.572-578, 2006.

SHEN, F.; CUI, Y.L.; YANG, L.F.; YAO, K.D.; DONG, X.H.; JIA, W.Y.; SHI, H.D. A study on the fabrication of porous chitosan/gelatin network scaffold for tissue engineering, **Polymer International**, vol.49, p.1596-1599, 2000.

TAN, H.P.; CHU, C.R.; PAYNE, K.A.; MARRA K.G. Injectable in situ forming biodegradable chitosan-hyaluronic acid based hydrogels for cartilage tissue engineering. **Biomaterials**, vol.30, p.2499–2506, 2009.

TIĞLI, R.S.; KARAKEÇİLİ, A.; GÜMÜŞDERELİOĞLU, M. In vitro characterization of chitosan scaffolds: influence of composition and deacetylation degree. **Journal of Materials Science: Materials in Medicine**, vol.18, p.1665-1674, 2007.

WANG, Y.; LIN, M.; WANG, D.; HSIEH H. Fabrication of a novel porous PGA–chitosan hybrid matrix for tissue engineering. **Biomaterials**, vol.24, p.1047–1057, 2003.



# CAPÍTULO 5 – IN VITRO BIOLOGICAL PERFORMANCE OF INJECTABLE CHITOSAN-TRIPOLYPHOSPHATE SCAFFOLDS COMBINED WITH PLATELET-RICH PLASMA

---

Artigo submetido ao periódico *Tissue Engineering and Regenerative Medicine*.

Andréa Arruda Martins Shimojo<sup>1</sup>, Sofia Elisa Moraga Galdames<sup>1</sup>, Amanda Gomes Marcelino Perez<sup>1</sup>, Thiago Heiji Ito<sup>2</sup>, Maria Helena Andrade Santana<sup>1\*</sup>

<sup>1</sup>Department of Engineering of Materials and Bioprocesses, School of Chemical Engineering, University of Campinas (UNICAMP), Campinas, SP, Brazil.

<sup>2</sup>Department of Physical Chemistry, Institute of Chemistry, University of Campinas, (UNICAMP), Campinas, SP, Brazil.

\*Corresponding author: Maria Helena Andrade Santana; PHONE: +55 19 35213921; FAX: +55 19 35213890; e-mail: [mariahelena.santana@gmail.com](mailto:mariahelena.santana@gmail.com)

**Abstract:** This study aimed to evaluate the *in vitro* biological effectiveness of chitosan-sodium tripolyphosphate microparticles in combination with activated platelet-rich plasma as an injectable composite scaffold for growth factor release, cell proliferation and osteogenic differentiation. The microparticles were prepared by vortexing the chitosan and TPP solutions. The ionic crosslinking of chitosan with TPP was made at mass ratios of 2:1, 5:1, and 10:1 at pH 4.0. Pure platelet-rich plasma (P-PRP) was obtained via the controlled centrifugation of whole blood. The composite scaffolds were prepared by adding the microparticles to immediately activated P-PRP. The results showed that the microparticles enhanced the physicochemical and mechanical properties of aP-PRP. The proliferation of human adipose-derived mesenchymal stem cells was lower than in aP-PRP but significant at a 2:1 chitosan:TPP mass ratio.

Osteogenic differentiation was stimulated at all studied mass ratios, as indicated by the ALP activity. These results offer perspectives for optimizing the composite scaffold, and to prove its potential as an injectable scaffold in regenerative medicine.

**Keywords:** Chitosan; tripolyphosphate; platelet-rich plasma; injectable scaffolds; composite.

## 5.1. Introduction

Due to their minimally invasive implantation procedures, injectable scaffolds have been widely investigated and are considered promising in tissue engineering (Kretlow *et al.*, 2007).

From the clinical perspective, the use of injectable scaffolds is advantageous because it minimizes patient discomfort, the risk of infection and scarring, and the cost of treatment (Hou *et al.*, 2004). Furthermore, injectable scaffolds can homogeneously fill the defect or repair point and can incorporate cells and various therapeutic agents such as growth factors prior to injection (Gutowska *et al.*, 2001).

From the biomaterial perspective, adequate injectable scaffolds must be nontoxic, biodegradable, and sterilizable. Moreover, they must solidify under mild conditions, show mechanical strength and resistance to in situ forces and allow for the incorporation of bioactive molecules.

Various types of biodegradable materials have been proposed for the preparation of injectable scaffolds used in tissue engineering. Considerable attention has been given to chitosan-based materials, primarily due to their similarities with the extracellular matrix, chemical versatility, good biological performance, and specific cellular interactions (Costa-Pinto *et al.*, 2011).

Chitosan scaffolds have been prepared as hydrogels by physical association (Berger *et al.*, 2004), coordination with metal ions (Brack *et al.*, 1997) and chemical crosslinking (Hennink & Van Nodtrum, 2002). However, the use of chemical crosslinking agents are a major obstacle to scaffold fluids due to their toxicity to the cells. Thus, tripolyphosphate (TPP) and genipin have become attractive alternatives to chitosan



crosslinking (Bhumkar & Pokharkar, 2006; Ibezim *et al.*, 2010; Harris *et al.*, 2010; Karnchanajindanun *et al.*, 2010).

The electrostatic interaction between chitosan and TPP leads to the formation of biocompatible crosslinked chitosan hydrogels, which could be used as injectable scaffolds in micro- and/or nanoparticles in non-surgical treatments.

Platelet-rich plasma (PRP) is an autologous concentrate of platelets and other components of plasma that is capable of releasing the growth factors and cytokines used in tissue regeneration (Anitua, 1999; Foster *et al.*, 2009). PRP has been successfully used in regenerative medicine (Crane & Everts, 2008; Cole *et al.*, 2010).

When activated, aP-PRP produces a fibrin network with a gel-like structure that supports cell proliferation and differentiation (Marx, 2004). Efforts have been made to improve the stability and rheological properties of the fibrin network.

In our previous studies, we have shown that porous chitosan sponges stabilized by crosslinking with TPP had adequate physicochemical properties for tissue engineering uses. Moreover, in combination with aP-PRP, the sponges supported the fibrin network, increased its stability, delayed the release of PDGF-AB and TGF- $\beta$ 1 compared to aP-PRP alone, and allowed the proliferation and differentiation of h-AdMSCs.

In the present work, we extended our previous findings by evaluating the performance of the combination of chitosan microparticles and activated P-PRP as a composite scaffold. Our hypothesis is that the crosslinked microparticles will also improve the properties of aP-PRP alone, with the benefits of an injectable formulation.

## **5.2. Materials and Methods**

### **5.2.1. Materials**

Chitosan (average molecular weight [Mw] =  $4 \times 10^5$  Da, degree of deacetylation =  $83 \pm 4\%$ ) was purchased from Polymar® (Fortaleza, Brazil) and purified according to the protocol described by Nasti *et al.* (2009). Other chemicals were reagent grade and were used without any further purification. All biological experiments were performed with human adipose-derived mesenchymal stem cells (h-AdMSCs) and approved by the

Ethics Committee of the Medical Sciences School of the University of Campinas (UNICAMP; CAAE: 0972.0.146.000-11). The donors were healthy individuals between 30 and 40 years old and were previously assessed through their clinical examinations.

### 5.2.2. Preparation of injectable scaffolds of chitosan-sodium tripolyphosphate (iCHT-TPPs)

The injectable scaffolds (iCHT-TPPs) prepared in this work are composed of hydrogels of chitosan microparticles that were ionically crosslinked with TPP. Initially, a chitosan solution 2.5% (w/v) was prepared by dissolution in acetic acid 5% (w/v). TPP solution was prepared as a 5% (w/v) solution in Milli-Q water. The solutions were mixed at mass ratios CHT-TPP of 2:1, 5:1 and 10:1 and vortexed for 5 minutes to obtain the microparticles. The crosslinking was carried out at 25°C for 24 hours at pH 4. The hydrogels were washed three times with water and phosphate buffered saline (PBS) (LB Laborclin, Pinhais, PR, Brazil) at pH 7.4 and centrifuged at 10,000 rpm for 10 minutes.

### 5.2.3. Physicochemical Characterization

#### 5.2.3.1. Chemical modification.

The ionic crosslinking was characterized by Fourier-transform infrared (FTIR) in a Thermo Scientific Nicolet model 6700 (Thermo Scientific Nicolet™, Waltham, MA, USA). Measurements were made in the ATR mode with accessory SMART OMNI-SAMPLER, in the spectral range of 4000-675  $\text{cm}^{-1}$  resolution of 4  $\text{cm}^{-1}$  and 64 scans. Pure chitosan was used as control.

ATR-IR (chitosan): 3500–3000 ( $\nu$  OH and  $\text{NH}_2$ ), 2875 ( $\nu$ CH), 1645 (amide I), 1550 (amide II) 1380, 1067, 1020  $\text{cm}^{-1}$  (Nasti *et al.*, 2009).

#### 5.2.3.2. Crosslink density Flory-Rehner calculations.

Crosslink density was evaluated by measuring the volumetric swelling and using a simplified version of the Flory-Rehner equation (Flory & Rehner, 1943), according to Collins & Birkinshaw (2008). The value used for chitosan–water interaction parameter ( $\chi$ ) was 0.5917 (Jin & Song, 2006).

#### 5.2.3.3. Particle diameter measurements

The mean diameter of the particles was evaluated by laser light scattering in a Mastersizer S particle size analyzer, model Long Bench-MAM 5005 (Malvern Instruments, Worcestershire, UK). The particle size analysis was performed with the hydrogels dispersed in water. The standard deviation was calculated from five measurements of the mean diameter.

#### 5.2.3.4. Rheology measurements.

Rheological measurements were performed in steady and oscillatory regimes at 25°C, using a parallel plate geometry of 20 mm. Steady shear measurements were obtained at shear rates of 0.1-50 s<sup>-1</sup>. Oscillatory measurements were conducted in the linear region, at a stress of 1.188 Pa and in the frequency range of 0.01 to 10 Hz. All rheological measurements were performed on a rheometer Haake RheoStress 1 (Haake, Karlsruhe, Germany).

#### 5.2.3.5. Extrusion force.

Initially the iCHT-TPPs were loaded in 1-mL plastic syringes with 30-gauge needles. Subsequently, the force required to extrude was measured using a MTS 810 Servo-hydraulic Universal Testing Machine (MTS Systems Corporation, Eden Prairie, MN, USA) (Load Cell 1.5 kN) at 25°C at a 5.0 mm/ min extrusion rate.

#### 5.2.3.6. Swelling ratio (SR).

The microparticles were weighed after swelling in phosphate buffered saline (PBS) at pH 7.4, and their dry weight was determined by drying under vacuum (1 mmHg) at 25°C after 3 days. SR was calculated using the Equation (1):

$$SR = \frac{ws}{wd} \quad \text{Equation (1)}$$

where ws and wd are the weights of the scaffolds at the swelling state and the dry state,

respectively.

#### 5.2.3.7. Degradation in phosphate buffered saline.

The degradation of iCHT-TPPs was examined with respect to weight loss. The weight loss of the initially weighed iCHT-TPPs ( $w_0$ ) was monitored as a function of incubation time in PBS at 37°C. At specified time intervals, iCHT-TPPs were removed from the PBS and weighed ( $w_t$ ). The weight loss ratio was defined as in Equation (2) (Tan *et al.*, 2009).

$$\text{weight loss (\%)} = \frac{(w_0 - w_t)}{w_0} \times 100 \quad \text{Equation (2)}$$

### 5.2.4. Biological characterization

#### 5.2.4.1. Cell compatibility.

The compatibility of the iCHT-TPPs was carried out by exposure to h-AdMSCs and cultivation at 37°C for 24 hours. The cell compatibility was evaluated using a modified MTT (3-[4,5-dimethyl-thiazol-2-yl]-2,5-diphenyltetrazolium bromide) assay (MTT, Molecular Probes®, São Paulo, SP, Brazil) (Mossmam, 1983). The MTT assay is a colorimetric test that is based on the reduction of yellow tetrazolium salt into a purple formazan product in presence of cells (Gümüşderelioğlu & Aday, 2011).

#### 5.2.5. Preparation of pure platelet-rich plasma (P-PRP)

P-PRP, a PRP type that is rich in platelets and poor in leukocytes, was prepared according to Perez *et al.* (2013). Briefly, whole blood (WB) was collected into 3.5 mL vacuum tubes (Vacuette®, Campinas, SP, Brazil) containing sodium citrate 3.2% (w/v) as an anticoagulant. WB was initially centrifuged in a Rotina 380R centrifuge (Hettich® Zentrifugen, Tuttlingen, Germany) at 100 xg for 10 minutes at 25°C. After the formation of three layers (a bottom layer composed primarily of red blood cells (RBCs); an upper layer composed of plasma, platelets and some WBCs; and an intermediate layer, or buffy coat, composed primarily of WBCs), only the upper layer was collected to obtain P-PRP. The concentrations of platelets, WBCs and RBCs in WB and in P-PRP were determined using the ABX Micros ES 60 hematology analyzer (HORIBA ABX

Diagnostics, Montpellier, France).

#### 5.2.5.1. Activation of P-PRP (aP-PRP)

aP-PRP was prepared via the activation of P-PRP with autologous serum (Ser) and 10% (w/v) CaCl<sub>2</sub> solution as agonists using the following proportions: agonist/P-PRP=20%; Ser/CaCl<sub>2</sub> volumetric ratio=9. Autologous serum was prepared by collecting 5 mL of WB in tubes without anticoagulant. After 30 minutes of clot formation, WB was centrifuged at 2000 xg for 10 minutes.

#### 5.2.6. Preparation of composite scaffold (aP-PRP/iCHT-TPPs)

aP-PRP/iCHT-TPPs was prepared by embedding by dripping aP-PRP, immediately after activation, into iCHT-TPPs. The preparation was carried out in 48-well microplates using 200 µL of aP-PRP/ 100-200 mg of iCHT-TPPs.

#### 5.2.7. Characterization of aP-PRP/iCHT-TPPs

##### 5.2.7.1. Release of GFs

The release of platelet-derived growth factor AB (PDGF-AB) and transforming growth factor β1 (TGF-β1) was performed after a 1 hour gelation of aP-PRP associated to iCHT-TPPs in the presence of the culture medium Dulbecco's Modified Eagle's Medium with low glucose concentration (DMEM-LG, Gibco, Grand Island, NY, USA). The culture medium (1.5 mL) was added to aP-PRP/iCHT-TPPs in 48-well microplates, which were maintained in an incubator with 5% CO<sub>2</sub> throughout the assays. The total volume of culture medium was withdrawn at 3, 6, 12, 24 and 72 hours, and the same volume of fresh medium was replaced without removing the hydrogels from the wells. The samples were stored at -80°C for further characterization. The concentrations of the released GFs PDGF-AB and TGF-β1 were measured using enzyme-linked immunosorbent assay (ELISA) kits (R&D Systems, Minneapolis, MN, USA) according to the manufacturer's instructions and specifications.

### 5.2.8. h-AdMSCs isolation and pre-cultivation

Human subcutaneous adipose tissue, initially acquired from liposuction surgery, was washed with sterile PBS, separated into fractions of 10 g, digested with 20 mg of collagenase type 1A and maintained in 20 mL of DMEM-LG containing 10% BSA (bovine serum albumin) and 10  $\mu$ L of gentamicin for 30 min in a bath at 37°C. After complete digestion, the reaction was quenched with 10 mL fetal bovine serum (FBS) and immediately centrifuged for 15 min at 1500 rpm. The supernatant was discarded, and the pellet was suspended in 10 mL DMEM-LG with 10% FBS. After pre-cultivation for 24 h, the culture medium was changed every 3 days; after the fourth passage, the cells were characterized by immunophenotyping using flow cytometry and by adipogenic, osteogenic and chondrogenic differentiation (data not shown) and were then used in the subsequent experiments.

### 5.2.9. Culture of h-AdMSCs-seeding in the composite scaffolds

The pre-cultured h-AdMSCs were trypsinized and resuspended in P-PRP to a final cell concentration of  $1 \times 10^4$  cells/mL. P-PRP containing h-AdMSCs was activated and immediately embedded into the iCHT-TPPs in a 24-well tissue culture plate, using 200  $\mu$ L of h-AdMSCs+aP-PRP/100-200 mg of iCHT-TPPs. The composite scaffolds with h-AdMSCs were kept at room temperature for 45 minutes for the consolidation of the fibrin network. Activated PRP was used as a control.

#### 5.2.9.1. h-AdMSCs proliferation

The cultivation of h-AdMSCs was carried out in 24-well tissue culture plates by adding 1 mL of the culture medium DMEM to the seeded composite scaffolds (n=4). The seeded composite scaffolds was maintained at 37°C along 10 days. Cell proliferation was quantified using the thiazolyl blue tetrazolium bromide (MTT) assay. At cultivation days 3, 5, 7 and 10, the composite scaffolds were removed and transferred to 24-well plates. MTT (1 mL of 1 mg/mL) was then added, and the cultivation proceeded at 37°C for 4 hours. The MTT solution was then discarded, and 1 mL of dimethylsulfoxide (DMSO) was added to dissolve the purple formazan crystals. The samples were shaken

at 120 rpm for 30 min to ensure the homogeneous dissolution of the formazan dye, and 200  $\mu$ L of each sample was then transferred to a 96-well plate. Optical density was measured at 595 nm using a microplate reader (FilterMax F5 Molecular Devices).

#### 5.2.9.2. Images of the cell-seeded composite scaffolds

The images of cell-seeded composite scaffolds were obtained by scanning electron microscopy after 5 days of h-AdMSCs proliferation. The cell-seeded composite scaffolds were fixed in a solution of 4% paraformaldehyde and 2.5% glutaraldehyde in phosphate buffer, pH 7.4, for 2 hours. The samples were then dehydrated in ethanol for 15-min intervals in aqueous 50%, 70%, 95% and 100% ethanol solutions (2x) and dried using the critical point dryer BAL-TEC CPD 030 (BAL-TEC<sup>®</sup>, Schalksmühle, Germany). After gold coating in Sputter Coater POLARON SC7620 (VG Microtech, Ringmer, UK), the cell-seeded composite scaffolds were visualized using a scanning electron microscope Leo440i (LEO Electron Microscopy/Oxford, Cambridge, UK) with an accelerating voltage of 20 kV.

#### 5.2.9.3. Induction of osteogenic differentiation

h-AdMSCs-seeding composite scaffolds were induced to differentiate into the osteogenic lineage by providing the osteogenic medium containing DMEM-LG supplemented with 10% FBS, 1%  $\beta$ -glycerol-phosphate (Sigma-Aldrich, St. Louis, MO, USA), 1% L-ascorbic acid (Sigma-Aldrich, St. Louis, MO, USA), 1% dexamethasone (Sigma-Aldrich, St. Louis, MO, USA) and 1% Penicillin/Streptomycin solution (Gibco, Grand Island, NY, USA). The medium was changed every 7 days.

#### 5.2.9.4. Alkaline phosphatase activity (ALP)

The alkaline phosphatase (ALP) activity produced by h-AdMSCs was determined on day 14. Here, 200  $\mu$ L of the supernatant was collected and mixed with 200  $\mu$ L of p-Nitrophenyl phosphate (SIGMAFAST<sup>™</sup> p-Nitrophenyl phosphate Tablets, Sigma, Saint Louis, MI, USA) as substrate and subsequently incubated at room temperature for 30 minutes. Absorbance was read immediately on a spectrophotometer at 405 nm.

## 5.2.10. Statistical analysis

Each experiment was carried out in triplicate unless otherwise specified. All results are presented as the mean  $\pm$  standard deviation (SD). The experimental data from all of the studies were analyzed using Analysis of Variance (ANOVA). Statistical significance was set at a p-value  $\leq 0.05$ .

## 5.3. Results and discussion

### 5.3.1. Crosslinking in the injectable scaffolds of chitosan-sodium tripolyphosphate (iCHT-TPPs).

According to Bhumkar and Pokharkar (2006), chitosan (pKa 6.3) may be crosslinked with TPP (pKa 9.7) by two different pH-dependent mechanisms (Figure 20).

The ionic crosslinking occurs at low pH values by a reaction between  $\text{NH}_3^+$  groups of chitosan and  $\text{P}_3\text{O}_{10}^{5-}$  of TPP [Figure 20(a)]. The deprotonation mechanism occurs at high pH values using the  $\text{OH}^-$  groups of TPP that are present in solution [Figure 20(b)]. In this work, the pH of the reaction mixture was maintained at pH 4, which favored the ionic crosslinking mechanism.

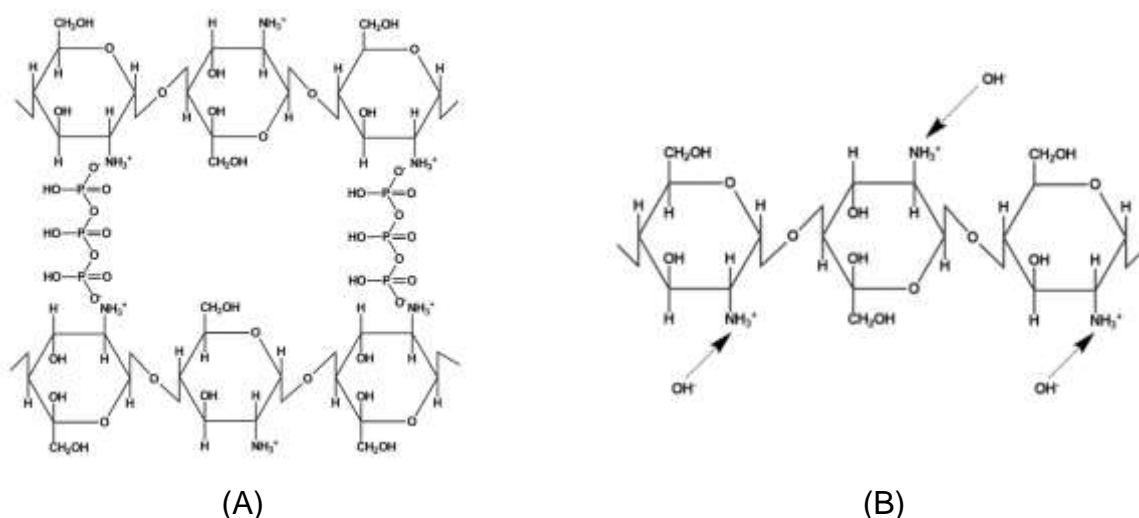


**Figure 20.** Interaction of chitosan with TPP by (a) ionic crosslinking or (b) deprotonation.

The FTIR spectra of pure chitosan and iCHT-TPPs 2:1 are shown in Figure 21.



Pure chitosan was characterized by bands at  $3449\text{ cm}^{-1}$  attributed to the  $-\text{NH}_2$  and  $-\text{OH}$  groups' stretching vibration and the band of amide I at  $1639\text{ cm}^{-1}$  (Bhumkar & Pokharkar, 2006).

The ionic crosslinking between the  $-\text{NH}_3^+$  group of chitosan and  $\text{P}_3\text{O}_{10}^{5-}$  of TPP in iCHT-TPPs (2:1) was characterized by the presence of the P=O and P-O groups at the frequencies of  $1100\text{ cm}^{-1}$  and  $1232\text{ cm}^{-1}$ , respectively (Mi *et al.*, 1999).

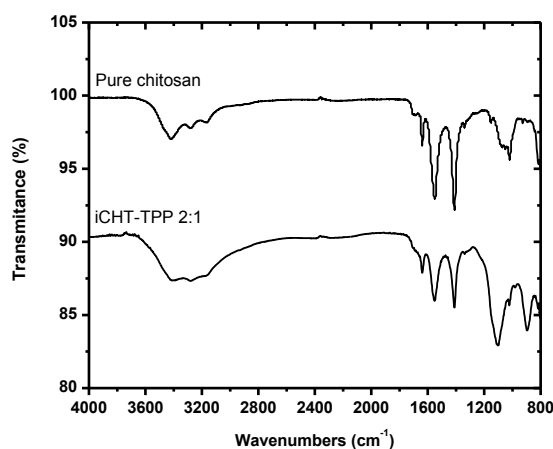


**Figure 21.** FTIR spectrum of pure chitosan and iCHT-TPPs 2:1.

### 5.3.2. Physicochemical and mechanical properties of iCHT-TPPs.

The water absorption capacity (swelling properties) of scaffolds must be carefully controlled to allow handling during cell implantation and promote cell growth. When hydrated, the scaffolds became fragile being deformed and/ or broken with the application of small forces. Thus, a balance between the viscoelastic and swelling properties is essential to maintain the integrity of scaffolds and support the cell proliferation and differentiation.

Table 2 shows the physicochemical and rheological properties of iCHT-TPPs prepared by varying the CHT-TPP mass ratio. The iCHT-TPPs showed a high swelling capacity (SR), allowing for fast hydration when culture medium was added. Moreover, SR decreased with the degree of crosslinking because of the decreased availability of functional groups to hydrogen bonds with water.

Flory-Rehner calculations were used to determine the effective crosslink density ( $V_e$ )

and the molecular weight between crosslinks ( $M_c$ ). The decrease of the CHT-TPP mass ratio increased  $V_e$ , as expected (Flory & Rehner, 1943). Moreover, we observed lower  $M_c$  values, indicating higher entanglement of chains.

We also estimated the charge ratio ( $R_{+/-}$ ) of iCHT-TPPs according to Rädler *et al.* (1998). The values of  $R_{+/-}$  were negative for iCHT-TPPs 2:1 and positive for iCHT-TPPs 5:1 and 10:1. Therefore, the increase in the crosslinking degree decreased the positive charge of chitosan in the complex. These modifications to the charge ratio may change the interactions with the fibrin network and alter the electrostatic interaction with growth factors.

The microparticles in iCHT-TPPs had a mean diameter in the range of 150 to 220  $\mu\text{m}$ , which was proportional to the CHT-TPP mass ratio. These diameters are within the adequate range for an injectable application ( $<700 \mu\text{m}$ ) (Kablik *et al.*, 2009).

**Table 2.** Physicochemical and mechanical properties of iCHT-TPPs.

Physicochemical properties					
Mass ratio CHT:TPP	SR	$V_e$ (mol.cm <sup>-3</sup> )	$M_c$ (g.mol <sup>-1</sup> )	$R_{+/-}$	Particle diameter ( $\mu\text{m}$ )
2:1	22 $\pm$ 1	2.4 x 10 <sup>-4</sup>	5110	0.7	152 $\pm$ 4
5:1	31 $\pm$ 1	1.3 x 10 <sup>-4</sup>	9450	1.8	205 $\pm$ 3
10:1	44 $\pm$ 1	7.5 x 10 <sup>-5</sup>	16669	3.6	215 $\pm$ 4
Rheological properties					
Mass ratio CHT:TPP	$G'$ in 1 Hz (Pa)	$n$	$\tan \delta$	Extrusion force (N)	
2:1	522	0.04	0.134	12.6 $\pm$ 0.9	
5:1	333	0.15	0.174	10.8 $\pm$ 0.4	
10:1	72	0.32	0.276	11.1 $\pm$ 0.8	

SR=swelling ratio;  
 $V_e$ =Effective crosslink density;  
 $M_c$ =Molecular weight between crosslinks;  
 $R_{+/-}$ =charge ratio;  
 $G'$ =elastic moduli;  
 $G''$ =viscous moduli;  
 $\tan \delta=G''/G'$ ;  
 $n$ = flow behavior index.

The rheological data (Table 2) show that the iCHT-TPPs exhibited behavior that is typical of so-called weak gels, irrespective of their mass ratios, as analyzed by the storage ( $G'$ ) and loss moduli ( $G''$ ). The moduli had low frequency dependence, and  $\tan \delta > 0.1$  (Ikeda & Nishimari, 2001; Clark & Ross-Murphy, 1987).

We also observed an increase in the  $G'$  values with the number of crosslinks or entanglements (high  $V_e$  and low  $M_c$ ), which indicated stiffer gels.

In addition, the values of  $\tan \delta$  indicated an increment in gel strength with an increase in  $V_e$ . Regardless of the CHT-TPP mass ratio, iCHT-TPPs showed  $G'$  values that are adequate ( $<700$  Pa) for injectable application (Kablik *et al.*, 2009).

Considering the Ostwald de Waele power law ( $\eta=K.\dot{\gamma}^{n-1}$ ), the flow indices ( $n$ ) of iCHT-TPPs showed a viscoelastic behavior that was dependent on mass ratio. The pseudoplastic behavior is an important parameter in injectable applications, where the flow viscosity should be lower than the rest viscosity.

In addition to the beneficial rheological properties and microparticle size, the injectable scaffolds must have an extrusion force to allow for their easy injection through an appropriately sized needle and thereby prevent side effects such as pain (Kablik *et al.*, 2009).

In iCHT-TPPs, we measured extrusion forces between 10 and 12 N, which were adequate ( $<20$  N) for injectable applications (De Melo & Marijnissen-Hofste, 2012; Öhrlund, 2010). No modifications were observed in the extrusion force with the degree of crosslinking, particle size and distribution, as reported by Bentkover (2009).

Figure 22 shows the loss weight of iCHT-TPPs after incubation in PBS, pH 7.4, at 37°C. The microparticles can be considered stable for 30 days, irrespective of the CHT-TPP mass ratio. The maximum loss weight was approximately 4%, for CHT-TPP 2:1.

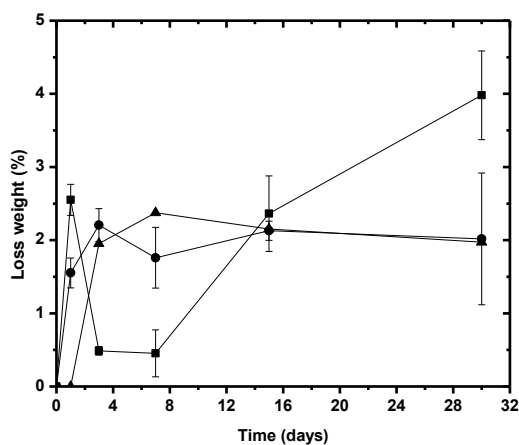


**Figure 22.** Degradation profile of iCHT-TPPs in PBS pH 7.4 at 37°C. (■) iCHT-TPPs 2:1; (●) iCHT-TPPs 5:1 and (▲) iCHT-TPPs 10:1.

### 5.3.3. Biological characterization

Figure 23 shows the PDGF-AB and TGF- $\beta$ 1 release kinetics from aP-PRP/iCHT-TPPs.

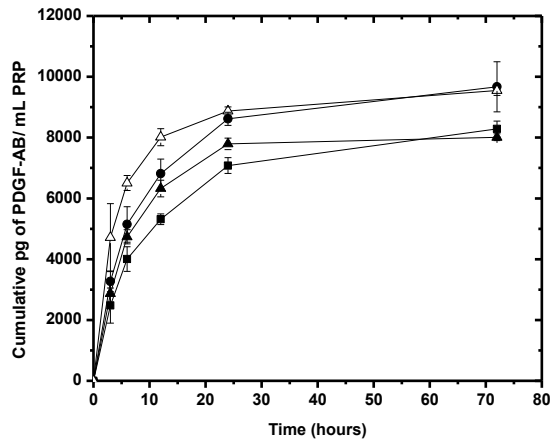
The curves show predominantly diffusive profiles, indicating no collapse of the scaffold structure at the time of the assays. Controlled GF release was achieved from aP-PRP/iCHT-TPPs compared with aP-PRP alone. The maximum PDGF-AB release was obtained at 24 hours [Figure 23(a)], whereas a concentration plateau was not observed for TGF- $\beta$ 1 at 72 hours [Figure 23(b)].

In addition to the barrier of the structures, the interactions of GF and scaffolds play an important role in the release. According to Hokugo *et al.* (2005) and De Cock *et al.* (2012), because GFs are generally basic proteins, in physiological conditions, they interact ionically with negatively charged surfaces.

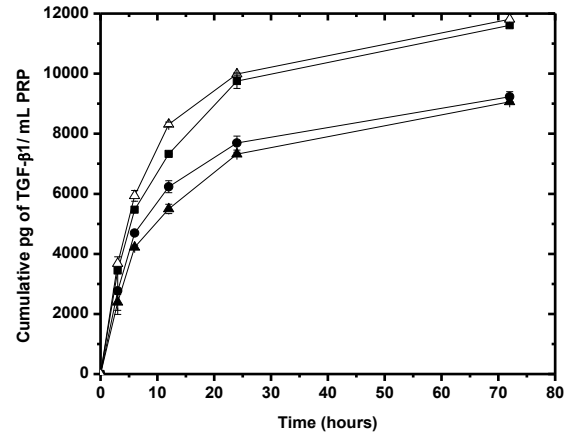
In this work, we observed a slower release in the PDGF-AB for the scaffold aP-PRP/iCHT-TPPs mass ratio 2:1 compared with aP-PRP, suggesting electrostatic interactions with negative charges of the scaffold. At physiological pH, PDGF-AB bore a net positive charge (isoelectric point 9.8-10.5) (De Cock *et al.*, 2012).

For TGF- $\beta$ 1, a slower release was observed for the scaffolds aP-PRP/iCHT-TPPs at mass ratios of 5:1 and 10:1 compared with aP-PRP. Because TGF- $\beta$ 1 has the isoelectric point of 8.2, which is near the physiological pH (7.4), the positive charges of the scaffolds had a smaller influence on controlled release (Wang *et al.*, 2011).

In this case, we hypothesized that the slower release was primarily due to the interaction of the negative fibrin network and the positive scaffold, which entrapped the GF molecules.



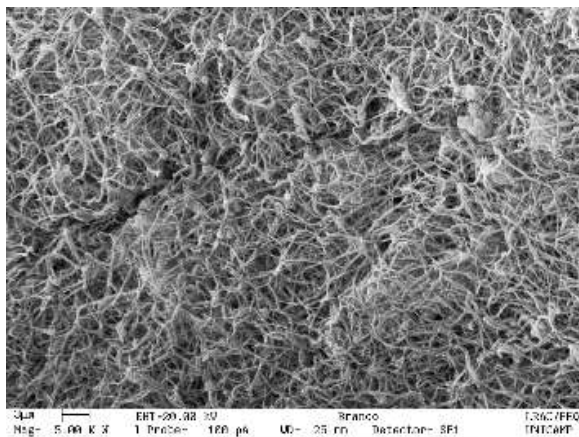
(a)



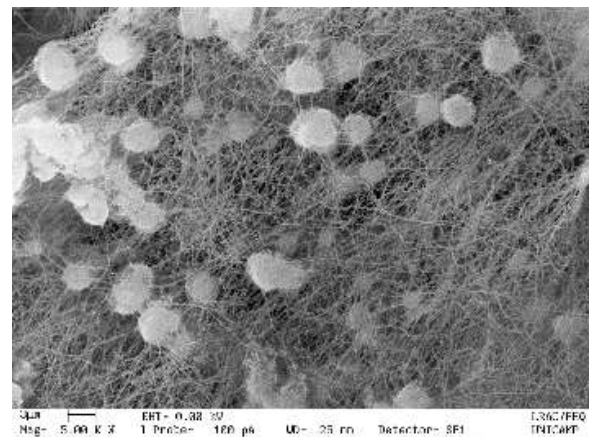
(b)

**Figure 23.** Growth factor release profiles from aP-PRP combined with CHT-TPP scaffolds. (a) PDGF-AB and (b) TGF- $\beta$ 1. ( $\Delta$ ) PRP activated with  $Ca^{+2}$ /serum used as control; ( $\blacksquare$ ) aP-PRP/iCHT-TPPs 2:1; ( $\bullet$ ) aP-PRP/iCHT-TPPs 5:1 and ( $\blacktriangle$ ) aP-PRP-iCHT-TPPs 10:1. The concentration of platelets in whole blood donors (average of 2 donors) was 234,250  $pq/mm^3$ . After preparation of the P-PRP, the platelets were concentrated approximately 2.09 times, with an average final concentration of 472,250  $pq/mm^3$ .

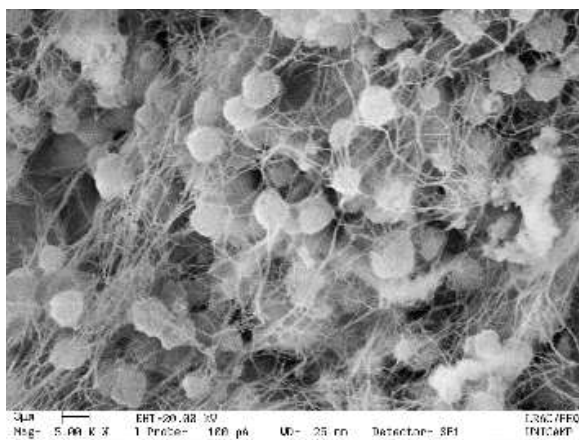
Scanning electronic microscopy (Figure 24) of aP-PRP showed a tangled network that was similar to the extracellular matrix. The microparticles were entrapped by the fibrin network, which provided an additional matrix for h-AdMSCs adherence and proliferation.



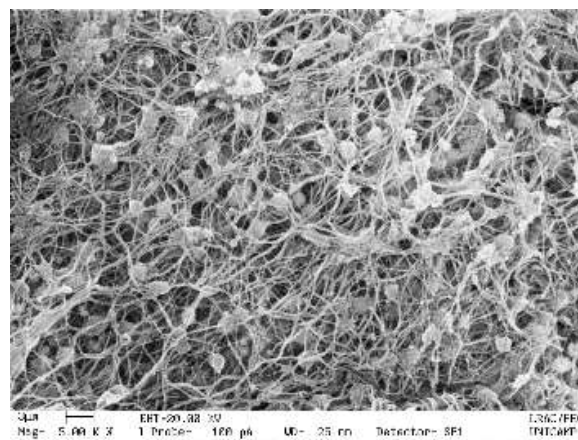
aP-PRP



aP-PRP/iCHT-TPPs 2:1



aP-PRP/iCHT-TPPs 5:1



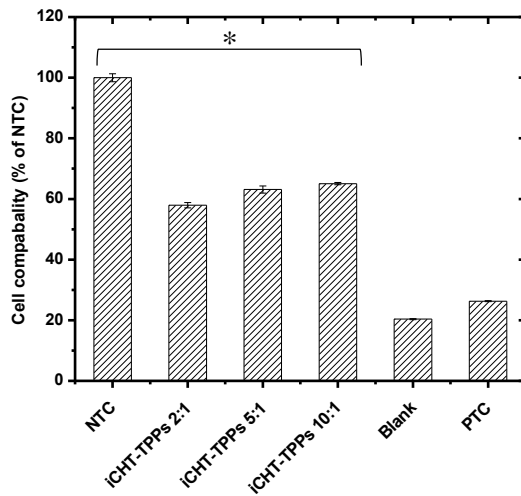
aP-PRP /iCHT- TPPs 10:1

**Figure 24.** Scanning electron microscopic images of aP-PRP and aP-PRP/iCHT-TPPs after 5 days of cultivation of h-AdMSCs.

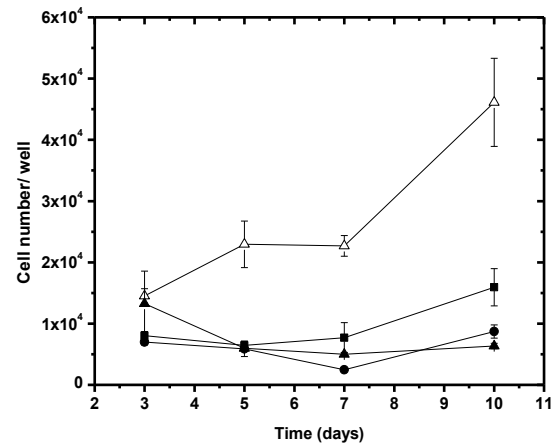
The proliferation of h-AdMSCs cultured in the presence of iCHT-TPPs, as assayed by MTT is shown in Figure 25(a). In all of the prepared mass ratios, the iCHT-TPPs had a higher proliferation compared with the positive control, which indicated compatibility.

The proliferation kinetic profiles in presence of PRP [Figure 25(b)] showed a long lag phase (~7 days) for aPRP and aP-PRP/iCHT-TPPs at 2:1 and 5:1.

The proliferation of h-AdMSCs was lower than aP-PRP in the composite scaffolds at 2:1 and 5:1 mass ratios, whereas no proliferation was observed at 10:1 aP-PRP/iCHT-TPPs.



(a)



(b)

**Figure 25.** (a) % of NTC as a measurement of the compatibility of h-AdMSCs that were exposed to the iCHT-TPPs. Negative control (NTC) = DMEM with 10% FBS; positive control (PTC) = DMEM with phenol 0.5%. The population means are significantly different from positive control at  $*p < 0.05$ . (b) Proliferation profile of h-AdMSCs cultured in aP-PRP/iCHT-TPPs scaffolds as a function of time. Activated PRP was used as control. (Δ) aP-PRP; (■) aP-PRP/iCHT-TPPs 2:1; (●) aP-PRP/iCHT-TPPs 5:1 and (▲) aP-PRP/iCHT-TPPs 10:1. The concentration of platelets in whole blood donors (average of 2 donors) was  $215,375 \text{ pq/mm}^3$ . After preparation of the P-PRP, the platelets were concentrated approximately 1.79 times, with an average final concentration of  $383,500 \text{ pq/mm}^3$ . Mean  $\pm$  standard deviation  $n = 3$ .

Figure 26 shows significant ALP activity in the aP-PRP/iCHT-TPPs, indicating stimulation of osteoblast differentiation. It is known that ALP enzymatic activity is essential for mineralization. Differences among the structures could not be inferred because ALP activity was determined in the culture medium and thus did not include the concentrations inside the gels. This may have also contributed to the lower values of ALP activities of the composite scaffolds compared with aP-PRP, due to the higher viscosity, which delayed the release of ALP.

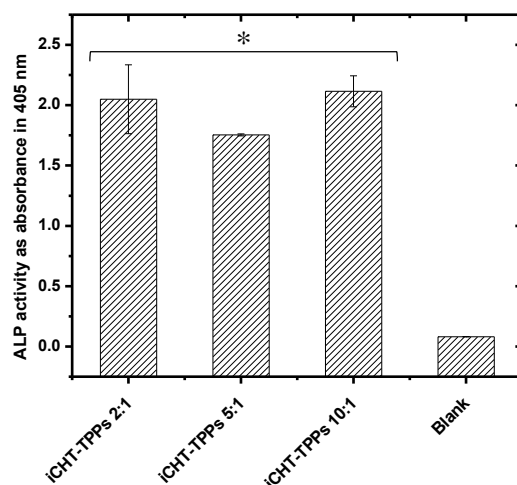


**Figure 26.** ALP activities of h-AdMSCs cultured on composite scaffolds (\*statistically significant differences from blank,  $n=3$ ,  $p<0.05$ ). Blank = the reagents used in the assay only). The concentration of platelets in whole blood donors (average of 2 donors) was 214,000  $\text{pq}/\text{mm}^3$ . After preparation of the P-PRP, the platelets were concentrated approximately 2.31 times, with an average final concentration of 473,500  $\text{pq}/\text{mm}^3$ .

## 5.4. Conclusions

We have demonstrated that the injectable composite scaffolds (aP-PRP/iCHT-TPP) promoted the controlled release of PDGF-AB and TGF- $\beta$ 1 from platelets primarily during the first 10 h. Although the physicochemical and rheological properties of iCHT-TPP increased the stability of the fibrin network, a significant proliferation of AdMSCs was observed only for the composite scaffold containing 2:1 chitosan:TPP. However, the osteogenic differentiation was promoted in all mass ratios. Thus, the injectable composite scaffolds could be optimized to demonstrate their potential for regenerative medicine applications.

**Acknowledgments.** The authors acknowledge the financial support from the National Council of Technological and Scientific Development (CNPq, Brazil). They also thank Prof. Dr. Edvaldo Sabadini of the Chemical Institute (University of Campinas) for the use of the rheometer; Prof. Dr. William Dias Belangero and Dr. Ana Amélia Rodrigues of the



Faculty of Medical Sciences (University of Campinas) for assistance, and Dr. Ângela Cristina Malheiros Luzo of the Haematology and Hemotherapy Center (University of Campinas) for the donation of h-AdMSCs.

**Conflict of Interest.** Andréa Arruda Martins Shimojo, Sofia Elisa Moraga Galdames, Amanda Gomes Marcelino Perez, Thiago Heiji Ito and Maria Helena Andrade Santana declare that they have no conflict of interest in the presented work.

## 5.5. References

ANITUA, E. Plasma Rich in Growth Factors: Preliminary Results of Use in the Preparation of Future Sites for Implants. **International Journal of Oral & Maxillofacial Implants**, vol.14, p.529-535, 1999.

BENTKOVER, S.H. The Biology of Facial Fillers. **Facial Plastic Surgery**, vol.25, n.2, p.73-85, 2009.

BERGER, J.; REIST, M.; MAYER, J.; FELT, O.; PEPPAS, N.; GURNY, R. Structure and interactions in covalently and ionically crosslinked chitosan hydrogels for biomedical applications. **European Journal of Pharmaceutics and Biopharmaceutics**, vol.57, p.19–34, 2004.

BHUMKAR, D.R.; POKHARKAR, V.B. Studies on Effect of pH on Cross-linking of Chitosan With Sodium Tripolyphosphate: A Technical Note. **AAPS Pharm Sci Tech**, vol.7, n.2, p.E138-143, 2006.

BRACK, H.P.; TIRMIZI, S.A.; RISEN JR, W.M. A spectroscopic and viscometric study of the metal ion-induced gelation of the biopolymer chitosan. **Polymer**, vol.38, p.2351-2362, 1997.

CLARK, A.H.; ROSS-MURPHY, S.B. Structural and mechanical properties of biopolymer gels. **Advances in Polymer Science**, vol.83, p.57-192, 1987.

COLE, B.J.; SEROYER, S.T.; FILARDO, G.; BAJAJ, S.; FORTIER, L.A. Platelet-Rich Plasma: Where Are We Now and Where Are We Going? **Sports Health**, vol.2, n.3, p.203-210, 2010.

COLLINS, M.N.; BIRKINSHAW, C. Investigation of the Swelling Behavior of Crosslinked Hyaluronic Acid Films and Hydrogels Produced Using Homogeneous Reactions. **Journal of Applied Polymer Science**, vol.109, p.923-931, 2008.

COSTA-PINTO, A.R.; REIS, R.L.; NEVES, N.M. Scaffolds Based Bone Tissue Engineering: The Role of Chitosan. **Tissue Engineering Part B**, vol.17, n.5, p.331-347, 2011.

CRANE, D.; EVERTS, P.A.M. Platelet Rich Plasma (PRP) Matrix Grafts. **PPM Communications**, vol.8, p.1-10, 2008.

DE COCK, L.J.; DE WEVER, O.; HAMMAD, H.; LAMBRECHT, B.N.; VANDERLEYDEN, E.; DUBRUEL, P.; DE VOS, F.; VERVAET, C.; REMON, J.P.; DE GEEST, B.G. Engineered 3D microporous gelatin scaffolds to study cell migration. **Chemical Communications**, vol.48, p.3512-3514, 2012.

DE MELO, F.; MARIJNISSEN-HOFSTE, J. Investigation of Physical Properties of a Polycaprolactone Dermal Filler when Mixed with Lidocaine and Lidocaine/Epinephrine. **Dermatology and Therapy**, vol.2, n.13, p.1-10, 2012.

FLORY, P.J.; REHNER, J. Statistical Mechanics of Cross-Linked Polymer Networks I. Rubberlike Elasticity. **Journal of Chemical Physics**, vol.11, p.512-520, 1943.

FOSTER, T.E.; PUSKAS, B.L.; MANDELBAUM, B.R.; GERHARDT, M.B.; RODEO, S.A. Platelet-Rich Plasma: From Basic Science to Clinical Applications. **American Journal of Sports Medicine**, vol.37, p.2259-2272, 2009.

GÜMÜŞDERELIOĞLU, M.; ADAY, S. Heparin-functionalized chitosan scaffolds for bone tissue engineering. **Carbohydrate Research**, vol.346, p.606-613, 2011.

GUTOWSKA, A.; JEONG, B.; JASIONOWSKI, M. Injectable Gels for Tissue Engineering. **Anatomical Record**, vol.263, p.342-349, 2001.

HARRIS, R.; LECUMBERRI, E.; HERAS, A. Chitosan-Genipin Microspheres for the Controlled Release of Drugs: Clarithromycin, Tramadol and Heparin. **Marine Drugs**, vol.8, p.1750-1762, 2010.

HENNINK, W.E.; VAN NODTRUM, C.F. Novel crosslinking methods to design hydrogels. **Advanced Drug Delivery Reviews**, vol.54, p.13-36, 2002.

HOKUGO, F.; OZEKI, M.; KAWAKAMI, O.; SUGIMOTO, K.; MUSHIMOTO, K.; MORITA, S.; TABATA, Y. Augmented Bone Regeneration Activity of Platelet-Rich Plasma by Biodegradable Gelatin Hydrogel. **Tissue Engineering**, vol.11, n.7/8, p.1224-1233, 2005.

HOU, Q.; BANK, P.A.; SHAKESHEFF, K.M. Injectable scaffolds for tissue regeneration. **Journal of Materials Chemistry**, vol.14, p.1915-1923, 2004.

IBEZIM, E.C.; ANDRADE, C.T.; MARCIA, C.; BARRETTO, B.; ODIMEGWU, D.C.; DE LIMA, F.F. Ionically Cross-linked Chitosan/Tripolyphosphate Microparticles for the Controlled Delivery of Pyrimethamine. **Ibnosina Journal of Medicine and Biomedical Sciences**, vol.3, n.3, p.77-88, 2010.

IKEDA, S.; NISHINARI, K. Weak Gel-Type Rheological Properties of Aqueous Dispersions of Nonaggregated K-Carrageenan Helices. **Journal of Agricultural and Food Chemistry**, vol.49, p.4436-4441, 2001.

JIN, J.; SONG, M. Chitosan and Chitosan–PEO Blend Membranes Crosslinked by Genipin for Drug Release. **Journal of Applied Polymer Science**, vol.102, p.436-444 (2006).

KABLIK, J.; MONHEIT, G.D.; YU, L.; CHANG, G.; GERSHKOVICH, J. Comparative Physical Properties of Hyaluronic Acid Dermal Fillers. **Journal of dermatologic surgery**, vol.35, p.302-312, 2009.

KARNCHANAJINDANUN, J.; SRISA-ARD, M.; SRIHANAM, P.; BAIMARK, Y. Preparation and characterization of genipin-cross-linked chitosan microparticles by water-in-oil emulsion solvent diffusion method. **Natural Science**, vol.2, n.10, p.1061-1065, 2010.

KRETLOW, J.D.; KLOUDA, L.; MIKOS, A.G. Injectable matrices and scaffolds for drug delivery in tissue engineering. **Advanced Drug Delivery Reviews**, vol.59, p.263-273, 2007.

MARX, R.E. Platelet-rich plasma: Evidence to support its use. **Journal of Oral and Maxillofacial Surgery**, vol.62, p.489–496, 2004.

MI, F-L.; SHYU, S-S.; LEE, S-T.; WONG T-B. Kinetic Study of Chitosan-Tripolyphosphate Complex Reaction and Acid-Resistive Properties of the Chitosan-Tripolyphosphate Gel Beads Prepared by in-Liquid Curing Method. **Journal of Polymer Science Part B: Polymer Physics**, vol.37, p.1551-1564, 1999.

MOSSMAM, T.J. A rapid colorimetric assay of cellular growth and survival: application to proliferation and cytotoxicity assays. **Journal of Immunological Methods**, vol.65, p.55-63, 1983.

NASTI, A.; ZAKI, M.N.; DE LEONARDIS, P.; UNGPHAIBOON, S.; SANSONGSAK, P.; RIMOLI, M.G.; TIRELLI, N. Chitosan/TPP and Chitosan/TPP-hyaluronic Acid Nanoparticles: Systematic Optimization of the Preparative Process and Preliminary Biological Evaluation. **Pharmaceutical Research**, vol.26, n.8, p.1918-1930, 2009.

ÖHRLUND Å. Lifting capacity of hyaluronic acid (HA) dermalaluronic acid (HA) dermal fillers. **Poster presentation at 8 th Anti-aging Medicine World Congress (AMWC)**, Monte-Carlo, Monaco, 2010.

PEREZ, A.G.M.; LICHY, R.; LANA, J.F.S.D.; RODRIGUES, A.A.; LUZO, A.C.M.; BELANGERO, W.D.; SANTANA, M.H.A. Prediction and Modulation of Platelet Recovery by Discontinuous Centrifugation of Whole Blood for the Preparation of Pure Platelet-Rich Plasma. **BioResearch Open Access**, vol.2, p. 307-314, 2013.

RÄDLER, J.O.; KOLTOVER, I.; JAMIESON, A.; SALDITT, T.; SAFINYA, C.R. Structure and Interfacial Aspects of Self-Assembled Cationic Lipid–DNA Gene Carrier Complexes. **Langmuir**, vol.14, n.15, p.4272-4283,1998.

TAN, H.P.; CHU, C.R.; PAYNE, K.A. Injectable In Situ Forming Biodegradable Chitosan-Hyaluronic acid Based Hydrogels for Cartilage Tissue Engineering. **Biomaterials**, vol.30, p.2499-2506, 2009.

WANG, C.; LI, J.; YAO, F. Application of Chitosan-Based Biomaterials in Tissue Engineering. In: YUJI, Y. (Eds.). **Chitosan-Based Hydrogels: Functions and Applications**. New York: CRC Press, p.424, 2011.

# CAPÍTULO 6 – IMPROVEMENTS IN PLATELET-RICH PLASMA PERFORMANCE BY ASSOCIATION WITH MICROPARTICLES OR SPONGES OF AUTO-CROSSLINKED HYALURONIC ACID

---

Artigo submetido ao periódico *Journal of Applied Polymer Science*.

Andréa Arruda Martins Shimojo<sup>a</sup>, Isabela Cambraia de Souza Brissac<sup>a</sup>, Sofia Elisa Moraga Galdames<sup>a</sup>, Amanda Gomes Marcelino Perez<sup>a</sup>, José Fábio Santos Duarte Lana<sup>b</sup> and Maria Helena Andrade Santana<sup>a,\*</sup>

<sup>a</sup>Department of Engineering of Materials and Bioprocesses- School of Chemical Engineering, University of Campinas, Campinas-SP, Brazil.

<sup>b</sup>Institute of Bone and Cartilage (IOC), Indaiatuba-SP, Brazil

\*Correspondence to: Maria Helena Andrade Santana, phone: +55-19-35213921, FAX: +55-19-35213890, e-mail: [mariahelena.santana@gmail.com](mailto:mariahelena.santana@gmail.com)

**Abstract.** The association of platelet-rich plasma (PRP) to fluid hyaluronic acid (HA) has yielded beneficial outcomes *in vivo* in orthopedic applications. However, aside from needing to repeat the applications, the literature is not conclusive about the improvements to efficiency or long-lasting effects related to PRP alone. Auto-crosslinked hyaluronic acid (ACP) may introduce benefits to the stability of fibrin network from activated PRP (aP-PRP) and to the mechanical properties of fluid HA. The main advantage of ACP is not introducing foreign molecules to the formulation. This study was undertaken to investigate *in vitro* association of aP-PRP and ACPs as composite scaffolds for growth factors release, the proliferation of human adipose-derived mesenchymal stem cells (h-AdMSCs) and differentiation by osteogenic marker alkaline phosphatase (ALP). ACP was prepared by organocatalyzed auto-esterification and

structured into microparticles or sponges to create injectable or solid scaffolds, respectively. The structured ACP were not cytotoxic and had better mechanical properties than does fluid HA. PRP was obtained by centrifuging whole blood without the buffy-coat layer (P-PRP). Autologous serum and calcium were used for P-PRP activation. Most of PDGF-AB (platelet-derived growth factor AB) and TGF- $\beta$ 1 (transforming growth factor  $\beta$ -1) was released from aP-PRP alone or from the composite scaffolds in the first 10 hours. The release occurred in concert with the degradation time of the structured ACPs. The composite scaffolds improved h-AdMSCs proliferation and promoted ALP activity suggesting potential osteogenic differentiation. Therefore, aP-PRP combined with ACP is a promising biomaterial for further biological studies and applications in regenerative medicine.

**Keywords:** auto-crosslinked hyaluronic acid; controlled release; microparticles; PDGF-AB; platelet-rich plasma; sponges; TGF- $\beta$ 1.

## 6.1. Introduction

Platelet-rich plasma (PRP) is a platelets concentrate prepared from whole blood, which is able to release growth factors following induced activation (Anitua 1999; Foster *et al.*, 2009). PRP have been widely applied in various regenerative therapies and its beneficial effects has been proven mainly in cartilage regeneration, wound healing and sports medicine (Crane & Everts, 2008; Civinini *et al.*, 2011; Kon *et al.*, 2011; Amable *et al.*, 2013).

Since the 1990s, when clinical application of PRP began, three generations of formulations can be identified: the first generation applied PRP only; the second-generation included bone marrow cells in PRP; and the third and current generation uses PRP and human adipose derived mesenchymal stem cells (h-AdMSCs). It has been reported that AdMSCs are comparable to bone marrow-derived MSCs (BM-MSCs) with respect to multi-lineage potential, growth kinetics, and cells senescence (de Ugarte *et al.*, 2003).

Recently, PRP has been used in combination to high molecular weight HA aimed to ensure better stability of the fibrin network, control release of GF and decrease pain

related to inflammation caused by injury in the application of PRP (Pak, 2012; de Angelis *et al.*, 2012; Chen *et al.*, 2014; Fathi, 2012; de Boulle *et al.*, 2013).

Pak (2012) has described different methods and pharmaceutical compositions comprising PRP, h-AdMSCs, HA and CaCl<sub>2</sub> for the treatment, preventions or alleviation of bone and cartilage diseases.

De Angelis *et al.* (2012) have treated patients with wound dehiscence and tendon exposure, showing that PRP combined with fluid hyaluronic acid (fHA) enables a more rapid regeneration of damaged tissues.

Recently, Chen *et al.* (2014) demonstrated synergic effects of the anabolic actions of PRP-fHA on cartilage regeneration and the inhibition of osteoarthritis inflammation. Cytokine-induced degeneration was reduced through the recovery of chondrogenic signaling.

The benefits of using platelet-rich plasma and hyaluronic acid when used alone or in combination on wound healing were evaluated by Fathi (2012). This author observed that the use of PRP alone or in combination with HA accelerate wound healing, while the use of low concentration of HA alone presents no improvement of wound healing in comparison with normal one.

However, the need for repeated applications of free HA *in vivo* has directed the studies for the use of biocompatible crosslinked derivatives (de Boulle *et al.*, 2013; Collins & Birkinshaw, 2013; Stern *et al.*, 2000).

Preliminary studies from our group have shown that the addition of divinyl sulfone (DVS) crosslinked HA microparticles to activated P-PRP (aP-PRP) improves the mechanical properties of the natural fibrin networks by increasing its viscoelasticity and eliminating strain hardening (unpublished data). Furthermore, the HA microparticles stimulate h-AdMSCs proliferation on the thin fibers (~65 nm) of the fibrin network. However, the long-term effects of DVS-crosslinked HA microparticles remain unclear, and the release of the chemical crosslinkers causes inflammatory outcomes (Prasadam *et al.*, 2013).

Thus, auto-crosslinked polysaccharide (ACP) represents an interesting strategy for improving the stability of HA. ACP polymers are inter- and intra-molecular esters of HA for which some of the carboxyl groups have been esterified with hydroxyl groups of

the same and/ or different molecules, thus forming a mixture of lactones and inter-molecular ester bonds (Mensitieri *et al.*, 1996).

The main advantage for ACP is the formation of ester bonds without the addition of toxic crosslinking agents. As no foreign molecules are used to create the crosslink, the gel is de-esterified upon degradation and hyaluronic acid is liberated. HA is a naturally occurring molecule that has a biological role and is eliminated through a known metabolic pathway (Mensitieri *et al.*, 1996).

Furthermore, ACP can be prepared with various degrees of crosslinking by modulating the reaction conditions, which allow the adaption of its mechanical and/or rheological properties for many applications (de Laco *et al.*, 1998)

ACP has been widely used on the prevention of postsurgical adhesions (de Laco *et al.*, 1998; Belluco *et al.*, 2001; Koçak *et al.*, 1999; Yerushalmi *et al.*, 1994). However, as far as we know, the application of ACP as scaffolds is still scarce.

Solchaga *et al.* (2005) demonstrated that porous sponges of ACP<sup>®</sup> seeded with chondrocytes or osteoblasts improve the cartilage and bone regeneration in osteochondral defects of rabbits compared to HYAFF<sup>®</sup>-11 (a benzyl ester of HA that is completely esterified). The degradation time of ACP<sup>®</sup> led to rapid bone formation while the slow degradation of HYAFF<sup>®</sup>-11 prolonged the presence of cartilage and delayed endochondral bone formation.

The present work extends the previous findings by investigating the association of activated aP-PRP and ACP structured in microparticles or sponges as a composite scaffold for growth factors (GFs) release, the proliferation of h-AdMSCs and osteogenic differentiation *in vitro*. Our hypothesis is that the composite scaffolds will improve proliferation and differentiation of h-AdMSCs by providing better structural and mechanical properties compared to fHA or aP-PRP alone.

This study might offer promising approaches for further biological applications and should provide alternatives in orthopedic treatments.

## **6.2. Experimental**



### 6.2.1. Materials

HA in sodium form ( $\overline{MW} = 2 \times 10^6$  Da) was obtained from Spec-Chem Ind. (Nanjing, China). All other reagents were purchased from Synth® (Diadema, SP, Brazil) unless specified otherwise. PRP was prepared from whole blood (WB) of donors, who were healthy individuals aged between 30 and 40 years old and previously assessed through their clinical examinations. The human adipose tissue-derived mesenchymal stem cells, h-AdMSCs, were provided by Umbilical Cord Blood Bank of Haematology and Hemotherapy Center of University of Campinas. All biological experiments were approved by the Ethics Committee of the Medical Sciences School of the University of Campinas (UNICAMP; CAAE: 0972.0.146.000-11).

### 6.2.2. Methods

#### 6.2.2.1. Preparation of HA-TBA

An aqueous solution of 0.5% (w/v) sodium hyaluronate (Na-HA) was stirred in strongly acidic ion exchange resin Dowex® 50-8WX-400 mesh (Sigma-Aldrich, St. Louis, MO, USA) for 8 hours. The suspension was centrifuged in a Rotina 380R centrifuge (Hettich® Zentrifugen, Tuttlingen, Germany) at 10,000 rpm for 10 minutes to remove the resin and neutralized with tetrabutylammonium hydroxide (TBA-OH)  $0.2 \text{ mol.L}^{-1}$  (Vetec®, Duque de Caxias, Rio de Janeiro, Brazil) to form the quaternary ammonium salt of HA (HA-TBA). The solution was then frozen and lyophilized in lyophilizer Liobras L101 (Liobras, São Carlos, SP, Brazil) for 48 hours (Khetan & Burdick, 2010).

#### 6.2.2.2. Preparation of ACP

The auto-crosslinked HA (ACP) was prepared by an autoesterification reaction according to the protocol described by Bellini *et al.* (2001) (Figure 27). HA-TBA with a molecular weight of approximately  $2 \times 10^6$  Da and corresponding to 10 mEq of monomeric units was solubilized in 50 mL of dimethylsulfoxide (DMSO) at 25°C. Triethylamine (0.5 mEq) was added and the resulting solution was agitated for 30 minutes. A solution of 2-chloro-1-methyl pyridinium iodide (CMPI) (0.5 mEq) (Sigma-Aldrich, St. Louis, MO, USA) in 15 mL of DMSO was slowly added drop by drop over 1

hour and the mixture was kept at 30°C for 15 hours. A solution of sodium chloride 2.5% (w/v) was then added and the resulting mixture was poured slowly into 150 mL of acetone, maintaining continual agitation. The formed precipitate was centrifuged at 10,000 rpm for 10 minutes, washed three times in 100 mL of 5:1 acetone: water and three times with 100 mL of acetone and vacuum-dried for 24 hours at 30°C.

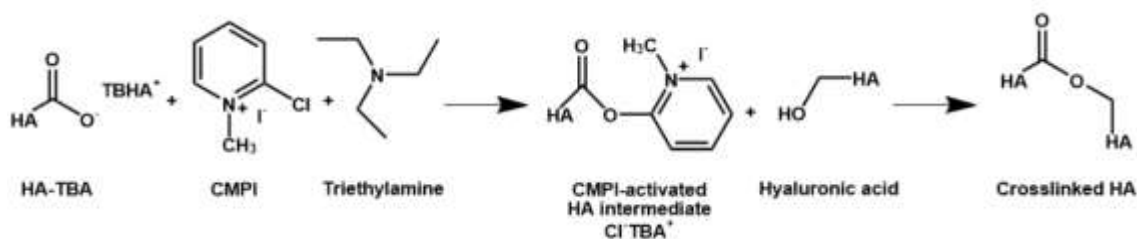


**Figure 27.** Auto-crosslinking reaction using CMPI-activated HA intermediate (Schanté *et al.*, 2011).

#### 6.2.2.3. Characterization of ACP

ACP was characterized by Fourier-transform infrared (FTIR) in a Thermo Scientific Nicolet model 6700 (Thermo Scientific Nicolet™, Waltham, MA, USA). Measurements were made in the ATR mode with accessory SMART OMNI-SAMPLER, in the spectral range of 4000-675  $\text{cm}^{-1}$  with a resolution of 4  $\text{cm}^{-1}$  over 64 scans.

#### 6.2.2.4. Preparation of structured ACP

The ACP structured in microparticles (mACP) or sponges (sACP) were prepared from plain ACP swollen in Milli-Q water. The microparticles were obtained by shearing in an Ultra-Turrax T25 homogenizer (IKA Labor Technik, Staufen, Germany) at 18,000 rpm by 20 minutes, according to Shimojo *et al.* (2013). The sponges were initially placed in polystyrene 24-well microplates (TPP®, Trasadingen, Switzerland), frozen at -20°C and lyophilized at temperature of approximately -30°C for 48 hours.

#### 6.2.2.5 Characterization of structured ACP

HA structured in sponges (sHA) and fluid HA (fHA) were characterized like the structured ACP and used as control as necessary.

*Morphology and pore size.* The morphology of ACP sponges was evaluated by scanning electron microscopy (SEM) using an LEO 440i Electron Microscopy/Oxford (Cambridge, England) operated at 5 kV accelerating voltage. The scaffolds were gold coated using a sputter coater POLARON SC7620, VG Microtech (Uckfield, England) for 180 s at a current of 3 mA. Pore size ( $n=20$ ) was measured using Image J 1.47t.

*Mechanical Properties.* Mechanical compression tests of ACP sponges ( $n = 3$ ) were performed using a Universal Testing Machine, MTS model 810-Flex Test 40 (MTS Systems Corporation, Eden Prairie, MN, USA) up to 60% strain, according to Correia *et al.* (2011). The testing machine was equipped with a 1.5 kN load cell, and the loading rate was 5 mm/min. Young's modulus was calculated in the initial linear section of the stress-strain curve, when the strain was lower than 10%.

*Degradation time.* The gravimetric method described by Tang *et al.* (2007) was used to estimate the degradation time of the structured ACP through measurements of remaining weight. The assay was carried out with the ACP microparticles and ACP sponges in phosphate buffer saline solution (PBS, pH 7.2) (LB Laborclin, Pinhais, PR, Brazil) at 37°C.

*Average diameter.* The average diameter was measured for the ACP microparticles suspended in water. The measurements were performed in a Malvern Mastersizer S laser diffraction (Malvern Instruments Ltd, Malvern, UK). The standard deviation was calculated from ten consecutive measurements.

*Rheology.* Rheological measurements were performed in steady and oscillatory regimes at 25°C using a parallel plate geometry of 20 mm. Steady shear measurements were obtained at shear rates of 0.1-50 s<sup>-1</sup>. Oscillatory measurements were conducted in the linear region with a stress of 1.188 Pa and in the frequency range of 0.01 to 10 Hz. All rheological measurements were performed using the swollen ACP microparticles equilibrated in Milli-Q on a rheometer Haake RheoStress 1 (Haake, Karlsruhe,

Germany).

*Extrusion force.* Initially the ACP microparticles were loaded in 1-mL plastic syringes with 30-gauge needles. Afterward, the force required to extrude was measured in a MTS 810 Servo-hydraulic Universal Testing Machine (MTS Systems Corporation, Eden Prairie, MN, USA) (Load Cell 1.5 kN) at 25°C at a 5.0 mm/min extrusion rate.

*Swelling ratio.* Swelling measurements of the ACP microparticles were performed in PBS at 25°C after 72 h of incubation, according to Shu *et al.* (2004). The swelling ratio (SR) was calculated using the following Equation (1).

$$SR = \frac{W_s}{W_d} \quad \text{Equation (1)}$$

where  $w_s$  and  $w_d$  are the weights of the scaffolds in the swelled state and the dry state, respectively.

The swelling measurements of the ACP sponges was determined by swelling the freeze-dried ACP sponges (with known weights) in PBS at 37°C for 24 hours. The swollen ACP sponges were weighed after the removal of excess of water by keeping the surfaces on a filter paper. The swelling ratio (SR) was also calculated using Equation (1).

*Porosity.* The porosity ( $\epsilon$ ) of the ACP sponges was determined according to the protocol used by Wang *et al.* (2011), and calculated by Equation (2).

$$\epsilon (\%) = \frac{V_m - \left(\frac{W_m}{\rho}\right)}{V_m} \cdot 100 \quad \text{Equation (2)}$$

where  $V_m$  is the total volume of ACP sponges ( $\text{cm}^3$ ),  $\rho$  is the density of non-porous HA ( $1.0016 \text{ g/cm}^3$ ) and  $w_m$  is the weight of sponges (g). Values are expressed as the mean  $\pm$  standard deviation (n=3).

*Cell compatibility.* The compatibility of the structured ACP with h-AdMSCs cells was carried out by exposing them to cell culture at 37°C for 24 hours. Then, cell viability was evaluated by using an MTT assay (3-[4,5-dimethyl-thiazol-2-yl]-2,5-diphenyltetrazolium bromide) (MTT, Molecular Probes), according to modified Mosmann method (1983). The MTT assay is a colorimetric test based on the reduction of yellow tetrazolium salt into a purple formazan product in presence of cells (Gümüşşderelioğlu & Aday, 2011).

#### 6.2.2.6. Preparation of PRP

PRP rich in platelets and poor in leukocytes (P-PRP) was prepared according to Perez *et al.* (2014). Briefly, whole blood (WB) was collected into 3.5 mL vacuum tubes (Vacuette®, Campinas, SP, Brazil) containing sodium citrate 3.2% (w/v) as anticoagulant. WB was initially centrifuged in a Rotina 380R centrifuge (Hettich® Zentrifugen, Tuttlingen, Germany) at  $100 \times g$  for 10 minutes, at 25°C. After the formation of three layers (a bottom layer composed mainly of red blood cells (RBCs); an upper layer composed of plasma, platelets and some WBCs; and an intermediate layer, or buffy coat, composed mostly of WBCs), only the upper layer was collected to obtain P-PRP. The concentration of platelets, WBCs and RBCs in WB and P-PRP was determined using the ABX Micros ES 60 hematology analyzer (HORIBA ABX Diagnostics, Montpellier, France).

#### 6.2.2.7. Preparation of activated P-PRP (aP-PRP)

aP-PRP was prepared via the activation of P-PRP with autologous serum (Ser) and 10% (w/v)  $\text{CaCl}_2$  solution as agonists using the following proportions: agonist/P-PRP=20% (v/v); Ser/ $\text{CaCl}_2$  volumetric ratio=9. Ser was prepared by collecting 5 mL of WB in tubes without anticoagulant. After 30 minutes for clot formation, WB was centrifuged at  $2000 \times g$  for 10 minutes (Perez *et al.*, 2013).

#### 6.2.2.8 Preparation of composite scaffolds

For preparation of the composite scaffolds, immediately after activation, aP-PRP was mixed with the ACP microparticles or embedded by dripping into the ACP sponges,

both in 48-well microplates. In all biological assays performed in this work, the following proportions of aP-PRP to structured ACP were used: aP-PRP: microparticles = 200  $\mu$ L:100-200 mg and aP-PRP: sponges = 200  $\mu$ L:10-20 mg in order to guarantee the same proportion PRP to HA.

#### 6.2.2.9. Characterization of composite scaffolds

*Release of growth factors.* The release of platelet-derived growth factor AB (PDGF-AB) and transforming growth factor  $\beta$ 1 (TGF- $\beta$ 1) was performed after a 1 hour gelation of composite scaffolds in the presence of the culture medium Dulbecco's Modified Eagle's Medium with low glucose concentration (DMEM-LG, Gibco, Grand Island, NY, USA) in 48-well microplates. The microplates were maintained in an incubator with 5% CO<sub>2</sub> over the assays. After sampling, the volume was replaced with fresh medium at 3, 6, 12, 48 and 72 hours without removing the hydrogels from the wells. The samples were stored at -80°C until all samples were collected. The concentrations of the released GFs were measured using enzyme-linked immunosorbent assay (ELISA) kits (R&D Systems, Minneapolis, MN, USA) according to the manufacturer's instructions and specifications.

*h-AdMSCs-seeding in the composite scaffolds.* The pre-cultured h-AdMSCs were trypsinized and resuspended in P-PRP to a final cell concentration of 1 x 10<sup>4</sup> cells/ mL. P-PRP containing h-AdMSCs was activated and immediately pipetted onto the surface of the microparticles or embedded into the sponges, both in 24-well tissue culture plates. The composite scaffolds were kept at room temperature for 45 minutes for consolidation of the fibrin network. The cells seeded in fHA or in sHA were used as controls.

*h-AdMSCs cultivation in the composite scaffolds.* Cultivation of the h-AdMSCs was carried out in 24-well tissue culture plates, by adding 1 mL of the culture medium (DMEM) to the seeded composite scaffolds (n=4). The culture was maintained at 37°C over 10 days. Cell proliferation was quantified using the thiazolyl blue tetrazolium bromide (MTT) assay. At 3, 5, 7 and 10 cultivation days, the substrates were removed and transferred to 24-well plates. MTT (1 mL of 1 mg/mL) was then added, and the

cultivation proceeded at 37°C for 4 hours. The MTT solution was then discarded, and 1 mL of DMSO was added to dissolve the purple formazan crystals. The samples were shaken at 120 rpm for 30 min to ensure homogeneous dissolution of the formazan dye, and then 200 µL of each sample was transferred to a 96-well plate. Optical density was measured at 595 nm using a microplate reader (FilterMax F5 Molecular Devices, Sunnyvale, CA, USA). The cell concentration was obtained from the previously built calibration curve.

*Images of the cell-seeded composite scaffolds.* Images of cell-seeded composite scaffolds were obtained by scanning electron microscopy (SEM) after 5 days of h-AdMSCs proliferation. The substrates were fixed in a solution of 4% paraformaldehyde and 2.5% glutaraldehyde in PBS, for 2 hours. The samples were then dehydrated in ethanol for 15-min intervals in aqueous 50%, 70%, 95% and 100% ethanol solutions (2x) and dried at the critical point dryer BAL-TEC CPD 030 (BAL-TEC®, Schalksmühle, Germany). After gold coating in a Sputter Coater POLARON, SC7620 (VG Microtech, Ringmer, UK), the samples were visualized with a scanning electron microscope Leo440i (LEO Electron Microscopy/Oxford, Cambridge, UK) with an accelerating voltage of 20 kV.

*Induction of osteogenic differentiation.* h-AdMSCs-seeding composite scaffolds were induced to differentiate into the osteogenic lineage by providing the osteogenic medium containing DMEM-LG supplemented with 10% fetal bovine serum (FBS), 1% β-glycerol-phosphate (Sigma-Aldrich, St. Louis, MO, USA), 1% L-ascorbic acid (Sigma-Aldrich, St. Louis, MO, USA), 1% dexamethasone (Sigma-Aldrich, St. Louis, MO, USA) and 1% Penicillin/Streptomycin solution (Gibco, Grand Island, NY, USA). The medium was changed every 7 days.

*Alkaline phosphatase activity (ALP).* The level of alkaline phosphatase (ALP) activity of h-AdMSCs was determined on day 14. Two hundred microliters of the supernatant was collected and mixed with 200 µL of p-nitrophenyl phosphate (SIGMAFAST™ p-Nitrophenyl phosphate Tablets, Sigma, Saint Louis, MI, USA) as

substrate and incubated at room temperature for 30 minutes. Absorbance was read immediately on a spectrophotometer at 405 nm.

#### 6.2.2.10. Statistical analysis

Each experiment was carried out in triplicate unless otherwise specified. All results are presented as the mean  $\pm$  standard deviation (SD). The experimental data from all the studies were analyzed using Analysis of Variance (ANOVA). Statistical significance was set to p-value  $\leq 0.05$ .

## 6.3. Results

### 6.3.1. Characterization of ACP

The IR spectra from ACP (Figure 28) shows peaks between 1000 and 850  $\text{cm}^{-1}$ , corresponding to deformation out of the plane of the OH group, which is related to the H-bonds; between 1250-1080  $\text{cm}^{-1}$ , corresponding to the asymmetrical stretching  $\text{CC}(=\text{O})\text{-O}$  and  $\text{CHO}$ ; at approximately 1400  $\text{cm}^{-1}$ , corresponding to the deformation of  $\text{COH}$  bond; and in the region of 1800-1700  $\text{cm}^{-1}$ , which is attributed to the stretching vibration of  $\text{C}=\text{O}$  of carboxylic acyl groups ( $\sim 1725 \text{ cm}^{-1}$ ) and ester groups (1780-1760  $\text{cm}^{-1}$ ) (Schanté *et al.*, 2011; Silverstein *et al.*, 1974).

These results ensured the auto-crosslinking and its unique feature that no foreign bridge molecules are present between the crosslinked HA chains.

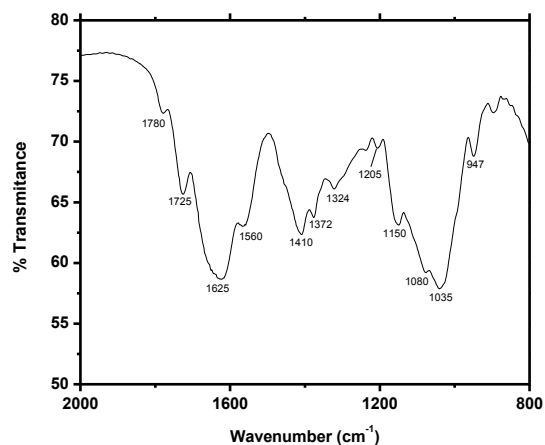


**Figure 28.** ATR-FTIR spectra of ACP with 5% of carboxylic groups esterified.



### 6.3.2. Characterization of ACPs structured scaffolds

The rheological behavior determined by oscillatory and steady measurements of the ACP structured in microparticles in relation to 1% fHA is shown in Figure 29(a) and 29(b), respectively. The microparticles exhibited the gel-like behavior, as analyzed by the storage ( $G'$ ) and loss moduli ( $G''$ ), where  $G'$  is higher than  $G''$  in all studied frequency ranges and the curves are parallel to the frequency axis, indicating crosslinking. The 1% fHA showed crossover ( $G'=G''$ ) around 1 Hz indicating concentrated solution behavior, as expected. Moreover, mACP exhibited behavior typical of so-called weak gels with  $\tan \delta$  ( $G''/G'$ )=0.19 in 1 Hz (Ikeda & Nishimari, 2001; Clark & Ross-Murph, 1987).

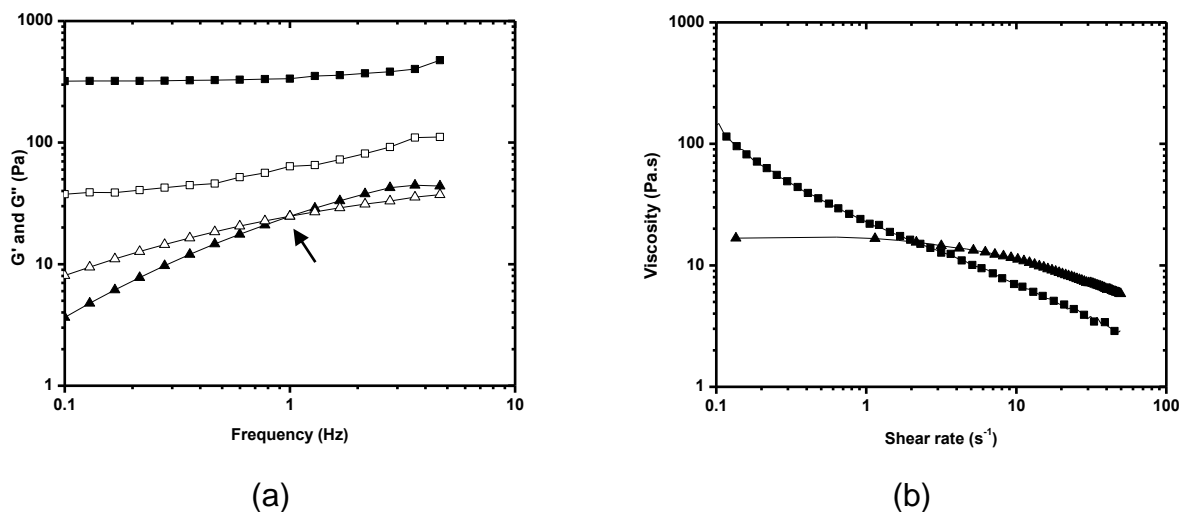


**Figure 29.** (a) Oscillation spectrum and (b) flow curve of (■) ACP Microparticles and (▲) fluid HA (1% wt.).  $G'$  (closed symbol) and  $G''$  (open symbol).

The flow curve (Figure 29b) showed a shear thinning behavior characteristic of pseudoplastic fluids for mACP and the microparticles were more resistant to shearing (up to  $1 s^{-1}$ ) than 1% fHA.

Moreover, the microparticles showed  $G'$  (~300 Pa) values between 100-700 Pa, which are adequate for injectable application (Kablik *et al.*, 2009).

In addition to the beneficial rheological properties and microparticle size, the injectable scaffolds must have an extrusion force to allow for their easy injection through an appropriately sized needle and thereby prevent side effects such as pain, bruising,

bleeding, and edema (Kablik *et al.*, 2009).

For injectable applications, extrusion force values must be smaller than 20 N and the mean diameter of particles smaller than 700  $\mu\text{m}$  (Shimojo *et al.*, 2013; Kablik *et al.*, 2009).

In ACP microparticles, we standardized the mean diameter to values smaller than 200  $\mu\text{m}$  by adequate conditions of shearing. Thus, the ACP microparticles showed extrusion forces around 20N, which is adequate for injectable applications (Table 3).

Moreover, the extrusion force of the microparticles was five times higher than the 1% fHA, indicating crosslinking and improvement of mechanical properties.

**Table 3.** Properties of fHA, sHA, and structured ACP (microparticles and sponges).

Scaffold	Extrusion Force (N)	Young' s moduli (kPa)	Swelling ratio (SR= $w_s/w_d$ )	Porosity (%)
ACP microparticles	20 $\pm$ 1	-	61 $\pm$ 8	-
fHA (1% w/v)	4.3 $\pm$ 0.1	-	-	-
ACP sponges	-	30 $\pm$ 0.1	91 $\pm$ 5	97.6 $\pm$ 0.2
sHA	-	< 10	-	97.8 $\pm$ 0.3

The Young's modulus of ACP sponges (Table 3) was approximately 3 times higher than for the sHA with similar porosity (~97%). This result is evidence of the improvements to mechanical resistance imparted by ACP, which is one of the most important requirements for scaffolds in tissue engineering.

The capacity to hydration is also an essential factor for cell migration inside the scaffolds. The 5% auto-crosslinking did not greatly affect the capacity for hydration of the structured ACP. Although the hydration capacity is directly linked to the functional groups capable of forming H-bonds with water, in this case, the higher hydration capacity of the ACP sponges (~90%) can be attributed to the porous structure of the scaffold, which retains greater amount of unbound water. For the ACP microparticles, the swelling was ~60%, due to a smaller porous size structure.

The porosities of the ACP sponges and sHA were similar, which evidence the superiority of the ACP sponges as a scaffold, when associated to its mechanical

resistance. The porosity values of ACP sponges and sHA ranged around 97%, which are adequate for tissue engineering.

Different aggregations of the HA chains in ACP sponges or sHA are shown in Figure 30. In both cases, highly porous structures were formed, confirming the determined values for porosity in Table 2. However, the structure of ACP sponges has more round pores [Figure 30(a)], whereas the sHA has a leaf structure [Figure 30(b)].

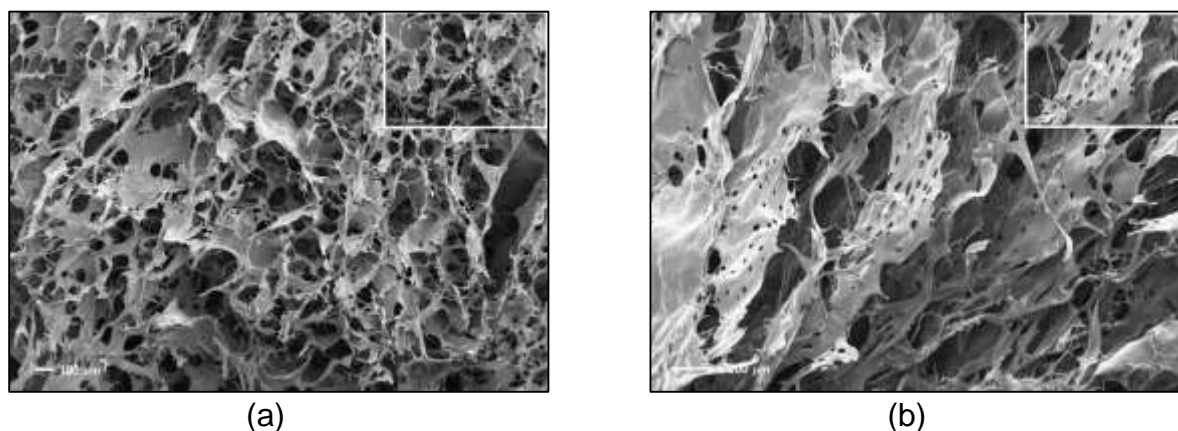


**Figure 30.** Figure 4. SEM micrographs of cross-sectional of (a) ACP sponges and (b) HA sponge.

The proliferation of h-AdMSCs results, as assayed by MTT, shown in Figure 31(a) indicated that the structured ACP, sHA and fHA could be considered compatible to the cells, by comparison with the positive toxicity control (PTC).

We also observed that the proliferation of h-AdMSCs on ACP sponges was significantly higher than the negative control ( $p < 0.05$ ).

Moreover, ACP microparticles showed lower cell proliferation compared to fHA, while there were no significant differences between the cell proliferation of ACP sponges and sHA.

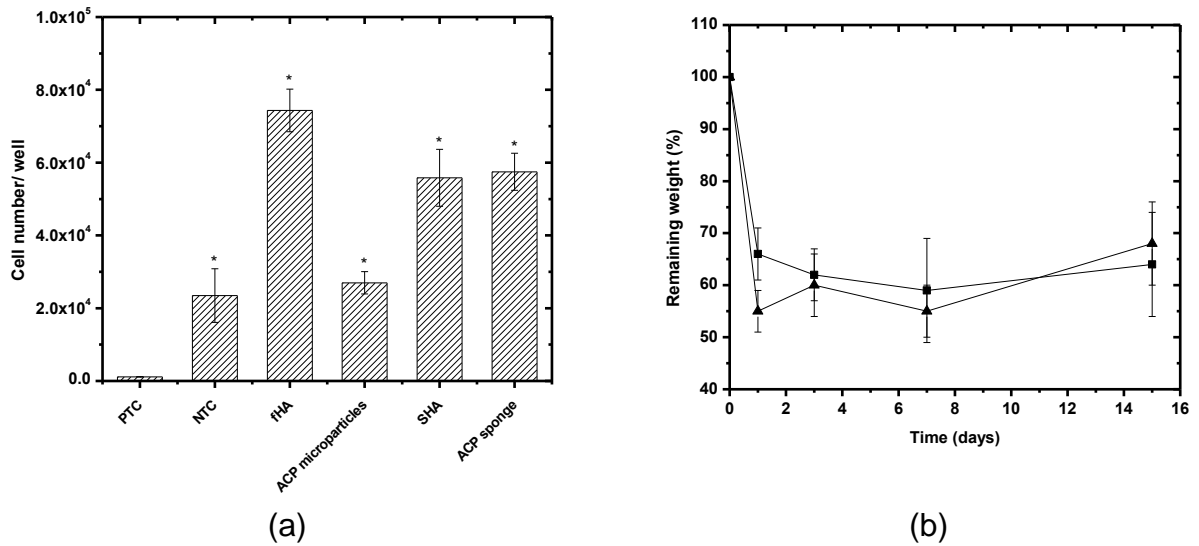


**Figure 31.** (a) Viability of h-AdMSCs exposed to the structured ACP or HA (fluid and sponge). Negative control (NTC) = DMEM with 10% FBS; positive control (PTC) = DMEM with phenol 0.5%. Mean  $\pm$  standard deviation  $n = 3$ . The population means are significantly different from the positive control at  $*p < 0.05$ . (b) The weight remaining of the structured ACP under the time course of degradation (at  $37^\circ\text{C}$ , in PBS). (■) ACP microparticles and (▲) ACP sponges.

Figure 31(b) shows the degradation kinetics of the structured ACP in PBS in terms of remaining weight. Most of the weight reduction, around 40% was observed in the first day for both structures. Scaffolds for regenerative medicine applications should degrade over the course of tissue regeneration to allow complete repair by host tissue. Therefore, degradation must be adjusted to release GFs and allow for cell proliferation.

### 6.3.3. Characterization of the composite scaffolds

Figure 32 shows the release kinetic of PDGF-AB and TGF- $\beta$ 1 from the composite scaffolds. The GFs were from aP-PRP containing average platelet concentration  $407,000 \text{ pq}/\text{mm}^3$ . The fibrin network from activated aP-PRP alone was used as control.

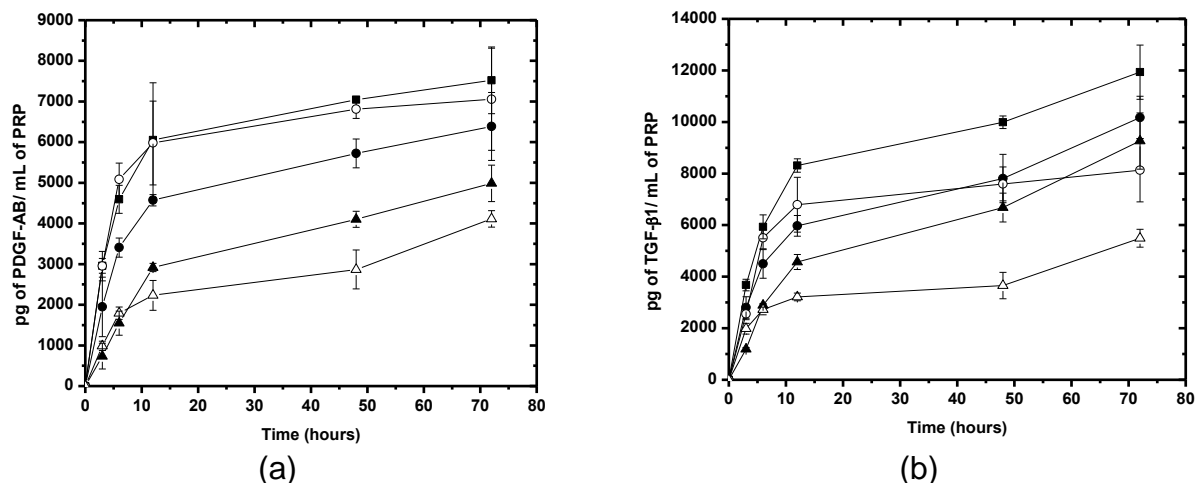


**Figure 32.** Growth factor release profiles from P-PRP combined with HA and ACP structured scaffolds. (a) PDGF-AB and (b) TGF- $\beta$ 1. (●) ACP microparticles; (▲) fHA; (■) P-PRP alone; (O) ACP sponges and (Δ) sHA. The concentration of platelets in P-PRP was 407,000  $\text{pq}/\text{mm}^3$ .

Controlled release of GFs was achieved from the composite scaffolds. The curves show parallel diffusive profiles. The bulk of the GFs were released in the first 12 hours. For both GFs, the initial release rate was higher in aP-PRP alone and aP-PRP-ACP sponges, followed by aP-PRP-ACP microparticles, aP-PRP-fHA and aP-PRP-sHA. Subsequently, the release rates reduced and different amounts of the GFs were released from the scaffolds over the 72 hours assay.

The release of the most of the GFs occurred in concert with the degradation time (12 hours) of the structured ACP [Figure 31(b)].

The structured ACP promoted proliferation of h-AdMSCs (Figure 33), which was evidence of the benefits of the porous structure, swelling and mechanical properties on cell adhesion and migration.

The importance of the stability of the porous structures for cultivation is clear from comparing the performances of aP-PRP-ACP microparticles and aP-PRP-ACP sponges.

The aP-PRP-ACP sponges showed better cell proliferation compared to aP-PRP alone. The effect was similar to aP-PRP-sHA [Figure 33(b)]. However, aP-PRP-ACP microparticles [(Figure 33(a)] showed reduced cell proliferation related to aP-PRP alone and fHA showed no cell proliferation attributed to the very small pore size and to high



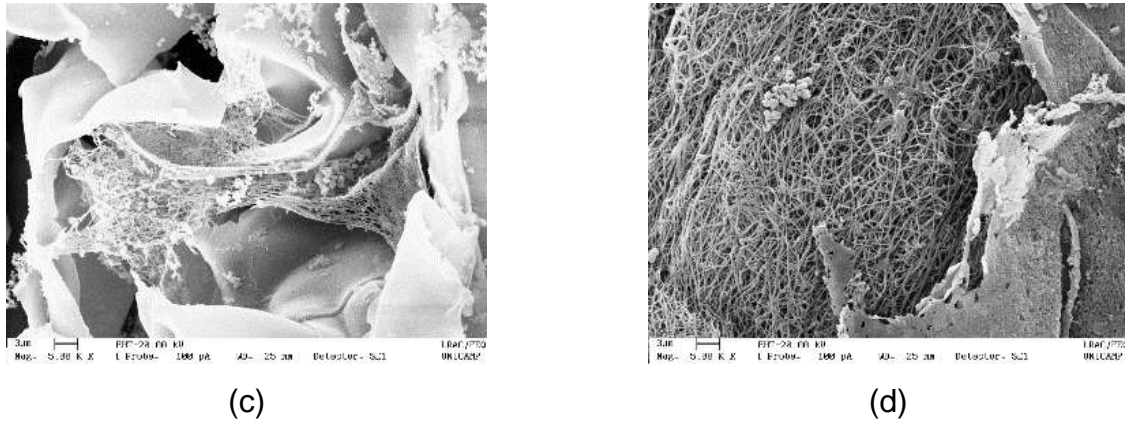


**Figure 34.** Scanning electron microscopy images of HA and ACP composite scaffolds after 5 days of cultivation of h-AdMSCs. (a) ACP microparticles; (b) fluid HA; (c) ACP sponges and (d) HA sponge. Original magnification is  $\times 5,000$  and the scale bar represents  $3 \mu\text{m}$ .

Osteogenic differentiation of h-AdMSCs was investigated after HA and ACP composite scaffolds induction at days 14. ALP activity, an early marker of osteogenic differentiation, was measured and shown in Figure 35. ALP activity was significantly higher in the sponges and in ACP microparticles compared with the fHA (control) suggesting stimulation of osteogenic differentiation.

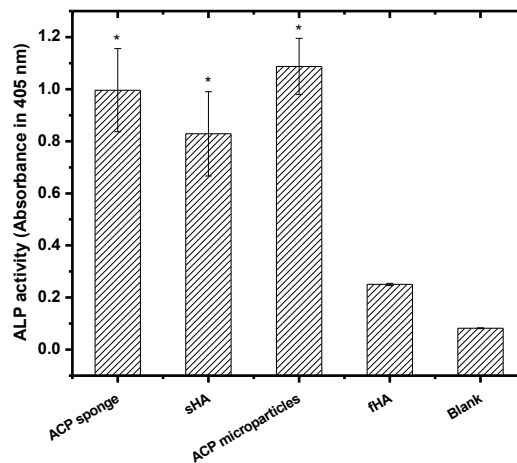


**Figure 35.** Alkaline phosphatase (ALP) activity of h-AdMSCs-seeded cultured in the HA and ACP composite scaffolds on day 14. Blank = the reagents used in the assay only.

Statistically significant differences from blank, n=3, \*p<0.05. The concentration of platelets in P-PRP was 473,500 pq/mm<sup>3</sup>.

## 6.4. Discussion

In this study, we prepared novel composite scaffolds by associating aP-PRP to 3D-ACP structured in microparticles or sponges.

ACP is a crosslinked derivative of hyaluronic acid biocompatible, obtained by organocatalyzed auto-esterification (Bellini *et al.*, 2001). ACP was used to increase the residence time at the site of application and improve the physicochemical and mechanical properties of free HA, reducing the need for repeated applications.

The auto-esterification reaction of HA was performed with the quaternary ammonium salt of HA (HA-TBA) as the intermediate. CMPI was used as activating agent of the carboxyl groups of HA according to Magnani *et al.* (2000). The anhydrous organic solvent DMSO was used to minimize CMPI hydrolysis. CMPI reacts with a carboxyl group of HA, forms a pyridinium intermediate and releases a chloride ion, which is neutralized by tetrabutylammonium. Triethylamine neutralizes the released iodide ion. When no amine is added to the reaction medium, esterification occurs as the CMPI-activated HA reacts with its own hydroxyl groups, forming an ester crosslink between the HA chains. The product is the auto-crosslinked HA, usually called ACP.

The ACP ensures that only the HA, a naturally occurring molecule that has a biologic role, is released and eliminated through a known metabolic pathway during its degradation in the organism (Mensitieri *et al.*, 1996). According Koçak *et al.* (1999), ACP is slowly resorbed within 2 weeks and is excreted within 40 days by the kidneys.

In this work, ACP was structured in microparticles and sponges to create injectable or solid scaffolds, respectively. Furthermore, aiming ensure better stability of the fibrin network from PRP and control the release of GFs, we associate PRP with structured ACP.

P-PRP was obtained by centrifugation to about twice the concentration relative to WB. Haynesworth *et al.* (2002) showed that the proliferation and differentiation of adult mesenchymal stem cells are directly related to the platelet concentration. Platelet



concentrations ranged from  $0.8$  to  $1.2 \times 10^6$  platelets/ $\mu\text{L}$  have been proposed to be effective for *in vivo* applications by Weibrich *et al.* (2004) and Fennis *et al.* (2005). In our biological assays, we used around  $0.5 \times 10^6$  platelets/ $\mu\text{L}$  due to the platelet concentration factor (2x) inherent to the process used to obtain PRP.

P-PRP was activated with autologous serum and  $\text{Ca}^{+2}$  in specific conditions to obtain fibrin network architectures with thin fibers with an average radius of approximately 65 nm. This type of fiber favors proliferation of h-AdMSCs due to its paracrine nature for the cells (Ye *et al.*, 2013)

The composite scaffolds were obtained by mixing the microparticles or embedding the sponges with immediately activated P-PRP to ensure that the fibrin network was gelled in the scaffold.

The structured ACP were characterized by physicochemical and mechanical properties.

The effect of ACP structured on biological performance of aP-PRP/ACP was evaluated by the kinetics of growth factor release (PDGF-AB and TGF- $\beta$ 1), h-AdMSCs proliferation and osteogenic differentiation by marker ALP.

Beyond that, the scaffolds structured in sponges were characterized in terms of porosity, pore shape and interconnectivity, because these aspects are determinant for cellular colonization *in vitro* since they affect the diffusion of physiological nutrients and cells through the scaffold (Leong *et al.*, 2003; Liu & Ma, 2004). In addition, the high porosity (>90%) and the interconnectivity of pores compromised the mechanical and structural stability of the scaffolds. According to Loh & Choong (2013), these aspects must be evaluated in accordance with the application and degradation rate of materials used. For order to guide tissue regeneration, the mechanical properties of scaffolds must maintain the spaces required for cell in-growth and matrix elaboration during *in vitro* cultivation (Leong *et al.*, 2003). The ACP sponges presented morphological properties adequate to tissue engineering, whereas the mechanical properties indicated application for soft tissues (Hollister, 2005).

The scaffolds structured in microparticles were characterized by rheological and mechanical properties, which allowed injectable applications (Kablik *et al.*, 2009). The average diameter of the microparticles of  $190 \pm 5 \mu\text{m}$  was supported by our previous

work on viscoelasticity and injection force (Shimojo *et al.*, 2013).

Moreover, we observed that h-AdMSCs cultured in ACP structured scaffolds proliferated ensuring the non-cytotoxicity.

It is well known that growth factors greatly contribute to wound healing and tissue regeneration at various stages of cell proliferation and differentiation (Stocum, 1997). Moreover, the fibrin converted from fibrinogen works in concert with these GF in promoting of tissue regeneration.

However, the release of most of these growth factors from PRP occurs within the first hours after platelet activation and the gradual release of GF is essential for cascade of events involved on regeneration process (McCarrel & Fortier, 2009).

Tsay *et al.* (2005) showed in their *in vitro* study that PRP gels had a burst release of 80% of PDGF-AB and 82% of TGF- $\beta$ 1 in the medium after 24 h and a sustained release for another 14 days. Thus, to protect the GFs against proteolysis and to extend its activity, Tabata (2003) suggested combining the functions of scaffolds with controlled release technology.

Scaffolds can be an interesting alternative to gradual release of GFs increasing the effectiveness of PRP, and therefore, the regeneration of tissues.

Aside from the barrier of the ACP structures, the interactions among GFs and the scaffolds also play an important role in the controlled release.

In order to control the release of growth factors into scaffolds, chemical bonding (covalent and non-covalent) or physical interaction have been used (Tabata, 2003; King & Krebsbach, 2012). However, the physical interactions using hydrophilic polymers has been the most commonly used approach to incorporate growth factors into scaffolds (King & Krebsbach, 2012). Increasing the magnitude of these electrostatic interactions decreases the initial burst release.

The increase of the concentration of charge on scaffold is the common technique to increase the electrostatic attraction between growth factors and scaffolds. Although, some studies reported that specific intermolecular interactions may be more effective at minimizing the initial burst release of growth factors when compared to non-specific electrostatic interactions because these interactions are stronger and localized (Gao *et al.*, 2001; Jha *et al.*, 2009; Lee *et al.*, 2011).

Because growth factors are generally basic proteins (isoelectric point > 7), in physiological pH, they will have positive charge interacting ionically with the acidic species. (Hokugo *et al.*,2005; Okuda *et al.*, 2003)

Thus, when a scaffold is prepared from a biodegradable polymer with negative charges, such as hyaluronic acid and ACP, the growth factors with a positively charged site interact electrostatically with the polymer and can be physically immobilized. If environmental changes, such as increasing in ionic strength, occurs, the immobilized growth factor will be released. However, if such an environmental change does not take place, degradation of the scaffolds will be responsible for growth factors release.

Hokugo *et al.* (2005) and Tabata & Ikada (1998) reported the controlled release of TGF- $\beta$ 1 and PDGF from the hydrogel of acidic gelatin and demonstrated successful bone regeneration in rabbit and monkey skull defects, in marked contrast to defects treated with free TGF- $\beta$ 1. According to these authors, TGF- $\beta$ 1 and PDGF are sorbed into the acidic gelatin hydrogel mainly due to electrostatic interaction between the gelatin and GFs molecules. The immobilized growth factors were released from the hydrogel since hydrogel degradation occurs.

Scaffold degradation plays an important role in controlled release in scaffolds that strongly interact with growth factors. Generally, growth factor released from these scaffolds has been correlated to the rate of degradation of material after the initial burst release period (King & Krebsbach, 2012).

*In vivo*, it is known that the growth factors are normally stored in the body ionically bound to the acidic polysaccharides of the ECM. These bounds protect growth factors against denaturation and enzymatic degradation *in vivo*. In this case, the growth factors are released from the ECM complex due to polysaccharide degradation according to the need (Tabata, 2003).

Growth factor released from degradable scaffolds can be tuned by controlling either factor diffusion or degradation. Fast degradation will lead to rapid release of growth factors, while slowing degradation will retard release of factors (Fournier *et al.*, 2003).

Despite the controlled release compared to aP-PRP alone, we observed that the initial burst of release within 12 hours occurred in concordance with higher degradation

of scaffolds. After this first step, both release and degradation rate are reduced, indicating that the GFs release is governed mainly by degradation of scaffolds.

Van der Dolder *et al.* (2006) and Lucarelli *et al.* (2003) showed that PRP had a stimulating effect on the initial cell growth and differentiation of osteoblast-like cells and stromal cells.

Moreover, according to Okuda *et al.* (2003), PRP modulates the cell proliferation by PDGF- and/or TGF- $\beta$ 1 mediated-mechanisms.

Although controversial, it is known that these effects are dependent of PRP concentration. Choi *et al.* (2005) and Arpornmaeklong *et al.* (2004) showed in their studies that the cell viability, proliferation and differentiation were affected by PRP concentrations. The results obtained by Choi *et al.* showed that the viability and proliferation of alveolar bone cells were suppressed by high PRP concentrations, but were stimulated by low PRP concentrations (1–5%). In contrast, Arpornmaeklong *et al.* (2004) showed that a high concentration of PRP inhibited osteoblastic differentiation and increased the proliferation of pre-osteoblast-like cells or osteoblast precursor cells. PRP in low concentration did not show a marked effect on cell proliferation or differentiation.

We found that despite the high concentration of PRP (20% v/v) used in the assays, the presence of aP-PRP in the scaffolds was benefic on cell proliferation and differentiation.

We also verified that the differences on structuration of scaffolds in microparticles or sponges produced a more prominent effect on cell proliferation of the composite scaffolds compared to stimulating of osteogenic differentiation.

## 6.5. Conclusions

We have demonstrated that the composite scaffolds released PDGF-AB and TGF- $\beta$ 1 from platelets mainly during the first 12 h. The released amounts depended on the architecture of the structures and on the interactions of the GFs and HA. We also showed the composite scaffolds in microparticles or sponges promoted h-AdMSCs proliferation and stimulated osteogenic differentiation as evaluated by ALP activity. Thus, our results provide evidence that composite scaffolds with superior mechanical

properties are promising biomaterials for future clinical use in osteoarthritis therapies. The flexibility to obtain injectable formulations (microparticles) or solid sponges opens perspectives to use the ACP-derived biomaterials in non-surgical applications, for surgical implants or even for wound healing.

**Acknowledgments.** The authors acknowledge the financial support from the National Council of Technological and Scientific Development (CNPq, Brazil). They also thank Prof. Dr. Edvaldo Sabadini of the Chemical Institute (University of Campinas) for the use of the rheometer; Prof. Dr. William Dias Belangero and Dr. Ana Amélia Rodrigues of the Faculty of Medical Sciences (University of Campinas) for assistance; and Dr. Ângela Cristina Malheiros Luzo of the Haematology and Hemotherapy Center (University of Campinas) for the donation of h-AdMSCs.

## 6.6. References

AMABLE, P.R.; CARIAS, R.B.; TEIXEIRA, M.V.; PACHECO, I.C.; AMARAL, R.J.C.; GRANJEIRO, J.M.; BOROJEVIC, R. Platelet-rich plasma preparation for regenerative medicine: optimization and quantification of cytokines and growth factors. **Stem Cell Research & Therapy**, vol.4, p.67-79, 2013.

ANITUA, E. Plasma Rich in Growth Factors: Preliminary Results of Use in the Preparation of Future Sites for Implants. **International Journal of Oral & Maxillofacial Implants**, vol.14, p.529-535, 1999.

ARPORNMAEKLONG, P.; KOCHER, M.; DEPPRICH, R.; KÜBLER, N.R.; WÜRZLER, K.K. **International Journal of Oral and Maxillofacial Surgery**, vol.33, p.60-70, 2004.

BELLINI, D.; PAPARELLA, A.; O'REGAN, M.; CALLEGARO, L. Autocross-linked hyaluronic acid and related pharmaceutical compositions for the treatment of arthropathies. **United States Patent: U.S. 6,251,876 B1**, 2001.

BELLUCO, C.; MEGGIOLARO, F.; PRESSATO, D.; PAVESIO, A.; BIGON, E.; DONA, M.; FORLIN, M.; NITTI, D.; LISE, M. Prevention of Postsurgical Adhesions with an Autocrosslinked Hyaluronan Derivative Gel. **Journal of Surgical Research**, vol.100, p.217–221, 2001.

CHEN, W-H.; LO, W-C.; HSU W-C.; WEI, H-J.; LIU, H-Y.; LEE, C-H.; CHEN, S-YT.; SHIEH, Y-H.; WILLIAMS, D.F.; DENG, W-P. Synergistic anabolic actions of hyaluronic acid and platelet-rich plasma on cartilage regeneration in osteoarthritis therapy. **Biomaterials**, vol.xxx, p.1-9, 2014.

CHOI, B-H.; ZHU, S-H.; KIM, B-Y.; HUH, J-Y.; LEE, S-H.; JUNG, J-H. Effect of platelet-rich plasma (PRP) concentration on the viability and proliferation of alveolar bone cells: an in vitro study. **International Journal of Oral and Maxillofacial Surgery**, vol.34, p.420–424, 2005.

CIVININI, R.; MACERA, A.; NISTRI, L.; REDL, B.; INNOCENTTI, M. The use of autologous blood-derived growth factors in bone regeneration. **Clinical Cases in mineral and bone metabolism**, vol.8, n.1, p.25–31, 2011.

CLARK, A.H.; ROSS-MURPHY, S.B. Structural and mechanical properties of biopolymer gels. **Advances in Polymer Science**, vol.83, p.57-192, 1987.

COLLINS, M.N.; BIRKINSHAW, C. Hyaluronic Acid Solutions—A Processing Method for Efficient Chemical Modification. **Journal of Applied Polymer Science**, vol.130, p.145-152, 2013.

CRANE, D.; EVERTS, P.A.M. Platelet Rich Plasma (PRP) Matrix Grafts, **PPM Communications**, vol.8, p.1-10, 2008.

DE ANGELIS, B.; LUCARINI, L.; ORLANDI, F.; AGOVINO, A.; MIGNER, A.; CERVELLI, V.; IZZO, V.; CURCIO, C. Regenerative surgery of the complications with Morton's neuroma surgery: Use of platelet rich plasma and hyaluronic acid. **International Wound Journal**, vol.10, n.4, p.372-376, 2012.

DE BOULLE, K.; GLOGAU, R.; KONO, T.; NATHAN, M.; TEZEL, A.; ROCA-MARTINEZ, J-X.; PALIWAL, S.; STROUMPOULIS, D. A Review of the Metabolism of 1,4-Butanediol Diglycidyl Ether-Crosslinked Hyaluronic Acid Dermal Fillers. **Dermatologic Surgery**, vol.39, p.1758-1766, 2013.

DE LACO, P.A.; STEFANETTI, M.; PRESSATO, D.; PIANA, S.; DONA, M.; PAVESIO, A.; BOVICELLI, L. A novel hyaluronan-based gel in laparoscopic adhesion prevention: preclinical evaluation in an animal model. **Fertility and Sterility**, vol.69, p.318–323, 1998.

DE UGARTE, D.A.; MORIZONO, K.; ELBARBARY, A.; ALFONSO, Z.C.; ZUK, P.A.; ZHU, M.; DRAGOO, J.L.; ASHJIAN, P.; THOMAS, B.; BENHAIM, P.; CHEN, I.; FRASER, J.; HEDRICK, M.H. Comparison of Multi-Lineage Cells from Human Adipose Tissue and Bone Marrow. **Cells Tissues Organs**, vol.174, p.101–109, 2003.

FATHI, W.K. The Effect of Hyaluronic Acid and Platelet - Rich Plasma on Soft Tissue Wound Healing: An Experimental Study on Rabbits. **Al-Rafidain Dental Journal**, vol.12, n.1, p.115-125, 2012.

FENNIS, J.P.M.; STOELINGA, P.J.W.; JANSEN, J.A. Reconstruction of the mandible with an autogenous irradiated cortical scaffold, autogenous corticocancellous bone-graft and autogenous platelet-rich plasma: an animal experiment. **International Journal of Oral & Maxillofacial Surgery**, vol.34, p.158-166, 2005.

FOSTER, T.E.; PUSKAS, B.L.; MANDELBAUM, B.R.; GERHARDT, M.B.; RODEO, S.A. Platelet-Rich Plasma: From Basic Science to Clinical Applications. **American Journal of Sports Medicine**, vol.37, p.2259-2272, 2009.

FOURNIER, E.; PASSIRANI, C.; MONTERO-MENEI, C.N.; BENOIT, J.P. Biocompatibility of implantable synthetic polymeric drug carriers: focus on brain biocompatibility. **Biomaterials**, vol.24, p.3311-3331, 2003.

GAO, T.; KOUSINIORIS, N.; WINN, S.R.; WOZNEY, J.M.; ULUDAG, H. Enhanced retention of rhBMP-2 in vivo by thermoreversible polymers. **Materwiss Werksttech**, vol.32, n.12, p.953-961, 2001.

GÜMÜŞDERELIOĞLU, M.; ADAY, S. Heparin-functionalized chitosan scaffolds for bone tissue engineering. **Carbohydrate Research**, vol.346, p.606-613, 2011.

HAYNESWORTH, S.E.; KADIYALA, S.; LIANG, L.N.; BRUDER, S.P. Mitogenic stimulation of human mesenchymal stem cells by platelet release suggest a mechanism for enhancement of bone repair by platelet concentrates. **Presented at the 48th Meeting of the Orthopedic Research Society**, Boston 2002.

HOKUGO, F.; OZEKI, M.; KAWAKAMI, O.; SUGIMOTO, K.; MUSHIMOTO, K.; MORITA, S.; TABATA, Y. Augmented Bone Regeneration Activity of Platelet-Rich Plasma by Biodegradable Gelatin Hydrogel. **Tissue Engineering**, vol.11, n.7/8, p.1224-1233, 2005.

HOLLISTER, S. J. Porous scaffold design for tissue engineering. **Nature Materials**, vol.4, p.518-590, 2005.

IKEDA, S.; NISHINARI, K. Weak Gel-Type Rheological Properties of Aqueous Dispersions of Nonaggregated K-Carrageenan Helices. **Journal of Agricultural and Food Chemistry**, vol.49, p.4436-4441, 2001.

JHA, A.K.; HULE, R.A.; JIAO, T.; TELLER, S.S.; CLIFTON, R.J.; DUNCAN, R.L.; POCHAN, D.J.; JIA, X. Structural Analysis and Mechanical Characterization of Hyaluronic Acid-Based Doubly Cross-Linked Networks. **Macromolecules**, vol.42, p.537-546, 2009.

KABLIK, J.; MONHEIT, G.D.; YU, L.; CHANG, G.; GERSHKOVICH, J. Comparative Physical Properties of Hyaluronic Acid Dermal Fillers. **Journal of dermatologic surgery**, vol.35, p.302-312, 2009.

KHETAN, S.; BURDICK, J.A. Patterning network structure to spatially control cellular remodeling and stem cell fate within 3-dimensional hydrogels. **Biomaterials**, vol.31, p.8228-8234, 2010.

KING, W.J.; KREBSBACH, P.H. Growth factor delivery: How surface interactions modulate release in vitro and in vivo. **Advanced Drug Delivery Reviews**, vol.64, n.12, p.1239-1256, 2012.

KOÇAK, I.; ÜNLÜ, C.; AKÇAN, Y.; YAKIN, K. Reduction of adhesion formation with cross-linked hyaluronic acid after peritoneal surgery in rats. **Fertility and Sterility**, vol.72, n.5, p.873-878, 1999.

KON, E.; MANDELBAUM, B.; BUDA, R.; FILARDO, G.; DELCOGLIANO, M.; TIMONCINI, A.; FORNASARI, P.M.; GIANNINI, S.; MARCACCI, M. Platelet-Rich Plasma Intra-Articular Injection Versus Hyaluronic Acid Viscosupplementation as Treatments for Cartilage Pathology: From Early Degeneration to Osteoarthritis. **Arthroscopy: The Journal of Arthroscopic and Related Surgery**, vol.27, n.11, p.1490-1501, 2011.

LEE, K.; SILVA, E.A.; MOONEY, D.J. Growth factor delivery-based tissue engineering: general approaches and a review of recent developments. **Journal of the Royal Society Interface**, vol.8, p.153-170, 2011.

LEONG, F.; CHEAH, C.M.; CHUA, C.K. Solid freeform fabrication of three-dimensional scaffolds for engineering replacement tissues and organs. **Biomaterials**, vol.24, p.2363–2378, 2003.

LIU, X.; MA, P.X. Polymeric Scaffolds for Bone Tissue Engineering. **Annals of Biomedical Engineering**, vol.32, n.3, p.477–486, 2004.

LOH, Q.L.; CHOONG, C.; Three-Dimensional Scaffolds for Tissue Engineering Applications: Role of Porosity and Pore Size. **Tissue Engineering: Part B**, vol.19, n.6, p.485-503, 2013.

LUCARELLI, E.; BECCHERONI, A.; DONATI, D.; SANGIORGIO, L.; CENACCHI, A.; DEL VENTO, A.M.; MEOTTI, C.; BERTOJA, A.Z.; GIARDINO, R.; FORNASARI, P.M.; MERCURI, M.; PICCI, P. Platelet-derived growth factors enhance proliferation of human stromal stem cells. **Biomaterials**, vol.24, p.3095-3100, 2003.

MAGNANI, A.; RAPPUOLI, R.; LAMPONI, S.; BARBUCCI, R. Novel Polysaccharide Hydrogels: Characterization and Properties. **Polymers for Advanced Technologies**, vol.11, p.488-495, 2000.

MCCARREL, T.; FORTIER, L. Temporal Growth Factor Release from Platelet-Rich Plasma, Trehalose Lyophilized Platelets, and Bone Marrow Aspirate and Their Effect on Tendon and Ligament Gene Expression. **Journal of Orthopaedic Research**, vol.27, p.1033–1042, 2009.

MENSITIERI, M.; AMBROSIO, L.; NICOLAIS, L.; BELLINI, D.; O' REGAN, M. Viscoelastic properties modulation of a novel autocrosslinked hyaluronic acid polymer. **Journal of Materials Science: Materials in Medicine**, vol.7, n.11, p.695-698, 1996.

MOSSMAM, T.J. A rapid colorimetric assay of cellular growth and survival: application to proliferation and cytotoxicity assays. **Journal of Immunological Methods**, vol.65, p.55-63, 1983



OKUDA K, KAWASE T, MOMOSE M, MURATA M, SAITO Y, SUZUKI H, WOLFF LF, YOSHIE H. Platelet-rich plasma contains high levels of platelet-derived growth factor and transforming growth factor- $\beta$  and modulates the proliferation of periodontally related cells in vitro. **Journal of Periodontology**, vol.74, p.849-857, 2003.

PAK, J. Compositions and methods for treating, preventing and alleviating bone or cartilage diseases. **United States Patent: 2012/0,171,169 A1**, 2012.

PEREZ, A.G.M.; LANA, J.F.S.D.; RODRIGUES, A.A.; LUZO, A.C.M.; BELANGERO, W.D.; SANTANA, M.H.A. Relevant Aspects of Centrifugation Step in the Preparation of Platelet-Rich Plasma. **ISRN Hematology**, vol.2014, p.1-8, 2014.

PEREZ, A.G.M.; LICHY, R.; LANA, J.F.S.D.; RODRIGUES, A.A.; LUZO, A.C.M.; BELANGERO, W.D.; SANTANA, M.H.A. Prediction and Modulation of Platelet Recovery by Discontinuous Centrifugation of Whole Blood for the Preparation of Pure Platelet-Rich Plasma. **BioResearch Open Access**, vol.2, p.307-314, 2013.

PRASADAM. I.; MAO, X.; SHI, W.; CRAWFORD, R.; XIAO, Y. Combination of MEK-ERK inhibitor and hyaluronic acid has a synergistic effect on anti-hypertrophic and pro-chondrogenic activities in osteoarthritis treatment. **Journal of Molecular Medicine**, vol.91, p.369-380, 2013.

SCHANTÉ, C.E.; ZUBER, G.; HERLIN, C.; VANDAMME, T.F. Chemical modifications of hyaluronic acid for the synthesis of derivatives for a broad range of biomedical applications. **Carbohydrate Polymer**, vol.85, p.469-489, 2011.

SHIMOJO, A.A.M.; PEREZ, A.G.M.; GALDAMES, S.E.M.; BRISSAC, I.C.S.; SANTANA, M.H.A. Performance of PRP Associated with Porous Chitosan as a Composite Scaffold for Regenerative Medicine. **The Scientific World Journal**, vol.2015, p.1-12, 2015.

SHIMOJO, A.A.M.; PIRES, A.M.B.; TORRE, L.G.; SANTANA, M.H.A. Influence of Particle Size and Fluid Fraction on Rheological and Extrusion Properties of Crosslinked Hyaluronic Acid Hydrogel Dispersions. **Journal of Applied Polymer Science**, vol.128, n.3, p.2180-2185, 2013.

SHU, X.Z.; LIU, Y.; PALUMBO, F.S.; LUO, Y.; PRESTWICH, G.D. In situ crosslinkable hyaluronan hydrogels for tissue engineering. **Biomaterials**, vol.25, p.1339-1348, 2004.

SILVERSTEIN, R.M.; BASSLER, G.C.; MORRILL, T.C. **Spectrometric identification of organic compounds**. 3rd ed. New York: John Wiley, 1974.

SOLCHAGA, L.A.; TEMENOFF, J.S.; GAO, J.; MIKOS, A.G.; CAPLAN, A.I.; GOLDBERG, V.M. Hyaluronic Acid-B based Polymers as Cell Carriers for Tissue-Engineered Repair of Bone and Cartilage. **Osteoarthritis and Cartilage**, vol.13, n.4, p.297-309, 2005.

STERN, S.; LINDENHAYN, K.; SCHULTZ, O.; PERKA, C. Cultivation of porcine cells from the nucleus pulposus in a fibrin/hyaluronic acid matrix. **Acta Orthopaedica**

**Scandinavica**, vol.71, n.5, p.496-502, 2000.

STOCUM, D.L. Frontiers in medicine: regeneration. **Science**, vol.276, p.59-87, 1997.

TABATA, Y. Tissue regeneration based on growth factor release. **Tissue engineering**, vol.9, n.1, p.S5-15, 2003.

TABATA, Y.; IKADA, Y. Protein release from gelatin matrices. **Advanced Drug Delivery Reviews**, vol.31, p.287-301, 1998.

TANG, S.; VICKERS, S.M.; HSU, H-P.; SPECTOR, M. Fabrication and characterization of porous hyaluronic acid–collagen composite scaffolds. **Journal of Biomedical Materials Research**, vol.82A, p.323–335, 2007.

TSAY, R.C.; VO, J.; BURKE, A.; EISIG, S.B.; LU, H.H.; LANDESBURG, R. Differential Growth Factor Retention by Platelet-Rich Plasma Composites. **Journal of Oral and Maxillofacial Surgery**, vol.63, p.521-528, 2005.

VAN DER DOLDER, J.; MOOREN, R.; VLOON, A.P.G.; STOELINGA, P.J.W.; JANSEN, J.A. Platelet-Rich Plasma: Quantification of Growth Factor Levels and the Effect on Growth and Differentiation of Rat Bone Marrow Cells. **Tissue Engineering**, vol.12, n.11, p.3067-3073, 2006.

WANG, C.; LI, J.; YAO, F. Application of Chitosan-Based Biomaterials in Tissue Engineering. In: YUJI, Y. (Eds.). **Chitosan-Based Hydrogels: Functions and Applications**. New York: CRC Press, p.424, 2011.

WEIBRICH, G.; HANSEN, T.; KLEIS, W.; BUCH, R.; HITZLER, W.E. Effect of platelet concentration in platelet-rich plasma on peri-implant bone regeneration. **Bone**, vol.34, p.665-671, 2004.

YE, L.; ZIMMERMANN, W-H.; GARRY, D.J.; ZHANG, J. Patching the Heart: Cardiac Repair from Within and Outside. **Circulation Research**, vol.113, n.7, p.1-28, 2013.

YERUSHALMI, N.; ARAD, A.; MARGALIT, R. Molecular and cellular studies of hyaluronic acid-modified liposomes as bioadhesive carriers for topical drug delivery in wound healing. **Archives of Biochemistry and Biophysics**, vol.313, n.2, p.267-273, 1994.

# CAPÍTULO 7 – STRUCTURATION OF HIGH MOLECULAR WEIGHT HYALURONIC ACID IN MICROPARTICLES OR SPONGES IMPROVES ITS PERFORMANCE WHEN ASSOCIATED TO PLATELET-RICH PLASMA

---

Artigo submetido ao periódico *Trends in Biomaterials & Artificial Organs*.

Andréa Arruda Martins Shimojo<sup>a</sup>, Sofia Elisa Moraga Galdames<sup>a</sup>, Adriana da Silva Santos Duarte<sup>b</sup>, Lucas Martins Pina<sup>a</sup>, Ana Amélia Rodrigues<sup>b</sup>, Ângela Cristina Malheiros Luzo<sup>b</sup>, William Dias Belangero<sup>c</sup> and Maria Helena Andrade Santana<sup>a,\*</sup>

<sup>a</sup>Department of Engineering of Materials and Bioprocesses, School of Chemical Engineering, University of Campinas, Campinas, SP, Brazil.

<sup>b</sup>Haematology and Hemotherapy Center, Umbilical Cord Blood Bank, University of Campinas, Campinas, SP, Brazil

<sup>c</sup>Department of Orthopedics and Traumatology, Faculty of Medical Sciences, University of Campinas, Campinas, SP, Brazil.

\*Correspondence to: Maria Helena Andrade Santana, telephone: +55-19-35213921, FAX: +55-19-35213890, e-mail: [mariahelena.santana@gmail.com](mailto:mariahelena.santana@gmail.com)

**Abstract.** Nowadays, high molecular weight hyaluronic acid (HA) has been widely used associated with platelet-rich plasma (PRP) in regenerative medicine. This study aimed to investigate *in vitro* the association of HA crosslinked with 1,4-butanediol diglycidyl ether (BDDE), structured in microparticles (mHA-BDDE) and sponges (sHA-BDDE), with PRP as composite scaffolds for growth factors release, proliferation of human adipose-derived mesenchymal stem cells (h-AdMSCs) and differentiation by osteogenic marker alkaline phosphatase (ALP). The reason for using BDDE is to increase the residence

time *in vivo*, improve the mechanical stability of free HA (fHA) and provide a larger surface area for cell proliferation and differentiation in a new tissue. PRP was obtained via controlled centrifugation of whole blood and activated with autologous serum and calcium. The results showed that structuration benefited the physicochemical and mechanical properties compared to fHA. Both structures were non-cytotoxic. The release of GFs from PRP was lower than fHA but higher than the fibrin network. The effects on the proliferation of seeded mesenchymal cells were not intense. However, a remarkable activity of the osteogenic marker alkaline phosphatase was observed. We concluded the structuration of HA provides injectable (mHA-BDDE) or solid (sHA-BDDE) formulations with better properties compared to fHA, which associated to PRP may be promising for regeneration of bone tissue.

**Keywords:** Platelet-rich plasma; hyaluronic acid; 1,4-butanediol diglycidyl ether; microparticles; sponges.

## 7.1. Introduction

Platelet Rich Plasma (PRP) is an autologous product prepared from whole blood, consisting of a concentrate of platelets, leukocytes, protein and other components dispersed in a small fraction of plasma (Marx *et al.*, 1998; Marx, 2004). Platelets and leukocytes are sources of growth factors (GFs) which promote wound healing and tissue regeneration, through proliferation and differentiation of specific cells.

In the last decade, PRP has been widely used in medical practice in various therapies, especially in orthopedics and sports medicine. This is mainly due to its ability to regenerate bone lesions, tendons and cartilage, often avoiding surgical interventions (Lana *et al.*, 2014).

Pure PRP, named as P-PRP, is rich in platelets and poor in leukocytes, according to the classification of Ehrenfest *et al.* (2009).

Preparation of PRP is composed of two main steps: concentration and activation. The fibrin network is formed by the activation of platelets and the breakdown of fibrinogen from plasma. The fibrin network is also a weak gel, which acts as a barrier for

release of growth factors and also as a natural scaffold for proliferation and differentiation of mesenchymal cells.

However, the fibrin network is fragile, has low viscosity and viscoelasticity, and also undergoes rapid degradation in a biological environment. In addition to this, the released GFs have a half-life of only few hours.

In order to overcome these limitations, in the last decade the PRP has been used in orthopedics, associated with free hyaluronic acid (HA) of high molecular weight (Pak, 2012; De Angelis *et al.*, 2012; Chen *et al.*, 2014). Clinical studies in literature have shown that tissue regeneration with free HA associated with PRP is greater than HA or PRP alone (Pak, 2012; De Angelis *et al.*, 2012). Furthermore, the presence of the HA in the formulation is responsible for the reduction of pain resulting from inflammation caused by injury in the application of PRP (Fathi, 2012; Chen *et al.*, 2014).

In our previous studies, we observed that free HA, when combined with PRP, interacted with fibrin network improving their mechanical and viscoelastic properties and promoting the gradual release of GFs. However, the low mechanical stability of the free HA and the need for repeated injections *in vivo* have limited their application in regenerative medicine.

Thus, aiming to overcome these limitations, we structured HA in microparticles or sponges, which were chemically crosslinked by 1,4-butanediol diglycidyl ether (BDDE) for stabilization. The microparticles must meet the requirements of injectable formulations while the sponges works as solid scaffolds.

Our hypothesis is that by improving the structural and mechanical properties of the fibrin network we benefit the proliferation and differentiation of h-AdMSCs, thereby increasing the efficiency of the PRP in tissue regeneration.

HA crosslinked by BDDE has been widely used in medical and cosmetic area, mainly as dermal fillers on tissue augmentation and regeneration (Allemann & Baumann, 2008; Andre, 2004; Beasley *et al.*, 2009; Falcone & Berg, 2008) and also as a viscosupplement for joint diseases (Schanté *et al.*, 2011; Malson & Lindqvist, 1987).

HA can be crosslinked by BDDE under alkaline conditions, in which it reacts with the deprotonated hydroxyl group of HA to form a stable covalent ether linkage between HA and the epoxide groups of the crosslinker (Kenne *et al.*, 2013; Malson & Lindqvist,

1986; Garg & Hales, 2004; Schanté *et al.*, 2011). Its ability to crosslink is attributed to the reactivity of the epoxide groups present at the two ends of the molecule (De Boule *et al.*, 2013).

Besides the biodegradability and stability of the ether bond relative to the ester or amide bond, BDDE shows lower toxicity (rat oral LD<sub>50</sub>=1134 mg/kg) compared to others crosslinkers (Yeom *et al.*, 2010).

La Gatta *et al.* (2013) obtained HA sponges for soft tissues regeneration by lyophilization and then reacted with BDDE in heterogeneous conditions. The scaffolds showed promising physicochemical and mechanical properties, good cellular viability, high stability in cell culture and for enzymatic degradation.

Zawko *et al.* (2009) engineered novel dual-crosslinked hyaluronic acid hydrogel scaffolds with photopatterned anisotropic swelling using BDDE and glycidyl methacrylate, but only the physicochemical and mechanical properties were evaluated.

Besides the limited number of studies with HA-BDDE, as far as we know, there is none report in the literature on the use of HA-BDDE associated to PRP for applications in tissue regeneration.

## 7.2. Experimental Section

### 7.2.1. Materials

HA in sodium form (MW = 2 x 10<sup>6</sup> Da) was obtained from Spec-Chem Ind. (Nanjing, China). 1,4-Butanediol diglycidyl ether (BDDE) was obtained from Aldrich Chemical Co. (Milwaukee, WI, USA). All other reagents were purchased from Synth® (Diadema, SP, Brazil) unless specified otherwise. PRP was prepared from whole blood (WB) of donors, who were healthy individuals aged between 30 and 40 years old and previously assessed through clinical examinations. The human adipose tissue-derived mesenchymal stem cells, h-AdMSCs, were provided by Haematology and Hemotherapy Center, Umbilical Cord Blood Bank, University of Campinas. All biological experiments were approved by the Ethics Committee of the Medical Sciences School of the

University of Campinas (UNICAMP; CAAE: 0972.0.146.000-11).

## 7.2.2. Methods

### 7.2.2.1. Preparation and characterization of HA crosslinked with BDDE

The plain hydrogel of HA/BDDE was prepared in a 1:1 ratio by weight, according to the methodology described by Wang (2005). Sodium hyaluronate was dissolved in 0.25 mol.L<sup>-1</sup> NaOH aqueous solution in a stirrer vessel at room temperature for 4 hours. BDDE was added to the solution under stirring, and then the solution was kept at 50°C for four hours. Then, phosphate buffer saline solution (PBS, pH 7.4) (LB Laborclin, Pinhais, PR, Brazil) was added to the stirrer vessel to wash and hydrate the obtained gel. After 2.5 days, washing with six changes of fresh PBS, the gel was centrifuged to remove free PBS. The HA-BDDE crosslinking was characterized by Fourier-transform infrared (FTIR) in a Thermo Scientific Nicolet model 6700 (Thermo Scientific Nicolet™, Waltham, MA, USA). Measurements were made in the ATR mode with accessory SMART OMNI-SAMPLER, in the spectral range of 4000-675 cm<sup>-1</sup> with a resolution of 4 cm<sup>-1</sup> over 64 scans.

### 7.2.2.2. Preparation of structured HA-BDDE

The HA-BDDE structured in microparticles (mHA-BDDE) or sponges (sHA-BDDE) were prepared from HA-BDDE plain hydrogel swollen in Milli-Q water. The microparticles were obtained by shearing in an Ultra-Turrax T25 homogenizer (IKA Labortechnik, Staufen, Germany) at 18,000 rpm by 20 minutes (Shimojo *et al.*, 2013). The sponges were initially placed in polystyrene 48-well microplates (TPP®, Trasadingen, Switzerland), frozen at -20°C and lyophilized at controlled temperature of approximately -30°C for 48 hours (Shimojo *et al.*, 2015). Non-crosslinked sponges (sHA) was also prepared as control, as well as fluid HA (fHA).

## 7.2.3. Characterization of the structures

Degradation time. The gravimetric method described by Tang *et al.* (2007) was used to estimate the degradation time in PBS at 37°C of the structured HA-BDDE

through measurements of remaining weight.

Cell compatibility. The compatibility of the structured HA-BDDE with h-AdMSCs cells was carried out by exposing them to cell culture at 37°C for 24 hours. Then, cell viability was evaluated by using an MTT assay (3-[4,5-dimethyl-thiazol-2-yl]-2,5-diphenyltetrazolium bromide) (MTT, Molecular Probes), according to modified Mosmann (1983) method. The MTT assay is a colorimetric test based on the reduction of yellow tetrazolium salt into a purple formazan product in presence of cells (Gümüşşderelioğlu & Aday, 2011).

#### 7.2.3.1. mHA-BDDE

Average diameter. The average diameter was measured for the mHA-BDDE suspended in water. The measurements were performed in a Malvern Mastersizer S laser diffraction (Malvern Instruments Ltd, Malvern, UK). The standard deviation was calculated from five consecutive measurements.

Rheology. Rheological measurements of mHA-BDDE were performed in steady and oscillatory regimes at 25°C using a parallel plate geometry of 20 mm. Steady shear measurements were obtained at shear rates of 0.1-50 s<sup>-1</sup>. Oscillatory measurements were conducted in the linear region with a stress of 1.188 Pa and in the frequency range of 0.01 to 10 Hz. All rheological measurements were performed using the swollen mHA-BDDE equilibrated in Milli-Q on a rheometer Haake RheoStress 1 (Haake, Karlsruhe, Germany).

Extrusion force. Initially the mHA-BDDE were loaded in 1 mL plastic syringes with 30 gauge needles. Afterward, the force required to extrude was measured in a MTS 810 Servo-hydraulic Universal Testing Machine (MTS Systems Corporation, Eden Prairie, MN, USA) (load cell 1.5 kN) at 25°C at a 5.0 mm/min extrusion rate.

Swelling ratio (SR). Swelling measurements of the HA-BDDE microparticles were performed in PBS at 37°C after 72 h of incubation, according to Shu *et al.* (2004). SR



was calculated using the following Equation (1).

$$SR = \frac{W_s}{W_d} \quad \text{Equation (1)}$$

where  $w_s$  and  $w_d$  are the weights of the scaffolds in the swelled state and the dry state, respectively.

#### 7.2.3.2. sHA-BDDE

Morphology and pore size. The morphology of sHA-BDDE was evaluated by scanning electron microscopy (SEM) using an LEO 440i Electron Microscopy/Oxford (Cambridge, England) operated at 5 kV accelerating voltage. The sponges were gold-coated using a sputter coater POLARON SC7620, VG Microtech (Uckfield, England) for 180 s at a current of 3 mA. Pore size ( $n=20$ ) was measured using Image J 1.47t.

Swelling ratio (SR). The swelling measurements of the HA-BDDE sponges was determined by swelling the freeze-dried HA-BDDE sponges (with known weights) in PBS at 37°C for 24 hours. The swollen HA-BDDE sponges were weighed after the removal of excess of water by keeping the surfaces on a filter paper. The swelling ratio was also calculated using Equation (1).

Porosity. The porosity ( $\epsilon$ ) of the sHA-BDDE was determined according to the protocol used by Wang *et al.* (2003), and calculated by Equation (2).

$$\epsilon (\%) = \frac{V_m - \left(\frac{W_m}{\rho}\right)}{V_m} \cdot 100 \quad \text{Equation (2)}$$

where  $V_m$  is the total volume of sHA-BDDE ( $\text{cm}^3$ ),  $\rho$  is the density of HA ( $1.0016 \text{ g/cm}^3$ ) and  $w_m$  is the weight of sHA-BDDE (g). Values are expressed as the mean  $\pm$  standard deviation ( $n=3$ ).

Mechanical Properties. Mechanical compression tests of sHA-BDDE ( $n = 3$ ) were

performed using a Universal Testing Machine, MTS model 810-Flex Test 40 (MTS Systems Corporation, Eden Prairie, MN, USA) up to 60% strain, according to Correia *et al.* (2011). The testing machine was equipped with a 1.5 kN load cell, and the loading rate was 5 mm/min. Young's modulus was calculated in the initial linear section of the stress-strain curve, when the strain was lower than 10%.

#### 7.2.4. PRP preparation and activation

The P-PRP (rich in platelets and poor in leukocytes) was prepared according to Perez *et al.* (2013). Briefly, whole blood (WB) was collected into 3.5 mL vacuum tubes (Vacuette®, Campinas, SP, Brazil) containing sodium citrate 3.2% (w/v) as an anticoagulant. WB was initially centrifuged in a Rotina 380R centrifuge (Hettich® Zentrifugen, Tuttlingen, Germany) at  $100 \times g$  for 10 minutes, at 25°C. After the formation of three layers (a bottom layer composed mainly of red blood cells (RBCs); an upper layer composed of plasma, platelets and some WBCs; and an intermediate layer, or buffy coat, composed mostly of WBCs), only the upper layer was collected to obtain P-PRP. The concentration of platelets, WBCs and RBCs in WB and P-PRP was determined using the ABX Micros ES 60 hematology analyser (HORIBA ABX Diagnostics, Montpellier, France).

Autologous serum (Ser) and 10% (w/v)  $\text{CaCl}_2$  solution were used as agonists to activate the PRP preparations (aP-PRP). The Ser was prepared by collecting 5 mL of WB in tubes without anticoagulant. After 30 minutes for clot formation, WB was centrifuged at  $2000 \times g$  for 10 minutes. The conditions of agonist/PRP=20%; Ser/ $\text{CaCl}_2$  volumetric ratio=9 were used for getting an architecture of the fibrin network composed of thin fibers (average radius 65 nm), according to Perez *et al.*, 2014).

#### 7.2.5. Release of growth factors

Immediately after activation, aP-PRP was mixed with the mHA-BDDE or embedded by dripping into the sHA-BDDE, both in 48-well microplates. In all biological assays performed in this work, the following proportions of aP-PRP to structured HA-BDDE were used: aP-PRP: microparticles = 200  $\mu\text{L}$ :100 mg and aP-PRP: sponges =

200  $\mu$ L:10 mg in order to guarantee the same proportion PRP to HA. After 1 hour of gelation, 1.5 mL of Dulbecco's Modified Eagle's Medium (DMEM) (Gibco, Grand Island, NY, USA) with low glucose concentration was added to the composed hydrogels. The microplates were maintained in an incubator with 5% CO<sub>2</sub> over the assays. After sampling, the volume was replaced with fresh medium at 3, 6, 12, 48 and 72 hours without removing the hydrogels from the wells. The samples were stored at -80°C until all samples were collected. The concentrations of the released GFs, platelet-derived growth factor AB (PDGF-AB) and transforming growth factor beta 1 (TGF- $\beta$ 1), were measured using enzyme-linked immunosorbent assay (ELISA) kits (R&D Systems, Minneapolis, MN, USA) according to the manufacturer's instructions and specifications.

#### 7.2.6. Association of mHA-BDDE or sHA-BDDE with P-PRP and h-AdMSCs-seeding

The pre-cultured h-AdMSCs were trypsinized and resuspended in P-PRP to a final cell concentration of  $1 \times 10^4$  cells/mL. P-PRP containing h-AdMSCs was activated and immediately pipetted onto the surface of the microparticles or embedded into the sponges, both in 24-well tissue culture plates. The plates were kept at room temperature for 45 minutes for consolidation of the fibrin network. The cells seeded in fHA or in sHA were used as controls.

#### 7.2.7. h-AdMSCs cultivation

Cultivation of the h-AdMSCs was carried out in 24-well tissue culture plates, by adding 1 mL of the culture medium (DMEM) to the seeded structures (n=4). The culture was maintained at 37°C for 10 days. Cell proliferation was quantified using the thiazolyl blue tetrazolium bromide (MTT) assay. At 2, 4, 7 and 10 cultivation days, the substrates were removed and transferred to 24-well plates. MTT (1 mL of 1 mg/mL) was then added, and the cultivation proceeded at 37°C for 4 hours. The MTT solution was then discarded, and 1 mL of DMSO was added to dissolve the purple formazan crystals. The samples were shaken at 120 rpm for 30 min to ensure homogeneous dissolution of the formazan dye, and then 200  $\mu$ L of each sample was transferred to a 96-well plate.

Optical density was measured at 595 nm using a microplate reader (FilterMax F5 Molecular Devices, Sunnyvale, CA, USA). The cell concentration was obtained from the previously built calibration curve.

#### 7.2.8. Images of the cell-seeded composite scaffolds

Images of cell-seeded composite scaffolds were obtained by scanning electron microscopy after 5 days of h-AdMSCs proliferation. The substrates were fixed in a solution of 4% paraformaldehyde and 2.5% glutaraldehyde in PBS for 2 hours. The samples were then dehydrated in ethanol for 15 min intervals in aqueous 50%, 70%, 95% and 100% ethanol solutions (2x) and dried at the critical point dryer BAL-TEC CPD 030 (BAL-TEC®, Schalksmühle, Germany). After gold coating in a Sputter Coater POLARON, SC7620 (VG Microtech, Ringmer, UK), the samples were visualized with a scanning electron microscope Leo440i (LEO Electron Microscopy/Oxford, Cambridge, UK) with an accelerating voltage of 20 kV.

#### 7.2.9. Induction of osteogenic differentiation

The seeded h-AdMSCs were induced to differentiate into the osteogenic lineage by providing the osteogenic medium containing DMEM-LG supplemented with 10% FBS, 1%  $\beta$ -glycerol-phosphate (Sigma-Aldrich, St. Louis, MO, USA), 1% L-ascorbic acid (Sigma-Aldrich, St. Louis, MO, USA), 1% dexamethasone (Sigma-Aldrich, St. Louis, MO, USA) and 1% Penicillin/Streptomycin solution (Gibco, Grand Island, NY, USA). The medium was changed every 7 days.

#### 7.2.10. Alkaline phosphatase activity (ALP)

The level of alkaline phosphatase (ALP) activity produced by h-AdMSCs was determined as an osteogenic marker on day 14 under differentiation conditions. Two hundred microliters of the supernatant was collected and mixed with 200  $\mu$ L of p-nitrophenyl phosphate (SIGMAFAST™ p-Nitrophenyl phosphate Tablets, Sigma, Saint Louis, MI, USA) as substrate and incubated at room temperature for 30 minutes. Absorbance was read immediately on a spectrophotometer at 405 nm.

### 7.2.11. Statistical analysis

Each experiment was carried out in triplicate unless otherwise specified. All results are presented as the mean  $\pm$  standard deviation (SD). The experimental data from all the studies were analyzed using Analysis of Variance (ANOVA). Statistical significance was set to p-value  $\leq 0.05$ .

## 7.3. Results and Discussion

### 7.3.1. Experimental design

In this study, we associated P-PRP to HA-BDDE structured into microparticles or sponges. First, the synthesized HA-BDDE was characterized by FT-IR to guarantee the absence of toxic non-bound chemicals before building the microparticles or sponges. Secondly, the structural and mechanical properties of the structured HA-BDDE were characterized and evaluated for cell compatibility. The association was obtained by mixing the microparticles or embedding the sponges with immediately activated P-PRP in a 24 well microplates. P-PRP was obtained by centrifugation to about twice the concentration relative to WB. Activation of P-PRP was performed by  $\text{Ca}^{+2}$  and autologous serum to obtain fibrin network architectures with thin fibers and an average radius of approximately 65 nm. This type of fiber favors proliferation of h-AdMSCs due to its paracrine nature for the cells. The release of the GFs (PDGF-AB and TGF- $\beta$ 1) was evaluated in DMEM culture medium. Cell seeded in the fibrin network alone or associated with HA-BDDE structured into microparticles or sponges was obtained by adding pre-cultured h-AdMSCs to P-PRP before activation. An in vitro examination of kinetics of h-AdMSCs proliferation was determined after 10 days of cultivation, whereas ALP activity as an osteogenic marker was evaluated under differentiation conditions after 14 days of cultivation.

### 7.3.2. Chemical modifications

The chemical modifications of HA crosslinked with BDDE were identified in FTIR

spectra of the HA-BDDE by the characteristic peak for BDDE appearing in  $1310\text{ cm}^{-1}$ , which was attributed to the stretch ether ( $\nu\text{C-O}$ ,  $1320\text{-}1100\text{ cm}^{-1}$ ) and in  $1460\text{ cm}^{-1}$  attributed to  $\text{CH}_2$  deformation (Silverstein *et al.*, 1974; Kim *et al.*, 2014). These results ensure the absence of free BDDE before structuring in microparticles or sponges.

### 7.3.3. Physicochemical and mechanical properties of HA forms

At physiological pH, the HA and its derivatives are hydrated extensively by water because the water forms hydrogen bonds with the N-acetyl and carboxyl groups. The dipole attraction of the hydrogen bond to the carboxyl group results in HA's affinity for retaining water. The swelling capacity is dependent upon concentration, crosslinking density, and the processes used for hydration.

The crosslinking reduced the water swelling in the HA-BDDE structures providing stability to HA (highly soluble), although they still exhibit high levels of water uptake, as shown in Table 4 by the SR values:  $43.2 \pm 0.7$  (sHA-BDDE) and  $28 \pm 2$  (mHA-BDDE). The larger hydration capacity of the sponges was attributed to its porous structure, which can retain unbound water (Collins & Birkinshaw, 2008; Shimojo *et al.*, 2014).

**Table 4.** Physicochemical and mechanical properties of HA in the forms: free (fHA), structured in sponge (sHA), crosslinked with BDDE and structured in sponges (sHA-BDDE) or microparticles (mHA-BDDE).

HA form*	SR	Young's moduli (kPa)	G' (Pa) at 1 Hz	Extrusion force (N)	Pore Size ( $\mu\text{m}$ )	Porosity (%)	Particle size ( $\mu\text{m}$ )
fHA	-	-	*	$4.3 \pm 0.1$	-	-	-
sHA	-	<10	-	-	-	$97.8 \pm 0.3$	-
sHA-BDDE	$43.2 \pm 0.7$	$14 \pm 5$	-	-	$218 \pm 24$	$97.4 \pm 0.1$	-
mHA-BDDE	$28 \pm 2$	-	3181	$78 \pm 7$	-	-	$160 \pm 18$

\*Forms prepared from 1% fHA.

\*\*Newtonian behavior.

The stability in PBS of the structures was studied by means of gravimetric analyses in terms of remaining weight up to 14 days incubation [Figure 36(a)]. Most of the weight reduction ( $\sim 40\%$ ) of HA-BDDE sponges was observed until the seventh day, whereas most of the weight reduction ( $\sim 40\%$ ) of HA-BDDE microparticles was observed

in the third day. The sHA did not retain their shape during incubation becoming a viscous gel.

We also evaluated the cytotoxicity of HA-BDDE structures by MTT method [Figure 36(b)]. The results showed that the HA-BDDE structures exhibit a good compatibility to the cells, not only because the proliferation was greater than the positive toxicity control (PTC), but it was also significantly higher than positive control NTC ( $p < 0.05$ ).

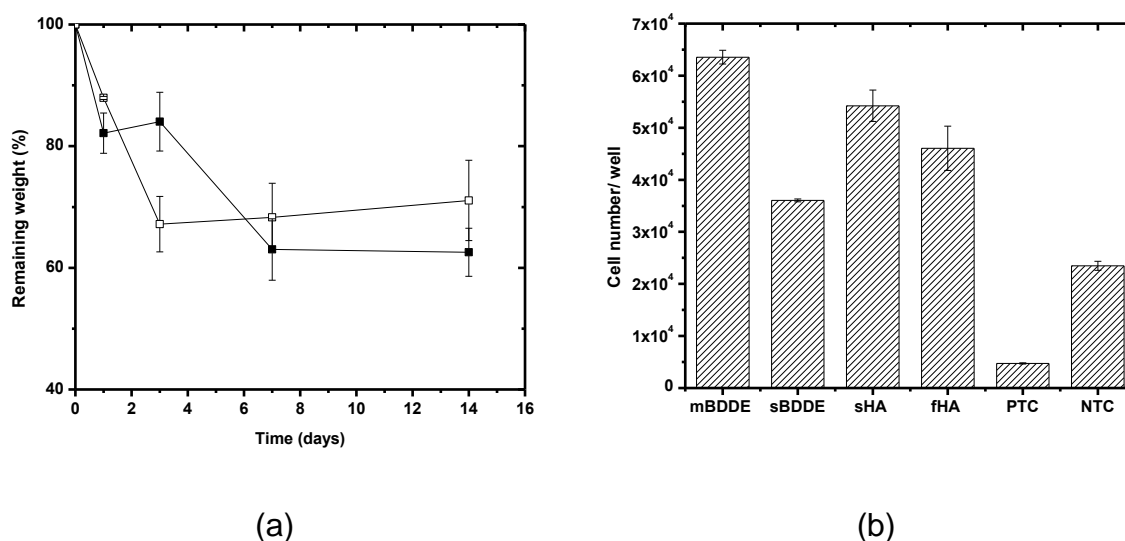


**Figure 36.** (a) The weight remaining of the HA-BDDE structures under the time course of degradation (At 37°C, in PBS). (■) sHA-BDDE and (□) mHA-BDDE. (b) Viability of h-AdMSC exposed to the HA-BDDE structures, sHA and fHA for 24 hours. Negative control (NTC) = DMEM with 10% FBS; positive control (PTC) = DMEM with phenol 0.5%. Mean  $\pm$  standard deviation  $n = 3$ . The population means are significantly different from positive control at  $p < 0.05$ .

Due to the nature of the assay, the higher cell number for mHA-BDDE could be justified due to their greater surface area available for cell adhesion compared to fHA. Moreover, the fewer number of cells for sHA-BDDE may indicate limitations in cell migration due to the porous structure created by the crosslinking.

### 7.3.3.1. mHA-BDDE

The mHA-BDDE [Figure 37(a)] exhibited typical gel-type mechanical spectra, with

$G'$  higher than  $G''$  in all studied ranges and both moduli lying parallel to the frequency axis (Ikeda & Nishimari, 2001).

The shear viscosity spectra of HA-BDDE showed a pseudoplastic behavior [Figure 37(b)], while fHA 1% is a Newtonian fluid. The pseudoplastic behavior is an important parameter in injectable applications, where the flow viscosity should be lower than the rest viscosity.

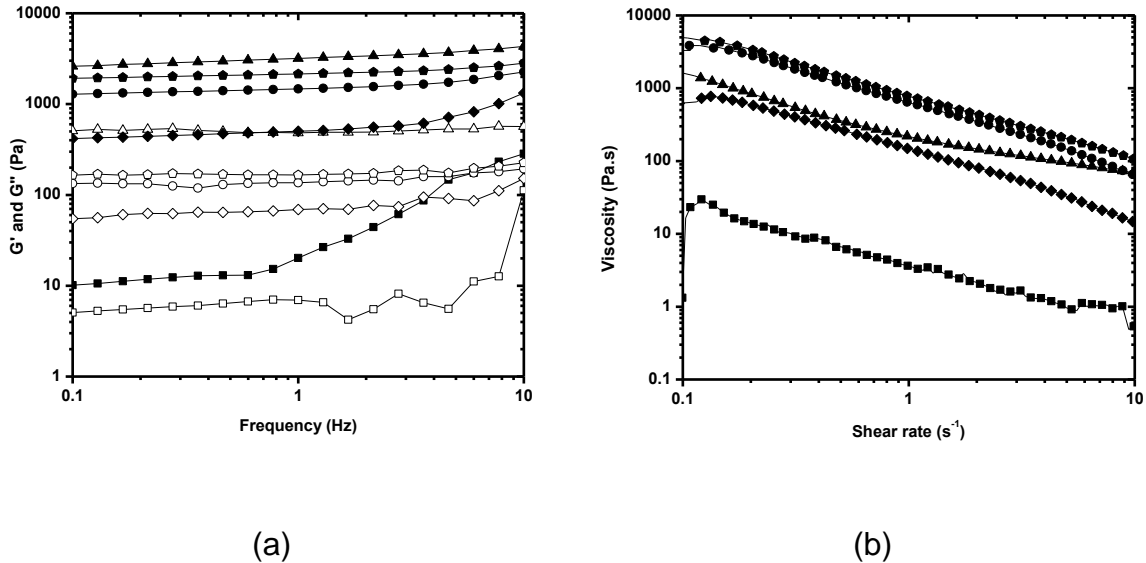


**Figure 37.** (a) Oscillation spectrum of mHA-BDDE and mHA-BDDE/aP-PRP. (■) aP-PRP; (▲) mHA-BDDE; (●) mHA-BDDE/aP-PRP 2:1; (●) mHA-BDDE/aP-PRP 1:1; (◆) mHA-BDDE/aP-PRP 1:2.  $G'$  (closed symbol) and  $G''$  (open symbol). (b) Shear viscosity spectra of (▲) fluid HA (1% wt.) and (■) mHA-BDDE.

The microparticles showed a mean diameter (Table 4) around 160  $\mu\text{m}$ , which is adequate for an injectable application ( $<700 \mu\text{m}$ ) (Shimojo *et al.*, 2013; Kablik *et al.*, 2009).

$G'$  values were around 3000 Pa in 1 Hz that are out of the adequate range (100-700 Pa) for injectable application. Therefore, they should be dispersed in a fluid phase or to have the crosslinking degree decreased to fit in the required range (Shimojo *et al.*, 2013; Kablik *et al.*, 2009).

In addition to viscoelasticity, the injectable scaffolds must have an extrusion force to allow their easy injection through an appropriately sized needle (27-30 g needle) and



thereby prevent side effects such as pain (Shimojo *et al.*, 2013; Kablik *et al.*, 2009). The crosslinking increased the extrusion force of HA-BDDE ( $78 \pm 7$  N) compared to fHA 1% ( $4.3 \pm 0.1$  N) as expected (Table 4), however, it was not adequate for injectable applications ( $<20$  N) (de Melo *et al.*, 2012; Öhrlund *et al.*, 2010).

Thus, the  $G'$  and extrusion force values obtained indicated the need to adjust the formulation for injectable application by adding a fluid phase and/or decreasing the degree of crosslinking (Shimojo *et al.*, 2013).

In this work, we utilized aP-PRP in different volumetric ratio as fluid phase. We observed that the addition of the activated P-PRP maintained the pseudoplastic gel-type behavior of composite and adequate the rheological properties with reduction of  $G'$ , as required. The volumetric ratio mHA-BDDE/aP-PRP 1:2 was more suitable for fit the requirements for injectable application. ( $G'$  in 1Hz = 503 Pa). This volumetric ratio was maintained in the biological assays.

#### 7.3.3.2. sHA-BDDE

The results of compression test (Table 4) showed that the crosslinking improved to mechanical resistance of the sHA-BDDE compared to non-crosslinked sHA. The Young's modulus value ( $\sim 14$  kPa) was higher for the sHA-BDDE than for the sHA with the same porosity ( $\sim 97\%$ ).

The porosity is also an important aspect of cell migration and proliferation, guiding and promoting the formation of new tissue. A porosity higher than 90% and pore interconnectivity are basic requirements for scaffolds in tissue engineering because they affect the diffusion of physiological nutrients and gases to and the removal of metabolic waste and by-products from cells that have penetrated the scaffold (Leong *et al.*, 2003; Liu & Ma, 2004). The porosity values of sHA-BDDE and sHA obtained in this study, both around 97%, are adequate for tissue, engineering, particularly for bone tissue.

The cross-section morphologies of sHA-BDDE and sHA obtained by SEM are shown in Figure 38. In both cases, highly porous structures were formed, confirming the determined values for porosity in Table 4. However, the structure of HA-BDDE sponges has more open round pores [Figure 38(a)], whereas the sHA has a leaf structure [Figure 38(b)].

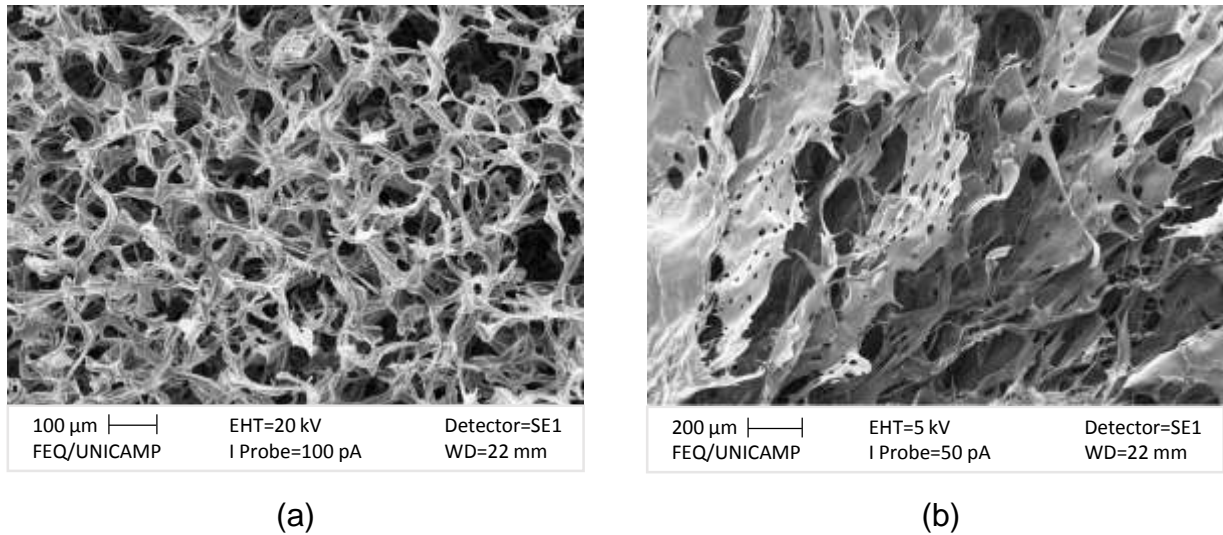


**Figure 38.** Scanning electron micrographs. Cross-section morphologies of (a) HA-BDDE scaffold and (b) sHA.

Although there is a large distribution of sizes, sHA-BDDE showed pores around 200 μm, which is adequate for regeneration of hard tissues (Salgado *et al.*, 2004). Moreover, because human adipose tissue-derived mesenchymal stem cells (h-AdMSCs) exhibit a spindle-like shape and are 80–100 μm in diameter and ~200 μm in length, the range of pore sizes in sHA-BDDE allows cells to migrate freely into the scaffolds, favoring the formation of a new tissue (Chavez-Munoz *et al.*, 2013).

These values were slightly larger than the ones reported by La Gatta *et al.* (2013) (70-130 μm) for the matrices crosslinked with comparable equivalents of BDDE. This difference may be due to the differences in processing conditions that used heterogeneous conditions for preparation.

### 7.3.4. Effects of the association with P-PRP

#### 7.3.4.1. SEM images

SEM images (Figure 39) shows the activated P-PRP associated to HA-BDDE form a composite scaffold with the fibrin network formed inside the microparticles or sponges.

Figure 39(b) also shows a cluster of cells on the fibrin fibers.

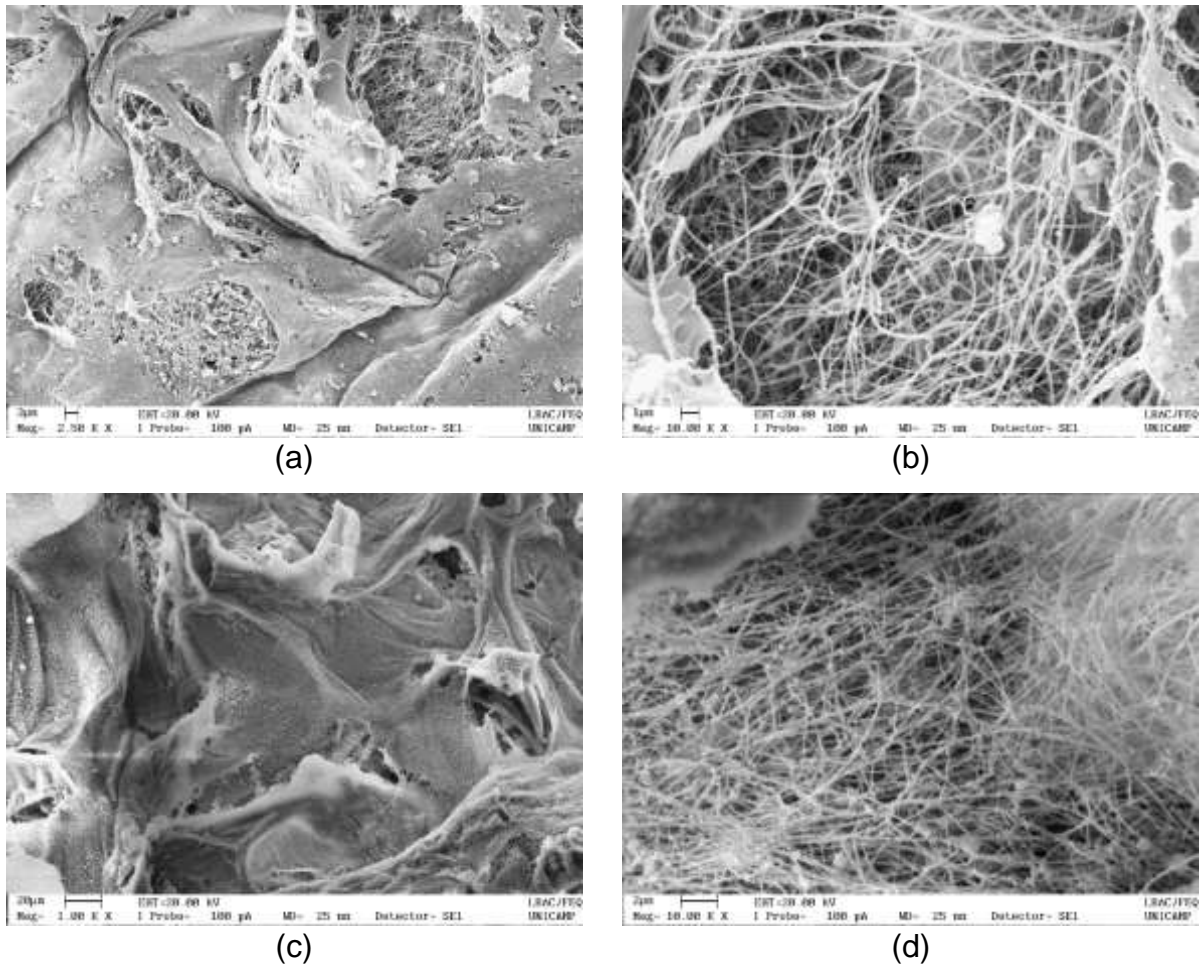


**Figure 39.** Scanning electron microscopic images of aP-PRP/HA-BDDE scaffolds after 5 days of cultivation of h-AdMSCs. Microparticles: (a) magnification of 2,500X and (b) magnification of 10,000X. Sponges: (c) magnification of 1,000X and (d) magnification of 10,000X.

#### 7.3.4.2. Release of growth factors

The release kinetics of PDGF-AB and TGF- $\beta$ 1 from the structured HA associated with activated P-PRP in DMEM are shown in Figure 40.

The curves show parallel diffusive profiles, indicating no collapse of the structure during the assays. The maximum TGF- $\beta$ 1 and PDGF-AB release was not observed up to 72 hours of assay.

For PDGF-AB, we observed a slower release from P-PRP/HA-BDDE than from P-PRP alone for the first 48 hours. For TGF- $\beta$ 1, we did not observe significant differences in the release profiles during the assay time.

The release of the most of GFs occurred in agreement with the degradation time of the scaffolds as could be observed in Figure 40 and Figure 36(a).

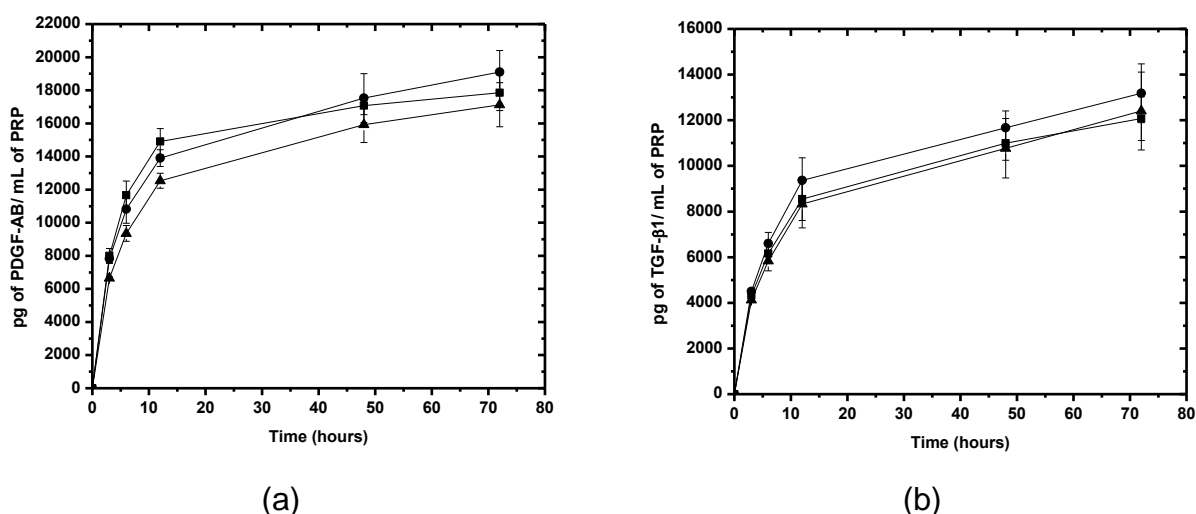


**Figure 40.** Growth factor release profile from PRP combined with HA-BDDE scaffolds. PDGF-AB (a) and TGF- $\beta$ 1 (b). (■) PRP activated with serum/Ca<sup>2+</sup> was used as control; (●) sHA-BDDE; (▲) mHA-BDDE. The GFs were measurements from activated P-PRP containing average platelet concentration 495,000 pq/mm<sup>3</sup>.

#### 7.3.4.3. Proliferation of h-AdMSCs and ALP activity

The kinetic profiles of proliferation were determined for h-AdMSCs cultured in the presence of composite scaffolds in 10 days, in comparison with fHA and the activated PRP alone [Figure 41(a)].

At a macroscopic observation, the scaffolds appeared homogeneously colored after the MTT treatment at each tested time thus supporting the presence of living and metabolically active cells. The cell number per well determined after 2 days exceeded the number of seeded cells ( $1.4 \times 10^4$  cells/ well) in the structures associated to PRP, meaning that the cells kept in the matrices retained their viability.

Although the cell proliferation was not intense in the composite scaffolds, it was higher than in fHA. The association of PRP with the structures reduced cell proliferation,

compared with the fibrin network (activated PRP alone), mainly for the crosslinked mHA-BDDE and sHA-BDDE.

In counterpart, the structured HA promoted the ALP activity [Figure 41(b)], an early osteoblastic marker, which reflected both the population of viable cells and the cell differentiation. The ALP activity was remarkable in mHA-BDDE. Although the necessity of determining other factors, the ALP activity points out to the structured HA associated to PRP is promising for osteogenic regeneration.

These results point to the opposite directions of the proliferation and ALP activity, which require more detailed studies regarding its mechanisms in the presence of growth factors and the composite scaffolds.

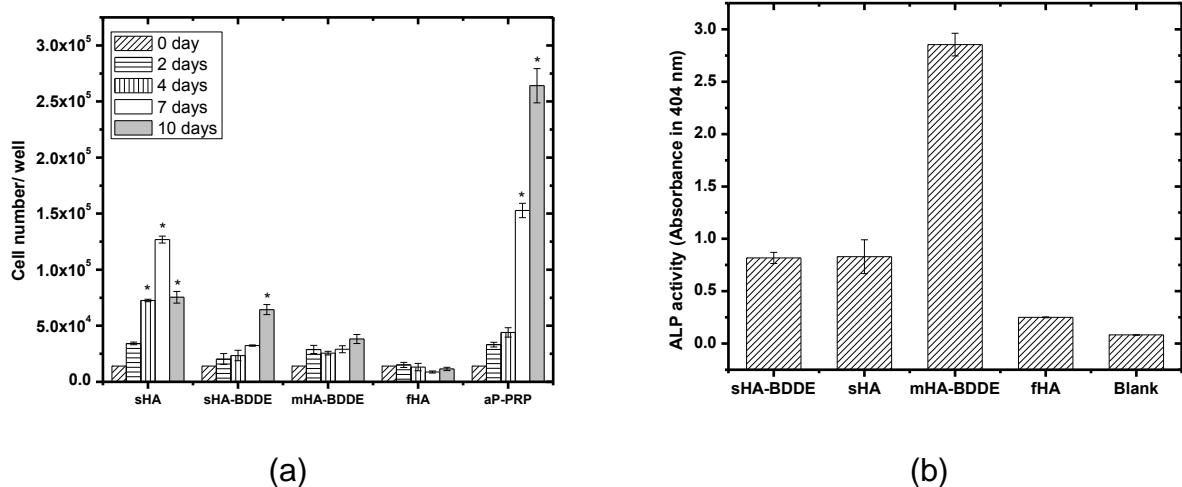


**Figure 41.** (a) Kinetic proliferation profiles of h-AdMSCs seeded in aP-PRP/HA-BDDE scaffolds structured in sponges and microparticles. aP-PRP was used as control. The concentration of platelets in P-PRP was 273,000 pq/mm<sup>3</sup>. (b) ALP activities of cells cultured on aP-PRP/HA-BDDE scaffolds structured in sponges and microparticles (statistically significant differences from blank, n=3, \*p<0.05). Blank = the colorimetric reagent used in the assay only. The concentration of platelets in whole blood donors (average of 2 donors) was 468,500 pq/mm<sup>3</sup>.

## 7.4. Conclusions

Novel composite scaffolds were prepared from hyaluronic acid crosslinked with

1,4-butanediol diglycidyl ether and structured in sponges and microparticles, in association with activated platelet-rich plasma. The crosslinked structures improved the physicochemical, mechanical and biological properties as compared to free hyaluronic acid. Thus, our results provide evidences that the composite scaffolds are promising biomaterials for future clinical use in tissue engineering, with perspectives for osteogenic regeneration. The flexibility to obtain injectable formulations (microparticles) or solid sponges expands their applications.

**Acknowledgments.** The authors acknowledge the financial support from the National Council of Technological and Scientific Development (CNPq, Brazil). They also thank Prof. Dr. Edvaldo Sabadini and Dr. Thiago Heiji Ito of the Chemical Institute (University of Campinas) for the use of the rheometer.

## 7.5. References

ALLEMANN, I.B.; BAUMANN, L. Hyaluronic acid gel (Juvederm™) preparations in the treatment of facial wrinkles and folds. **Clinical Interventions in Aging**, vol.3, n.4, p.629-634, 2008.

ANDRE, P. Hyaluronic acid and its use as a “rejuvenation” agent in cosmetic dermatology. **Seminars in Cutaneous Medicine and Surgery**, vol.23, p.218-222, 2004.

BEASLEY, K.L.; WEISS, M.A.; WEISS, R.A. Hyaluronic acid fillers: A comprehensive review. **Facial Plastic Surgery**, vol.25, p.86-94, 2009.

CHAVEZ-MUNOZ, C.; NGUYEN, K.T.; XU, W.; HONG, S.J.; MUSTOE, T.A.; GALIANO, R.D. Transdifferentiation of adipose-derived stem cells into keratinocyte-like cells: engineering a stratified epidermis. **PLOS One**, vol.8, n.12, p.1-13, 2013.

CHEN, W-H.; LO, W-C.; HSU, W-C.; WEI, H-J.; LIU, H-Y.; LEE, C-H.; CHEN, S-Y.T.; SHIEH, Y-H.; WILLIAMS, D.F.; DENG, W-P. Synergistic anabolic actions of hyaluronic acid and platelet-rich plasma on cartilage regeneration in osteoarthritis therapy. **Biomaterials**, vol.35, n.36, p.9599-9607, 2014.

COLLINS, M.N.; BIRKINSHAW, C. Investigation of the Swelling Behavior of Crosslinked Hyaluronic Acid Films and Hydrogels Produced Using Homogeneous Reactions. **Journal of Applied Polymer Science**, vol.109, p.923-931, 2008.

CORREIA, C.R.; TEIXEIRA, L.S.M.; MORONI, L.; REIS, R.L.; VAN BLITTERSWIJK, C.A.; KAPERIEN, M.; MANO, J.F. Chitosan Scaffolds Containing Hyaluronic Acid for

Cartilage Tissue Engineering. **Tissue Engineering – Part C**, vol.17, n.7, p. 717-730, 2011.

DE ANGELIS, B.; LUCARINI, L.; ORLANDI, F.; AGOVINO, A.; MIGNER, A.; CERVELLI, V.; IZZO, V.; CURCIO, C. Regenerative surgery of the complications with Morton's neuroma surgery: Use of platelet rich plasma and hyaluronic acid. **International Wound Journal**, vol.10, n.4, p.372-376, 2012.

DE BOULLE, K.; GLOGAU, R.; KONO, T.; NATHAN, M.; TEZEL, A.; ROCA-MARTINEZ, J-X.; PALIWAL, S.; STROUMPOULIS, D. A Review of the Metabolism of 1,4-Butanediol Diglycidyl Ether–Crosslinked Hyaluronic Acid Dermal Fillers. **Dermatologic Surgery**, vol.39, p.1758-1766, 2013.

DE MELO, F.; MARIJNISSEN-HOFSTE, J. Investigation of Physical Properties of a Polycaprolactone Dermal Filler when Mixed with Lidocaine and Lidocaine/Epinephrine. **Dermatology and Therapy**, vol.2, n.13, p.1-10, 2012.

EHRENFEST, D.M.D.; RASMUSSEN, L.; ALBREKTSSON, T. Classification of platelet concentrates: from pure platelet-rich plasma (P-PRP) to leucocyte- and platelet-rich fibrin (L-PRF). **Trends Biotechnology**, vol.27, p.158-167, 2009.

FALCONE, S.J.; BERG, R.A. Crosslinked hyaluronic acid dermal fillers: A comparison of rheological properties. **Journal of Biomedical Materials Research**, vol.87A, p.264-271, 2008.

FATHI, W.K. The Effect of Hyaluronic Acid and Platelet - Rich Plasma on Soft Tissue Wound Healing: An Experimental Study on Rabbits. **Al-Rafidain Dental Journal**, vol.12, n.1, p.115-125, 2012.

GARG, H.G.; HALES, C.A. **Chemistry and Biology of Hyaluronan**, Boston: Elsevier, 2004.

GÜMÜŞDERELIOĞLU, M.; ADAY, S. Heparin-functionalized chitosan scaffolds for bone tissue engineering. **Carbohydrate Research**, vol.346, p.606-613, 2011.

IKEDA, S.; NISHINARI, K. Weak Gel-Type Rheological Properties of Aqueous Dispersions of Nonaggregated K-Carrageenan Helices. **Journal of Agricultural and Food Chemistry**, vol.49, p.4436-4441, 2001.

KABLIK, J.; MONHEIT, G.D.; YU, L.; CHANG, G.; GERSHKOVICH, J. Comparative physical properties of hyaluronic acid dermal fillers. **Dermatologic Surgery**, vol.35, n.1, p.302-312, 2009.

KENNE, L.; GOHIL, S.; NILSSON, E.M.; KARLSSON, A.; ERICSSON, D.; KENNE, A.H.; NORD, L.I. Modification and cross-linking parameters in hyaluronic acid hydrogels—Definitions and analytical methods. **Carbohydrate Polymer**, vol.91, p.410-418, 2013.

KIM, Z.H.; LEE, Y.; KIM, S.M.; KIM, H.; YUN, C.K.; CHOI, Y.S. A Composite Dermal Filler Comprising Cross-Linked Hyaluronic Acid and Human Collagen for Tissue

Reconstruction. **Journal of Microbiology and Biotechnology**, 2014. [Epub ahead of print]

LA GATTA, A.; SCHIRALDI, C.; PAPA, A.; D'AGOSTINO, A.; CAMMAROTA, M.; DE ROSA, A.; DE ROSA, M. Hyaluronan scaffolds via diglycidyl ether crosslinking: Toward improvements in composition and performance. **Carbohydrate Polymer**, vol.96, p.536-544, 2013.

LANA, J.F.S.D.; SANTANA, M.H.A.; BELANGERO, W.D.; LUZO, A.C.M. **Platelet-Rich Plasma: Regenerative Medicine: Sports Medicine, Orthopedic, and Recovery of Musculoskeletal Injuries** (Lecture Notes in Bioengineering), 1st ed., Springer, 2014.

LEONG, F.; CHEAH, C.M.; CHUA, C.K. Solid freeform fabrication of three-dimensional scaffolds for engineering replacement tissues and organs. **Biomaterials**, vol.24, p.2363-2378, 2003.

LIU, X.; MA, P.X. Polymeric Scaffolds for Bone Tissue Engineering. **Annals of Biomedical Engineering**, vol.32, n.3, p.477-486, 2004.

MÄLSON, T.; LINDQVIST, B. Gels of crosslinked hyaluronic acid for use as a vitreous humor substitute. **United States Patent: U.S. 1987/4,716,154**, 1987.

MARX, R.E. Platelet-rich plasma: Evidence to support its use. **Journal of Oral and Maxillofacial Surgery**, vol.62, p.489-496, 2004.

MARX, R.E.; CARLSON, E.R.; EICHSTAEDT, R.M.; SCHIMMELE, S.R.; STRAUSS, J.E.; GEORGEFF, K.R. Platelet-rich plasma: Growth factor enhancement for bone grafts. **Oral Surgery, Oral Medicine, Oral Pathology, Oral Radiology**, vol.85, p.638-646 1998.

MOSSMAM, T.J. A rapid colorimetric assay of cellular growth and survival: application to proliferation and cytotoxicity assays. **Journal of Immunological Methods**, vol.65, p.55-63, 1983.

ÖHRLUND Å. Lifting capacity of hyaluronic acid (HA) dermalalauronic acid (HA) dermal fillers. **Poster presentation at 8 th Anti-aging Medicine World Congress (AMWC)**, Monte-Carlo, Monaco, 2010.

PAK, J. Compositions and methods for treating, preventing and alleviating bone or cartilage diseases. **United States Patent: U.S. 2012/0,171,169 A1**, 2012.

PEREZ, A.G.M.; LICHY, R.; LANA, J.F.S.D.; RODRIGUES, A.A.; LUZO, A.C.M.; BELANGERO, W.D.; SANTANA, M.H.A. Prediction and Modulation of Platelet Recovery by Discontinuous Centrifugation of Whole Blood for the Preparation of Pure Platelet-Rich Plasma. **BioResearch Open Access**, vol.2, p. 307-314, 2013.

PEREZ, A.G.M.; RODRIGUES, A.A.; LUZO, A.C.M.; LANA, J.F.S.D.; BELANGERO, W.D.; SANTANA M. H. A. Fibrin network architectures in pure platelet-rich plasma as characterized by fiber radius and correlated with clotting time. **Journal of Materials Science: Materials in Medicine**, vol.25(8), p.1967-1977, 2014.



SALGADO, J.; COUTINHO, O.P.; REIS, R.L. Bone Tissue Engineering: State of the Art and Future Trends. **Macromolecular Bioscience**, vol.4, p.743-765, 2004.

SCHANTÉ, C.E.; ZUBER, G.; HERLIN, C.; VANDAMME, T.F. Chemical modifications of hyaluronic acid for the synthesis of derivatives for a broad range of biomedical applications. **Carbohydrate Polymer**, vol.85, n.3, p.469-489, 2011.

SHIMOJO, A.A.M.; PEREZ, A.G.M.; GALDAMES, S.E.M.; BRISSAC, I.C.S.; SANTANA, M.H.A. Performance of PRP Associated with Porous Chitosan as a Composite Scaffold for Regenerative Medicine. **The Scientific World Journal**, vol.2015, p.1-12, 2015.

SHIMOJO, A.A.M.; PIRES, A.M.B.; LICHY, R.; RODRIGUES, A.A.; SANTANA, M.H.A. The crosslinking degree controls the mechanical, rheological, and swelling properties of hyaluronic acid microparticles. **Journal of Biomedical Materials Research**, vol.103A, n.2, p.730-737, 2014.

SHIMOJO, A.A.M.; PIRES, A.M.B.; TORRE, L.G.; SANTANA, M.H.A. Influence of Particle Size and Fluid Fraction on Rheological and Extrusion Properties of Crosslinked Hyaluronic Acid Hydrogel Dispersions. **Journal of Applied Polymer Science**, vol.128, p.2180-2185, 2013.

SHU, X.Z.; LIU, Y.; PALUMBO, F.S.; LUO, Y.; PRESTWICH, G.D. In situ crosslinkable hyaluronan hydrogels for tissue engineering. **Biomaterials**, vol.25, p.1339-1348, 2004.

SILVERSTEIN, R.M.; BASSLER, G.C.; MORRILL, T.C. **Spectrometric identification of organic compounds**. 3<sup>rd</sup> Ed., New York: John Wiley, 1974.

TANG, S.; VICKERS, S.M.; HSU, H-P.; SPECTOR, M. Fabrication and characterization of porous hyaluronic acid–collagen composite scaffolds. **Journal of Biomedical Materials Research**, vol.82A, p.323-335, 2007.

WANG, W. Methods for making injectable polymer hydrogels. **United States Patent: U.S. 2005/0,281,880 A1**, 2005.

WANG, Y.; LIN, M.; WANG, D.; HSIEH, H. Fabrication of a novel porous PGA–chitosan hybrid matrix for tissue engineering. **Biomaterials**, vol.24, p.1047-1057, 2003.

YEOM, J.; BHANG, S.H.; KIM, B-S.; SEO, M.S.; HWANG, E.J.; CHO, H.; PARK, J.K.; HAHN, S.K. Effect of Cross-Linking Reagents for Hyaluronic Acid Hydrogel Dermal Fillers on Tissue Augmentation and Regeneration. *Bioconjugate Chemistry*, vol. 21, p.240–247, 2010.

ZAWKO, S.A.; SURİ, S.; TRUONG, Q.; SCHMIDT, C.E. Photopatterned anisotropic swelling of dual-crosslinked hyaluronic acid hydrogels. **Acta Biomaterialia**, vol.5, p.14-22, 2009.



# CAPÍTULO 8 – STERILIZATION OF AUTO-CROSSLINKED HYALURONIC ACID STRUCTURED IN MICROPARTICLES OR SPONGES

---

Artigo submetido ao periódico *Biotechnology Letters*.

Andréa Arruda Martins Shimojo<sup>a</sup>, Isabela Cambraia de Souza Brissac<sup>a</sup>, Lucas Martins Pina<sup>a</sup>, Carlos Salles Lambert<sup>b</sup>, Maria Helena Andrade Santana<sup>a,\*</sup>

<sup>a</sup>Department of Engineering of Materials and Bioprocesses, School of Chemical Engineering, University of Campinas, Campinas-SP, Brazil.

<sup>b</sup>Department of Applied Physics, Institute of Physics "Gleb Wataghin", University of Campinas, Campinas-SP, Brazil.

Correspondence to: M. H. A. Santana (e-mail: [mariahelena.santana@gmail.com](mailto:mariahelena.santana@gmail.com))

**Abstract.** This work aimed to evaluate the effects of UV irradiation, plasma radiation, steam and 70% ethanol treatments on the sterilization and integrity of auto-crosslinked hyaluronic acid (HA-ACP) structured in microparticles or sponges. The integrity of the microparticles was characterized by rheological behavior, while for the sponges it was characterized by scanning electron microscopy, Fourier transform infrared spectroscopy and differential scanning calorimetry. The effectiveness of the sterilization treatment was verified by count of microorganism colonies in the samples after the treatments. In conclusion, plasma radiation was the best treatment for the sponges, while steam sterilization in autoclave at 126°C (1.5 kgf/cm<sup>2</sup>) for 5 minutes was the best one for the microparticles.

**Key Words:** auto-crosslinked hyaluronic acid, sterilization, plasma radiation, steam, UV

irradiation, ethanol treatment.

## 8.1. Introduction

Hyaluronic acid (HA) and its crosslinked derivatives have been widely used as scaffolds for tissue engineering (Collins and Birkinshaw, 2013; Unterman *et al.* 2012). Sterilization is of fundamental importance for storage as well as for *in vitro* and *in vivo* applications.

Several sterilization methods have been used for the sterilization of natural polymers structured as scaffolds for cell culture. These methods use dry heat, high-pressure vapor, ethylene oxide gas, supercritical carbon dioxide or radiation treatments (Danillof *et al.* 2009). An efficient treatment must provide sterility to the scaffold preserving its structure (Faraj *et al.* 2011).

HA and its crosslinked derivatives are heat-sensitive and sensible to  $\gamma$ -rays, presenting chemical degradation and depolymerisation with a decrease of molecular weight average (Rehakova *et al.* 1994). Besides degrading effects, the porous structure of scaffolds can be destroyed because of plastic deformation from the heat treatment (Plikk *et al.* 2006).

Moreover, since scaffolds usually have a porous structure, a sterilization method must penetrate materials without leaving residues (Siritientong *et al.*, 2011; Plikk *et al.* 2002).

In this study, we evaluated the effects of different treatments (70% ethanol; UV irradiation; plasma radiation and steam) on sterilization and the integrity of auto-crosslinked hyaluronic acid (HA-ACP) structured in microparticles or sponges. The integrity of the microparticles was characterized by rheological behavior, while for the sponges it was characterized by scanning electron microscopy, Fourier transform infrared spectroscopy and differential scanning calorimetry. The effectiveness of the sterilization method was verified by colonies counts of microorganisms after the treatments.

## 8.2. Materials and Methods

### 8.2.1. Materials

HA in sodium form ( $\overline{MW} = 2 \times 10^6$  Da) was obtained from Spec-Chem. Ind. (Nanjing, China). All other reagents were purchased from Synth® (Diadema, SP, Brazil) unless specified otherwise.

### 8.2.2. Methods

#### 8.2.2.1. Preparation of the HA-ACP scaffolds

*HA-ACP preparation.* The auto-crosslinked HA was prepared by an autoesterification reaction according to protocol described by Bellini *et al.* 2001. HA-TBA (tetrabutylammonium hyaluronate) with a molecular weight of approximately  $2 \times 10^6$  Da and corresponding to 10 mEq of monomeric units was solubilized in 50 mL of dimethylsulfoxide (DMSO) at 25°C. Triethylamine (0.5 mEq) was added and the resulting solution was agitated for 30 minutes. A solution of 2-chloro-1-methyl pyridinium iodide (CMPI) (0.5 mEq) (Sigma-Aldrich, St. Louis, MO, USA) in 15 mL of DMSO was slowly added drop by drop over 1 hour and the mixture was kept at 30°C for 15 hours. A solution of sodium chloride 2.5% (w/v) was then added and the resulting mixture was poured slowly into 150 mL of acetone, maintaining continual agitation. The formed precipitate was centrifuged at 10,000 rpm for 10 minutes, washed three times in 100 mL of 5:1 acetone: water and three times with 100 mL of acetone and vacuum-dried for 24 hours at 30°C.

*Preparation of structured HA-ACP scaffolds.* The HA-ACP scaffolds structured in microparticles (*mHA-ACP*) or sponges (*sHA-ACP*) were prepared from plain HA-ACP swollen in Milli-Q water. The microparticles were obtained by shearing in an Ultra-Turrax T25 homogenizer (IKA Labortechnik, Staufen, Germany) at 18,000 rpm by 20 minutes, according to Shimojo *et al.* 2013. For preparation of the sponges, the microparticles were initially placed in polystyrene 48-well microplates (TPP®, Trasadingen, Switzerland), frozen at -20°C and lyophilized at controlled temperature of approximately -30°C for 48 hours.

#### 8.2.2.2. Sterilization Treatments

HA-ACP microparticles were submitted to UV-irradiation, plasma radiation, steam, 70% ethanol treatments, aiming sterilization or disinfection. HA-ACP sponges were submitted to the same treatments except to steam. Non-treated scaffolds were used as control.

*Ethanol Treatment.* The HA-ACP scaffolds were disinfected with 70% (v/v) ethanol, according to Faraj *et al.* 2011. They were washed with 70% ethanol at ambient temperature for 3×1 h and 1×16 h. Thereafter, three short washings with sterile phosphate buffered saline (PBS) (pH 7.4) were performed with changes of washing fluid directly after one another, and finally 5×1 h and 1×16 h washings with PBS were performed. All washing changes were performed in a laminar flow cabinet. sHA-ACP was re-frozen at -20°C and lyophilized again.

*Plasma Irradiation.* The scaffolds were evacuated and then, a pressure of 1 Torr was established with the introduction of argon (Ar) gas that combined with an electrical potential difference (EPD) create Ar plasma inside the chamber. This treatment was performed along 5 minutes.

*UV Irradiation.* Irradiation was carried out with an ultraviolet lamp (Germetec, Rio de Janeiro, RJ, Brazil) at 254-nm wavelength at a distance of 5 cm (UV1) and at a distance of 60 cm (UV2). HA-ACP microparticles and HA-ACP sponges were irradiated for a total time of 30 min and were turned over halfway through the treatment to irradiate the top and bottom surfaces.

*Steam.* Steam treatment was applied to the microparticles only. The treatment was achieved by wet heating at 126°C, under a vapor pressure of 1.5 kgf/cm<sup>2</sup> for 1, 2.5, 5, 10 and 15 minutes in autoclave.

#### 8.2.2.3. HA-ACP sponges characterization

*Fourier-transform Infrared (FTIR).* FTIR was used to identify possible chemical modifications on scaffolds resulting from sterilization processes. Infrared spectra were obtained using a Thermo Scientific Nicolet model 6700 (Thermo Scientific Nicolet™, Waltham, MA, USA). Measurements were made in the ATR mode with accessory SMART OMNI-SAMPLER, in the spectral range of 4000 – 675  $\text{cm}^{-1}$  with a resolution of 4  $\text{cm}^{-1}$  over 64 scans.

*Scanning electronic microscopy (SEM).* The morphology of HA-ACP sponges sterilized was evaluated by scanning electron microscopy (SEM) using an LEO 440i Electron Microscopy/Oxford (Cambridge, England) operated at 5 kV accelerating voltage. The scaffolds were gold-coated using a sputter coater POLARON SC7620, VG Microtech (Uckfield, England) for 180 s at a current of 3 mA.

*Differential scanning calorimetry (DSC).* The thermal characterization of the scaffolds was achieved by DSC using a Mettler-Toledo DSC1 (Mettler Toledo Co., Zürich, Switzerland) module under a nitrogen atmosphere (nitrogen flow rate 50 mL/min) with a sample mass around 10 mg and a heating rate of 10°C/min.

#### 8.2.2.4. HA-ACP microparticles characterization

*Rheological properties.* HA-ACP microparticles sterilized were evaluated by rheological properties. The measurements were performed on a Rheometer Haake model RheoStress 1 (Haake, Karlsruhe, Germany). The properties of the scaffolds were characterized in the steady and oscillatory regimes at 25°C, using a parallel plate geometry of 20 mm. Oscillatory measurements were conducted in the linear region, at a stress of 1.188 Pa and in the frequency range of 0.01 to 10 Hz. Steady shear measurements were obtained at shear rates of 0.1-50  $\text{s}^{-1}$ .

#### 8.2.2.5. Sterility Tests

All the scaffolds were tested for sterility for heterotrophic bacterial, molds and yeasts, immediately following the treatments using a standard assay (Method 61, USP –

2012).

### 8.3. Results and Discussion

#### 8.3.1. Effects of the treatments on physicochemical properties of the HA-ACP sponges

The effects of the treatments on HA-ACP sponges were evaluated by scanning electron microscopy (SEM), Fourier transform infrared spectroscopy (FTIR) and differential scanning calorimetry (DSC).

The micrographs of sponges obtained by SEM (Figure 42) showed that except to ethanol disinfection [Figure 42(e)], the scaffolds remained their porous structure without major differences in morphology, regardless the treatments. Ethanol disinfection reduced substantially the porosity of HA-ACP sponge. Moreover, we observed loss in the scaffold shape by swelling after washing with PBS.

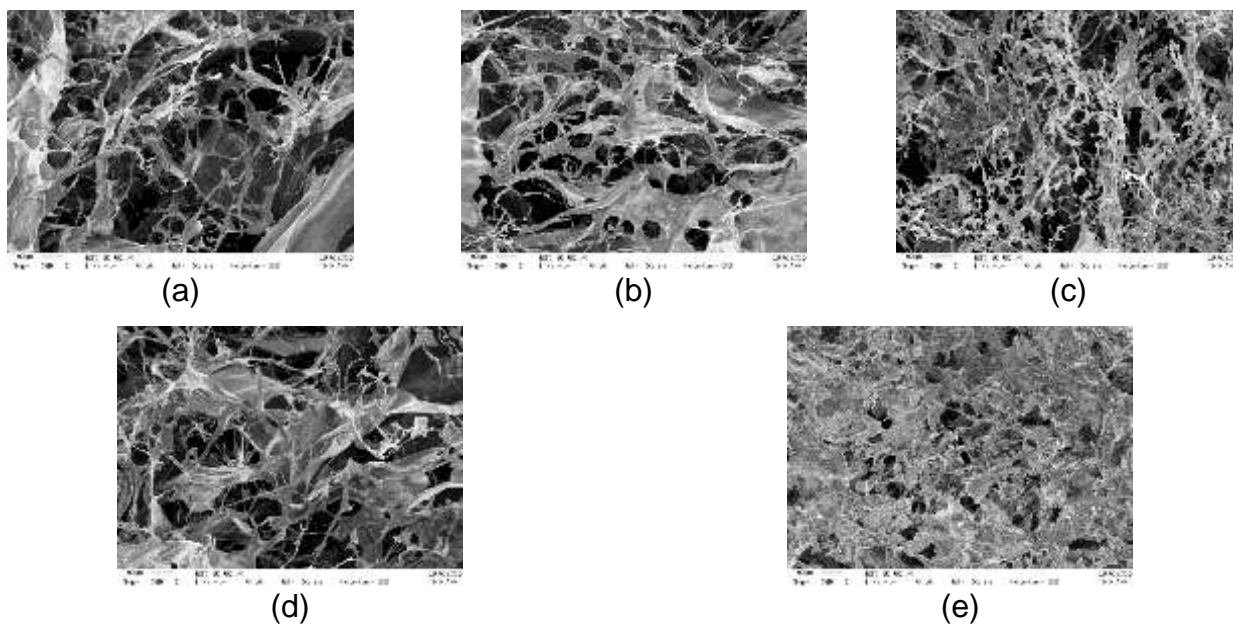


**Figure 42.** SEM cross-section images of HA-ACP sponges. (a) Unsterile; (b) UV (5 cm); (c) UV (60 cm); (d) Plasma and (e) Ethanol disinfection. Bar = 100 μm.

Figure 43(a) shows the FT-IR spectra of HA-ACP sponges. The spectra showed bands at 1617 and 1413  $\text{cm}^{-1}$  attributed to the asymmetric (C=O) and symmetric (C-O)



stretching modes of the planar carboxyl groups in the hyaluronate. The absorption bands at about 1650, 1561, and 1320  $\text{cm}^{-1}$  are characteristic of the amide I, II, and III band, respectively. The weak absorption band around 1740  $\text{cm}^{-1}$  was attributed to the stretching vibration of ester groups. The three signals centered at 1150, 1072, and 1040  $\text{cm}^{-1}$  were assigned to C-O-C (O-bridge), C-O (exocyclic), and C-OH group, respectively. The band at 945  $\text{cm}^{-1}$  was assigned to asymmetrical out-of-phase ring vibration.

The spectra of HA-ACP disinfected with 70% ethanol showed a band at 990  $\text{cm}^{-1}$  attributed to C-O of primary alcohols indicating ethanol residual in the structure.

Therefore, except for the HA-ACP disinfected with 70% ethanol, the spectra were very similar indicating that their chemical structure did not change significantly with the treatments.

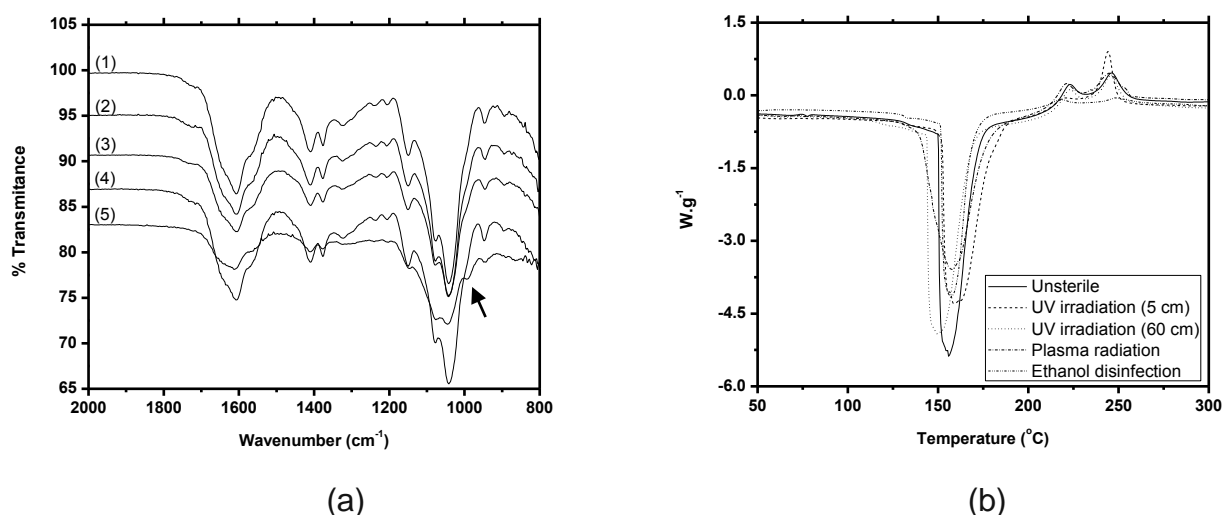


**Figure 43.** (a) FT-IR spectra and (b) DSC of HA-ACP sponges after the different treatments. (1) Unsterile; (2) UV irradiation (5 cm); (3) UV irradiation (60 cm); (4) plasma radiation and (5) ethanol disinfection.

The effects of treatments on the thermal behavior of the sponges are shown in Figure 43(b). All the scaffolds showed the presence of a broad endothermic peak between 150 and 160  $^{\circ}\text{C}$  associated with the loss of moisture remaining after the drying procedure. In addition, significant sharp exothermic peaks around 220 and 245  $^{\circ}\text{C}$  were observed, which probably represent decomposition (Collins & Birkinshaw, 2008). We

consider, none significant changes in the thermal profiles after the treatments.

### 8.3.2. Effects of the treatments on physicochemical properties of HA-ACP microparticles

Initially, we evaluated the influence of the steam treatment in autoclave, at 126°C, under a vapor pressure of 1.5 kgf/cm<sup>2</sup>, on the rheological properties of HA-ACP microparticles. The rheological behavior determined by oscillatory and steady measurements are shown in Figure 44(a) and 44(b), respectively.

We observe that until 5 minutes of steam treatment, the microparticles maintained the gel-like behavior, as analyzed by the storage ( $G'$ ) and loss moduli ( $G''$ ). (Ikeda & Nishimari, 2001). Moreover, considering the Ostwald de Waele power law ( $\eta=K.\dot{\gamma}^{n-1}$ ), the flow indices ( $n$ ) indicate a viscoelastic behavior that is an important parameter in injectable applications where the flow viscosity should be lower than the rest viscosity. According to the curves, we should consider no significant differences on rheological behavior of the microparticles up to 5 minutes of autoclave.

After the first 5 minutes of treatment, the mechanical spectra showed a crossover and due to very low viscosity, it was not possible to determine the flow curve using the parallel plate geometry previously used. Thus, these results indicate rheological behavior of solution and degradation of the structure.

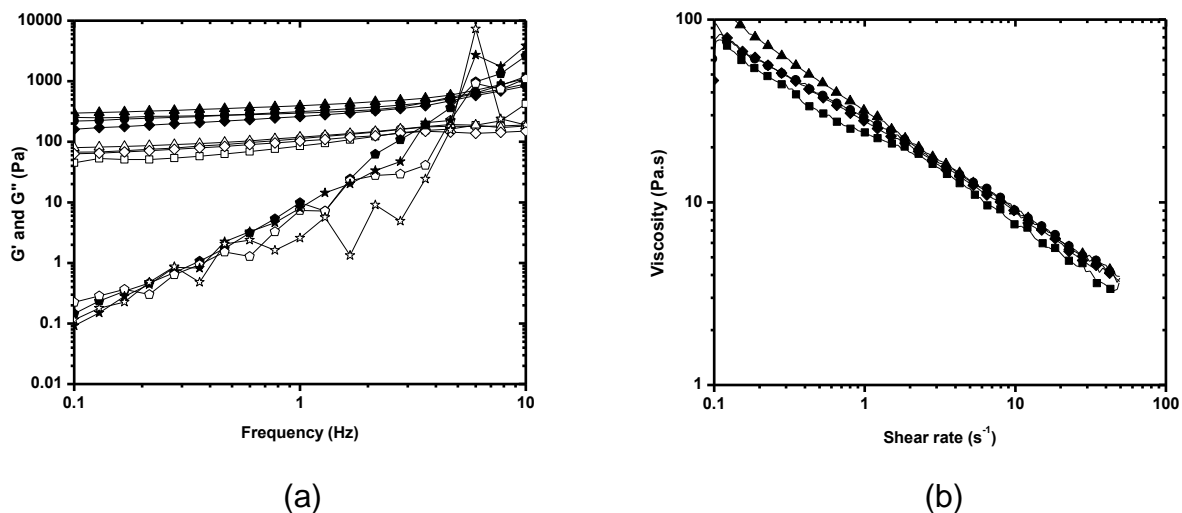


**Figure 44.** Rheological characterization of HA-ACP microparticles after treatment in autoclave at 126°C, under a vapor pressure of 1.5 kgf/cm<sup>2</sup> for: (■) 0 minute; (●) 1

minute; ( $\blacktriangle$ ) 2.5 minutes; ( $\blacklozenge$ ) 5 minutes; ( $\blacklozenge$ ) 10 minutes and ( $\blackstar$ ) 15 minutes. (a) Oscillation spectrum and (b) flow curves.  $G'$  (closed symbol) and  $G''$  (open symbol) moduli.

Figures 45a and 45b show the rheological behavior of the microparticles under UV1, UV2, plasma and 70% ethanol treatments. The  $G'$  and  $G''$  profiles show that only the UV1 treatment, in which the ultraviolet lamp was at a distance of 5 cm from the sample, affected the rheological behavior of the microparticles [Figure 45(a)]. Moreover, there was a drastic decreased of shear viscosity [Figure 45(b)]. This behavior was attributed to degradation of HA by the high UV intensity due to the very small distance between the lamp and the sample.

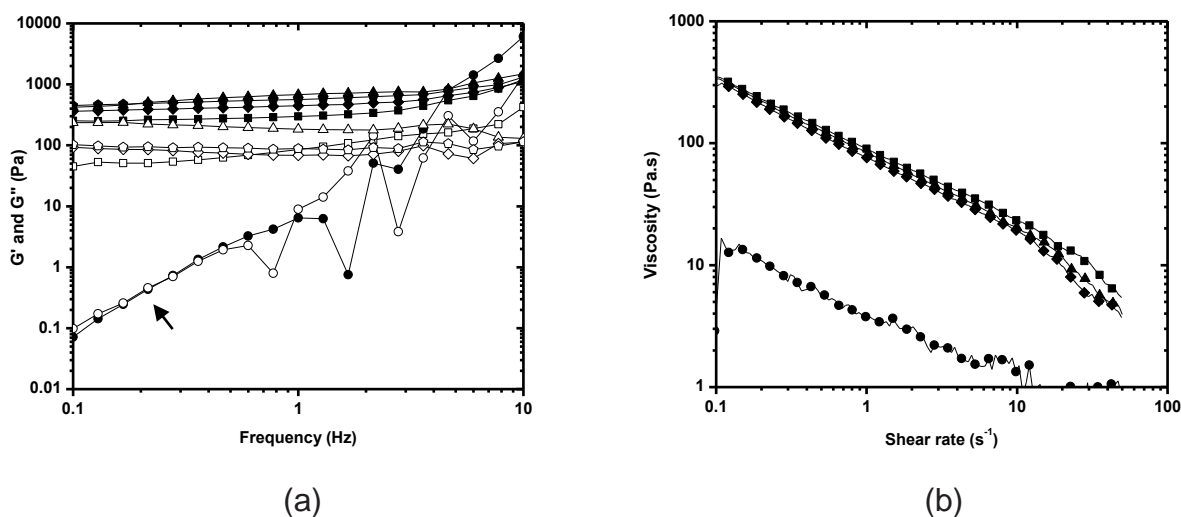


**Figure 45.** Rheological characterization of HA-ACP microparticles after the treatments: ( $\blacksquare$ ) untreated; ( $\bullet$ ) UV1; ( $\blacktriangle$ ) UV2; ( $\blacklozenge$ ) plasma and ( $\blacklozenge$ ) ethanol disinfection. (a) Oscillation spectrum and (b) flow curves.  $G'$  (closed symbol) and  $G''$  (open symbol) moduli.

### 8.3.3. Sterility evaluation

Tables 5 and 6 show the results of the sterility test for the sponges and the microparticles, respectively. The counts of colonies indicated that 70% ethanol disinfection and UV2 treatment were the least effective, while plasma radiation and UV1 were the most effective treatments for the sponges (Table 5).

**Table 5.** Results of heterotrophic plate count (bacteria) and fungal count (molds and yeasts) obtained after treatment of HA-ACP sponges.

Treatment	Heterotrophic Plate Count		Fungal Count	
	Bacteria (CFU/mL)	Molds (CFU/mL)	Yeasts (CFU/mL)	
UV (1)	-	-	-	
UV (2)	++	-	++	
PLASMA	-	-	-	
70% ETHANOL	+	-	+	
UNSTERILISED	++	+	++	

\*CFU=colony-forming units

- no growth (detection limit=10 CFU/mL), + amount of microorganism below  $1 \times 10^4$  CFU/mL, ++ amount of microorganism between  $1 \times 10^4$  and  $1 \times 10^6$  CFU/mL, +++ amount of microorganism between  $1 \times 10^6$  and  $1 \times 10^8$  CFU/mL.

The results in Table 6 indicate that only steam sterilization in autoclave was effective for sterilization of the microspheres.

**Table 6.** Results of heterotrophic plate count (bacteria) and fungal count (molds and yeasts) obtained after sterilization of HA-ACP microparticles.

Time (minute)		Heterotrophic Plate Count		Fungal count	
		Bacteria (CFU/mL)	Molds (CFU/mL)	Yeasts (CFU/mL)	
S T E A M	1	-	-	-	
	2.5	-	-	-	
	5	-	-	-	
	10	-	-	-	
	15	-	-	-	
UV (1)		++	+	++	
UV (2)		++	++	+	
PLASMA		++	++	+	
70% ETHANOL		+	-	-	
UNSTERILISED		++	+	++	

\*CFU=colony-forming units.

- no growth (detection limit=10 CFU/mL), + amount of microorganism below  $1 \times 10^4$  CFU/mL, ++ amount of microorganism between  $1 \times 10^4$  and  $1 \times 10^6$  CFU/mL, +++ amount of microorganism between  $1 \times 10^6$  and  $1 \times 10^8$  CFU/mL.

Comparing the effects of the treatments on the sterilization and physicochemical properties of the sponges and microparticles, our results showed that sterilization by plasma radiation was the most efficient treatment for sterilizing the auto-crosslinked hyaluronic acid sponges because it ensures the sterility and preserve their chemical composition and 3-D morphology. In contrast, the steam treatment in autoclave (at  $126^\circ\text{C}$ ,  $1.5 \text{ kgf/cm}^2$ ) up to 5 minutes was the method most adequate for sterilization of

the auto-crosslinked hyaluronic acid microspheres, because it did not change their rheological properties.

## 8.4. Conclusion

The sterilization by plasma radiation was the most efficient treatment for sterilizing the auto-crosslinked hyaluronic acid sponges, while the steam treatment in autoclave (at 126°C, 1.5 kgf/cm<sup>2</sup>) during 5 minutes was the most efficient treatment for the microspheres. Thus, these methods can be used for sterilization of ACP structured scaffolds.

**Acknowledgments.** The authors acknowledge the financial support from the National Council of Technological and Scientific Development (CNPq, Brazil). They also thank Prof. Dr. Edvaldo Sabadini of the Chemical Institute (University of Campinas) for the use of the rheometer.

## 8.5. References

BELLINI, D.; PAPARELLA, A.; O'REGAN, M.; CALLEGARO, L. Autocross-linked Hyaluronic Acid and Related Pharmaceutical Compositions for the Treatment of Arthrophaties. **United States Patent: U.S. 2001/6,251,876 B1**, 2001.

COLLINS, M.N.; BIRKINSHAW, C. Comparison of the Effectiveness of Four Different Crosslinking Agents with Hyaluronic Acid Hydrogel Films for Tissue-Culture Applications. **Journal of Applied Polymer Science**, vol.104, p.3183-3191, 2007.

COLLINS, M.N.; BIRKINSHAW, C. Hyaluronic acid based scaffolds for tissue engineering – A review. **Carbohydrate Polymer**, vol.92, p.1262–1279, 2013.

DANILOFF, G.Y.; SPIRO, R.C.; GRAVETT, D.M.; HILLAS, P.J.; HE, P. Sterile hyaluronic acid polymer compositions and related methods. **United States Patent Application: U.S. 2009/0,017,091**, 2009.

FARAJ, K.A.; BROUWER, K.M.; GEUTJES, P.J.; VERSTEEG, E.M.; WISMANS, R.G.; DEPREST, J.A.; CHAJRA, H.; TIEMESSEN, C.M.; FEITZ, W.F.J.; OOSTERWIJK, E.; DAAMEN, W.F.; VAN KUPPEVELT, T.H. The Effect of Ethylene Oxide Sterilisation, Beta Irradiation and Gamma Irradiation on Collagen Fibril-Based Scaffolds. **Tissue Engineering & Regenerative Medicine**, vol.8, n.5, p.460-470, 2011.

IKEDA, S.; NISHINARI, K. Weak Gel-Type Rheological Properties of Aqueous Dispersions of Nonaggregated K-Carrageenan Helices. **Journal of Agricultural and Food Chemistry**, vol.49, p.4436-4441, 2001.

PLIKK, P.; ODELIUS, K.; HAKKARAINEN, M.; ALBERTSSON, A.C. Finalizing the properties of porous scaffolds of aliphatic polyesters through radiation sterilization. **Biomaterials**, vol.27, p.5335–5347, 2006.

REHAKOVA. M.; BAKOS, D.; SOLDAN, M.; VIZAROVA, K. Depolymerization reactions of hyaluronic acid in solution. **International Journal of Biological Macromolecules**, vol.16, n.3, p.121-124,1994.

SHIMOJO, A.A.M.; PIRES, A.M.B.; TORRE, L.G.; SANTANA, M.H.A. Influence of Particle Size and Fluid Fraction on Rheological and Extrusion Properties of Crosslinked Hyaluronic Acid Hydrogel Dispersions. **Journal of Applied Polymer Science**, vol.128, n.3, p.2180-2185, 2013.

SIRITIENTONG, T.; SRICHANA, T.; ARAMWIT, P. The Effect of Sterilization Methods on the Physical Properties of Silk Sericin Scaffolds. **AAPS Pharm Sci Tech**, vol.12, n.2, p.771-781, 2011.

United States Pharmacopeial Convention, Inc. USP/NF: The official compendia of standards, 35th edition. Rockville: USP, 2012.

UNTERMAN, S.A.; GIBSON, M.; LEE, JH.; CRIST, J.; CHANSAKUL, T.; YANG, E.C.; ELISSEFF, J.H. Hyaluronic Acid-Binding Scaffold for Articular Cartilage Repair. **Tissue Engineering – Part A**, vol.18, n.23-24, p.2497-2506, 2012.

# CAPÍTULO 9 – CONCLUSÕES

---

## 9.1. Conclusões

Neste trabalho foram preparados e caracterizados os seguintes *scaffolds* compósitos de quitosana (CHT) e/ ou ácido hialurônico (AH) estruturados em esponjas (aP-PRP/PCHTs, aP-PRP/SPCHTs, aP-PRP/ACPs, aP-PRP/HA-BDDE e aP-PRP/PECs) e micropartículas (aP-PRP/iCHT-TPPs, aP-PRP/ACPs, aP-PRP/HA-BDDE e aP-PRP/PECs).

A efetividade *in vitro* dos *scaffolds* compósitos, foi avaliada através da cinética de liberação de fatores de crescimento (PDGF-AB e TGF- $\beta$ 1) do P-PRP em meio DMEM, proliferação e diferenciação de h-AdMSCs através do marcador osteogênico fosfatase alcalina (ALP).

O desempenho individual dos *scaffolds* foi apresentado nos artigos e na patente que compõem este trabalho.

Os resultados obtidos permitem as seguintes conclusões gerais:

- Os polímeros naturais CHT e AH podem ser estruturados em esponjas ou micropartículas que atuam como *scaffolds* para o PRP em formulações sólidas (esponjas) ou fluidas injetáveis (micropartículas), com diferentes propriedades físico-químicas e mecânicas.
- As esponjas apresentaram elevada porosidade (>90%), alto grau de intumescimento adequados para a migração e proliferação celular e resistência mecânica adequada ao manuseio e cultivo celular.
- As micropartículas apresentaram propriedades reológicas e mecânicas adequadas para a injeção.
- Para os *scaffolds* de CHT estruturados em esponjas, a estabilidade em termos de perda de massa com o tempo em PBS foi atribuída à presença de acetato residual, enquanto que nas micropartículas foi atribuída ao grau de reticulação. Nos *scaffolds* de AH, a estabilidade refletiu somente do grau de reticulação.
- Todos os *scaffolds* preparados neste trabalho não apresentaram citotoxicidade.
- Nas esponjas a rede de fibrina formou-se preferencialmente no interior dos poros, enquanto que nas micropartículas a partição da rede de fibrina entre o interior e a superfície das partículas foi dependente da sua rigidez, a qual é

função do grau de reticulação.

- A liberação dos fatores de crescimento (PDGF-AB e TGF- $\beta$ 1) foi predominantemente difusiva em todos os *scaffolds*. A maior parte dos fatores (~80%) foi liberada nas primeiras 12 horas em concordância com a estabilidade dos *scaffolds*.
- A proliferação de h-AdMSCs foi maior ou igual a do PRP para as esponjas de ambos os polímeros, exceto quando reticuladas com TPP (CHT) ou BDDE (AH). Nas micropartículas, a proliferação foi menor em relação ao PRP e dependente da dureza e grau de reticulação.
- A capacidade das h-AdMSCs para a produção do marcador de diferenciação osteogênica ALP foi favorecida nas micropartículas em relação às esponjas.
- A capacidade de diferenciação osteogênica apresentou uma tendência oposta à proliferação celular.
- A radiação por plasma foi o processo mais adequado para a esterilização por das esponjas de ACP, enquanto que o tratamento com vapor em autoclave (126°C, 1,5 kgf/cm<sup>2</sup>), até 5 minutos foi o processo mais eficaz para as microesferas de ACP.

Embora a reprodutibilidade de produção dos *scaffolds* e o cultivo celular possam ser bem controlados pelas condições operacionais, a comparação precisa do desempenho dos vários *scaffolds* é complexa por contemplar os fatores inerentes ao PRP, tais como a variabilidade da concentração de plaquetas e fatores de crescimento de diferentes doadores nos vários ensaios.

Assim, concluímos que os *scaffolds* compósitos preparados neste trabalho são promissores para engenharia de tecidos, particularmente para a cicatrização e regeneração óssea, no âmbito da medicina regenerativa.

## 9.2. Trabalhos Futuros

- Minimização da variabilidade do PRP para uma precisa comparação do desempenho dos *scaffolds*.
- Produzir e caracterizar *scaffolds* com diferentes tamanhos e formatos para ensaios pré-clínicos.
- Estender os estudos realizados com P-PRP para o L-PRP (plasma rico em plaquetas e em leucócitos).
- Estudar a influência das esponjas e micropartículas na ativação do PRP.



- Caracterizar as interações moleculares entre a rede de fibrina e os *scaffolds*.



# ANEXO 1

---

## COMPOSIÇÃO E FORMULAÇÃO DE *SCAFFOLDS* DE ÁCIDO HIALURÔNICO E QUITOSANA PARA ASSOCIAÇÃO COM PLASMA RICO EM PLAQUETAS E SEUS USOS EM TERAPIA REGENERATIVA

A presente invenção refere-se a *scaffolds* compostos de ácido hialurônico (AH) e quitosana (CHT) em formulações sólida ou fluida (injetável), para associação com plasma rico em plaquetas (PRP), em aplicações no campo da medicina regenerativa, mais especificamente no campo da ortopedia. Nas formulações sólidas os polímeros são estruturados em esponjas e nas formulações fluidas em micropartículas. A invenção baseia-se no fato de que a associação de PRP ao ácido hialurônico livre tem sido amplamente usado na clínica, em tratamento de lesões musculoesqueléticas. Ensaio *in vitro* mostraram que a estruturação do AH autorreticulado ou de quitosana estabilizada em esponjas ou micropartículas, promoveu a liberação gradual dos fatores de crescimento provenientes do PRP, estimulou a proliferação de células tronco mesenquimais humanas de tecido adiposo, assim como a osteogênese. A associação do PRP com os *scaffolds* melhorou a estabilidade da rede de fibrina, e a estruturação em esponjas ou micropartículas melhorou as propriedades mecânicas em relação aos polímeros livres. Entretanto, a elevada densidade de carga negativa do AH reduz a adesão celular que interfere na regeneração tecidual, enquanto que a elevada carga positiva da CHT pode resultar em danos celulares *in vivo*. Nesse contexto, a presente invenção que trata de *scaffolds* de AH autorreticulado e quitosana para associação com PRP evidencia que esses *scaffolds* constituem biomateriais para uso clínico que beneficiam as aplicações do PRP em terapia regenerativa.